Stereochemistry of small molecules: Configurational and conformational control

Yiqun Zhang

Dissertation submitted to the faculty of the Virginia Polytechnic Institute and State University in partial fulfillment of the requirements for the degree of

Doctor of Philosophy
In
Chemistry

Dr. Paul R. Carlier, Chairman
Dr. Felicia A. Etzkorn
Dr. Brian E. Hanson
Dr. David G. I. Kingston
Dr. James M. Tanko

March 15, 2007
Blacksburg, VA

Keywords: configurational stability, cyclopropylnitrile, halogen-metal exchange, chiral Grignard reagents, conformational control, nitrile aldol, *syn*-pentane interaction, allylic 1,3-strain

Stereochemistry of small molecules: Configurational and conformational control

Yiqun Zhang

ABSTRACT

Stereochemistry is important aspect of chemistry that customarily includes the study of the relative spatial arrangement of atoms within molecules (*static stereochemistry*), and the study of the stereochemical requirements and outcomes of chemical reactions (*dynamic stereochemistry*). These two branches complement each other in modern stereochemistry.

Chiral organometallics feature prominently in organic synthesis as reactive intermediates. The possibility of exploring their stereochemistry in synthesis is associated with the configurational stability of the metal-bearing stereogenic center. We were interested in the configurational stability of lithiated and magnesiated nitriles. We developed a new series of lithio-cyclopropylnitriles bearing chelating groups for intramolecular coordination, as a possible strategy to impart configurational stability. Although this strategy has not yet been successful, using density functional theory (DFT) method, we addressed the effect of chelating groups on racemization *via* the "conducted tour" mechanism. We then explored metal-bromine exchange on enantiopure bromonitrile as alternative route to metalated nitriles. In this way, we demonstrated that magnesiated 2,2-diphenyl cyclopropylnitrile is configurationally stable on the macroscopic timescale. No other metallated nitrile has ever demonstrated configurational stability on this timescale. In contrast, bromine-lithium exchange of 1-bromo-2,2-diphenyl-cyclopropylnitrile demonstrated fast racemization under the same conditions.

Another major project focused on conformational control of acyclic molecules. Using X-ray crystallography and NMR spectroscopy, we found that the 2,6-disubstituted aryl group eclipses its geminal hydrogen, and induces an antiperiplanar relationship of the geminal and vicinal hydrogens. Interestingly, *anti*-nitrile aldols or *syn*-ketone aldols bearing 2,6-disubstituted aryl groups demonstrate unanticipated remote effects on acyclic conformation: the 2,6-disubstituted aryl group prefers to be in a gauche position to the largest vicinal group. The minimization of allylic 1,3-strain and *syn*-pentane-like interaction works together in establishing this conformational preference.

Acknowledgements

I would like to express in depth my sincere gratitude to my advisor, Dr. Paul R. Carlier for his inspiration, guidance and continue support throughout my graduate years. His encouragement, patience and confidence in me have made my Ph.D. study a smooth and enjoyable experience. Without his ever-present mentoring this research never could become reality. I would like also to thank the members of my advisory committee, Dr. Felicia Etzkorn, Dr. Brian Hanson, Dr. David Kingston, and Dr. James Tanko for their advices.

My deep felt thanks to Mrs. Kay Castagnoli for her encouragement and support. I would also like to thanks Bill Bebout (high resolution Mass Spectroscopy), Tom Glass (NMR), and Carla Slebodnick (X-ray analysis) for all their help and support. I acknowledge the financial support of the Department of Chemistry at Virginia Tech.

I am also grateful to all my group members, Dr. Dawn Wong, Nipa Deora, Dr. Ming, Ma, Danny Hsu, Jason Harmon, Larry Williams, Josh Hartsel, Yang-sheng Sun, Christopher Monceaux, Dr. Hongwu Zhao, Dr. Stephanie MacQuarrie-Hunter, Dr. Ella Clement, Dr. Joseph DeGuzman, and Dr. Polo Lam. Many valuable discussions with them contributed to my success. Thanks each of them for their patience and for sharing their knowledge with me.

Many thanks for my Chinese friends in Blacksburg, Fangfang Huang, Wenjuan Shi, Suolong Ni, Jun Zheng, Ran Miao, Jun Qi, Ting Cai, Hang Wang, Xin Zhao, Haiyan Zhao, Henry Yip, Liping Xing, etc. They lighted up my time in Virginia Tech.

Finally, my deepest thanks are extended to my family for their love and support during my entire education. Without them I couldn’t overcome difficulties during the tough time.

Dedication

To my parents for their constant love and encouragement.

Table of Contents

List of Schemes

List of Figures

List of Tables

Chapter 1 Configurational stability of organolithium and organomagnesium reagents.

1.1 Introduction.

Organometallics have played an important role in organic synthesis, such as organolithiums and organomagnesiums.[1] In the last dozen years, organolithiums have been widely used in developing methods for asymmetric synthesis.[2] Grignard reagents also have been reported for stereoselective synthesis.[3-6] If the metal-bearing carbon atom is the sole source of chiral information and if no chiral additive is present in a preceding step, the configurational stability of the carbanionic intermediate ***1*-1** is the essential precondition for its utilization in asymmetric synthesis (Scheme 1.1).[7]

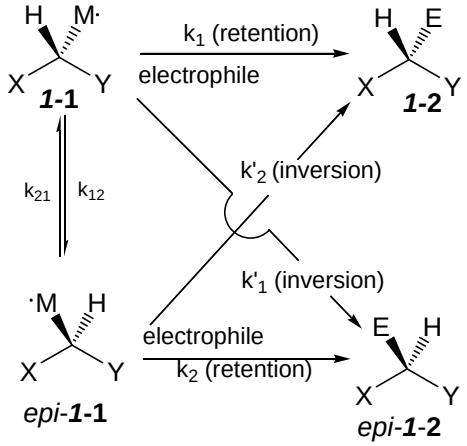

Scheme 1.1 The configurational stability of chiral organometallic as the precondition for its utilization in asymmetric synthesis.

The configuration of the formed product ***1*-2** is dependent on the stereochemical behavior of the chiral organometallics, and the stereospecificity towards electrophiles. Understanding the configurational behavior of chiral organolithium intermediates is

crucial for identifying the stereochemistry of their reactions. Furthermore, determination of the relationship of structures, reaction pathways and the stereochemical consequences can provide a basis for rational improvement of synthetic methodology.

Organolithiums have been excellently reviewed by Clayden.[8] He has noted that the term "configurational stability" has meaning only when it is associated with a temperature and a timescale. Hoffmann described that the timescale on which organometallics were configurationally stable was defined by the rate of the reaction of organometallics with electrophiles.[9] In this dissertation, three types of timescales are defined, according to experimental methods: NMR timescale, microscopic timescale and macroscopic timescale (Table 1.1).[8]

Table 1.1 Three types of timescales

Type	Experimental method
NMR timescale	dynamic NMR
Microscopic timescale	Hoffmann test[a]; or *in situ* quench conditions
Macroscopic timescale	sequential quench conditions

[a] Organolithiums, which are configurationally stable on macroscopic timescale, will pass the Hoffmann test.

In dynamic NMR experiments, the isomerization of a stereogenic center is evaluated by the interconversion of diastereotopic signals with a frequency difference $\Delta\nu$. The exchange rate of the diastereotopic signals increases with an increase in temperature. When the exchange rate of those two signals is large compared with $\Delta\nu$, a coalescence of two signals will be observed. Dynamic NMR timescale is taken as the coalescence

lifetime by an equation $\tau_{coalescence} = \left(\sqrt{2}\pi\Delta\nu\right)^{-1} = k^{-1}$.[10] Thus, NMR timescale on a 400 MHz spectrometer ranges from 0.2 s to 56 μs.[11, 12] Microscopic timescale and macroscopic timescale, which are associated with chemical methods, can be defined by the delay time between the formation of organolithiums and their reaction with electrophiles. Configurational stability on the microscopic timescale (a matter of seconds at most) is studied by the Hoffmann test, or by formation of organolithiums in the presence of electrophiles (*in situ* quench conditions). The term macroscopic timescale is used for sequential quench conditions, under which enantiomerically pure or enantioenriched organolithiums are formed first and subsequently react with electrophiles. Furthermore, a number of other factors are believed to affect configurational stability, including reagent structure, ligands, solvents.[13]

1.2 The Hoffmann test for assessing microscopic configurational stability

Hoffmann and his coworkers developed a chemical test of configurational stability based on kinetic resolution during the electrophilic substitution step.[9, 14] The Hoffmann test is a powerful chemical method and is widely used in the field because enantiomerically enriched or racemic organolithium reagents can be employed. Two reactions are carried out in the Hoffmann test (Scheme 1.2).

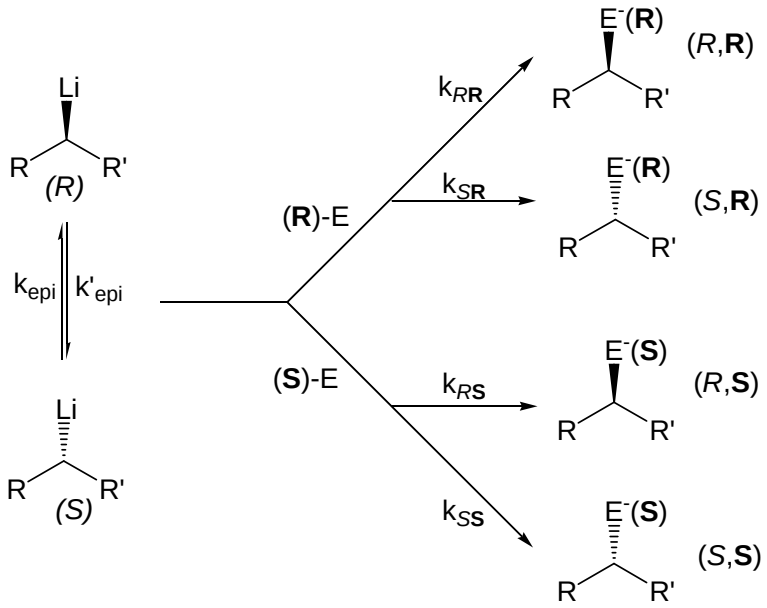

Reaction 1: use (**RS**)-E $\rho_{rac} = \frac{R.\mathbf{R} + S.\mathbf{S}}{S.\mathbf{R} + R.\mathbf{S}}$ and $3 > \rho_{rac} > 1.5$

Reaction 2: use (**R**)-E $\rho_R = \frac{R.\mathbf{R}}{S.\mathbf{R}}$

if $\rho_R = \rho_{rac}$, then configurationally labile

if $\rho_{rac} > \rho_R > 1$, then partially configurationally labile

if $\rho_R = 1$, then configurationally stable

Scheme 1.2 Overview of the Hoffmann test to determine the configurational stability.

In the first reaction, which is the control reaction, the racemic organolithium of interest is treated with a racemic chiral electrophile ((**R**)-E and (**S**)-E), such that the diastereomeric ratio ρ_{rac} of the resulting products lies between 1.5 and 3.0. If the diastereomeric ratio ρ_{rac} is outside of this range, there are difficulties in the subsequent analysis; thus different chiral electrophiles are explored until the diastereomeric ratio ρ_{rac} falls within this range. The degree of the conversion is not important in the first control reaction. In the second reaction, the racemic organolithium compound is allowed to react with the corresponding enantiopure (in this case **R**) electrophile. A high conversion (>90 %) has to be reached in

the second reaction. If the diastereomeric ratio ρ_R of the products is the same as that obtained in the control reaction (ρ_{rac}), the organolithium compound is configurationally labile on the reaction time scale. Otherwise, if the diastereomer ratios from the two reactions are different, the organolithium is at least partially configurationally stable. In the case of an organolithium compound that is completely configurationally stable on the time scale of the reaction, the diastereomeric ratio from the second reaction ρ_R should be equal to one.

A modified Hoffmann test, which also relies on a rate difference between diastereomeric transition states, is used to study the configurational stability of organolithiums in the presence of an enantiomerically pure chiral ligand. Two reactions are performed during this modified Hoffmann test: enantioenriched organolithiums reacting with excess achiral electrophiles; enantioenriched organolithiums reacting with deficit of achiral electrophiles (Scheme 1.3). When the organolithium is configurationally stable, the excess of achiral electrophiles allow the diastereomeric complexes of organolithium and chiral ligands to react completely, and ideally lead to racemic products. However, with a deficit of achiral electrophiles, the reaction stops before it goes to the completion. One diastereomer of the organolithium-ligand complexes, with a lower transition state for reacting with electrophiles, produces more products than the slower-reacting complex. Consequently, some degree of enantiomeric excess is observed for products (kinetic resolution). In contrast, for the configurationally labile organolithium, the rapid inversion causes the same enantiomeric excess of products

ensuing from the excess electrophiles as from the deficit of electrophiles.

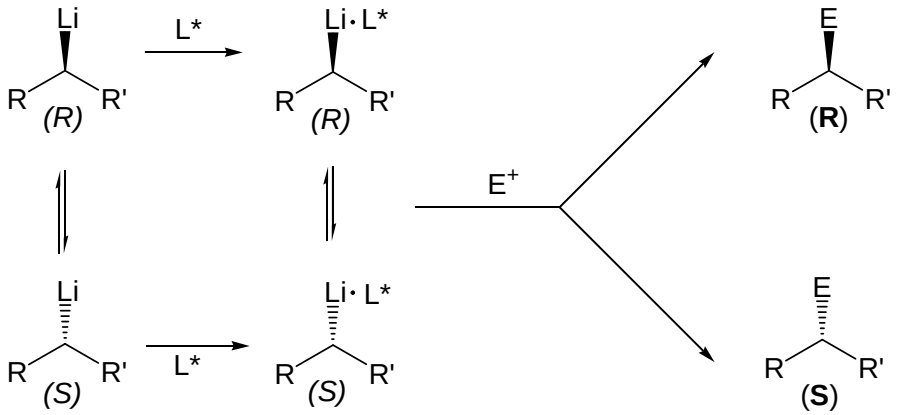

Reaction 1: use an excess of achiral E^+, $\rho_{excs} = \frac{\mathbf{R}_{excs}}{\mathbf{S}_{excs}}$

Reaction 2: use a deficit of achrial E^+, $\rho_{def} = \frac{\mathbf{R}_{def}}{\mathbf{S}_{def}}$

if $\rho_{excs} = \rho_{def}$, then configurationally labile

if $\rho_{excs} \neq \rho_{def} \neq 1$, then partially configurationally labile

if $\rho_{excs} = 1$, then configurationally stable

Scheme 1.3 Overview of the modified Hoffmann test to determine the configurational stability of organolithiums in the presence of an enantiomerically pure chiral ligand.

1.3 The relation of temperature to configurational stability.

"Configurationally stable" is associated with a temperature and a timescale. In general, the low energy barrier of inversion for enantiomerically enriched organolithium reagents requires that reactions be performed at low temperature. To perform practical organic reactions with these reagents, we may require macroscopically configurational stability. Following Öki's analysis,[15] it is possible to calculate the racemization rate from the activation barrier for racemization (equation 1), where we assume the pre-exponential is kT/h:[15, 16]

$$k_{rac} = 2 * kT/h * \exp(-\Delta G^{\ddagger}/RT), \quad \text{equation (1)}$$

$\tau_{1/2} = \ln 2/k_{rac}$

Table 1.2 demonstrates the relationship between temperature, half life, and activation barrier. If we require a racemization half-life of one hour (3600 s), it is possible to determine what the required activation barrier would be at various temperatures. At 100 °C (373 °K), an activation barrier of 28.9 kcal/mol is required; at –78 °C (195 °K), the required barrier is only 14.8 kcal/mol. A 5 min (300 s) half-life at this temperature requires a barrier of 13.9 kcal/mol (Table 1.2). Thus, as a minimum, 13.9 kcal/mol is required as a racemization barrier, if we wish to perform reactions on the minute time scale at -78 °C. Consequently, the lower the temperature is, the lower is the racemization barrier required for the minute time scale configurational stability. Even at 173 K, a 12.3 kcal/mol barrier is necessary.

Table 1.2 Free energies of activation ($\Delta G^{\ddagger}$)

T (K)	Half-life (s)	$\Delta G^{\ddagger}$ (kcal/mol)
373	3600	28.9
298	3600	22.9
273	3600	20.9
233	3600	17.8
195	3600	14.8
195	1800	14.6
195	300	13.9
195	1	11.7
173	300	12.3

From this stand point many of organolithium reagents ***1-3*** **~ 8** studied by dynamic NMR (Figure 1.1)[17-19] do not fit this requirement. In contrast, the chiral non-racemic

potassium enolates ***1*-9** of Fuji and Kawabata exhibited an inversion barrier of 16.0 kcal/mol at –78 °C,[20] and were indeed very useful in asymmetric alkylation, as a consequence of their macroscopically configurational stability.

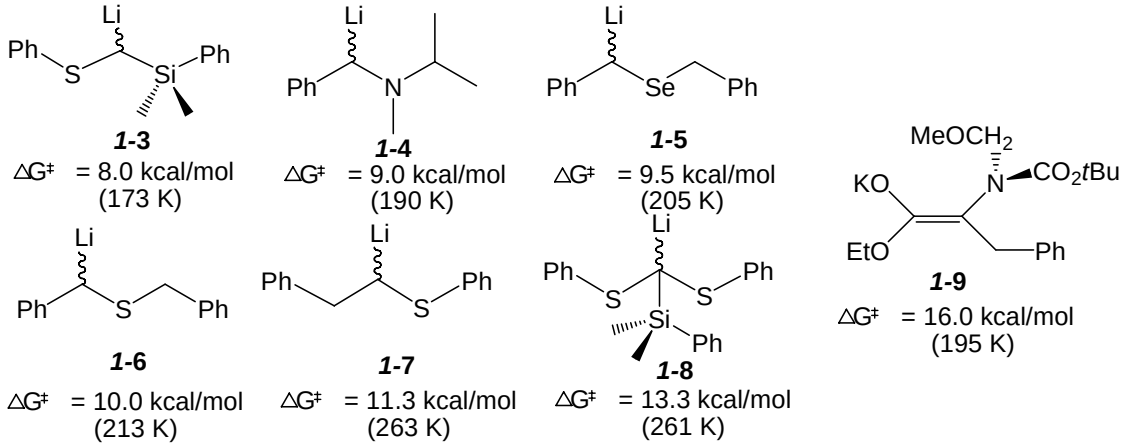

Figure 1.1 The free energies of enantiomerization of organolithium reagents ***1*-3 ~ 9**.

1.4 Effect of solvents on configurational stability.

Solvent can play an important role in configurational stability. Intermolecular coordination occurs between lithium and a Lewis base solvent, such as TMEDA (tetramethylethylene diamine), DME (dimethoxyethane), THF and DEE (diethyl ether).[21] The effect of these additives on configurational stability varies with the particular substrate.

Chiral organolithium intermediates were first reported by Letsinger,[22] Applequist[23] and Curtin[24] half a century ago. The half-lives for the racemization of secondary, unfunctionalized organolithiums ***1*-10a** and ***1*-10b** in the presence of Et_2O are only seconds at -70 ºC.[22,24] We can estimate an approximate racemization barrier of 12.2 kcal/mol for these unfunctionalized organolithiums at -70 °C in presence of Et_2O. However, in

non-polar solvents, such as pure pentane, ***1*-10b** had retained 83 % of its optical activity even after 4 hours at -40 °C.[24] A dissociation process[21] has been proposed for racemization since a polar solvent promotes the ionic character of the C-Li bonds and accelerates racemization (Scheme 1.4).

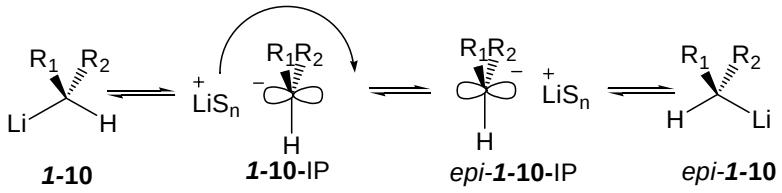

***1*-10** ***1*-10-IP** *epi-**1**-10-IP* *epi-**1**-10*

***1*-10a**: R1 = CH_3, R2 = C_7H_{15}
***1*-10b**: R1 = CH_3, R2 = C_2H_5 S: solvent molecule

Scheme 1.4 Racemization of ***1*-10a** and ***1*-10b** *via* a dissociation process.

Kerrick and Beak found that lithiated *N*-Boc-pyrrolidine intermediate ***1*-11** was configurationally stable for at least 30 min at –78 °C in the presence of TMEDA.[25] Organolithium intermediate ***1*-12**, which was generated from Li-Sn exchange, could retain its configuration at –78 °C for at least one hour in the absence of or in the presence of TMEDA.[26, 27] However, Pearson and Lendbeck reported that addition of the coordinating solvent TMEDA caused a much more rapid epimerization for organolithium ***1*-13** (Figure 1.2).[28]

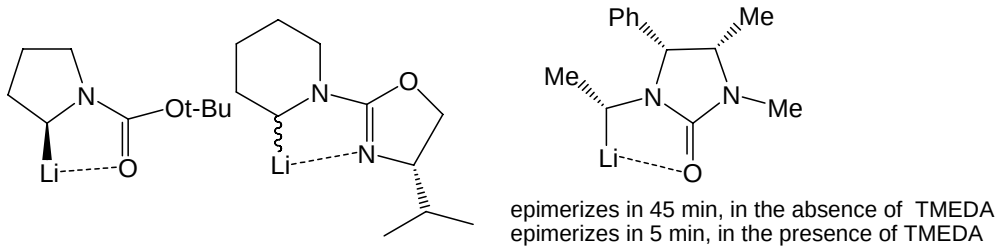

epimerizes in 45 min, in the absence of TMEDA
epimerizes in 5 min, in the presence of TMEDA

***1*-11** ***1*-12** ***1*-13**

Figure 1.2 The structure of α-aminoorganolithium ***1*-11** ~ **13**.

Reich et al. investigated the configurational stability of lithio-diphenylcyclohexane ***1*-14** (the axial isomer, Figure 1.3) formed from the lithium-metal exchange (by *sec*-BuLi). He found that the rate of inversion of ***1*-14** to its equatorial isomer was strongly dependent on the total organolithium concentration; it was faster at higher concentration.[29] A reasonable interpretation of this concentration dependence, suggested by Reich, was that the inversion was an associative process. If ***1*-14**, like *sec*-BuLi, was largely monomeric in THF, then the inversion might involve higher aggregates of ***1*-14**. An aggregate might provide mechanistic opportunities for inversion, for example, a rapidly inverting free carbanion ***1*-15**, a triple ion intermediate ***1*-16** with a symmetrically dilithiated planar carbanion (Figure 1.3), or by pseudo rotation of 5-coordinated carbon in dimer ***1*-17**.[30]

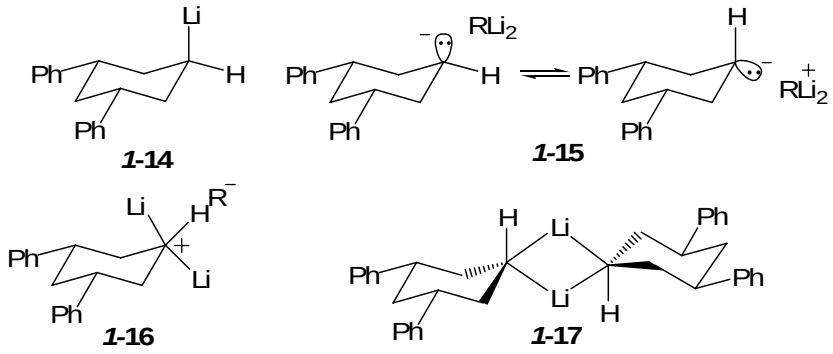

Figure 1.3 Lithio-diphenylcyclohexane and its inversion forms. (Reprinted with permission from Reich et al, *J. Am. Soc. Chem*. **1992**. *114*, 11003. Copyright (1992) American Chemical Society)

Reich investigated the above aggregation hypothesis.[29] A complexing reagent PMDTA (*N,N,N',N'',N''*-pentamethyldiethylenetriamine) that effectively prevents dimerization might enhance the configurational stability of ***1*-14** by preventing aggregate-based lithium exchange. Though the equilibrium constant was not significantly affected, the

isomerization rate of ***1*-14** was 20-fold lower (a half-life > 2h) in the presence of PMDTA than that (a half-life ≈ 9 min) in the sole solvent THF. However, the rate of isomerization increased when run in ether/THF mixtures compared to pure THF (most lithium reagents form higher aggregates in ether than in THF).[29] In this case, the configurational isomerization of the lithium reagent ***1*-14** was slowed by increase in the strength of solvent coordination to lithium. In contrast, Reich's other studies indicated that the addition of HMPA to the reaction decreased the inversion barrier of α-thio organolithium compounds.[31] Similar results were observed in 1-substituted cyclopropyllithium,[32] 1-styryllithium[19] and α-aminoalkylithiums.[33] At this point, the presence of ligands (as co-solvent) may function in two different ways: 1) prevent the aggregate-assisted isomerization; 2) facilitate the dissociative S_E1 isomerization.

1.5 Configurational stability of organolithiums

1.5.1 Formation of chiral organolithiums and transformation of their stereochemical information.

Organolithiums may be formed by one of four distinct methods as shown in Scheme 1.5: 1) lithiation by deprotonation using commercially available alkyllithium is feasible way; 2) transmetallation; 3) halogen-lithium exchange; and 4) reductive lithation.[34] The formation of organolithium from secondary alkyl halide is difficult by halogen-lithium exchange,[35] and reductive lithiation is usually preferable. Though reductive lithiation can be used for regioselective synthesis of organolithiums, stereoselective and stereospecific

synthesis of organolithiums is normally performed through asymmetric deprotonation, transmetallation or lithium-halogen exchange.[8]

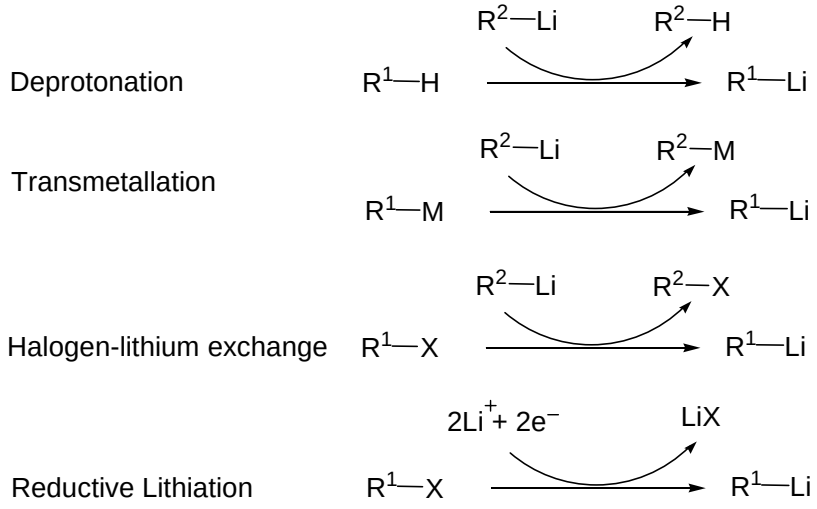

Scheme 1.5 Formation of organolithiums.

Chiral organolithium intermediates can to be generated by asymmetric deprotonation (Scheme 1.4). Basu and Thayumanavan have summarized Beak's work in lithiation/substitution.[36] The enantiodetermining step of the overall reaction can be asymmetric deprotonation or asymmetric substitution.[36, 37]

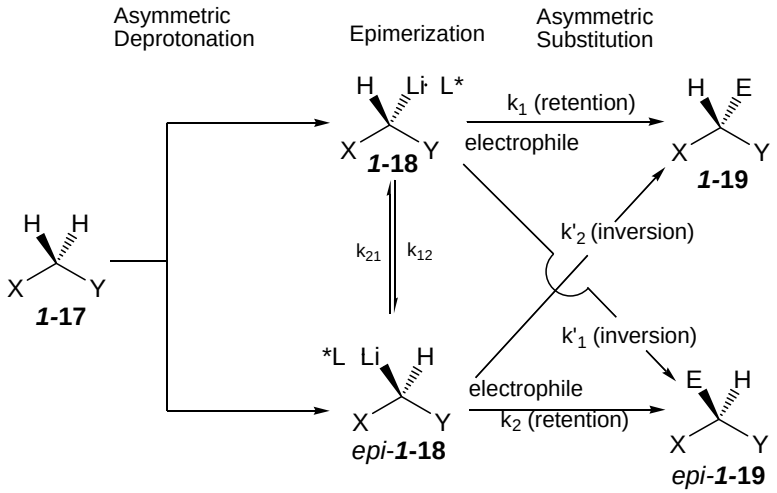

Scheme 1.6 Overview of step involved in the lithiation and substitution of prochiral methylene group[36].

For asymmetric deprotonation, the enantiodetermination step is the lithiation itself. The organolithium reagent, complexed to the chiral ligand, functions as a chiral base that selectively abstracts one enantiotopic proton from the prochiral substrate ***1*-17** to generate a macroscopic configurationally stable intermediate ***1*-18** or *epi*-***1*-18**. The intermediate reacts stereoselectively with an electrophile, providing the enantioenriched product ***1*-19** or *epi*-***1*-19**.

In asymmetric substitution, the enantiodetermining step occurs after deprotonation. Two limiting pathways can be envisioned for asymmetric substitutions--*dynamic thermodynamic resolution* or *dynamic kinetic resolution*. In dynamic thermodynamic resolution pathway, the diastereomeric complexes ***1*-18** and *epi*-***1*-18** are macroscopically configurationally stable. In this case the enantioselectivity of the product is determined by the ratio of the diastereomeric complexes that are formed before the substitution step. The term dynamic thermodynamic resolution is defined for this case because the ratio of complexes is dynamically controlled prior to reaction with electrophiles.

In dynamic kinetic resolution pathway, the diastereomeric complexes are configurationally labile with respect to their rate of a reaction with electrophiles. The lithiated intermediates ***1*-18** and *epi*-***1*-18** undergo rapid epimerization and one of the diastereomeric complexes reacts preferentially under the reaction conditions. In this case, the stereoselectivity arises as a result of the differences in the transition state energies of electrophilic substitution for each diastereomeric intermediate. Thus by introducing a

chiral ligand to these organolithium intermediates, enantioselective alkylation can be realized.

1.5.2 Configurational stability of organolithiums bearing α-heteroatoms

The presence of a heteroatom adjacent to a lithium-bearing carbon atom can significantly influence the stereochemical properties of organolithium compounds. The reported configurational stability investigations have concentrated on oxygen-,[38, 39] nitrogen-,[40, 41] sulfur-, selenium-,[42 43] and phosphorus-[44] stabilized organolithium derivatives. In general, sulfur- and selenium-stabilized organolithiums require a low temperature and/or a short timescale of investigation for microscopically configurational stability. This is in contrast to oxygen-and nitrogen-stabilized organolithiums that exhibit macroscopically configurational stability at –78 °C and sometimes at even higher temperature.[38-41]

1.5.2.1 Nondipole-stabilized organolithiums

A configurationally stable α-alkoxyorganolithium ***1*-21** was first reported by Still (Figure 1.4).[45] The enantioenriched α-methoxymethyl (MOM) organolithium compound ***1*-21** was prepared through lithio-destannylation of the enantioenriched tributyltin substituted precursor ***1*-20**. After trapping with acetone, *anti*- and *syn*-***1*-21** led to different products *anti*- or *syn*- ***1*-22** each with no trace of the other. This result suggested that the

configuration of ***1*-21** was stable over periods of at least minutes at –30 °C. Other α-alkoxyorganolithiums ***1*-23a ~ e** (Figure 1.4) were configurationally stable over a period of up to 30 min at -78 °C.[46-49]

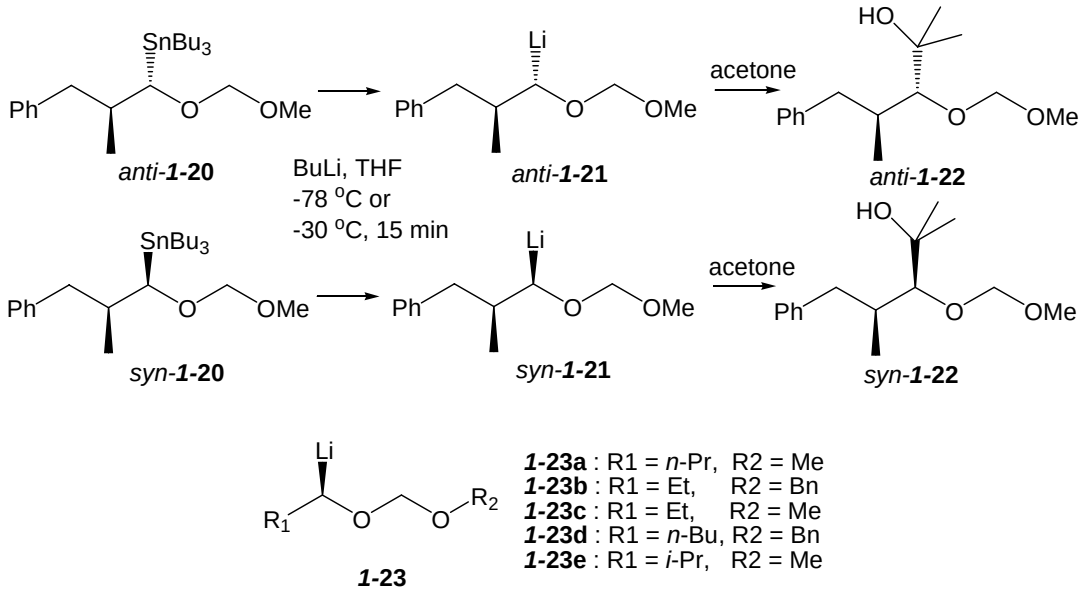

Figure 1.4 Macroscopically configurational stability of α-alkoxyorganolithiums ***1*-21** and ***1*-23**.

Gawley et al.[50] reported the macroscopically configurational stability of 2-lithio-*N*-methylpyrrolidine ***1*-24** and 2-lithio-*N*-methylpiperidine ***1*-25** (Figure 1.5), which were generated from the corresponding enantioenriched organostannanes. Both 2-lithiopyrrolidines and piperidine resisted racemization in THF or in the presence of TMEDA at temperature as high as –40 °C for at least 45 min. The increased configurational stability of ***1*-24** and ***1*-25** was attributed to bridging of the lithium across the carbon-nitrogen bond (structure ***1*-26** and ***1*-27**), which was probably more important in the absence of chelating substituent. The existence of the bridged structure ***1*-27** was confirmed by the observation of $^{15}N–^{6}Li$ coupling in the NMR spectra of the doubly labeled

material.[51]

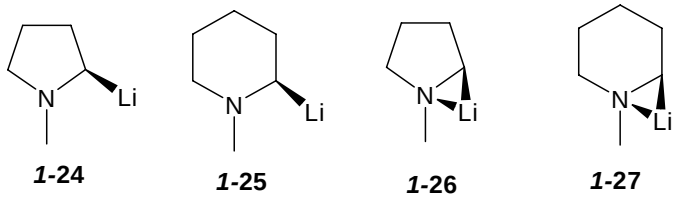

Figure 1.5 Macroscopically configurationally stable 2-lithiopyrrolidine ***1*-24** and 2-lithiopiperidine ***1*-25**, which attributed the configurational stability to their C-N bridging structures ***1*-26**, ***1*-27**.

Using the Hoffmann test, Hoffmann confirmed that α-arylthioorganolithium ***1*-28** was configurationally stabile on the microscopic timescale (Scheme 1.7).[14] The reaction of ***1*-28** with racemic ***1*-29** gave a 7:3 ratio of diastereoisomers ***1*-30a** and ***1*-30b** at -120 °C in methyl-THF; the repeat reaction with (*S*)-***1*-29** led to a 52:48 ratio.

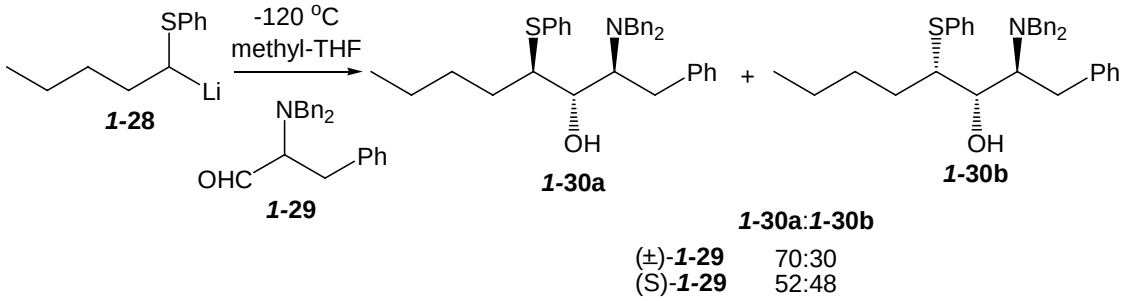

Scheme 1.7 Microscopically configurational stability of α-alkylthioorganolithium ***1*-28** (by the Hoffmann test).

Hoffmann reported that following the transmetallation of ***1*-31** (90% ee) to give the lithium compound ***1*-32**, the ring opening occurred quickly ($t_{1/2} \leq 5$min) with retention of configuration to provide chiral α-durylhomoallyllithium intermediate ***1*-33** (Scheme 1.8).[52, 53] After the methylation and hydrogenation of ***1*-33**, the compound ***1*-35** revealed 83% ee. It indicated that the α-durylhomoallyllithium ***1*-33** was configurationally stable

on the macroscopic timescale at -108 °C.[53]

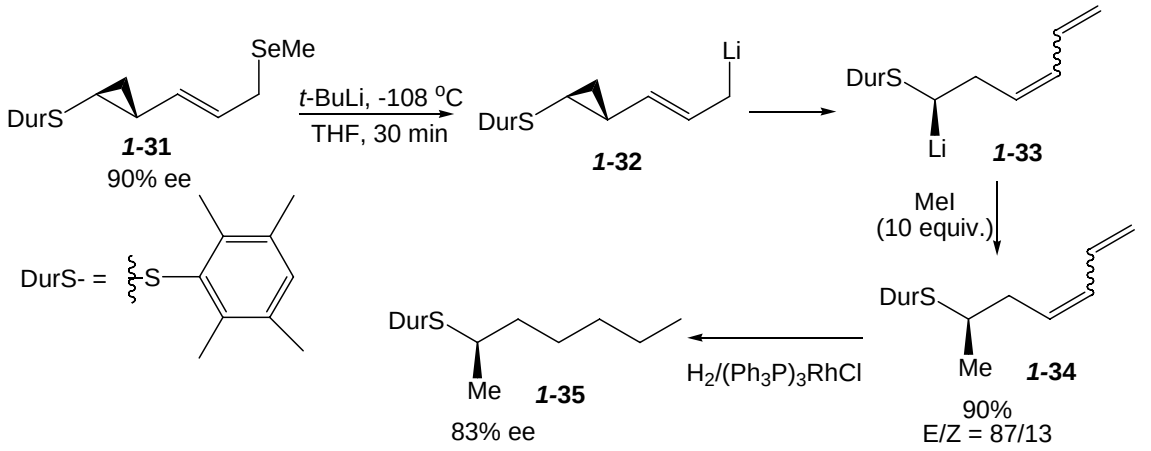

Scheme 1.8 Macroscopically configurational stability of α-durylhomoallyllithium ***1*-33.**

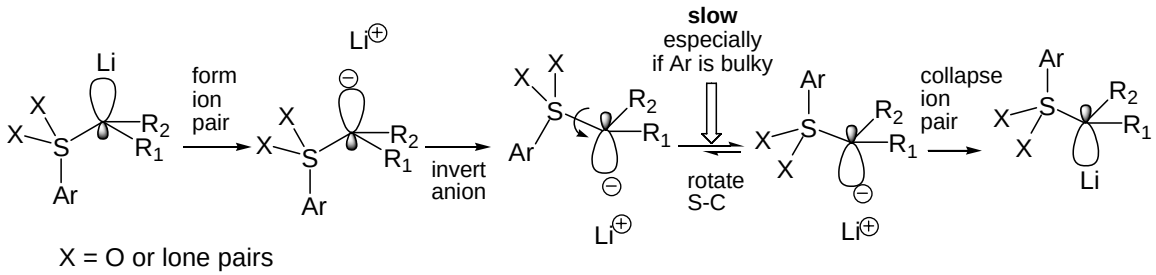

Scheme 1.9 Enantiomerization mechanism of sulfur-substituted organolithium.

The α-arylthio organolithium ***1*-28** and ***1*-33** exhibited microscopically and macroscopically configurational stability respectively. Reich[17] and Hoffman[18] provided an enantiomerization mechanism of sulfur-substituted organolithiums, which consists of four steps as shown in Scheme 1.9. Because the n → σ* conjugation features to place the S-C σ* orbital antiperiplanar to the C-Li bond or the carbanionic sp^3 orbital, the rotation of S-C bond is involved in the enantiomerization of α-thio substituted organolithiums (Scheme 1.9).[17] Consequently, the enantiomerization of α-arylthio organolithiums is expected to be slow when a bulky aryl group restricts the rotation of S-C bond. Dynamic

NMR studies by Hoffmann[18] showed that the enantiomerization barrier of ***1*-7** was 11.3 kcal/mol at 263 K whereas the durylsulfide ***1*-36** had a barrier greater than 13.9 kcal/mol at 263 K (Figure 1.6).

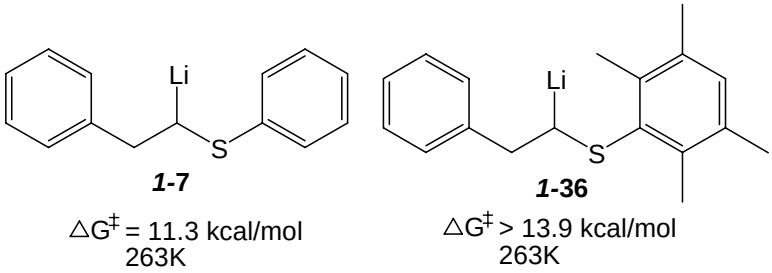

***1*-7** $\triangle G^{\ddagger}$ = 11.3 kcal/mol 263K

***1*-36** $\triangle G^{\ddagger}$ > 13.9 kcal/mol 263K

Figure 1.6 The enantiomerizaiton barriers of α-arylthioorganolithium ***1*-7** and ***1*-36** are influenced by the size of their arylthio groups.

α-Halo organolithium reagents are useful intermediates for the synthesis of epoxides and cyclopropanes. Hoffmann conducted the Hoffmann test on a racemic α-bromoalkyllithium ***1*-37** (Scheme 1.10) generated by Li/halogen exchange of the dibromide.[14] The organolithium ***1*-37** underwent addition to aldehyde ***1*-29** followed by the conversion of the β-bromo-alkoxides into epoxides. The reaction furnished two diastereomeric products ***1*-38a** and ***1*-38b**. When racemic ***1*-29** was used, the reaction afforded a 60:40 ratio of diastereoisomers ***1*-38a** and ***1*-38b**. The repeat reaction using (*S*)-***1*-29** reached a 50:50 diastereomer ratio. These facts showed that the compound ***1*-37** was configurationally stable on the microscopic timescale at -110 °C.

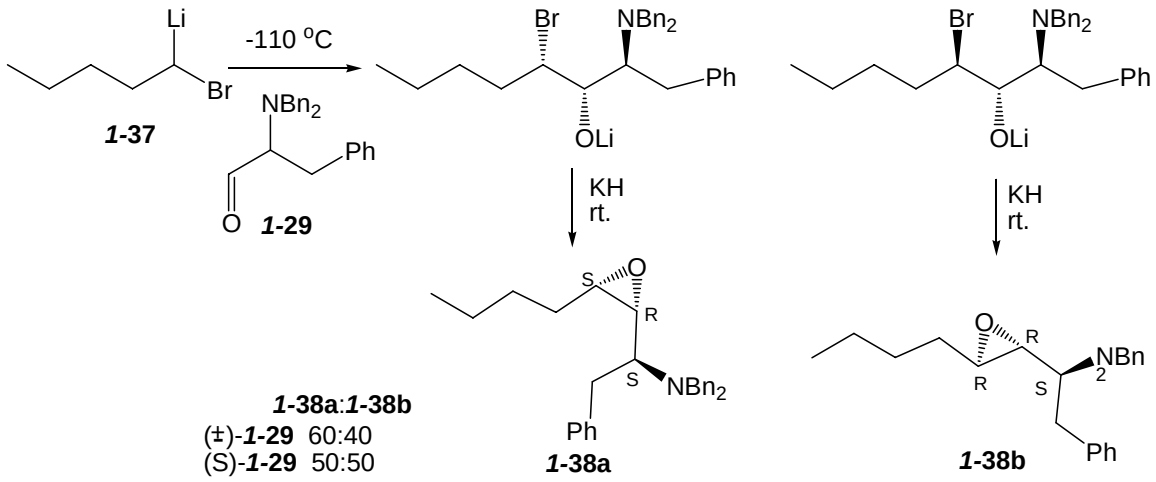

Scheme 1.10 Microscopically configurational stability of α-bromoalkyllithium ***1*-37**.

1.5.2.2 Dipole-stabilized organolithiums

The dipole-stabilization effect plays an important role in configurational stability of α-heteroatom substituted organolithium reagents.[26, 54-58] Representation of a dipole-stabilized organolithium ***1*-39** is shown in Scheme 1.11 where X represents the α-heteroatom, such as nitrogen, oxygen or sulfur. The carbonyl group beside the heteroatom is capable of inducing a formal positive charge on X. If ***1*-39b** is a significant contributor to the hybrid, the dipole stabilized form ***1*-39d** is an important factor in the stability of ***1*-39**.

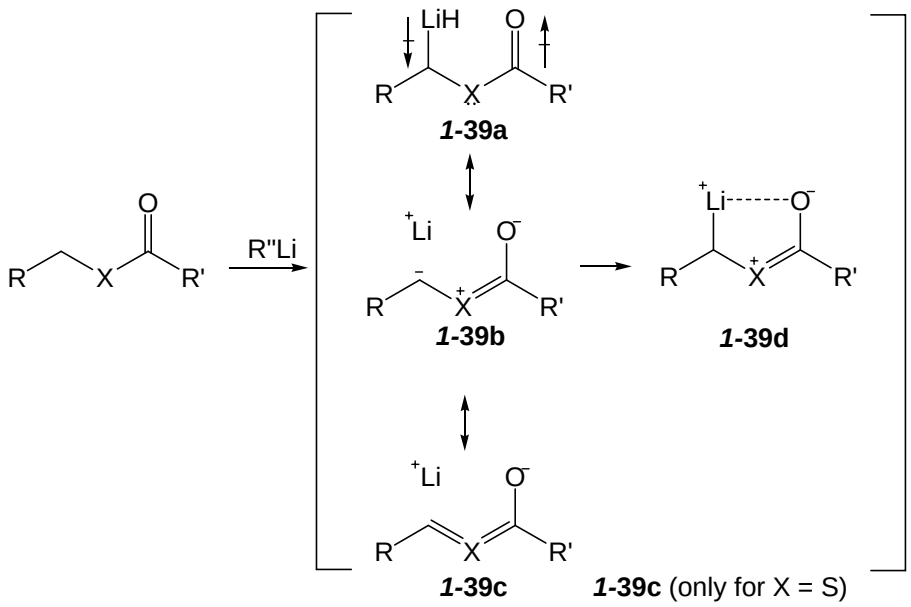

Scheme 1.11 Dipole stabilized organolithium reagents.

Kerrick and Beak found that the chiral 2-lithio-*N*-BOC-pyrrolidine ***1*-11** (Figure 1.7)**,** obtained by tin-lithium exchange in the presence of TMEDA, was macroscopically configurationally stable at –78 °C when ***1*-11** was trapped by trimethylsilyl chloride. However, ***1*-11** was configurationally labile at -78 °C in the absence of TMEDA.[25] In contrast, at the same reaction condition, Meyers and Elworthy reported that the organolithium ***1*-40** (Figure 1.7) was macroscopically configurationally stable at -78 °C in the absence of TMEDA.[59] Meyers suggested that the harder oxygen atom in ***1*-11** loosened the lithium-carbon attraction and allowed carbanion inversion to occur more readily, whereas the nitrogen atom in ***1*-40** was a poorer electron donor and allowed the C-Li bonding to remain closely associated, therefore inhibiting carbanion inversion.[59]

***1*-11** ***1*-40**

Figure 1.7 The structure of dipole-stabilized lithiated pyrrolidines ***1*-11** and ***1*-40**.

Many investigations have been carried out on dipole-stabilized benzylic organolithium intermediates.[60] A Hoffmann test on the secondary organolithium compound ***1*-41** indicated that ***1*-41** was microscopically configurationally stable at –78 °C in TMEDA/Et_2O (Figure 1.8).[60] The related tertiary lithium intermediates ***1*-42** and ***1*-43**, obtained from deprotonation of the corresponding carbamates, were macroscopically configurationally stable at -78 °C in TMEDA/hexane or in toluene/Et_2O.[61, 62] The chiral lithium intermediate ***1*-42** afforded products with retention of configuration after treatment with acetic acid, d-methanol, or dimethyl carbonate. In contrast, its reaction with carbon dioxide or alkyl halides provided inversion products.[39, 61, 63] This result reminds us that electrophilic substitution on organolithiums can occur with retention or inversion and that poor selectivity may reflect a mixture of these trajectories rather than poor configurational stability. Hammerschmidt confirmed that stannylation did occur with inversion of configuration in reactions of ***1*-43**.[62, 64] The related derivatives ***1*-44** and ***1*-45** exhibited macroscopically configurational stability for deuteration at –78 °C in TMEDA/hexane.[65]

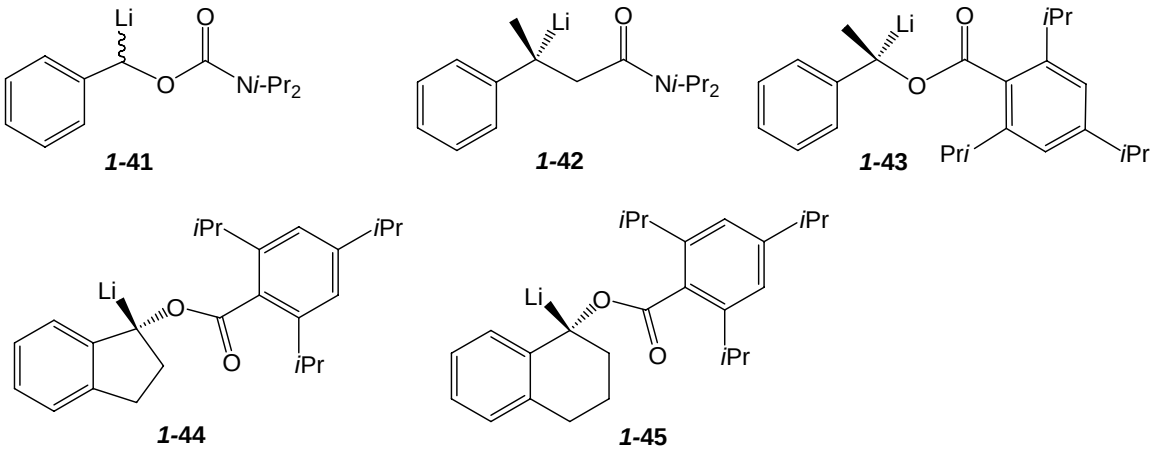

Figure 1.8 The structures of dipole stabilized benzylic organolithium ***1*-41** ~ **45**.

Chong reported that a chiral organolithium intermediate ***1*-46** (Figure 1.9), afforded from Li/Sn exchange, was configurationally stable at -78 °C for 3 h. However, the presence of a coordinating solvent HMPA made the ***1*-46** configurationally labile at -78 °C.[33] The benzylic organolithium ***1*-47** (Figure 1.9) was macroscopically configurationally stable at –78 °C in toluene in the presence of (–)-sparteine ***1*-50** (Figure 1.9). Treatment of (*R*)-***1*-47**/***1*-50** or (*S*)- ***1*-47**/***1*-50** with methyl triflate both provided methylated invertive products with 90% ee.[41, 66]

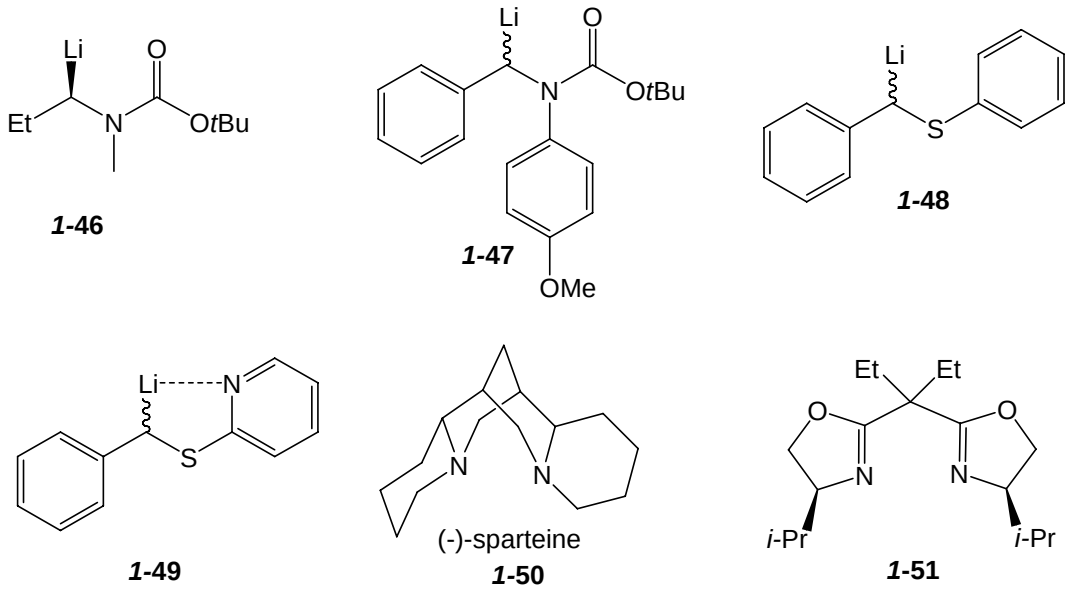

Figure 1.9 Structures of ***1*-46** ~ ***1*-49**, (-)-sparteine and ligand ***1*-51**.

A Hoffmann test indicated that the thiophenyl substituted organolithium ***1*-48** (Figure 1.9) was configurationally labile in cumene at -78 °C , even in the presence of TMEDA or ***1*-51**.[60,67] In contrast, Nakamura reported that the enantioselectivity in the reaction of the thiopyridyl substituted benzylic organolithium ***1*-49** with deficit of electrophiles turned out different from the reaction using stoichiometric amounts of electrophiles (a modified Hoffmann test). Furthermore, the highest enantiomeric ratio was obtained after a "warm-cool" sequence.[68] Thus, the organolithium ***1*-49** was macroscopically configurationally stable in the presence of ligand ***1*-51** (Figure 1.9) at –78 °C.[68]

1.5.3 Intramolecular coordination of a Lewis base

An appropriately placed heteroatom can serve as a Lewis base and coordinate with the lithium atom of an alkyllithium. This coordination can either improve or reduce the

configurational stability. In the previous discussion, 2-lithio-*N*-methylpyrrolidine ***1*-24** and 2-lithio-*N*-methylpiperidine ***1*-25** (Figure 1.10) were macroscopically configurationally stable at –40 °C in the presence of TMEDA (TMEDA was required in order to obtain acceptable yields). Without TMEDA, the organolithium ***1*-25** was both chemically and configurationally less stable over a period of hours at -60 °C.[50] Gawley also made ***1*-52** (Figure 1.10) and treated it under similar conditions to assess the effect of intramolecular chelation in this class of organolithiums. It was observed that ***1*-52** with a coordinating methoxy group was chemically and configurationally stable at –60 °C for up to 45 min in THF (with or without TMEDA), though TMEDA slightly lessened the configurational stability of ***1*-52**. Nonetheless, the organolithium ***1*-52** was considerably more configurationally stable than its acyclic analogue ***1*-53** (Figure 1.10) which could maintain its configuration at –95 °C for only 10 min in THF.[69]

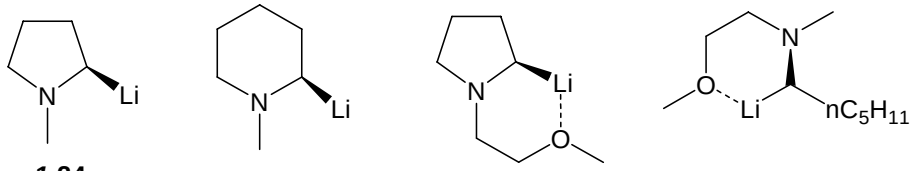

***1*-24** ***1*-25** ***1*-52** ***1*-53**

Figure 1.10 α-Aminoorganolithiums with intramolecular chelating substituents, ***1*-24** ~ **25**, and ***1*-52** ~ **53**.

1.5.4 Configurational stability of organolithiums with small ring systems.

In 1955, Walborsky first reported reactions of a cyclopropyl carbanion that was formed by the reaction of lithium diisopropylamide or sodium methoxide with 2,2-diphenylcyclopropyl cyanide ***1*-54** (Scheme 1.12)**.** The deuterium exchange of ***1*-54** could be accomplished with greater than 99.9% retention in basic CH_3OD. Walborsky

attempted methylation of (*R*)-***1*-54** in diethyl ether relative to methanol at room temperature, following deprotonation by LDA or sodium methoxide with times ranging from 10 seconds to 2 min. Racemization was observed in both cases. Walborsky proposed that lithiated or sodiated ***1*-54** had lower configurational stability in diethyl ether.[70, 71]

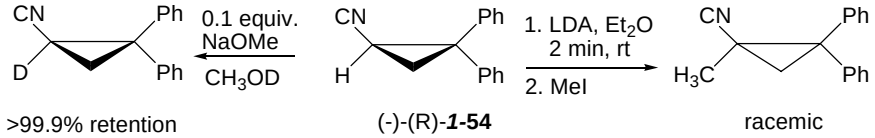

Scheme 1.12 The deuteration and methylation of 2,2-diphenylcylcopropylnitrile ***1*-54**.

It was recognized that the cyano group was playing a significant role in this racemization by participating in the delocalization of the negative charge. In an effort to obtain a cyclopropyl carbanion that was not adjacent to an unsaturated substituent, the Haller-Bauer cleavage of 1-benzoyl-1-methyl-2,2-diphenylcyclopropane ***1*-55** was investigated.[72] When optically active ***1*-55** was cleaved with sodium amide in toluene, the product 1-methyl-2,2-diphenylcyclopropane ***1*-56** retained its optical activity as well as the configuration at 1-carbon (Scheme 1.13). The cleavage presumably formed the 1-methyl-2,2-diphenylcyclopropyl carbanion, which then was protonated instantaneously by the benzamide co-product.

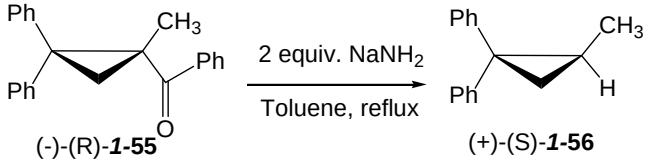

Scheme 1.13 Haller-Bauer cleavage of 1-benzoyl-1-methyl-2,2-diphenylcyclopropane ***1*-55**.

Some further insights into the stability of the 1-methyl-2,2-diphenylcyclopropyl

carbanion was undertaken by investigating 1-bromo-2,2-diphenylcyclopropane ***1*-57** (Scheme 1.14).[73] The corresponding organolithium was generated by halogen-metal exchange of ***1*-57** with *n*-butyllithium, cooled to –78 °C, followed by protonolysis in methanol. The reaction proceeded with a high degree of retention of optical purity and configuration. The reaction was independent of solvents, time and temperatures. When the organolithium underwent carbonation with carbon dioxide, or reaction with bromine, the reactions proceeded with complete retention of optical purity and configuration.

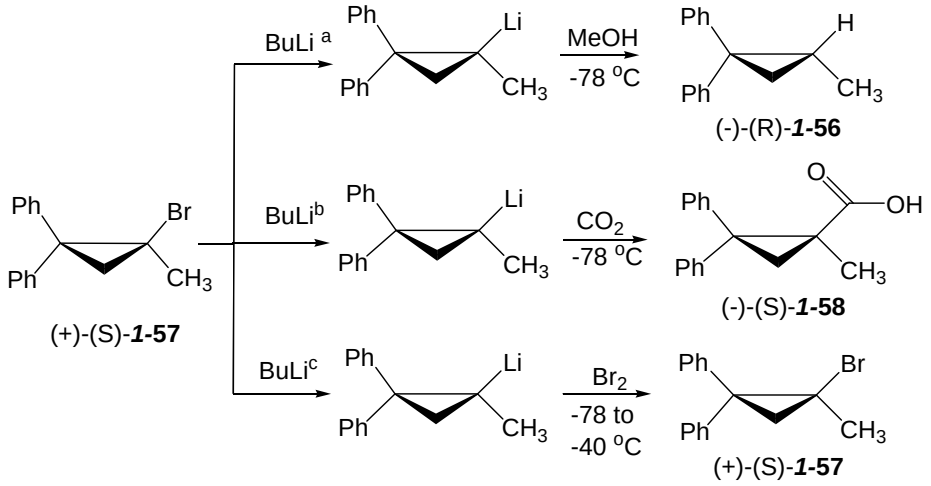

[a]. 1) in Ether-benzene-petroleum ether (2:1:1), 35°C, 10 min, 77% optical purity for ***1*-56**
2) in Ehter, 35 °C, 10 min, 84% optical purity for ***1*-56**
3) in Ether, -3 to 0 °C, 30 min, 76% optical purity for ***1*-56**

[b]. 1) in Ether, 28 °C, 30min, 100% optical purity for ***1*-58**
2) in Ether, 28 °C, 10 min, 100% optical purity for ***1*-58**
3) in Ether, -8 °C, 30 min, 100% optical purity for ***1*-58**
4) in THF, -8 °C, 20 min, 100% optical purity for ***1*-58**

[c]. 1) in Ether, rt, 10 min, 95% optical purity for product ***1*-57**

Scheme 1.14 The reactions of 1-bromo-1-methyl-2,2-diphenylcyclopropane ***1*-57**.

Similarly, treatment of the two diastereoisomeric cyclopropyl bromides *cis*- and *trans*-***1*-59** with isopropyllithium at 0 ºC in 94:6 pentane:ether for few minutes led to the corresponding organolithium ***1*-60**. The *cis*- or *trans*-***1*-60** was macroscopically

configurationally stable and afforded overall >95% retentive products ***1*-61** on treatment with CO_2 (Scheme 1.15).[23]

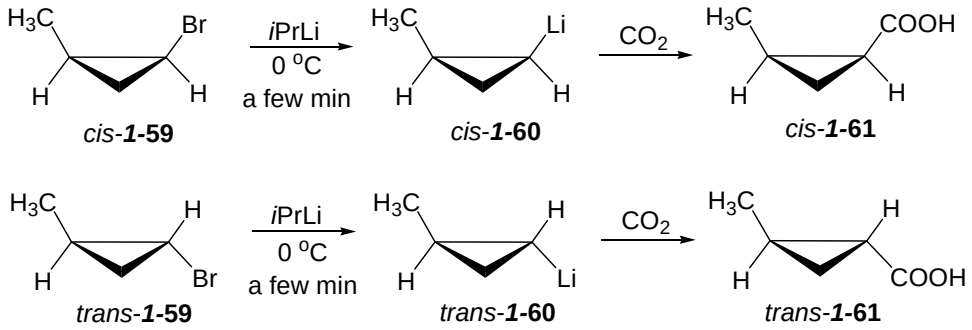

Scheme 1.15 The reaction of *cis*- and *trans*- 1-bromo-2-methylcyclopropane ***1*-59**.

Walborsky and Periasamy demonstrated that a cyclopropyl carbanion with an α-isocyano substituent was configurationally stable at -72 °C in THF for at least 30 min (Scheme 1.16).[74] The 1-isocyano-2,2-diphenylcyclopropane ***1*-62** was deprotonated by treating with LDA in THF at –72 °C, followed by reaction with methyl iodide. The product, 1-isocyano-1-methyl-2,2-diphenylcyclopropane ***1*-63**, had complete retention of configuration. The sodium *t*-butoxide was applied for cation exchange of lithiated ***1*-62**. The corresponding sodiated ***1*-62** was deuterated in MeOD and afforded the retentive product ***1*-64.** This result indicated that the sodiated ***1*-62** was capable of maintaining its configurational stability also.

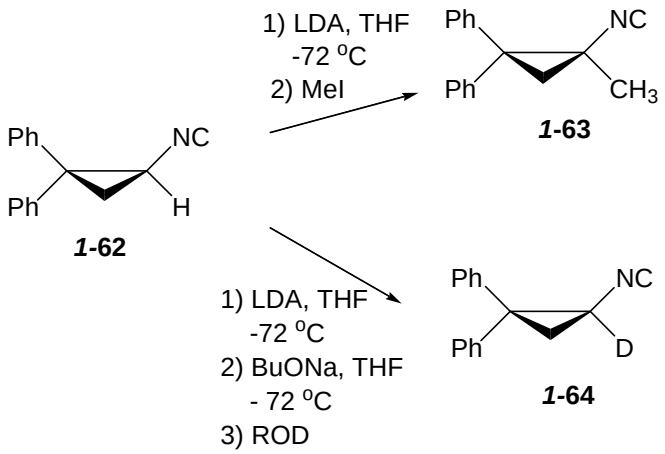

Scheme 1.16 The methylation and deuteration of 1-isocyano-2,2-diphenylcyclopropane ***1*-62**.

In a small ring, racemization requires that the pyramidal carbanion becomes planar or undergo an inversion. The configurational stability of cyclopropyl carbanions is higher than that of analogous carbanion derivatives from saturated carbon acids. Hopkinson et al. provided an early calculation of inversion barriers of isopropyl and cyclopropyl carbanions (7.7 and 20.8 kcal/mol respectively, DZ//3-21G).[75] The hybridization of the carbon and the angle strain in a small ring are factors which affect the energy barrier of the racemization. In the cyclopropane system the hybridization has been reported to be $sp^{2.20}$ for exocyclic bonds and $sp^{4.16}$ for endocyclic bonds.[76] Going to a planar state would require a rehybridization of the ring carbon to sp^2, leading to a more strained intermediate.[77] In the case of α-cyano cyclopropyl carbanion, the cyano group provides a driving force for the planarity of the carbanion though the energy gained by delocalization of the negative charge.[78] Such a delocalization mechanism was not favorable for the isocyano group.

1.6 Configurational stability of organomagnesiums

1.6.1 Formation of organomagnesiums

Victor Grignard found that a compound of general formula RMgX was prepared by the reaction of an alkyl halide and magnesium in Et_2O. The resulting organomagnesium halide, also called a Grignard reagent, reacted with carbonyl compounds to afford the corresponding alcohols.[79] Grignard reagents have proved to be a powerful synthetic tool in the formation of C-C bonds and carbon heteroatom bonds.

At present, the most common method to prepare an organomagnesium halide is the reaction of organic halides with magnesium. However, in 1931, Prévost reported the first example of bromine-magnesium exchange between cinnamyl bromide ***1*-65** and EtMgBr, which furnished cinnamylmagnesium bromide ***1*-66** (Scheme 1.17).[80] Urion also reported the bromine-magnesium exchange of bromocyclohexane ***1*-67** and EtMgBr and the resulting cyclohexylmagnesiumbromide ***1*-68** was formed in 12% yield (Scheme 1.17).[81] Although the halogen-magnesium exchange was observed in the early 1930s, it was not widely used until recently. Through the work of Knochel, it has became a very important mean of preparation of functionalized organomagnesium reagents.[82-85]

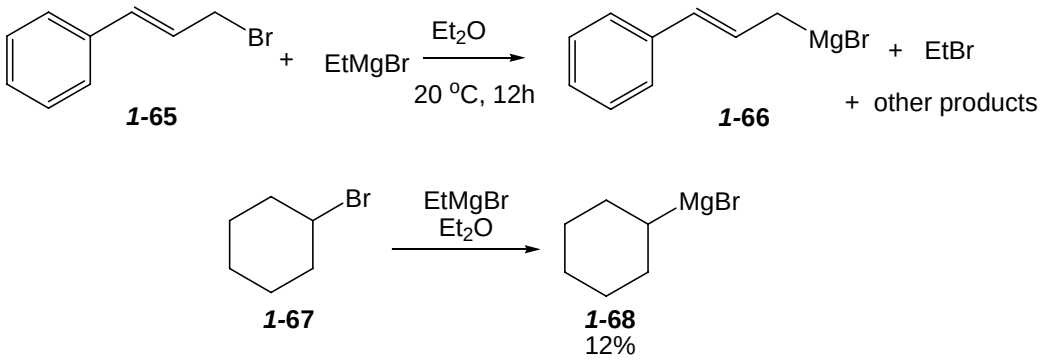

Scheme 1.17 Discovery of halogen-magnesium exchange.

Halogen-magnesium exchange is generalized in Scheme 1.18. Analogous to halogen-lithium exchange, the equilibrium shifts to right when the resulting organomagnesium compound is more stable and less basic than the Grignard reagent used for the reaction. The stability of organomagnesium species can be estimated by that of the corresponding carbanions. The trend of stability of organomagnesium is $sp > sp^2 > sp^3$.

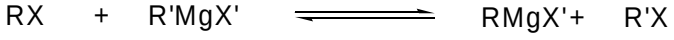

Scheme 1.18 Generation of organomagnesiums *via* halogen-magnesium exchange.

The reactivity of organic halides is dependent on the exchangeable halide atom and the organic substituents of halides. The order of the reactivity of halide atoms is I > Br >> Cl >> F. Although iodides are most reactive, bromides are widely used because of their availability and stability. The use of chlorides is rare. The work of Tamborski and Moore demonstrated that electron-withdrawing substituents were able to accelerate the halogen-magnesium exchange.[86, 87] They found that bromopentafluorobenzene ***1*-69** was easily converted to pentafluorophenylmagnesium bromide ***1*-70** within 1 min at 0 ºC when

EtMgBr was used for the exchange reaction. In contrast, the bromo-magnesium exchange between hexabromobenzene ***1*-71** and EtMgBr required 4h at 0 ºC to furnish pentabromophenylmagnesium bromide ***1*-72**. Interestingly, perfluoroalkyl iodides such as ***1*-73** readily reacted with EtMgBr at -78 ºC to afford the corresponding Grignard reagent ***1*-74,** which was reactive towards carbonyl compounds (Scheme 1.19).[88, 89]

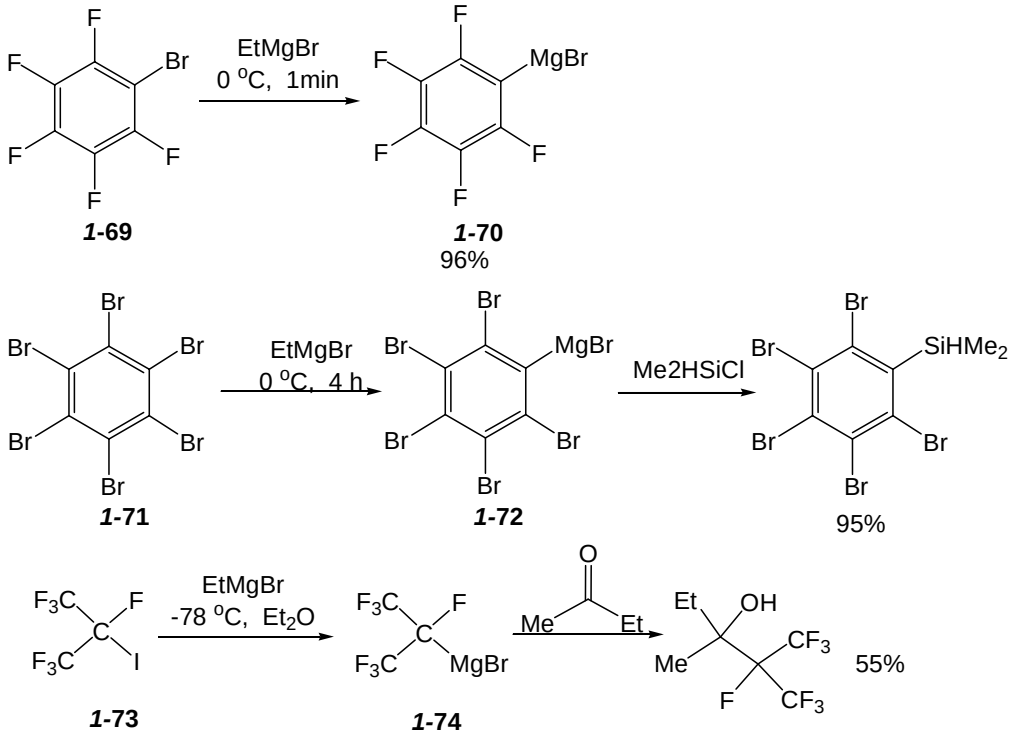

Scheme 1.19 Electron withdrawing groups accelerate the halogen-magnesium exchange.

THF is a common solvent that is used in halogen-magnesium exchange. Mukaiyama et al. and Markó et al studied the effect of solvents on the exchange reaction.[90, 91] The extent rate of exchange is proportional to the solvating power of solvents and increases in the order diethyl ether < diethoxyethane < methoxyethoxyethane < diglyme < tetrahydronfuran < dimethoxyethane.

1.6.2 Mechanism of halogen-magnesium exchange

The halogen-metal exchange reaction has been the focus of considerable mechanistic speculation.[92] However, mechanisms of the halogen/magnesium exchange reaction are far from being settled. A free radical pathway has been proposed for iodine-magnesium exchange.[93-95] A four-center transition state ***1*-75** was proposed by Villiéras.[96] Wittig and Schöllkopf postulated an ate-complex ***1*-76** as the intermediate in halogen-lithium exchange, which involved the attack of organolithiums on the halogen.[97, 98] An ate complex was isolated and characterized in 1986[99] and the other analogous lithium ate complex was detected by NMR in 1999.[100] If carbon-halogen bond formation precedes carbon-metal bond formation, the arrangement ***1*-77** might be the transition state of halogen-metal exchange.[101, 102] The comprehensive picture was shown by Hoffmann (Scheme 1.20).[102, 103] The R^1 and R^2 residues are functional groups which can stabilize the formed ate complex ***1*-76**. When this stabilization leads to the lower energy of ***1*-76** than the starting system in Situation A, the ate complex ***1*-76** can be observed or isolated. In Situation B, the stabilizing effect of the R^1 and R^2 groups are moderate and the complex ***1*-76** might not be observed. When an arrangement is strongly destabilized relative to the starting system, Situation C would prevail. In Situation C, the transition state ***1*-77** might be approximated by the contact ion pair.

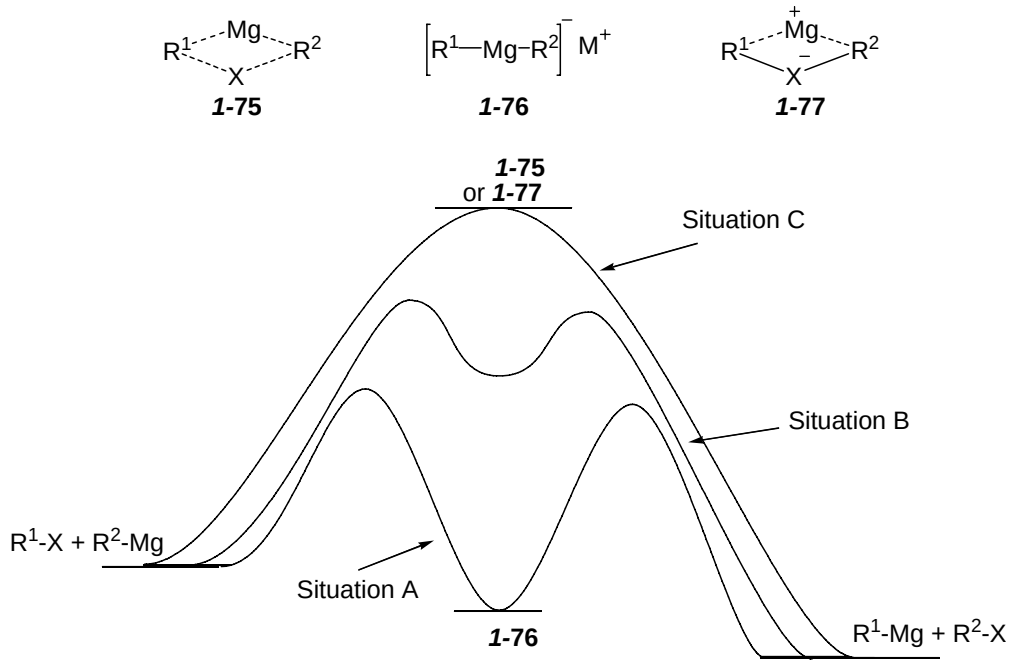

Scheme 1.20 Mechanism of halogen-magnesium exchange reactions.[103] (Reprinted with permission from Müller et al, *Organometallics* **2003**, *22*, 2931. Copyright (2003) American Chemical Society)

Hoffmann reported the first example of the formation of an ate complex intermediate during iodine-magnesium exchange reaction.[104] Treatment of 1,1-diiodoalkane ***1*-78** with *i*PrMgBr, an intense yellow color formed immediately and faded over about two hours. After the yellow color disappeared after 2 hours, the colorless solution was quenched by CH_3OH/CH_3OD, leading to an isotope effect of $k_H/k_D = 1.1$ (Scheme 1.21). The formation of iodoalkane ***1*-81** suggested the existence of Grignard reagent ***1*-80** in the colorless solution. However, quenching of the yellow solution two minutes after mixing of **69** with *i*PrMgBr resulted in an isotope effect of $k_H/k_D = 2.6$ (Scheme 1.16). This suggested that the substrates in the yellow solution were different from that Grignard reagent ***1*-80** in colorless solution. The long-lived ate complex ***1*-79** was proposed to be the source of the yellow color.[103, 105]

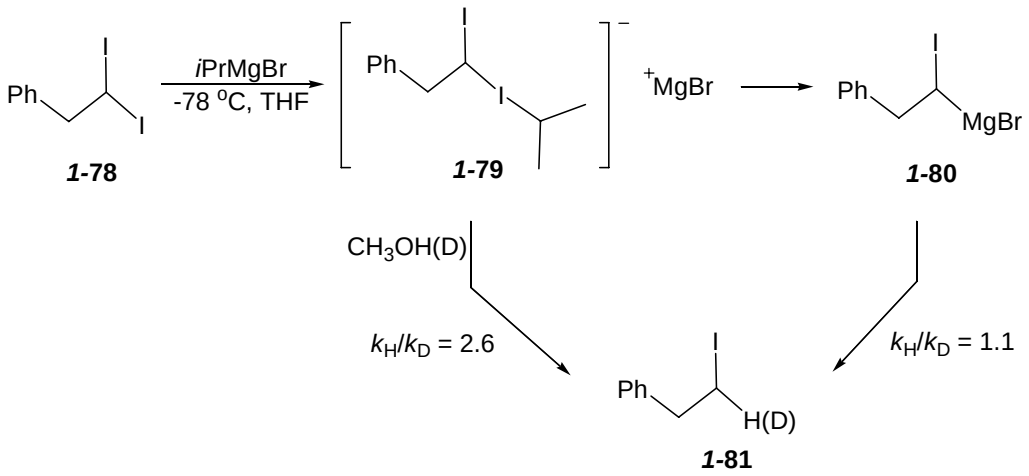

Scheme 1.21 Formation of the ate complex intermediate ***1*-79** *via* the halogen-magnesium exchange.

Further investigation by Hoffmann[102] suggested that the conversion of the ate complex ***1*-79** to the Grignard reagent ***1*-80** was a bimolecular process involving both the anion and an unspecified cationic magnesium species. And this conversion proceeded at a constant rate in numerous experiments in the absence of an additive. Interestingly, addition of 0.1 to 2.0 equiv. of electrophiles to the ate complex ***1*-79** accelerated the decolorization of the solution. The reaction was quenched after 30-120 min decolorization leading to a high yield of iodoalkane ***1*-81**. Electrophiles did not intercept the ate complex ***1*-79** and the Grignard reagent ***1*-80** to afford compounds of the type ***1*-82** under the reaction conditions (Scheme 1.22a). The Grignard reagent ***1*-80** could produce ***1*-82** at higher temperature or long reaction time. The same results from diverse electrophiles in the reaction suggested that the electrophiles served as an initiator for an electron transfer chain process and the ate complex ***1*-79** was converted to Grignard reagent ***1*-80** *via* a SET process (Scheme 1.22b).[102]

a) Reaction of the ate complex ***1*-79** or Grignard ***1*-80** with electrophiles.

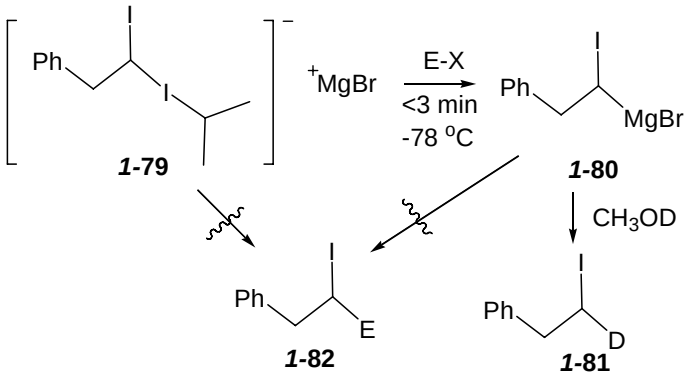

b) Conversion of the ate complex ***1*-79** to Grignard reagent ***1*-80** (& *i*-PrI) *via* SET process.

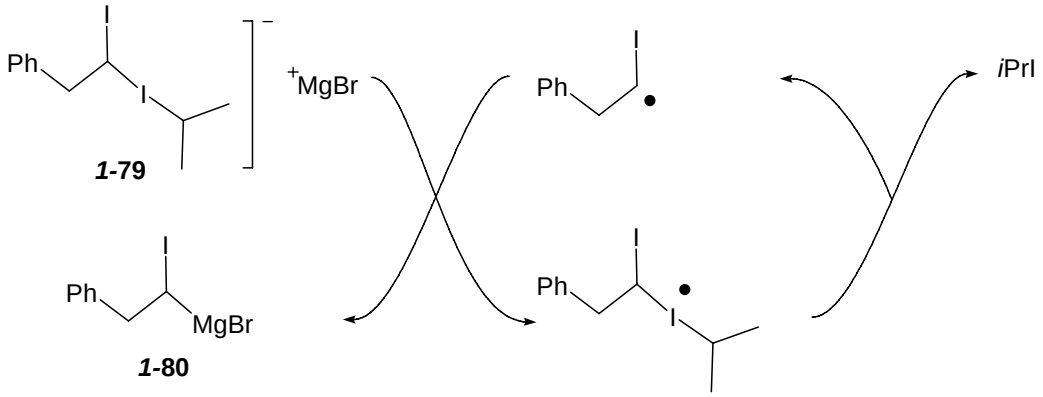

Scheme 1.22 Conversion of the ate complex ***1*-79** to Grignard reagent ***1*-80**.[102] (Reprinted with permission from Hoffmann et al, *Org. Lett.* **2003**, *5*, 313. Copyright (2003) American Chemical Society)

1.6.3 Chiral organomagnesium derivatives

Organomagnesiums with sp^3 hybridization on the Mg-bearing carbon can be prepared from halides and magnesium in ether and normally are reactive, such as EtMgBr, *i*PrMgBr and *i*PrMgCl. However, this method is not suitable to prepare functionalized alkyl magnesium compounds. A number of functionalized alkyl organomagnesium reagents have been reported through halogen-magnesium exchange.[106]

Yoshino and Manabe found that *cis*- or *trans*- β-styrenemagnesium bromides ***1*-84**, which were prepared from the corresponding bromide ***1*-83** and magnesium in THF, maintained their original *cis*- or *trans*- configuration after quenching with D_2O (Scheme 1.23).[107]

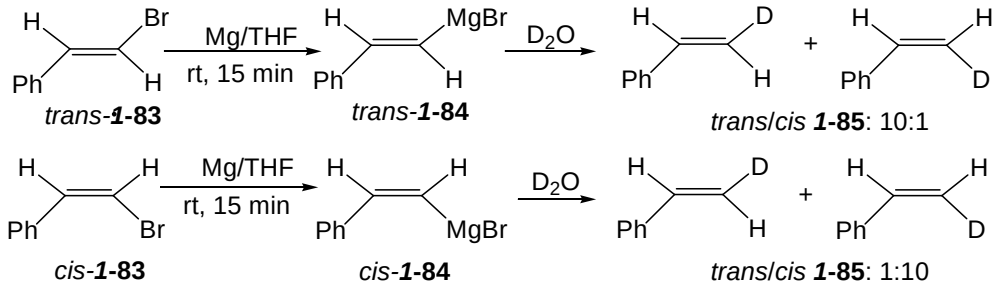

Scheme 1.23 The reaction of *cis*- and *trans*- β-styrenemagnesium bromides ***1*-74**.

Early work by Whitesides demonstrated that primary alkyl magnesium reagents underwent rapid inversion of configuration.[108, 109] Meanwhile, Whitesides' studies also suggested that the barrier to inversion of configuration was higher in secondary than in primary Grignard reagents.[109] Walborsky reported the first chiral Grignard reagent. The reaction of (+)-(*S*)-1-bromo-1-methyl-2,2- diphenylcyclopropane ***1*-86** with magnesium led to the formation of a chiral Grignard reagent ***1*-87** and after the carbonation the resulting cyclopropanecarboxylic acid ***1*-58** and cyclopropane ***1*-56** were optically active with predominant retention of configuration (Scheme 1.24a).[110] Walborsky demonstrated that when the cyclopropylmagnesium reagent ***1*-89** was obtained from the reaction of $MgBr_2$ and the corresponding configurationally stable lithium reagent ***1*-88**, the carbonation of ***1*-89** yielded optically pure ***1*-58**. This result suggested that the cyclopropylmagnesium reagent ***1*-89** was configurationally stable on the macroscopic

timescale and that partial racemization occurred in the Grignard formation step.[110]

a) Reaction of Grignard reagent ***1*-87**

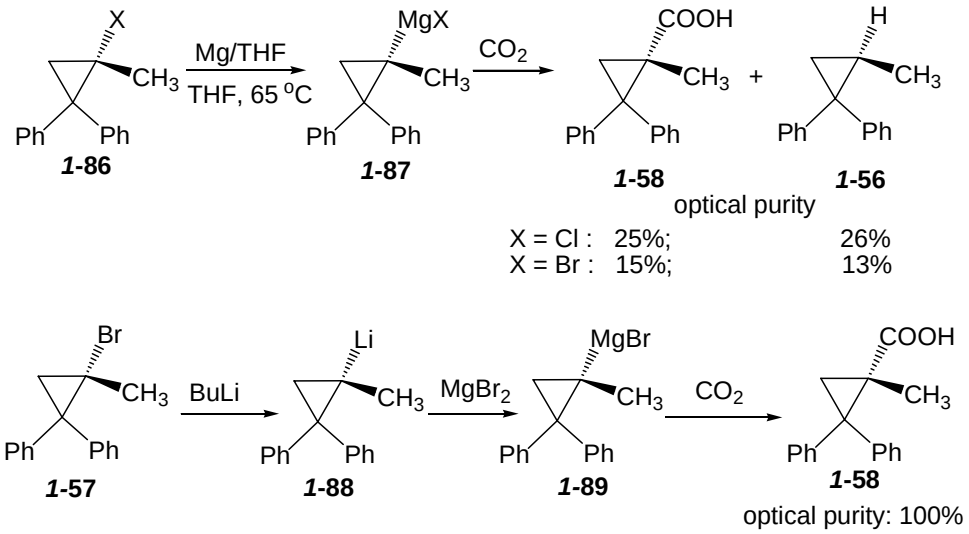

b) Reaction of Grignard reagent ***1*-90**

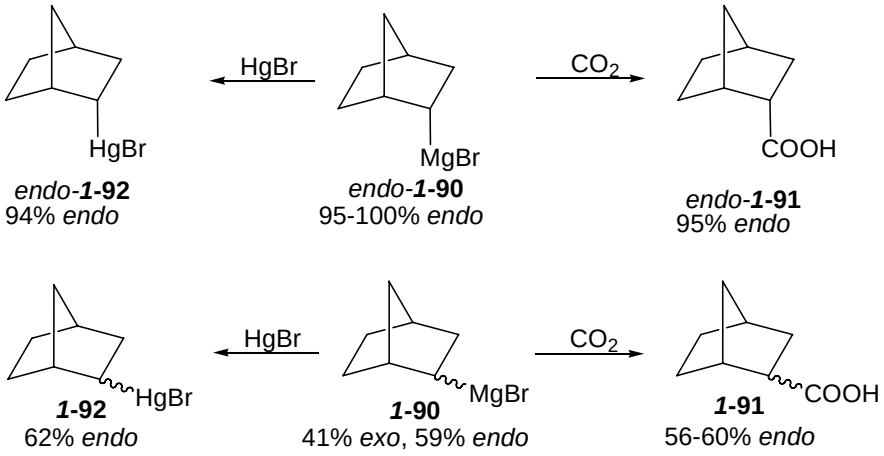

Scheme 1.24 Configurational stability of alkyl organomagnesium reagent ***1*-87** and ***1*-90**. (Reprinted with permission from Jensen et al, *J. Am. Soc. Chem.* **1966**, *88*, 3437. Copyright (1966) American Chemical Society)

The *endo*-norbornyl Grignard reagent ***1*-90** was also demonstrated to be macroscopic configurationally stable (Scheme 1.24b).[111] Jensen reported that the reaction of *endo*-norbornylmagnesium bromide (95-100%) with CO_2 and mercuric bromide afforded respectively 95% *endo* acid ***1*-91** and 94% *endo*-norbornylmercuric bromide ***1*-92**

(Scheme 1.24b). When the mixture of *exo*- and *endo*- ***1*-90** with (*exo*- 41%, *endo*- 59%) were used, the reaction furnished 56-60% *endo*-***1*-91** and 62% *endo*-***1*-92**. It indicated that both isomers underwent substitution with retention of configuration.[111]

Hoffmann found an iodine-magnesium exchange occurred between 1,1-diiodoalkanes ***1*-78** and a chiral Grignard reagent ***1*-93** in THF at -78 ºC, leading to two diastereomeric α-iodoalkylmagnesium reagents ***1*-94a** and ***1*-94b** (Scheme 1.25).[112] After trapping by benzaldehyde/dimethylaluminum chloride, the reaction provided the enantiomerically enriched iodohydrins ***1*-95** (53 %ee) plus some of epoxide ***1*-96** (50 %ee). Meanwhile, a modified Hoffmann test demonstrated that the enantiomeric enrichment of the resulting iodohydrins ***1*-95** was variable with changes of the amount of benzaldehyde. The high enantiomeric excess (68% ee) of ***1*-95** was observed with low conversion (17% yield) when a deficit benzaldehyde was used. These observations proved an important fact that α-iodoalkylmagnesium reagent ***1*-94** was microscopically configurational stable. α-Bromoalkylmagnesium reagent ***1*-98** was prepared from 1-bromo-1-iodoalkanes ***1*-97** and *i*PrMgCl, followed by reaction with benzaldehyde/dimethylaluminum chloride. The product ***1*-99** possessed the same degree of enantiomeric enrichment as the starting ***1*-97**. Thus, α-bromoalkylmagnesium reagent ***1*-98** was macroscopically configurational stable at -78 °C.[112]

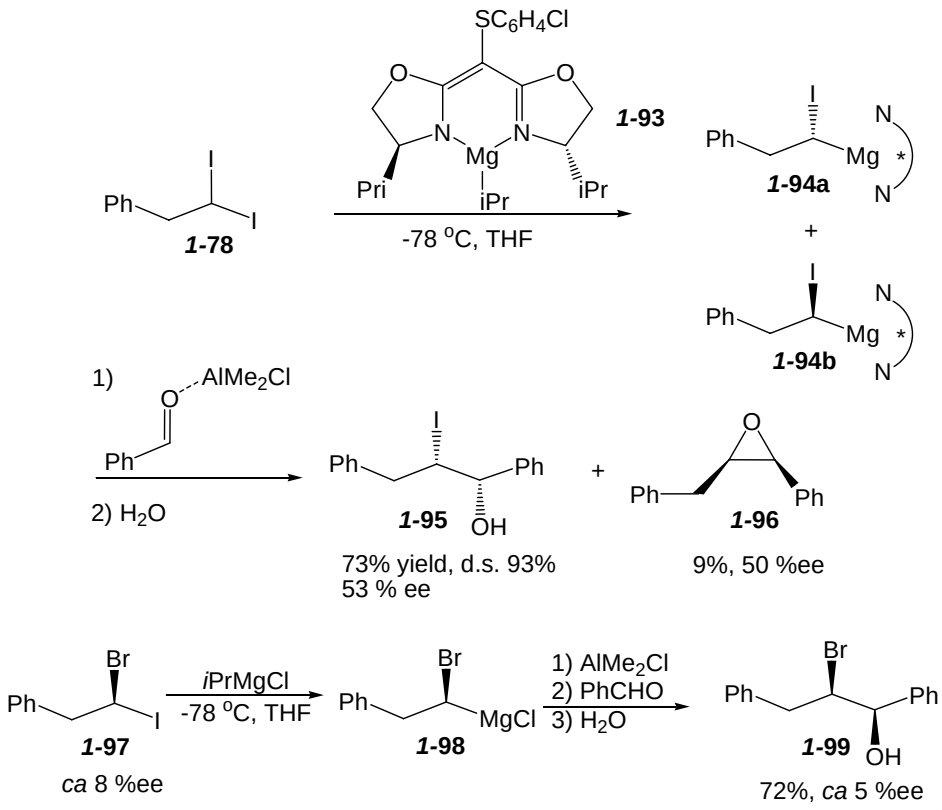

Scheme 1.25 The reaction of 1,1-diiodoalkanes ***1*-78** and a chiral Grignard reagent ***1*-93**.

Hoffmann reported the generation of enantiomerically pure secondary Grignard reagents by a sulfoxide-magnesium exchange reaction on diastereomerically pure α-chloro-alkyl sulfoxide ***1*-100** (Scheme 1.21).[113-115] When 1.3 equivalent EtMgBr was used for the exchange, the chiral Grignard reagent ***1*-101** was produced which was trapped with benzaldehyde/dimethylaluminium chloride, followed by conversion of the chlorohydrins to the epoxide ***1*-104**. The enantiomeric purity of the *cis*-epoxide ***1*-104** was shown to be 93 ± 3% (Scheme 1.26) which suggested that the Grignard reagent ***1*-101** had at least 93 ± 3% ee. The configuration of the chiral Grignard reagent ***1*-101** was stable at -78 ºC and was racemized by the influence of external halide ions,[115] such as magnesium bromide, most likely in a S_N2-type halide exchange process.[116, 117]

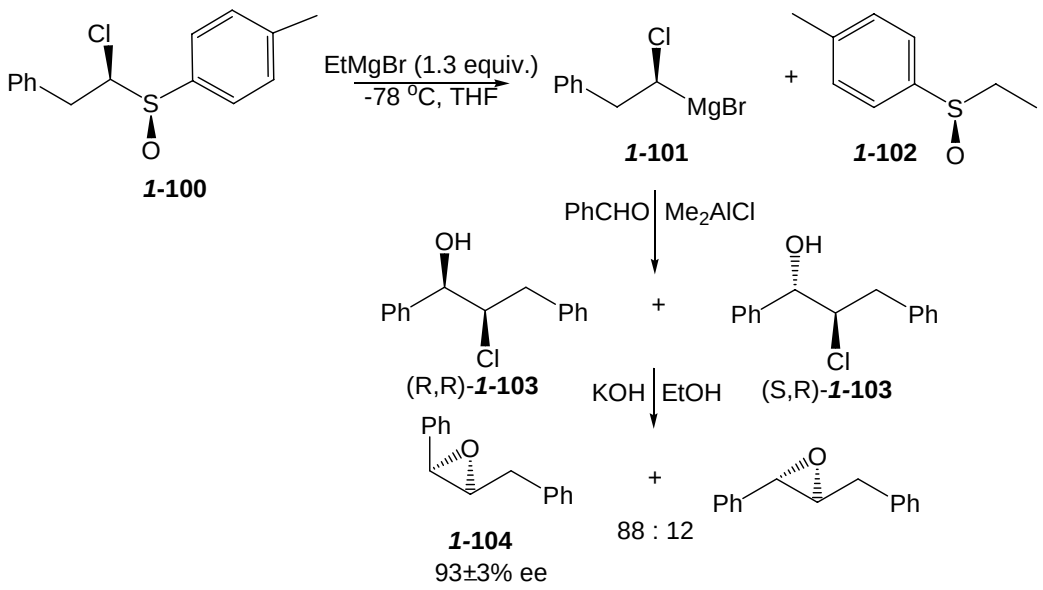

Scheme 1.26 Formation of the configurationally stable secondary alkyl organomagnesium ***1*-101**

The treatment of compound ***1*-105** with more excess EtMgCl (5-10 equiv.) furnished a Grignard reagent ***1*-106** (Scheme 1.27).[114] The thioamide product ***1*-107** (93% ee) was obtained when the Grignard reagent ***1*-106** was treated with phenylisothiocyanate. Hoffmann proposed that the addition of ***1*-106** to phenylisothicyanate proceeded with retention of configuration. Consequently, the enantiomeric excess of ***1*-106** was around 93%. The secondary Grignard reagent ***1*-106** appeared to be configurationally stable at -78 ºC. Warming of the solution of ***1*-106** to -10 ºC led to slow racemization in a first order process with a half life of about 5 hours.[114]

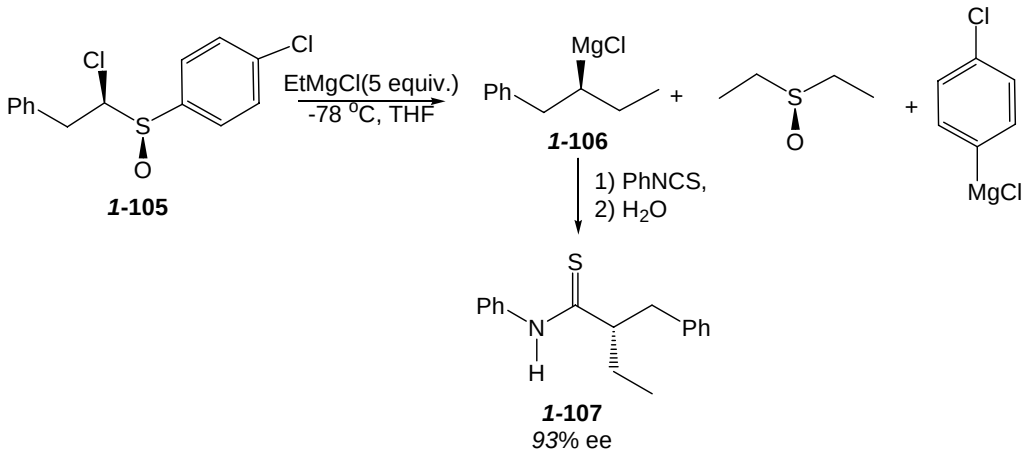

Scheme 1.27 Formation of the configurationally stable secondary alkyl organomagnesium ***1*-106**.

1.6.4 Application of chiral alkyl magnesium reagents: a probe for concerted or stepwise SET pathway.

The reaction of Grignard reagents with electrophiles could proceed by a polar concerted route, which should be characterized by retention of configuration at the stereogenic center if the Grignard reagents were chiral. The reaction could also proceed in a stepwise addition, initiated by SET-process followed by bond formation with a radical pair.[118] The SET-process should lead to racemic products because inversion barriers of alkyl radicals are extremely low.[119] Therefore, the configurationally stable chiral organometallics provide an opportunity to study the mechanism of electrophilic substitution.

The secondary chiral Grignard reagent ***1*-106** was configurationally stable at -78 ºC and was racemized with $t_{1/2}$ = 5 h at -10 ºC. It reacted with various electrophiles and the stereochemical outcomes were reported by Hoffmann.[113, 114, 120-122] The addition of ***1*-106** to PhNCS, CO_2 provided the product ***1*-108** and ***1*-109** with the same level of

enantiomeric purity, which represented the purity of ***1*-106** (entries 1 and 2, Table 1.3).[114, 120] The amination of ***1*-106** was found to produce the acetamide ***1*-110** with full retention of configuration (entry 3, Table 1.3).[122] The retentive products reflected a polar concerted pathway. Addition of ***1*-106** to benzaldehyde generated two diastereomeric adducts (D1 and D2) and the formation of major diastereomer proceeded without loss in enantiomeric purity (***1*-111**, D1: 88 %ee, entry 4, Table 1.3). The reaction of ***1*-106** and benzophenone, which had low reduction potential, led to extensive racemization (***1*-112**, 12 %ee, entry 5, Table 1.3).[120] When ***1*-106** was treated with allylic halides at low temperature (-90 ºC to -60 ºC), the allylic chloride and allylic bromide led to partial retentive products ***1*-113** (entries 6 and 7, Table 1.3) but the allylic iodide produced racemic ***1*-113** (entry 8, Table 1.3).[120] The partial racemization observed in ***1*-112** (entry 5, Table 1.3)and ***1*-113** (entry 8, Table 1.3) was caused by a competition between a polar concerted addition and a SET-process or between a polar S_N2-reaction and a SET-process.[120, 123] The SET process was accelerated with an electron withdrawing group. A racemic product, ***1*-114**, was obtained from ethyl α-bromomethylacrylate (entry 9 Table 1.3), compared to 57% ee of ***1*-113** from allylic bromide (entry 7, Table 1.3).

Table 1.3 The reaction of the chiral secondary organomagnesium ***1*-106** with various electrophiles.

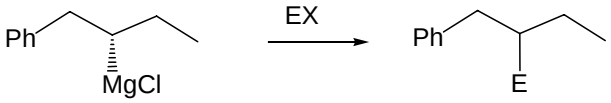

***1*-106**

entry	EX	product	configuration	yield (%)	%ee
1	PhNCS	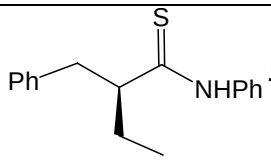 ***1*-108**	S	56	93
2	CO_2	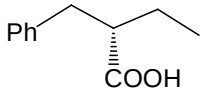 ***1*-109**	S	80	92
3	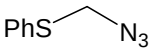	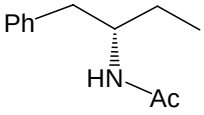 ***1*-110**	S	82	92
4	PhCHO	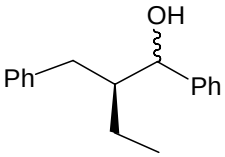 ***1*-111**	S	42	D1:88 D2:84
5	Ph_2CO	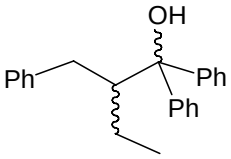 ***1*-112**	-	85	12
6	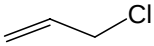	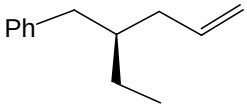 ***1*-113**	S	90	70
7	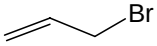	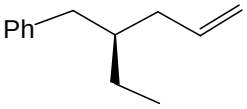 ***1*-113**	S	90	57
8	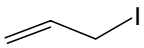	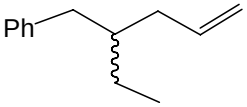 ***1*-113**	-	90	0
9	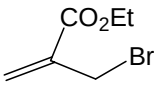	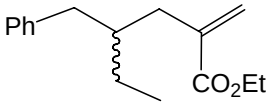 ***1*-114**	-	70	0

Compound ***1*-106** was also used to probe the Kumad-Corrie coupling of Grignard reagents with vinylic halides (Table 1.4).[121] The coupling reaction furnished the product

***1*-115** and the hydride-elimination product ***1*-116**. High enantiomeric purity of the coupling product ***1*-115** for Ni(0)- and Pd(0) mediated reaction suggested the full retention of configuration during the transmetallation. Thus the transmetallation of ***1*-106** to Ni(II) or Pd(II) proceeded via a concerted S_E2-ret process.[124] However, when the coupling reaction was catalyzed by Fe and Co, the partially racemized products were observed because of an SET process in the transmetallation step (Scheme 1.28).

Table 1.4 Kumada-type couplings of the Grignard reagent ***1*-106** with vinyl bromide.

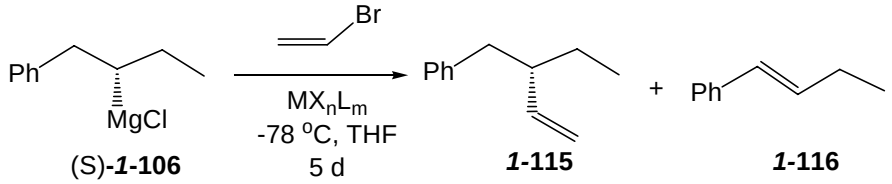

entry	catalyst	*1*-115/*1*-116 ratio	*1*-115: yield (%)	% ee
1	$NiCl_2$(dppf)	95:5	60	88
2	$NiCl_2$[(-)diop]	89:11	80	89
3	$PdCl_2$(dppf)	95:5	58	88
4	$PdCl_2$[(-)diop]	86:14	55	89
5	$Fe(acac)_3$	>95:5	35	53
6	$Co(acac)_2$	>95:5	30	55

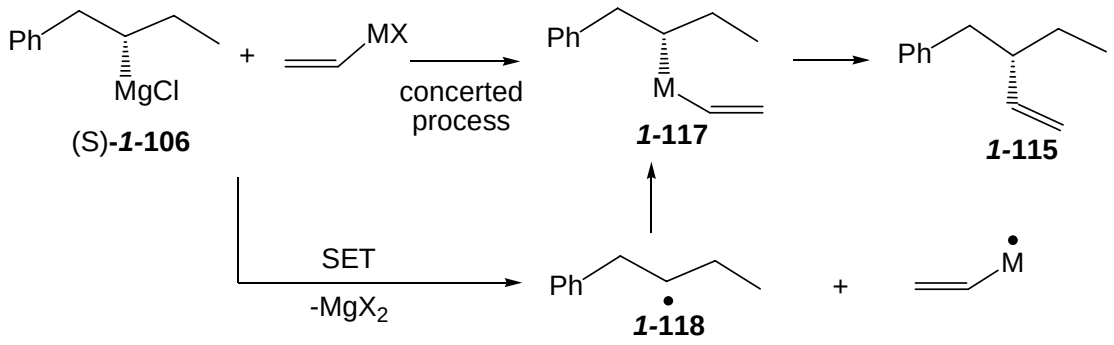

Scheme 1.28 Transmetallation step of ***1*-106** *via* a concerted process and a SET process. ([Hölzer et al, *Chem. Comm.* **2003**, 732] – Reproduced by permission of the Royal Society of Chemistry)

1.7 Proposed direction of research

The term configurational stability of organometallics is associated with a timescale, a temperature, and a solvent. A range of macroscopically or microscopically configurationally stable organolithiums present a heteroatom adjacent to a lithium-bearing carbon atom, such as α-oxy, α-amino, and α-thio. The dipole-stabilization highly influences the configurational stability of α-heteroatom substituted organolithiums. However, for organolithium species lacking this hetero-substituent, the factors underlying configurational stability are not well understood. We devised a strategy to impart configurational stability by intramolecular coordination that will be discussed in the following chapter.

Chapter 2 Evaluation of the effect of chelating groups on configurational stability of 2,2-disubstitutedcyclopropylnitriles: Deprotonation

2.1 Introduction

In Chapter 1, we discussed the concept of macroscopically configurational stability and the usefulness of this property in organic synthesis. The stereospecificity of electrophilic substitution is directly related to the configurational stability of chiral organolithium intermediates. The presence of an α-heteroatom, such as α-oxy, α-amino, or α-thio group, can provide configurational stability on the macroscopic timescale, allowing stereospecific substitution of enantiopure organolithiums. However, for organolithium species lacking this hetero-substituent, the factors underlying configurational stability are not well understood. This chapter describes our attempts to generate configurationally stable metallated cyclopropylnitriles by deprotonation. We will evaluate the influence of chelating groups on configurational stability of metalated cyclopropylnitriles in this chapter.

We chose to examine cyclopropylnitriles for several reactions. Firstly, the cyclopropane unit is important in natural products and medicinal chemistry. A cyclopropane fragment was found in natural oxidized fatty acid metabolites of Marine organisms, such as constanolactones,[125] solandelactones,[126] and halicho neohalicholactones.[127] Recently, Kirchhausen and Pelish et al. found that a natural product-like small molecule, secramine A bearing a cyclopropyl ring, inhibited membrane

traffic out of the Golgi apparatus.[128] Secondly, metalated nitriles are powerful and useful nucleophiles in organic synthesis.[5, 129, 130] Arseniyadis has given an excellent review on the application of metalated nitriles in synthesis.[129] Metalated nitriles would prove more useful if they could be generated as enantiopure reactive intermediates that possess configurational stability on the macroscopic timescale. However, no macroscopically configurationally stable metalated nitriles are known. Walborsky established microscopically configurational stability for a sodiated cyclopropylnitrile (Scheme 2.1). Deuteration of 2,2-diphenylcyclopropylnitrile ***2*-1** gave a highly retentive product at 50 °C (reaction a, Scheme 2.1).[78] In contrast, its acyclic analogue, 2-methyl-3,3-diphenylpropionitrile ***2*-3**, led to a racemic deuterio-product under the same reaction conditions (reaction b, Scheme 2.1).[78]

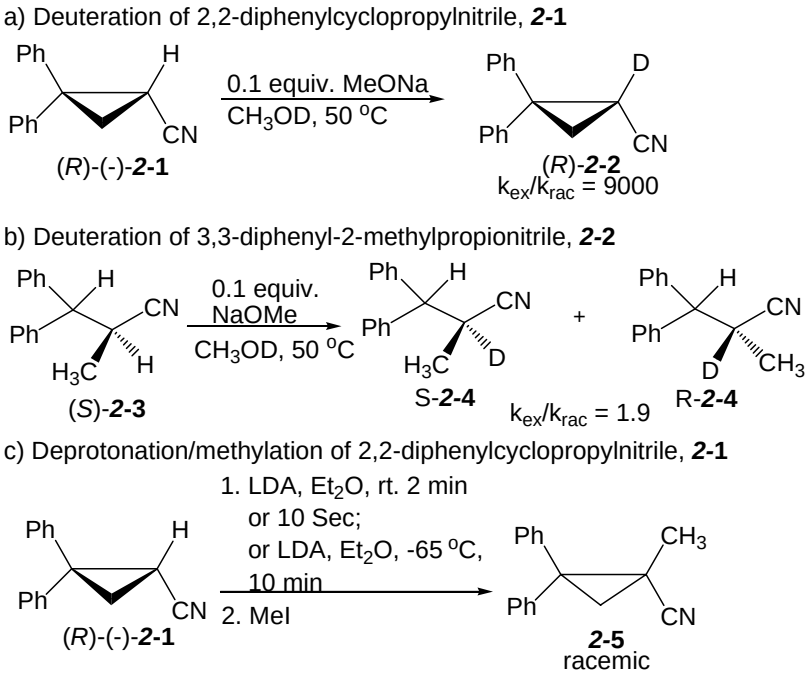

Scheme 2.1 Walborsky's studies on 2,2-diphenylcyclopropylnitrile (*R*)-(-)-***2*-1**: Deuteration and methylation.

Although the deuteration of *lithio*-2,2-diphenylcyclopropyl nitrile exhibited microscopically configurational stability, a sequential deprotonation/trapping with MeI at -65 °C gave a racemic product (reaction c, Scheme 2.1).[70] We envisioned that *lithio*-cyclopropylnitriles (*lithio*-***2***-**6** ~ ***2***-**8**, Figure 2.1) bearing chelating groups might exhibit configurational stability on the macroscopic timescale. The designed cyclopropylnitriles (***2***-**6** ~ ***2***-**8**) possess a sole stereogenic center at C1. Thus, at the same reaction condition, any differences of enantiomeric purity of alkylated products could be attributed to the chelating groups.

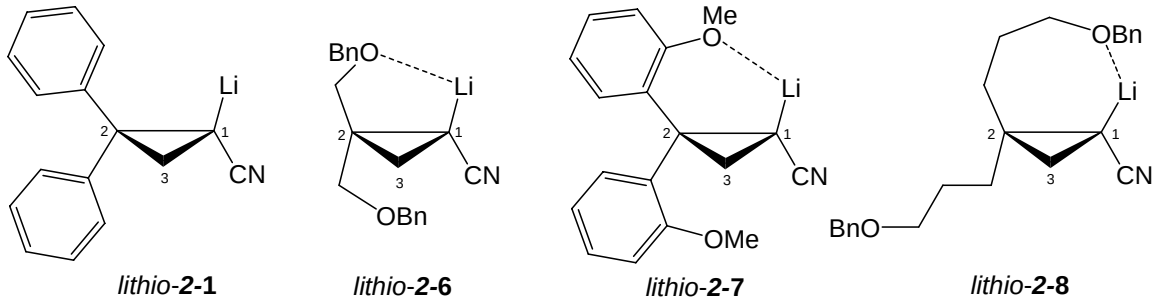

lithio-***2***-**1** *lithio*-***2***-**6** *lithio*-***2***-**7** *lithio*-***2***-**8**

Figure 2.1 Lithiated 2,2-diphenylcyclopropylnitrile ***2***-**1**, and designed lithiated cyclopropylnitriles (***2***-**6** ~ ***2***-**8**) bearing chelating groups. (Bn is benzyl group)

In this chapter, we discuss the synthesis of 2,2-disubstituted cyclopropylnitriles *via* Cu(I) triflate-catalyzed cyclopropanation of 1,1-disubstituted alkenes by α-diazoesters. Significant levels of asymmetric induction were achieved using the bis(oxazoline) ligand ***2***-**9** (Figure 2.2). H-D Exchange and deprotonation/alkylation experiments of 2,2-disubstituted cyclopropylnitriles were performed to evaluate the chelating effect. The chapter closes with computational studies of potential racemization pathways *via* the "conducted tour" mechanism.

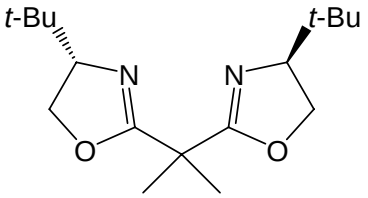

***2*-9**

Figure 2.2 Structure of ***2*-9**, 2,2-isopropylidenebis[(4*S*)-4-*tert*-butyl-2-oxazoline]. ((*S,S*)-BOX).

2.2 Synthesis of 2,2-disubstituted cyclopropylnitriles

The cyclopropanation of olefins using a transition metal-catalyzed reaction of diazoalkenes has been extensively investigated.[131, 132] The most useful diazo reagents for intermolecular cyclopropanation reactions are α-diazoester and α-diazo reagents containing one electron withdrawing group.[133, 134] The α-diazoester decomposes and cyclopropanates alkenes in the presence of metal catalysts. The mechanism of the transition metal-catalyzed decomposition of α-diazocarbonyl compounds is believed to initially proceed *via* the formation of a metal carbene complex.[135] It has been demonstrated that Cu(I) salts are the catalytically active species in the decomposition of α-diazoesters,[136, 137] and copper-based catalysts effectively produce the *trans* isomer in the reaction of α-diazoester with mono-substituted alkenes. Evans reported that the copper (I) complex of bis(oxazoline) achieved high enantioselectivities and diastereoselectivities in the cyclopropanation reaction with mono- and 1,1-disubstituted alkenes.[138, 139] We synthesized enantiomerically enriched ethyl 2,2-disubstituted cyclopropylcarboxylate using ethyl diazoacetate and appropriate 1,1-disubstituted ethene in the presence of copper (I) triflate and the bis(oxazoline) ligand ***2*-9** (Figure 2.2).

2.2.1 Synthesis of 1,1-disubstituted ethene

Compound ***2*-11**, 1,3-bisbenzyloxy-2-methylidenepropane, was prepared from ***2*-10** in 97% yield (Scheme 2.2).[140]

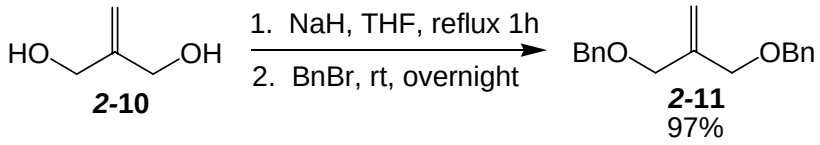

***2*-10** ***2*-11** 97%

Scheme 2.2 Synthesis of 1,3-bisbenzyloxy-2-methylidenepropane ***2*-11**.

To prepare 1,1-bis(2-methoxyphenyl)ethene ***2*-14**, the methoxy benzene was treated with *n*-butyl lithium and ethyl acetate. The resulting alcohol ***2*-13** was eliminated in acetic anhydride to give the compound ***2*-14** in 53% yield (Scheme 2.3).[141]

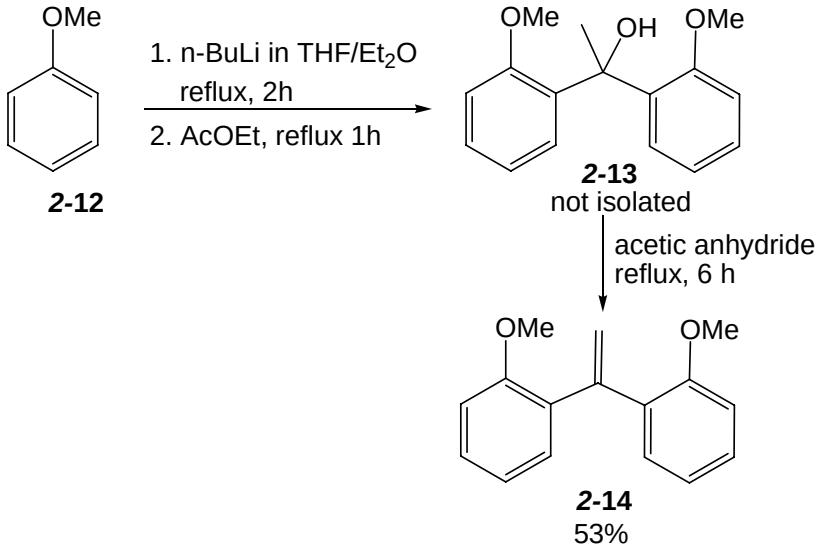

***2*-12** ***2*-13** not isolated ***2*-14** 53%

Scheme 2.3 Synthesis of 1,1-bis(2-methoxyphenyl)ethene ***2*-14**.

Diethyl 4-oxopimelate ***2*-16** was prepared from a mixture of furylacrylic acid ***2*-15** and thionyl chloride.[142] The diethyl 4-methylidenepimelate ***2*-17** was synthesized by the reaction of ***2*-16** with $CH_2Br_2/Zn/TiCl_4$ in 59% yield.[143] Treatment of ***2*-17** with $LiAlH_4$

afforded 4-methylideneheptane-1,7-diol ***2*-18** in 60% yield as shown in Scheme 2.4. The 1,7-bisbenzyloxy-4-methylideneheptane ***2*-19** was obtained similarly to the preparation of ***2*-11**.

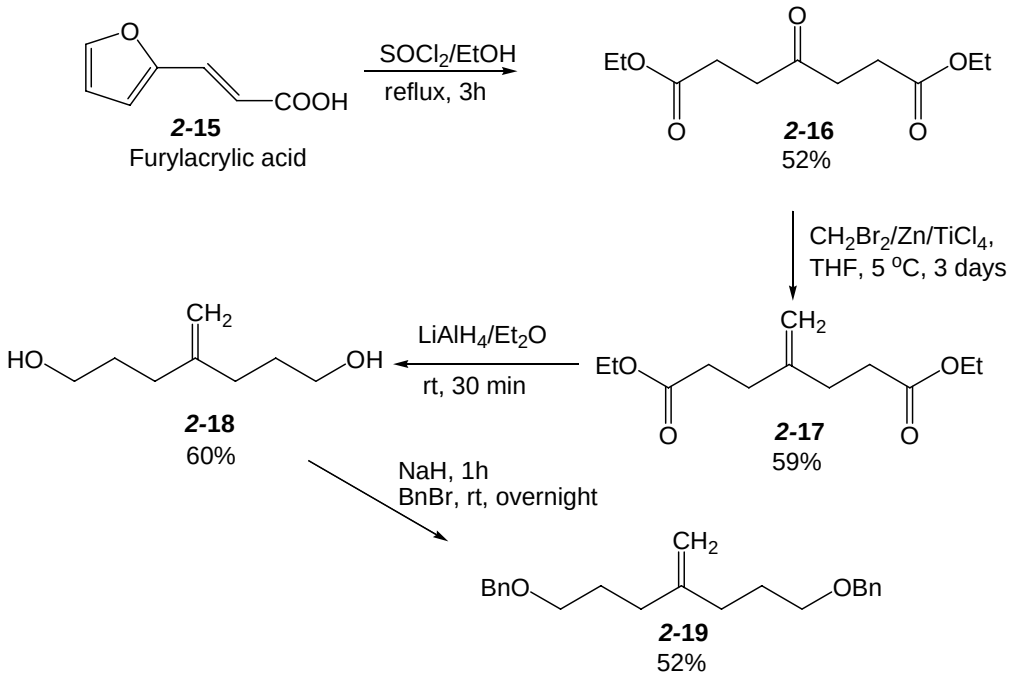

Scheme 2.4 Synthesis of 1,7-bisbenzyloxy-4-methylideneheptane ***2*-19**.

2.2.2 Synthesis of 2,2-disubstituted cyclopropylnitriles

The cyclopropanation reaction of 1,1-disubstituted ethenes and ethyl diazoacetate successfully afforded enantiomerically enriched ethyl cyclopropylcarboxylates in a respectable 56-81% yield in the presence of copper(I) triflate and the bidentate ligand ***2*-9** (BOX) (Scheme 2.5). The enantiomeric excesses for these compounds ranged from 46% to 92%, which were determined by chiral stationary phase HPLC. Unfortunately, we did not get separation of ***2*-21a** using OD and AD chiral columns.

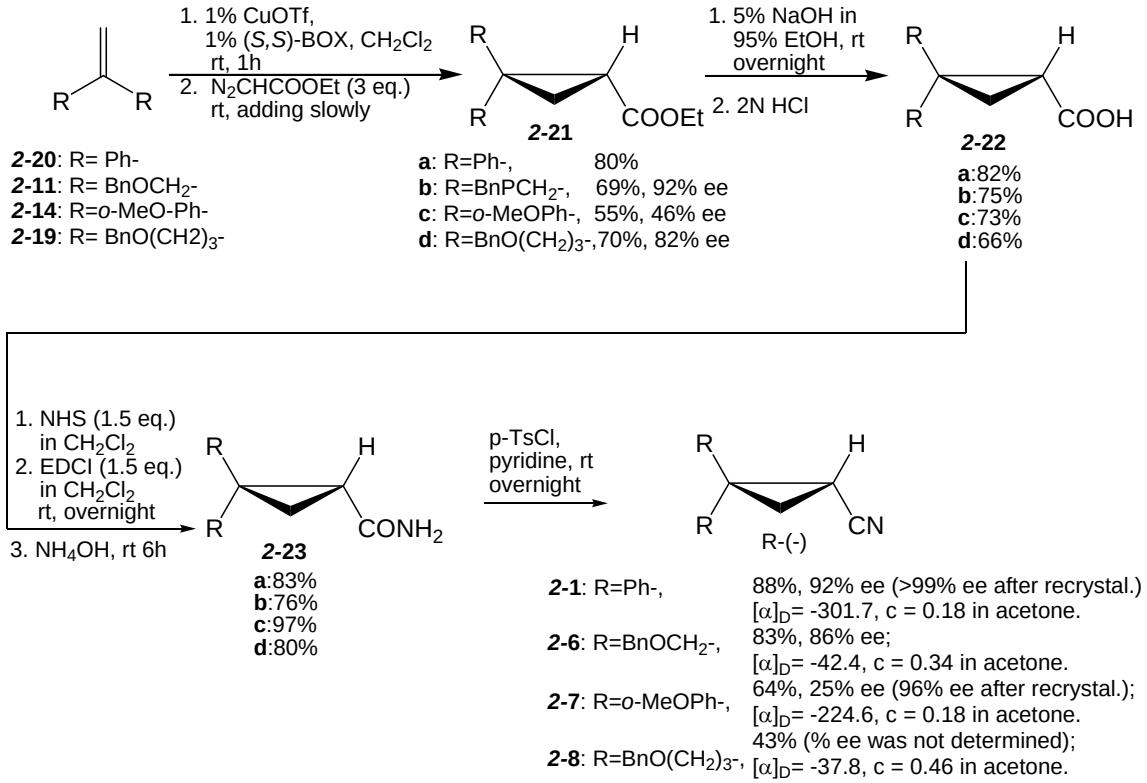

Scheme 2.5 Synthesis of 2,2-disubstituted cyclopropylnitriles ***2*-1** and ***2*-6** ~ ***2*-8**.

After the hydrolysis of ethyl cyclopropylcarboxylate ***2*-21** yielded the corresponding cyclopropylcarboxylic acid ***2*-22**, compound ***2*-22** was converted to amide ***2*-23** in 76-97% yield by treatment of NHS, EDCI and NH_4OH. The reaction of amide ***2*-23** and *p*-TsCl in pyridine afforded final cyclopropylnitriles (***2*-1**, ***2*-6** ~ ***2*-8**) in 43-88% yield. The enantiomeric excess for cyclopropylnitriles (***2*-1**, ***2*-6** ~ ***2*-7**) before recrystallization ranged from 25% to 92% (HPLC). However, we failed to separate the enantiomers of ***2*-8** using chiral stationary HPLC columns (AD, OD, AD-H and OD-H). Recrystallization of ***2*-1** and ***2*-7** successfully gave the enantiomerically enriched compounds with >99% and 96% of enantiomeric excess respectively. All four compounds were levorotatory. Walborsky reported (-)-***2*-1** (-307 ± 6 in acetone) was (*R*)- configured.[70, 78] Furthermore, we obtained

the X-ray structure for (-)-***2*-7**, which also showed the *R* configuration.

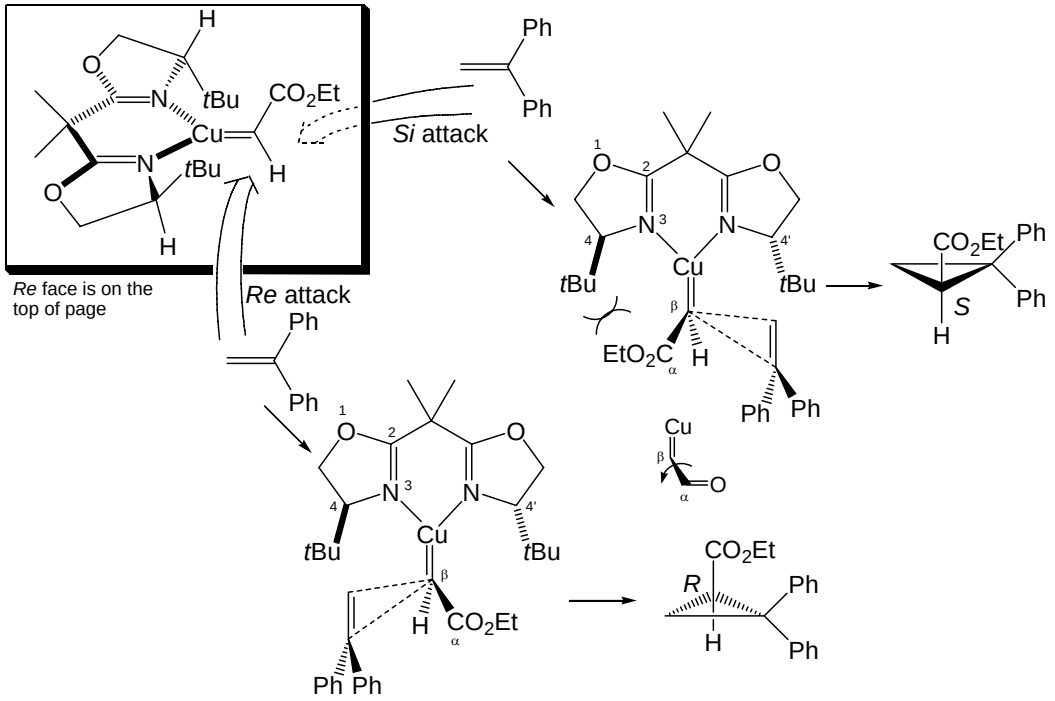

Scheme 2.6 Cyclopropanation: Olefin approach *Re* and *Si* face of the catalyst-carbene complex.

The *R* configuration originated from the cyclopropanation step. The stereochemical course of a chiral (*S,S*) bis(oxazoline) copper(I)-catalyzed cyclopropanation has been rationalized by Salvatella and Garacía using DFT calculations.[144] The olefin molecule approached the two alternative *Re* and *Si* faces of the plane defined by the Cu=C-C arrangement, leading to changes of the dihedral angle Cu-C_β-C_α-O. Salvatella and Garacía indicated that the attack of propene on the *Si* face of the catalyst-carbene complex resulted in a steric interaction between the COOEt group and the *t*-Bu group at C4, leading to the preference of *Re* face attack. In our case, 1,1-disubstituted ethene also preferred to approach the copper-carbene complex from its *Re* face, and resulted in the predominance of the *R* configuration (Scheme 2.6).

2.3 Deuteration of 2,2-disubstituted cyclopropylnitriles.

Walborsky investigated the rate of H-D exchange and racemization of 2,2-diphenylcyclopropylnitrile, (*R*)-(-)-***2*-1**. He concluded the retentive deuteration of (*R*)-(-)-***2*-1** based on a large ratio of the rate constants of the exchange and the racemization (k_{ex}/k_{rac} = 9000) (Scheme 2.1).[78] We re-studied the H-D exchange on enantiomerically enriched 2,2-disubstituted cyclopropylnitrile, and determined the enantiomeric excesses of deuterated products by chiral stationary phase HPLC.

Table 2.1 Deuteration of 2,2-disubstituted cyclopropylnitriles by NaOMe/MeOD at 50 ºC.

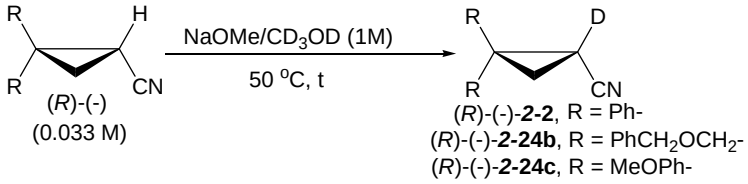

entry	R-	starting material	% ee of starting material	product	t (day)	% yield	% deut.[a]	% ee[b]
1	Ph-	(*R*)-(-)-***2*-1**	>99	***2*-2**	3	97	>99	>99
2	$PhCH_2OCH_2$-	(*R*)-(-)-***2*-6**	86	***2*-24b**	1	70	>99	81
3	*o*-CH_3OPh-	(*R*)-(-)-***2*-7**	96	***2*-24c**	8	87	56	94

[a] Determined by ^1H NMR

[b] Determined by chiral stationary phase HPLC

It was shown that enantioselective deuteration occurred in good yield (70-97%) and with little racemization at 50° C to give deuterated products ***2*-2** and ***2*-24b~c** (Table 2.1). Retentive deuteration was established based on chiral stationary phase HPLC in comparison to the protio starting material. Even though the deuteration reaction of (*R*)-(-)-***2*-7** required longer reaction time than other two compounds and only achieved

56% deuteration, high enantiomeric excess was still obtained for ***2*-24c** (entry 3, Table 2.1). The reason for the lower reactivity of (*R*)-(-)-***2*-7** towards deprotonation is currently unknown. This result indicates that the presence of chelating groups does not interfere with the retentive deuteration in CH_3ONa/CH_3OD. Walborsky proposed that the high degree of retentive configuration in the cyclopropyl nitrile was due to the hydrogen-bonding effect of the solvent and the ring constraint effects.[78, 145] The weaker hydrogen-bonded carbanion complex was less constrained and more able to invert or to become free and planar.[78] We attribute it simply to fast capture of a pyramidalized carbanion.

Table 2.2 Deuteration of (*R*)-(-)-***2*-1** by different bases.

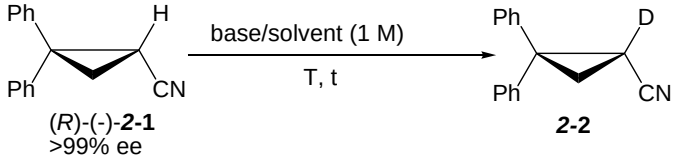

(*R*)-(-)-***2*-1**
>99% ee

***2*-2**

entry	base	solvent	T (° C)	t (day)	% yield	% deut.[a]	% ee[b]
1	MeONa	CD_3OD	50	3	97	>99	>99
2	MeOK	CD_3OD	50	2	90	84	>99
3	*t*-BuOK	*t*-BuOD	r.t	0.08	93	95	8.5

[a] Determined by ^1H NMR

[b] Determined by chiral stationary phase HPLC

The deuteration reaction of 2,2-diphenylcyclopropylnitrile (*R*)-(-)-***2*-1** was also performed using different bases, as shown in Table 2.2. When MeONa and MeOK were used as bases, the reaction afforded >99% (3 days) and 84% (2 days) deuteration respectively (entries 1 and 2, Table 2.2). The deuterated retentive products from these two reactions were obtained in >99% ee (HPLC). Interestingly, when the base was switched to

t-BuOK, the deuteration in *t*-BuOD occurred much faster than in MeONa/CD_3OD and in MeOK/CD_3OD. It just took 2 hours to get 95% deuteration (entry 3, Table 2.2). However, a nearly racemic deuterated product (8.5% ee) was afforded during the reaction (entry 3, Table 2.2). Walborsky reported slightly less stereoselective deuteration of (*R*)-(-)-***2*-1** in *t*-BuONa/*t*-BuOD (only 98.7% retention), which was deduced from the ratio of the rate constants of the exchange and the racemization (k_{ex}/k_{rac} = 77),[78].

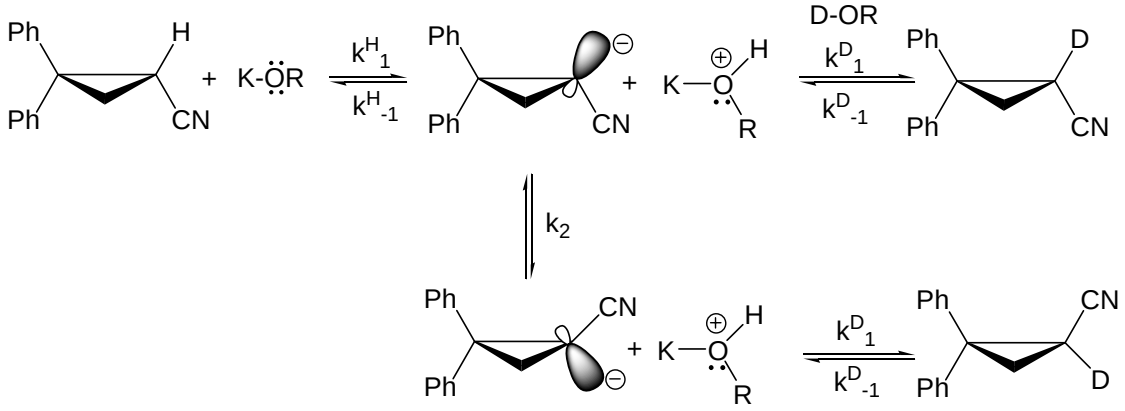

Scheme 2.7 Racemization pathway of 2,2-diphenylcyclopropylnitrile in *t*-BuOK/*t*-BuOD.

We propose a racemization pathway, as shown in Scheme 2.7. The rate of deprotonation (k_1) is directly related to the basicity of the alkoxide. A faster deprotonation (k_1) comes with a slower re-protonation (k^H_{-1}) or deuteration (k^D_1). The racemization (k_2) occurs in competition with the re-protonation (k^H_{-1})/deuteration (k^D_1) reactions. Consequently, the racemization (k_2) is more competitive if the re-protonation (k^H_{-1}) or the deuteration (k^D_1) is relatively slow. The faster deuteration for our deuteration reaction by *t*-BuOK/*t*-BuOD is due to the superior basicity of *t*-BuOK in *t*-BuOH relative to MeOK and MeONa in MeOH.

2.4 Evaluation of configurational stability of lithiated 2,2-disubstituted cyclopropylnitriles.

2.4.1 Evaluation of configurational stability of lithiated 2,2-diphenylcyclopropylnitrile.

Walborsky reported the racemic product was obtained when enantiomerically pure cyclopropylnitrile (*R*)-(-)-***2*-1** was deprotonated by LDA at -65 °C for 10 min and then treated with MeI.[70] This results suggested that lithiated (*R*)-(-)-***2*-1** had a low inversion barrier and racemized under these conditions. Assuming that complete racemization would take 5 half-lives, we estimated possible inversion barrier of 14.5 kcal/mol at -65 °C using Eyring equation. This same inversion barrier would result in a racemization $t_{1/2}$ = 25 min at -78°C or 56 h of half life at -100 °C. Thus, lowering the reaction temperature was the next logical step to study the configurational stability of (*R*)-(-)-***2*-1**. Considering the long deprotonation time would allow lithiated (*R*)-(-)-***2*-1** to racemize, we did alkylation reactions using an in situ strategy, where electrophiles and nitriles are combined before adding a base. In situ deprotonation/alkylation will possibly decrease the delay between deprotonation and alkylation.

Table 2.3 Deprotonation/alkylation of (*R*)-(-)-***2*-1**

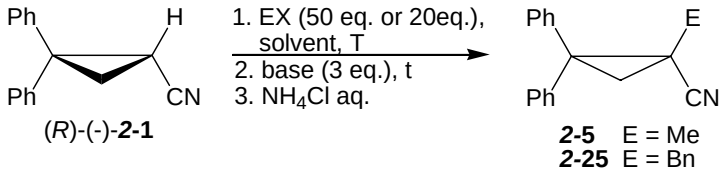

(*R*)-(-)-***2*-1**

***2*-5** E = Me
***2*-25** E = Bn

entry	EX	Pdt	base	T (° C)	solvent	t (min)	yield (%)[a]	% ee[b]
1	MeI	***2*-5**	LiHMDS	-100	THF	60	69	2
2	MeI	***2*-5**	LiHMDS	-100	THF	5	56	1
3	MeI	***2*-5**	LiHMDS	-100	Et_2O	1	NR	-
4	MeI	***2*-5**	LiHMDS	-100	Et_2O	5	NR	-
5	MeI	***2*-5**	KHMDS	-100	Et_2O	1	57	2
6	MeI	***2*-5**	KHMDS	-135	Me_2O	5	44	1
7	BnI	***2*-25**	LiHMDS	-100	THF	15	82	3
8	BnI	***2*-25**	LiHMDS	-100	THF	5	88	13
9	BnI	***2*-25**	LiHMDS	-100	THF	1	45	8

[a] Determined by ^{1}H NMR

[b] Determined by chiral stationary phase HPLC

After a 60 min in situ methylation in THF at -100 °C using LiHMDS as a base, we obtained a moderate yield (69 %) of racemic methylated product ***2*-5** (2 % ee, entry 1, Table 2.3). When the reaction time was decreased to 5 min, a lower yield (56% yield) was observed, however the product was still racemic (entry 2, Table 2.3). Since THF is highly solvating solvent, and may promote separated ion pair formation and subsequent racemization, we also used diethyl ether as a solvent because it is less effective for ion pair separation.[146] Unfortunately, we were not able to observe the formation of methylated product using LiHMDS in this solvent (entries 3 and 4, Table 2.3); note that the recovered starting material ***2*-1** in entries 3 and 4 had 99% ee. The methylated product ***2*-5** was obtained in 57% yield in Et_2O when the base was changed to KHMDS (entry 5, Table 2.3). However, in this case, the product was racemic. Apparently, in ether, LiHMDS is less

basic than that in THF. At the lowest reaction temperatures that we explored (-135 °C), only racemic product was obtained using KHMDS as a base even with a 5 min in situ reaction time (entry 6, Table 2.3). Extending the electrophile to benzyl iodide gave the desired products ***2*-25** in satisfactory yields but low % ee (3-13 %ee in entries 7-9). Shortening reaction time slightly improved % ee from 3% to 13% ee (entry 7 and entry 9). The nearly racemic products suggested that the lithated-***2*-1** has a very low racemization barrier and is unable to keep its configuration on the alkylation timescale.

2.4.2 Evaluation of configurational stability of lithiated 2,2-di(benzyloxymethyl) cyclopropylnitrile.

Previous investigations on alkylation of (*R*)-(-)-***2*-1** show that lithiated-***2*-1** racemizes quickly on the alkylation timescale. Compound (*R*)-(-)-***2*-6** possesses two identical chelating groups. After the deprotonation, the oxygen of one chelating group could coordinate to lithium and form a five-member ring. The coordination of oxygen and lithium could potentially increase configurational stability at C1. We carried out deprotonation/alkylation of (*R*)-(-)-***2*-6** using various bases under various temperatures and reaction time.

Table 2.4 Deprotonation/alkylation of (*R*)-(-)-***2*-6**.

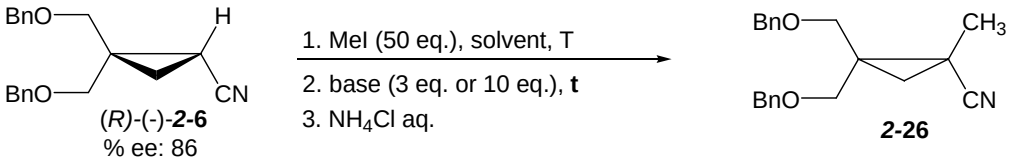

(*R*)-(-)-***2*-6**
% ee: 86

***2*-26**

entry	base	T (° C)	solvent	t (min)	yield (%)[a]	% ee[b]
1	LiHMDS (10 equiv)	-78	THF	60	100	5
2	LiHMDS (10 equiv)	-78	Et_2O	60	15	7
3	LiHMDS (10 equiv)	-100	Et_2O	30	9	10
4	LDA (3 equiv.)	-78	Et_2O	60	100	0
5	LDA (3 equiv.)	-100	Et_2O	1	100	0
6	KHMDS (3 equiv)	-100	Et_2O	1	71	1
7	KHMDS (3 equiv)	-100	Et_2O	5	100	-

[a] Determined by ^{1}H NMR

[b] Determined by chiral stationary phase HPLC

The initial trial of methylating the cyclopropylnitrile derivative (*R*)-(-)-***2*-6** in THF at -78 °C for 60 min using LHMDS led to a methylated product in 100% yield with 5% ee (entry 1, Table 2.4). The change of solvent from THF to Et_2O decreased the yield to 15% but did not change the enantiomerical excess of the methylated product (entry 2, Table 2.4). A decrease in temperature to -100 °C and reaction time to 30 min led to slight increase in % ee (10% ee) but lowered yield (9% yield) (entry 3, Table 2.4). Once LDA was used as a base, we were able to get 100% yield of the methylated product (entries 4-5, Table 2.4). The results indicates that LDA is a very active base and able to deprotonate the cyclopropylnitrile ***2*-6** within 1 min. However, the racemic methylated product indicates that the lithiated ***2*-6**, as an intermediate, is quickly racemized within 1 min in situ reaction timescale. The racemic products from the deprotonation/methylation by KHMDS indicates that potassiated ***2*-6** quickly racemizes on the alkylation timescale. Even though the chelating group ($BnOCH_2$) appears well situated to coordinate to lithium atom and form a

five-member ring, this feature does not noticeably improve configurational stability of the metalated cyclopropylnitrile.

2.4.3 Evaluation of configurational stability of lithiated 2,2-di(*o*-methoxyphenyl) cyclopropylnitrile.

For compound (*R*)-(-)-***2*-7**, the coordination of the oxygen of the chelating group (*o*-methoxyphenyl) after lithiation would form a six-member ring. However, unlike previous two cyclopropylnitriles, the deprotonation/methylation of (*R*)-(-)-***2*-7** did not successfully afford the desired products using LiHMDS or KHMDS at -78 ^{o}C (entries 1-2, Table 2.5). Extending the protocol to benzyl iodide was also unsuccessful even at -20 ^{o}C (entry 4, Table 2.5). In each case, the starting materials were recovered in >95% ee, suggesting that the deprotonation did not occur even at -20 ^{o}C. The low reactivity of the compound (*R*)-(-)-***2*-7** is consistent with its slow H/D exchange reaction (Table 2.1). In a final attempt to achieve alkylation, we carried out a sequential deprotonation/alkylation at 0 ^{o}C. After a 30 min deprotonation of ***2*-7** with LDA**,** the treatment with MeI for 60 min afforded methylated product ***2*-27** in 45% yield. We did not repeat this sequential deprotonation/alkylation on enantiomerically enriched starting materials because of the predictable racemic outcome at high temperature conditions.

Table 2.5 Deprotonation/alkylation of (*R*)-(-)-***2*-7**.

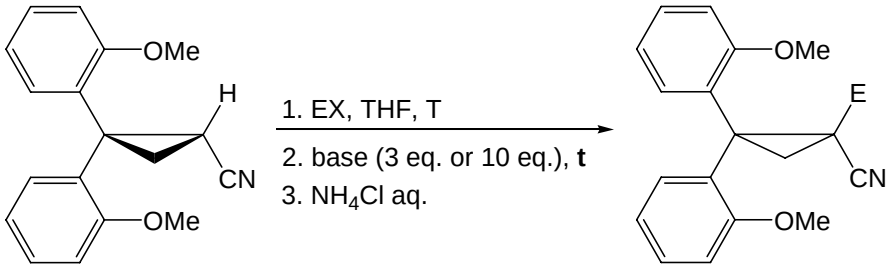

(*R*)-(-)-***2*-7**
% ee: 96

***2*-27**

entry	EX	Pdt	base	T (^{o}C)	t (min)	yield (%)[a]
1	MeI	***2*-27a**	LiHMDS	-78	30	0
2	MeI	***2*-27a**	KHMDS	-78	60	0
3	BnI	***2*-27b**	LiHMDS	-42	30	0
4	BnI	***2*-27b**	LiHMDS	-20	60	0
5[b]	MeI	***2*-27a**	LDA	0	$t_1 = 30$, $t_2 = 60$	45

[a] Determined by ^{1}H NMR

[b] The racemic ***2*-7** was used as the starting material. The reaction was the sequential deprotonation (t_1) /alkylation (t_2), which was done by Henry Yip.

2.4.4 Intramolecular reaction as a strategy to achieve enantioselective deprotonation/alkylation.

The in situ alkylation of the previous cyclopropylnitriles ***2*-1** and ***2*-6** afforded racemic products, demonstrating that metalated derivatives of cyclopropylnitriles had low racemization barriers. Even under in situ alkylation conditions, we still faced a delay between deprotonation and alkylation. Therefore, we aimed to design a cyclopropylnitrile that would allow an intramolecular alkylation. This strategy would involve the shortest possible delay between deprotonation and alkylation, and might be a viable way to compete against racemization of the lithiated cyclopropylnitrile.

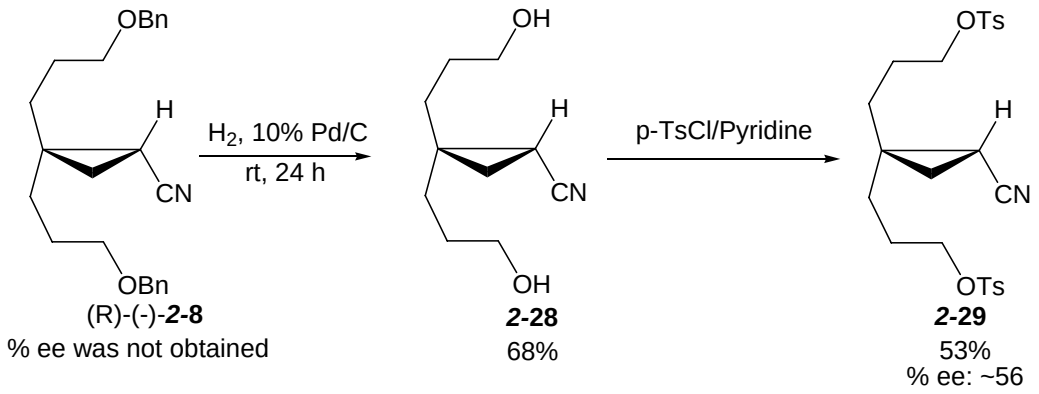

Scheme 2.8 Synthesis of 2,2-di(3-(*p*-toluenesufonyloxy)propyl)cyclopropylnitrile ***2*-29.**

The benzyl group in compound (*R*)-(-)-***2*-8** was removed and provided a diol ***2*-28** in 68% yield. The precursor cyclopropylnitrile ***2*-29** was prepared as liquid in 53% yield by the tosylation of ***2*-28** (Scheme 2.8). The enantiomerical excess of ***2*-29** was estimated at 56% ee, although base-line separation using various chiral HPLC column (AD,AD-H, and OD) could not be achieved. Furthermore, since ***2*-29** was an oil, it could not be recrystallized to higher % ee.

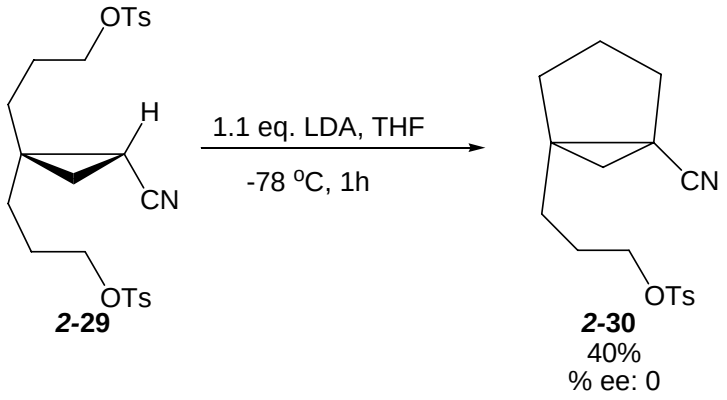

Scheme 2.9 Intramolecular alkylation of ***2*-29**

Nevertheless, ***2*-29** was treated with LDA in THF at -78 °C, as shown in Scheme 2.9. The bicyclic product ***2*-30** was isolated in 40% yield. However, chiral HPLC revealed that this bicyclic ***2*-30** was racemic. Because cyclization to five-membered ring is expected to

be very fast, we conclude that racemization of lithiated cyclopropylnitriles is indeed extremely fast.

2.5 Calculational estimation of racemization barriers of 2,2-disubstituted cyclopropylnitriles *via* the conducted-tour mechanism.

Walborsky reported that 2,2-diphenylcyclopropylnitrile afforded a racemic product during the methylation even though this compound was able to produce a retentive deuterated product at 50 º C.[70, 78] These divergent results were previously explained in terms of a S_E1 racemization pathway of the free anions of cyclopropylnitriles (S_E1 pathway, Scheme 2.10). However, in diethyl ether it was not clear how facile ion pair separation would be,[147, 148] and we sought to explain these divergent results in terms of a mechanism that did not involve separated ions. Thus, "conducted tour" mechanism may be possible. For example, as shown in Scheme 2.10, *lithio*-***2*-1** might racemize by isomerization to give ***2*-33**, followed by *N*-inversion.

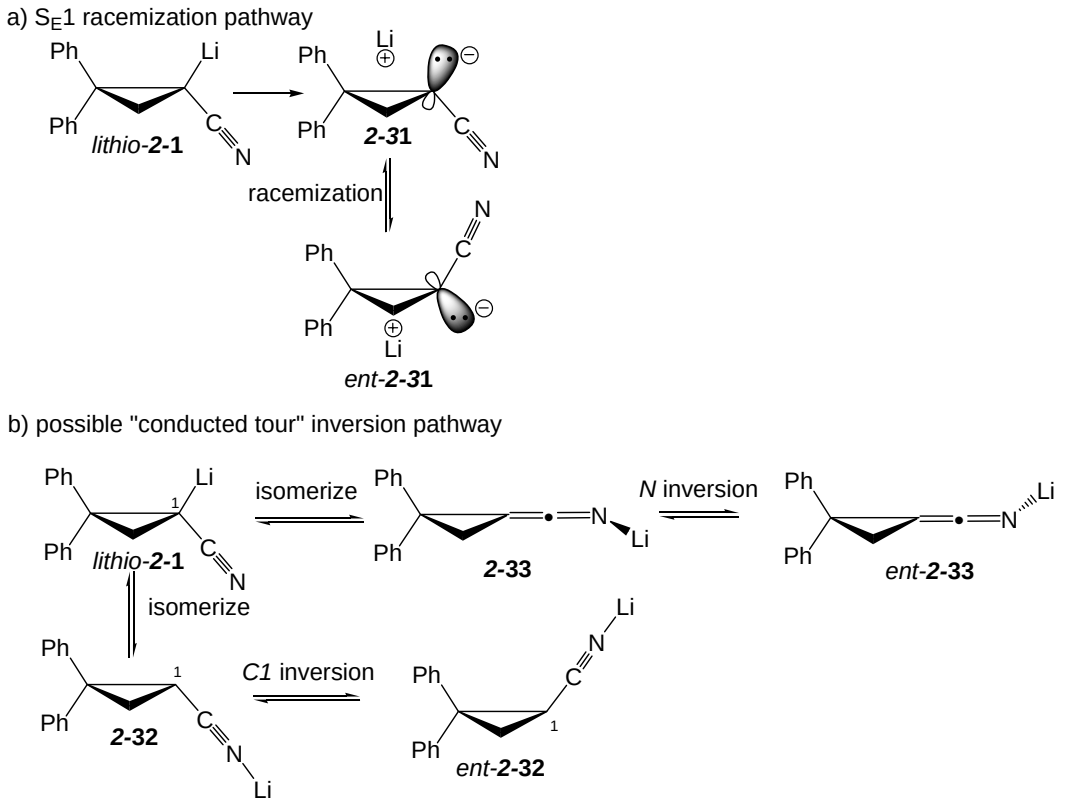

Scheme 2.10 Racemization of 2,2-diphenylcyclopropylnitrile. a) S_E1 racemization pathway of cyclopropyl anion; b) possible “conducted tour” inversion pathway.

A computational (B3LYP/6-31+G*) study on racemization of cyclopropylnitrile ***2*-34** *via* a “conducted tour” mechanism was previously reported by Carlier.[149] In this chapter, we focused on evaluating the effect of chelating groups on racemization of lithiated 2,2-disubstituted cyclopropylnitriles *via* the “conducted tour” mechanism. Our specific findings will be discussed in detials below; the major results are: 1) on the “conducted tour” pathway, deprotonation of 2,2-susbstituted cyclopropylnitriles can afford *N*-lithiated nitriles (*N*-lithiation) and *C*-lithiated nitriles (*C*-lithiation), followed by racemization. Note that *N*-lithiation is a deprotonation step which leads to a *N*-lithiated nitrile. Similarly, *C*-lithiation leads to a *C*-lithiated nitrile. Compared to the reported racemization barrier of

cyclopropylnitrile ***2*-34**,[149] our calculation indicated that the presence of 2,2-diphenyl substituents in compound ***2*-1** did not significantly change the barrier for *N*-lithiation/racemization. In contrast, chelating groups in compound ***2*-6** and ***2*-7** increased barriers for *N*-lithiation/racemization. 2) However, in the presence of solvent molecules, the barrier for *N*-lithiation/racemization of ***2*-7** was low enough to rapidly racemize. 3) Furthurmore, we found that chelating groups could facilitate the *C*-lithiation, and the lithium could be delivered to the opposite face of cyclopropyl ring by chelating groups.

2.5.1 *N*-Lithiation/racemization of 2,2-disubstituted cyclopropylnitriles *via* the "conducted tour" mechanism.

Carlier's previous *ab initio* studies on deprotonation of cyclopropylnitrile ***2*-34** by $LiNH_2$ and conducted tour racemization demonstrated an excellent correspondence of equilibrium geometries at three levels, HF/6-31G*, B3LYP/6-31G* and B3LYP/6-31+G* (Scheme 2.11).[149] Cyclopropylnitrile ***2*-34** and $LiNH_2$ formed a van der Waals complex (vdW) ***2*-35**. This complex ***2*-35** was precursor to *N*-lithiation transition state (*N*-Li. TS) ***2*-36**; following the reaction coordinate led to *N*-lithiated nitrile (*N*-Li.) ***2*-37**. The transition structure (*C*-Li. TS) ***2*-40**, which led directly to a *C*-lithiated nitrile (*C*-Li.) ***2*-39**, was much higher in energy than ***2*-36**. This result indicated that a *N*-lithiation of cyclopropylnitrile ***2*-34** was significantly kinetically preferred. The *N*-lithiated nitrile ***2*-37** racemized through the inversion transition state (inv. TS) ***2*-43**. Therefore, the inversion

barrier of *N*-lithiated cyclopropylnitrile was found to be 6.4 kcal/mol at B3LYP6-31G* (4.3 kcal/mol at B3LYP/6-31+G*).[149]

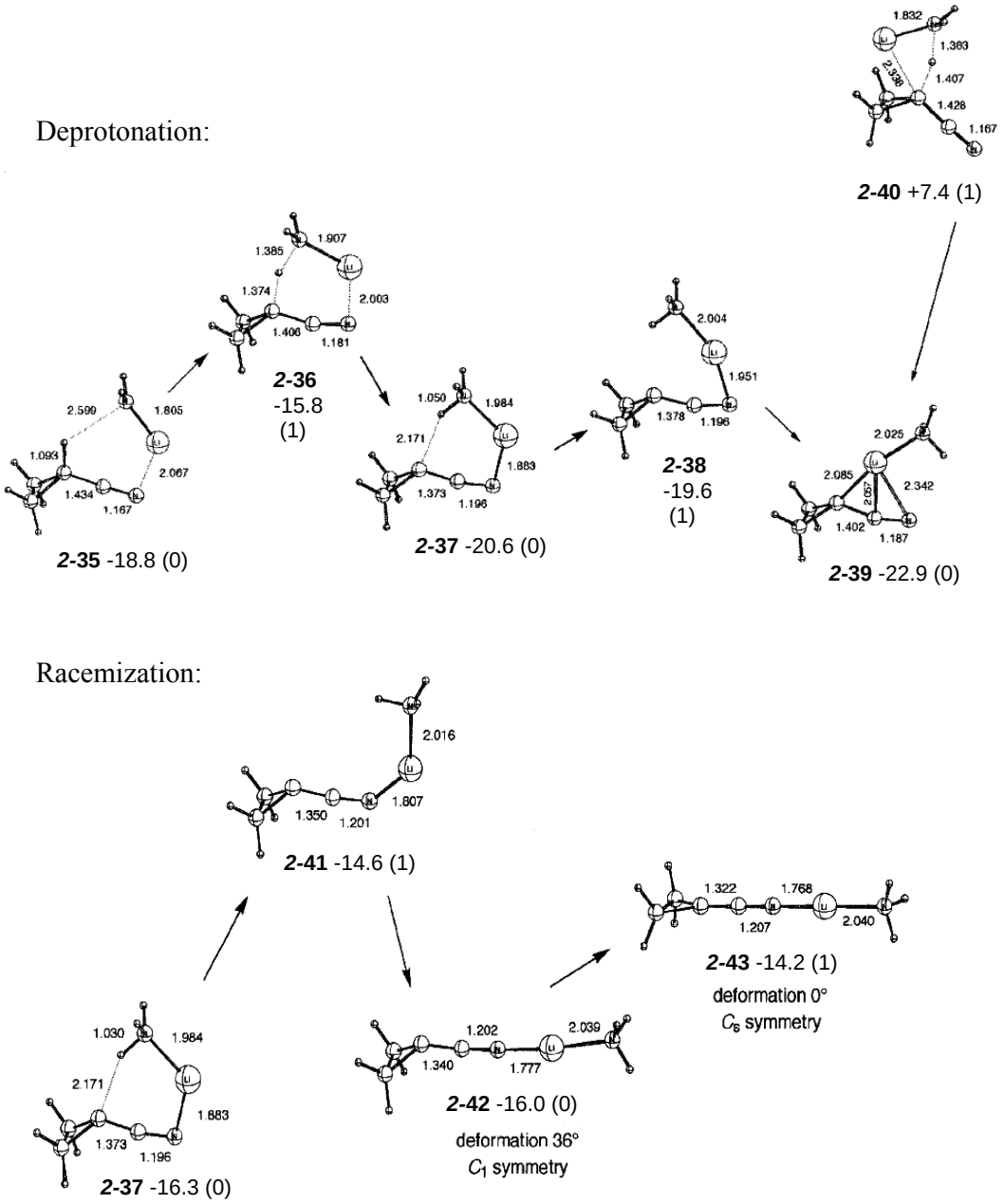

Scheme 2.11 Deprotonation/racemization of cyclopropylnitrile ***2*-34** by $LiNH_2$ *via* the "conducted tour" mechanism. Energies are given in kcal/mol at B3LYP/6-31G*, relative to separated ***2*-34** and $LiNH_2$; the number of imaginary frequencies for each structure is given in parenthesis. (Carlier et al, *Chirality* **2003**, *15*, 340. Copyright © (2003 and Carlier). Reprinted permisstion of Wiley-Liss, Inc. a subsidiary of John Wiley & Sons, Inc.)

Note that the inversion transition structure ***2*-43** was responsible for the highest energy species at B3LYP/6-31G*, while the *N*-lithiation transition structure ***2*-36** was highest in energy at B3LYP/6-31+G*.[149] Thus, in this computational study on racemization of 2,2-disubstituted cyclopropylnitriles, we only located their van der Waals complexes (vdW), deprotonation transition structures (*N*-Li.TS, or *C*-Li.TS), lithiated nitriles (*N*-Li., or *C*-Li.), and inversion transition structures (inv.TS) to estimate racemization barriers.[149-151] The geometry of each structure was optimized at B3LYP/6-31G*. All stationary points were characterized as minima (zero imaginary frequencies) or transition states (one imaginary frequency) by vibrational frequency analysis. Energies of minima and transition structures, throughout this chapter, were given in kcal/mol at B3LYP/6-31G* relative to the sum of the corresponding separated 2,2-disubstituted cyclopropyl nitriles and $LiNH_2$.

2.5.1.1 *N*-Lithiation and "conducted tour" racemization of 2,2-phenyl cyclopropylnitriles *2*-1 by $LiNH_2$.

To evaluate the effect of chelating groups on racemization, we initially investigated the *N*-lithiation and "conducted tour" racemization of 2,2-diphenylcyclopropylnitrile ***2*-1**. Structures derived from ***2*-1** and $LiNH_2$ at B3LYP/6-31G* are shown in **Error! Reference source not found.**. Selected bond lengths and distances are listed in Table 2.6.

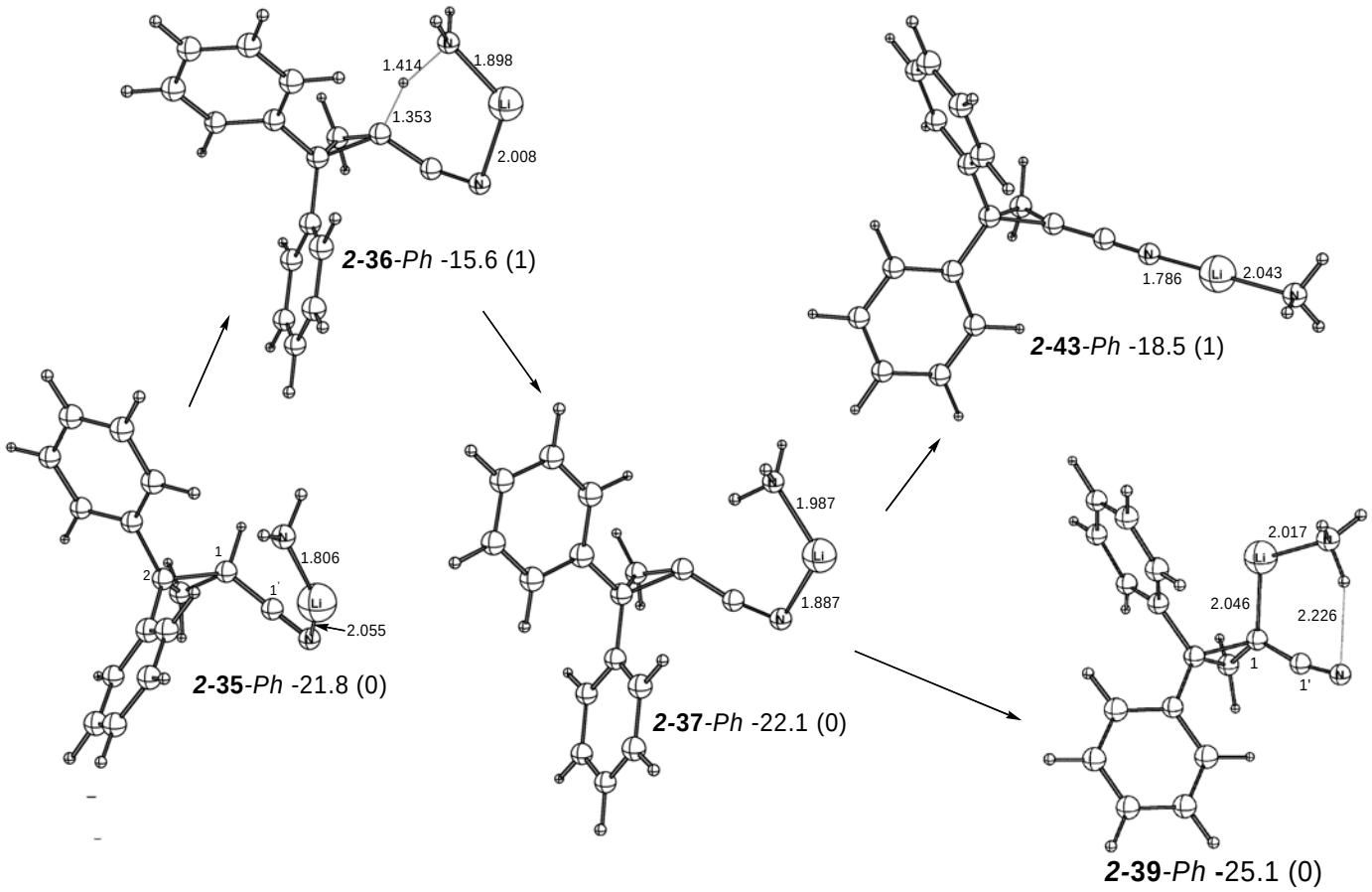

Scheme 2.12 B3LYP/6-31G* Structures for *N*-lithiation/racemization of ***2*-1** by $LiNH_2$. Energies are given in kcal/mol, relative to separated ***2*-1** and $LiNH_2$; the number of imaginary frequencies for each structure is given in parenthesis. Selected bond lengths are given in Å.

Table 2.6 Selected bond lengths and distances (Å) for structures derived from ***2*-1** and $LiNH_2$.

structure	Li-N	Li-NH2	C1′-N	C1-C1′	NH2-H1	C1-H1	C1-Li
2-35-Ph (vdW)	2.055	1.806	1.166	1.430	3.790	1.086	-
2-36-Ph (*N*-Li. TS)	2.008	1.898	1.179	1.411	1.414	1.353	-
2-37-Ph (*N*-Li.)	1.887	1.987	1.194	1,372	1.046	2,198	-
2-39-Ph (*C*-Li.)	3.397	2.017	1.178	1.406	-	-	2.046
2-43-Ph (inv. TS)	1.786	2.043	1.204	1.322	-	-	-

As seen for cyclopropylnitrile,[149] a van der Waals complex ***2*-35-*Ph*** is formed between ***2*-1** and $LiNH_2$. The deprotonation transition state ***2*-36-*Ph*** is located and requires 6.2 kcal /mol to reach it. The reaction coordinate leads to internally hydrogen-bond *N*-lithiated nitrile·amine complex ***2*-37-*Ph*** which is 0.3 kcal/mol more stable than the starting van der Waals complex ***2*-35-*Ph***. The ring inversion transition structure ***2*-43-*Ph*** is located at -18.5 kcal/mol. Though the *C*-lithiated nitrile·amine complex ***2*-39-*Ph*** (-25.1 kcal/mol) is slightly stable than the *N*-lithiated complex ***2*-37-*Ph*** (-22.1 kcal/mol), we failed to locate the deprotonation transition structure, an analog of ***2*-40**, directly leading to *C*-lithiated nitrile. Thus, the *C*-lithiated structure may be formed by isomerization of the *N*-lithiated nitrile. Therefore, the calculated inversion barrier for this *N*-lithiation/racemization of ***2*-1** by $LiNH_2$ is only 3.6 kcal/mol at B3LYP/6-31G*.

The relative energies of structures derived from ***2*-1**, as well as from cyclopropylnitrile ***2*-34**, at B3LYP/6-31G*, are listed in Table 2.7. Note that the 2,2-diphenyl substituents of ***2*-1** do not significantly affect relative energies (within 4.3

kcal/mol differences), compared to the corresponding structures derived from cyclopropylnitrile ***2*-34**.

Table 2.7 Calculated relative energies of structures derived from ***2*-1** and ***2*-34**.

entry	Relative energies[a]			
	Structures derived from ***2*-34**[b]		Structures derived from ***2*-1**	
	structure	B3LYP/6-31G*	structure	B3LYP/6-31G*
1	***2*-35** (vdW)	-18.8	***2*-35**-*Ph* (vdW)	-21.8
2	***2*-36** (*N*-Li. TS)	-15.8	***2*-36**-*Ph* (*N*-Li. TS)	-15.6
3	***2*-37** (*N*-Li.)	-20.6	***2*-37**-*Ph* (*N*-Li.)	-22.1
4	***2*-39** (*C*-Li.)	-22.9	***2*-39**-*Ph* (*C*-Li.)	-25.1
5	***2*-43** (inv. TS)	-14.2 [c]	***2*-43**-*Ph* (inv. TS)	-18.5
6	Inversion barrier	6.4	Inversion barrier	3.6

[a] All energies are relative to separated ***2*-1** and $LiNH_2$, or separated cyclopropylnitrile and $LiNH_2$. Energies are reported in kcal/mol after ZPVE correction.
[b] Relative energies of structures derived from cyclopropylnitriles are adopted from previous study by Carlier.[149]
[c] B3LYP/6-31G*//HF/6-31G*.

In the presence of chelating groups, the nitrile N and the chelating group are expected to both coordinate to lithium atom. Structures from *N*-lithiation/racemization of ***2*-6** by $LiNH_2$ at B3LYP/6-31G* are shown in Scheme 2.13, and selected bond lengths are listed in Table 2.8. In the case of ***2*-7**, B3LYP/6-31G* structures for *N*-lithiation/racemization of ***2*-7** by $LiNH_2$ are shown in Scheme 2.14, and selected bond lengths are listed in Table 2.9.

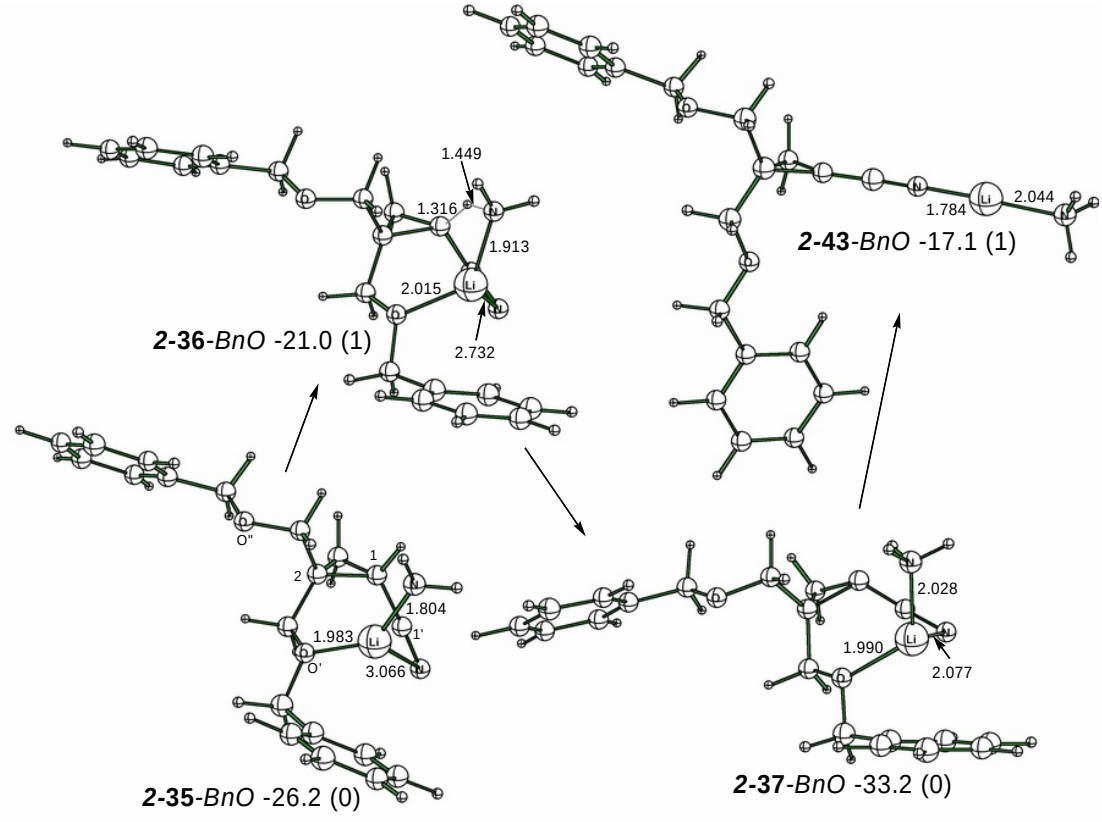

Scheme 2.13 B3LYP/6-31G* Structures for N-lithiation/racemization of ***2*-6** by $LiNH_2$. Energies are given in kcal/mol, relative to separated ***2*-6** and $LiNH_2$; the number of imaginary frequencies for each structure is given in parenthesis. Selected bond lengths are given in Å.

Table 2.8 Selected bond lengths and distances (Å) for structures derived from *N*-lithiation/racemization of ***2*-6**

structure	Li-N	Li-O′	Li-NH2	C1′-N	C1-C1′	NH2-H1	C1-H1
***2*-35**-*BnO* (vdW)	3.066	1.983	1.804	1.164	1.440	2.781	1.087
***2*-36**-*BnO* (N-Li.TS)	2.732	2.015	1.913	1.171	1.428	1.449	1.316
***2*-37**-*BnO* (N-Li.)	2.077	1.990	2.028	1.187	1.390	1.032	2.354
***2*-43**-*BnO* (inv.TS)	1.784	-	2.044	1.205	1.322	-	-

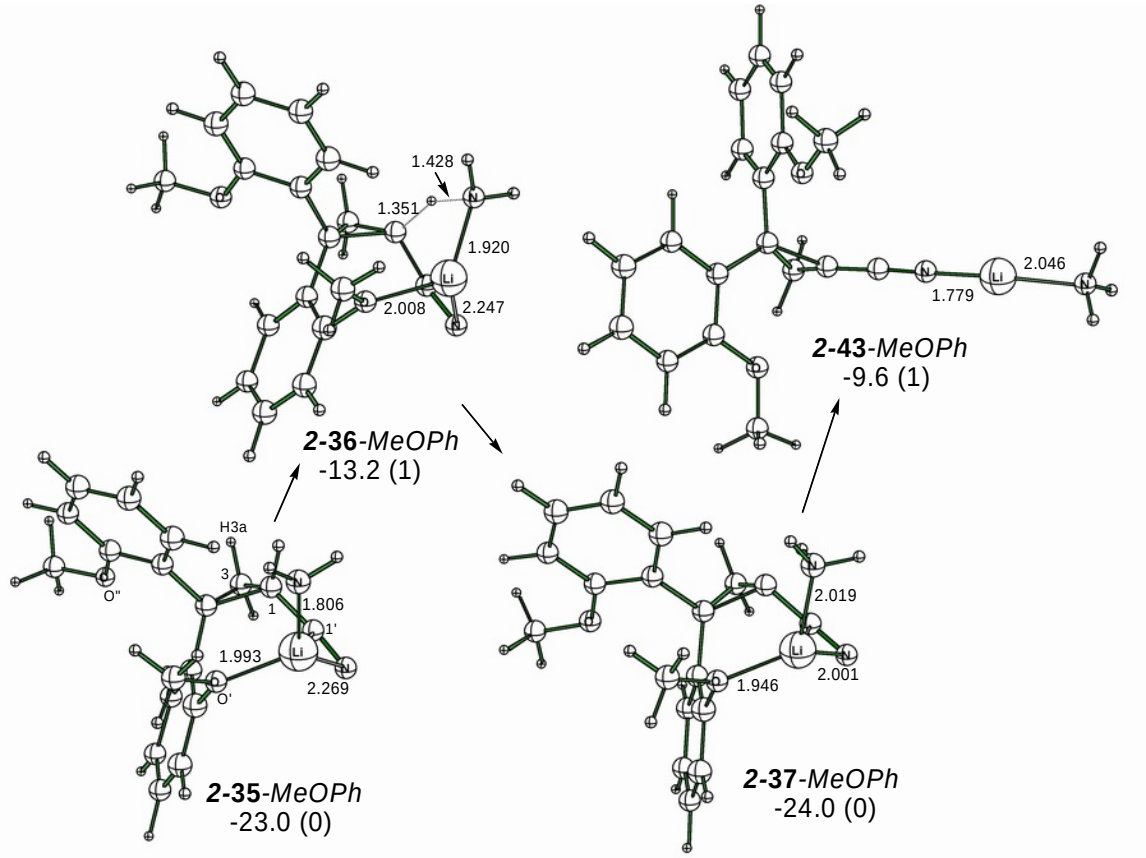

Scheme 2.14 B3LYP/6-31G* Structures for deprotonation of ***2*-7** by $LiNH_2$. Energies are given in kcal/mol, relative to separated ***2*-7** and $LiNH_2$; the number of imaginary frequencies for each structure is given in parenthesis. Selected bond lengths are given in Å

Table 2.9 Selected bond lengths or distances (Å) for structures derived from *N*-lithiation/racemization of ***2*-7**

structure	Li-N	Li-O′	Li-NH2	C1′-N	C1-C1′	NH2-H1	C1-H1
2-35-MeOPh (vdW)	2.269	1.993	1.806	1.165	1.434	3.160	1.085
2-36-MeOPh (*N*-Li.TS)	2.247	2.008	1.920	1.174	1.425	1.428	1.351
2-37-MeOPh (*N*-Li.)	2.001	1.946	2.019	1.189	1.385	1.031	2.488
2-43-MeOPh (inv.TS)	1.779	-	2.046	1.206	1.320	-	-

For the *N*-lithiation of ***2*-6** (Scheme 2.13), the van der Waals complex ***2*-35**-*BnO* (-26.2 kcal/mol) forms weaker coordination between lithium and the nitrile N, which is demonstrated by longer Li-N distance (3.066 Å). This Li-N distance is 2.732 Å for structure ***2*-36**-*BnO* (-21.0 kcal/mol), which is the deprotonation transition structure leading to the *N*-lithiated nitrile ***2*-37**-*BnO*. The strongest coordination in structure ***2*-37**-*BnO* (2.077 Å, Li-N bond length) dramatically stabilizes the *N*-lithiated nitrile ***2*-37**-*BnO* with -33.2 kcal/mol relative energy. The Li-O′ distances are 1.983 Å, 2.015 Å, 1.990 Å for ***2*-35**-*BnO, **2*-36**-*BnO,* and ***2*-37**-*BnO* respectively. The ring inversion structure ***2*-43**-*BnO* has the highest relative energy (-17.1 kcal/mol), because of the absence of the coordination between Li and the chelating group. Thus, the inversion barrier for the *N*-lithiated nitrile ***2*-37**-*BnO* is 16.1 kcal/mol.

In the case of *N*-lithiation of ***2*-7** (Scheme 2.16), the coordination between lithium and the nitrile N (Li-N), as well as between lithium and one of Methoxy O (Li-O′) are observed in the van der Waals complex ***2*-35**-*MeOPh,* the deprotonation transition structure ***2*-36**-*MeOPh,* and the *N*-lithiated nitrile ***2*-37**-*MeOPh*. The distances of Li-N are observed as 2.269 Å in ***2*-35**-*MeOPh*, 2.247 Å in ***2*-36**-*MeOPh*, and 2.001 Å in ***2*-37**-*MeOPh*, while the distances of Li-O′ are 1.993 Å, 2.008 Å, 1.946 Å in ***2*-35**-*MeOPh*, ***2*-36**-*MeOPh*, ***2*-37**-*MeOPh* respectively. The active barrier for deprotonation (*N*-lithiation) is 9.8 kcal/mol, which is higher than that of ***2*-35**-*Ph* and ***2*-35**-*BnO*. The ring inversion transition structure ***2*-43**-*MeOPh* has a relative energy of -9.6 kcal/mol. Therefore, by forming the *N*-lithiated nitrile, the complex ***2*-35**-*MeOPh* needs at least 14.4 kcal/mol to

approach the ring inversion transition state.

Table 2.10 Calculated relative energies of structures derived from *N*-lithiation/racemization of cyclopropylnitrile ***2*-34**, and their analogs derived from 2,2-disubstituted cyclopropylnitrile ***2*-1**, ***2*-6**, and ***2*-7** at B3LYP/6-31G*.

entry	structures	Relative energies[a]			
		***2*-34**	***2*-1** (*Ph*)	***2*-6** ($BnOCH_2$)	***2*-7** (o-$MeOC_6H_4$)
1	***2*-35** (vdW)	-18.8	-21.8	-26.2	-23.0
2	***2*-36** (*N*-Li.TS)	-15.8	-15.6	-21.0	-13.2
3	***2*-37** (*N*-Li.)	-20.6	-22.1	-33.2	-24.0
4	***2*-43** (inv.TS)	-14.2	-18.5	-17.1	-9.6
5	Inversion barriers	6.4	3.6	16.1	14.4

[a] All energies are relative to separated nitriles and $LiNH_2$. Energies are reported in kcal/mol after ZPVE correction.

To evaluate the effect of chelating groups on *N*-lithiation/racemization, calculated relative energies of structures at B3LYP/6-31G*, are shown in Table 2.10. Compared to structures derived from ***2*-1**, the coordination of the $BnOCH_2$ group of ***2*-6** with Li atom stabilizes the van der Waals complex (entry 1, Table 2.10), the *N*-lithiation transition structure (entry 2, Table 2.10), the *N*-lithiated nitrile (entry 3, Table 2.10), but is not possible in the ring inversion structure (entry 4, Table 2.10). Thus, a large inversion barrier (16.1 kcal/mol) is observed for *N*-lithiation/racemization of ***2*-6** with $BnOCH_2$ chelating groups (entry 6, Table 2.10). The MeOPh group of ***2*-7** has a different influence. At B3LYP/6-31G*, the MeOPh group slightly stabilizes the van der Waals complex and the *N*-lithiated nitrile compared to structures derived from ***2*-1**. However, a destabilization is observed for the *N*-lithiation transition structure and the inversion transition structure. It

is not clear the origin of this destabilization. As the effect of the MeOPh group, we also observe a large inversion barrier (14.4 kcal/mol) for ***2*-7**. This calculation demonstrates that the chelating group serves to increase the inversion barriers on *N*-lithiation/racemization pathway in the absence of solvent molecules. Obviously however, the experimental data do not provide evidence of higher racemization barriers. Below we discuss the effect of solvents and simultaneous coordination by both chelating groups on the inversion barrier.

2.5.1.2 *N*-Lithiation/racemization of solvated 2,2-di(*o*-methoxyphenyl)cyclopropyl nitriles

Several studies have shown that solvents (and cosolvents such as TMEDA) significantly influence configurational stability of organolithiums.[69, 152] Therefore, we investigated *N*-lithiation/racemization of monomeric 2,2-di(*o*-methoxyphenyl)cyclopropylnitrile ***2*-7** by explicitly solvated $LiNH_2$ at gas phase to understand the influence of solvents on racemization. Solvated $LiNH_2$ was characterized by placing two dimethyl ether molecules around lithium atom. In this work, we did not calculate structures in solution using polarizable continuum model (PCM).[153] Solvated structures derived from *N*-lithiation/racemization of ***2*-7** by $LiNH_2{\cdot}2(Me_2O)$ at B3LYP/6-31G* are shown in Scheme 2.15. Selected bond lengths are listed in Table 2.11.

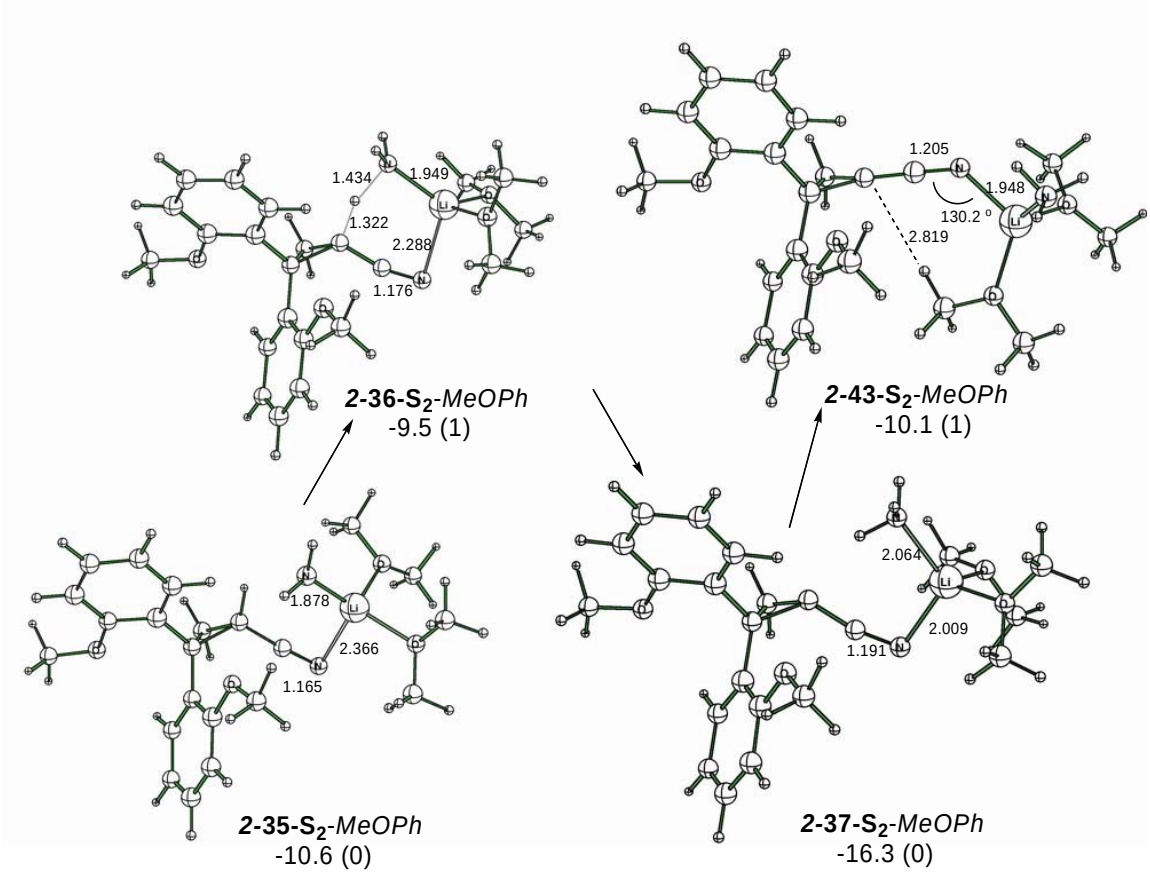

Scheme 2.15 B3LYP/6-31G* Structures for *N*-lithiation/racemization of ***2*-7** by $LiNH_2{\cdot}2(Me_2O)$. Energies are given in kcal/mol, relative to separated ***2*-7** and $LiNH_2{\cdot}2(Me_2O)$; the number of imaginary frequencies for each structure is given in parenthesis. Selected bond lengths are given in Å.

Table 2.11 Selected bond lengths and distances (Å) of solvated structures derived from *N*-lithiation/racemization of ***2*-7** by $LiNH_2{\cdot}2(Me_2O)$.

structure	Li-N	Li-NH2	C1′-N	C1-C1′	NH2-H1	C1-H1
2-**35-S_2**-*MeOPh* (vdW)	2.366	1.878	1.165	1.436	2.547	1.089
***2*-36-S_2**-*MeOPh* (*N*-Li.TS)	2.289	1.947	1.176	1.414	1.434	1.322
***2*-37-S_2**-*MeOPh* (*N*-Li.)	2.009	2.064	1.191	1.376	1.045	2.149
***2*-43-S_2**-*MeOPh* (inv.TS)	1.948	2.091	1.205	1.330	-	-

As shown in Table 2.12, at B3LYP/6-31G*, solvation significantly increases relative energies for the van der Waals complex ***2*-35-S_2-*MeOPh*** (-10.6 kcal/mol) and the *N*-lithiated nitrile ***2*-37-S_2-*MeOPh*** (-16.3 kcal/mol) compared to the corresponding unsolvated structures, ***2*-35- -*MeOPh*** (-23.0 kcal/mol) and ***2*-37-*MeOPh*** (-24.0 kcal/mol) (entries 1-2, Table 2.12). However, a lower relative energy is found for the inversion transition structure ***2*-43-S_2-*MeOPh*** compared to the corresponding ***2*-43-*MeOPh*** (entry 4, Table 2.12), since the external solvent molecules compensate for the loss of internal salvation by the chelating groups. Thus, the inversion barrier for solvated structures is 6.2 kcal/mol, which is much lower than that for unsolvated structures (14.4 kcal/mol) (entry 5, Table 2.12). Therefore, the solvation is one reason for rapid racemization of lithiated 2,2-distubstituted cyclopropylnitriles.

Table 2.12 Calculated relative energies of solvated structures derived from 2,2-(*o*-methoxyphenyl) cyclopropylnitrile ***2*-7** at B3LYP/6-31G*.

	Relative energies[a] (kcal/mol)			
entry		Unsolvated structures derived from ***2*-7** and $LiNH_2$		Solvated structures derived from ***2*-7** and $LiNH_2{\cdot}2(Me_2O)$
1	***2*-35-*MeOPh*** (vdW)	-23.0	***2*-35-S_2-MeOPh** (vdW)	-10.6
2	**2-36-*MeOPh*** (*N*-Li.TS)	-13.2	***2*-36-S_2-MeOPh** (*N*-Li.TS)	-9.5
3	**2-37-*MeOPh*** (*N*-Li.)	-24.0	***2*-37-S_2-MeOPh** (*N*-Li.)	-16.3
4	**2-43-*MeOPh*** (inv.TS)	-9.6	***2*-43-S_2-MeOPh** (inv.TS)	-10.1
5	Inversion barrier	14.4	Inversion barrier	6.2

[a] All energies are relative to separated nitriles and $LiNH_2$ or $LiNH_2{\cdot}2(Me_2O)$. Energies are reported in kcal/mol after ZPVE correction.

2.5.2 *C*-Lithiation/racemization of 2,2-substituted cyclopropyl nitriles.

Carlier's studies on racemization of cyclopropylnitrile ***2*-34** indicated that the directly formation of a *C*-lithiated nitrile was not kinetically favorable, which was demonstrated by the high *C*-lithiation transition state ***2*-40** in Scheme 2.11. We observed an alternative deprotonation of ***2*-6** and ***2*-7** at B3LYP/6-31G*, which featured the formation of a C-lithiated nitrile (C-Lithiation).

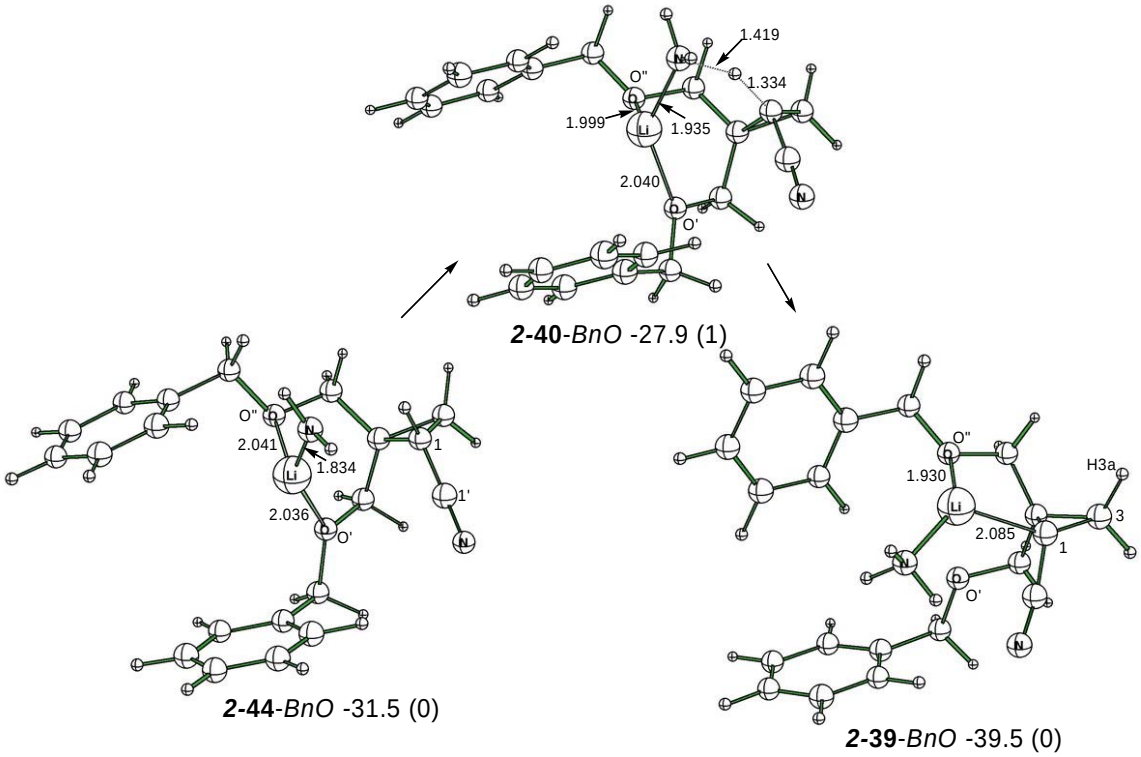

Scheme 2.16 B3LYP/6-31G* Structures for C-lithiation of ***2*-6** by $LiNH_2$. Energies are given in kcal/mol, relative to separated ***2*-6** and $LiNH_2$; the number of imaginary frequencies for each structure is given in parenthesis. Selected bond lengths are given in Å.

Table 2.13 Selected bond lengths and distances (Å) of structures derived from *C*-lithiation of ***2*-6** by $LiNH_2$.

structure	Li-N	Li-O′	Li-NH2	C1′-N	C1-C1′	NH2-H1	C1-H1	Li-O″	C1-Li
***2*-44**-BnO (vdW)	-	2.036	1.834	1.163	1.443	2.480	1.093	2.041	2.981
***2*-40**-BnO (*C*-Li.TS)	-	2.040	1.935	1.169	1.431	1.419	1.334	1.999	2.819
***2*-39**-BnO (*C*-Li.)	3.303	3.220	2.020	1.178	1.413	-	-	1.930	2.085

C-Lithiation of ***2*-6** by $LiNH_2$ is shown in Scheme 2.16. The relative energies of each structures for *C*-lithiation are given in Table 2.14 , which are compared to the corresponding structures from *N*-lithiation. In *C*-lithiation, the chelation of both $BnOCH_2$ groups with lithium atom is observed in the van der Waals complex ***2*-44**-*BnO* (-31.5 kcal/mol), and the *C*-lithiation transition structure (*C*-Li.TS) ***2*-40**-*BnO* (-27.9 kcal/mol). Though these two structures are around 6 kcal/mol more stable than the corresponding structures from *N*-lithiation (entries 1-3, Table 2.14), the deprotonation barriers for *C*-lithiation is only 1.6 kcal/mol less than that for *N*-lithiation (entry 5, Table 2.14). In the *C*-lithiated nitrile ***2*-39**-*BnO*, only one $BnOCH_2$ group coordinates to lithium, which is demonstrated by the distance of Li-C1 (2.085 Å), Li-O″ (1.931 Å) and Li-O′ (3.220 Å). Even though the dihedral angle of C2-C3-C1-Li is -46.26° and makes Li not right above the C1 carbanion, the chelating group is still able to keep Li on one face of the cyclopropyl ring. According to calculated relative energies of ***2*-39**-*BnO* (-39.5kcal/mol) and ***2*-37**-*BnO* (-33.2 kcal/mol), *C*-lithiation is thermodynamically and slightly kinetically favored compared to *N*-lithiation. However, it is unknown whether racemization of the *C*-lithiated nitrile ***2*-39**-*BnO* undergoes the inversion transition structure ***2*-43**-*BnO*.

Table 2.14 Relative energies (kcal/mol) of structures derived from ***2*-6**.

entry	*C*-Lithiation[a]		*N*-Lithiation[a]	
	structures	B3LYP/6-31G*	structures	B3LYP/6-31G*
1	***2*-44**-*BnO* (vdW)	-31.5	***2*-35**-*BnO* (vdW)	-26.2
2	***2*-40**-*BnO* (*C*-Li.TS)	-27.9	***2*-36**-*BnO* (*N*-Li.TS)	-21.0
3	***2*-39**-*BnO* (*C*-Li.)	-39.5	***2*-37**-BnO (N-Li.)	-33.2
4	-	-	***2*-43**-*BnO* (inv.TS)	-17.1
5	Deprotonation barrier	3.6	Deprotonation barrier	5.2

[a] All energies are relative to separated ***2*-6** and $LiNH_2$, Energies are reported in kcal/mol after ZPVE correction.

Alternative *C*-lithiation of ***2*-7** by LiNH2 is also observed at B3LYP/6-31G* as shown in Scheme 2.17, selected bond lengths are shown in Table 2.15, and relative energies of structures from *C*-lithiation and *N*-lithiation of ***2*-7** are listed in Table 2.16. In the van der Waals complex ***2*-34**-*MeOPh,* the *C*-lithiation transition structure ***2*-40**-*MeOPh*, and the *C*-lithiated nitrile ***2*-39**-*MeOPh*, both methoxy groups chelate with Li atom, which are demonstrated by bond lengths of Li-O′ and Li-O′′ in Table 2.15. The deprotonation barrier of *C*-lithiation is 3.6 kcal/mol lower than that of *N*-lithiation (entry 5, Table 2.16). The *C*-lithiated nitrile ***2*-39**-*MeOPh* (-32.1 kcal/mol) is much more stable than the *N*-lithiated nitrile ***2*-37**-*MeOPh* (-24.0 kcal/mol).

Table 2.15 Selected bond lengths and distances (Å) of structures derived from *C*-lithiation of ***2*-7** by $LiNH_2$.

structure	Li-O′	Li-NH2	C1′-N	C1-C1′	NH2-H1	C1-H1	Li-O′′	C1-Li
***2*-44**-MeOPh (vdW)	1.976	1.815	1.162	1.444	3.782	1.088	1.980	2.597
***2*-40**-MeOPh (C-Li.TS)	1.998	1.898	1.169	1.431	1.401	1.354	1.958	2.413
***2*-39**-MeOPh (C-Li.)	2.075	2.059	1.180	1.409	-	-	1.949	2.105

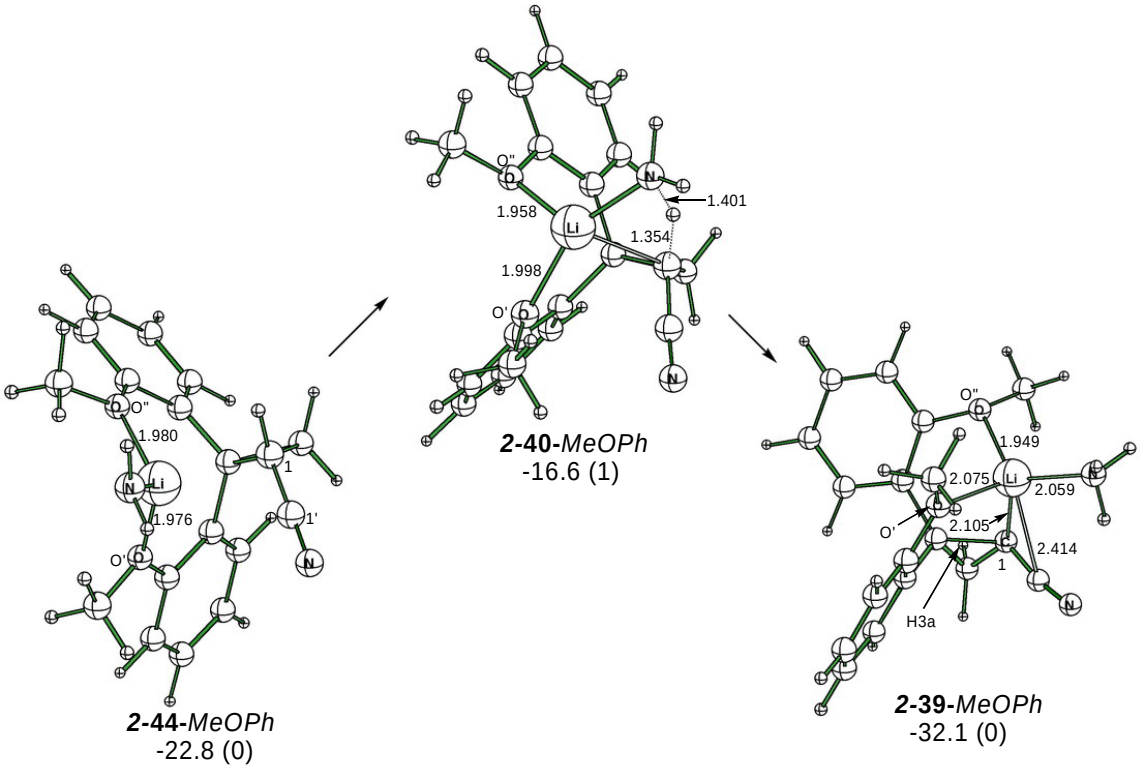

Scheme 2.17 B3LYP/6-31G* Structures for *C*-lithiation of ***2*-7** by $LiNH_2$. Energies are given in kcal/mol, relative to separated ***2*-7** and $LiNH_2$; the number of imaginary frequencies for each structure is given in parenthesis. Selected bond lengths are given in Å.

Table 2.16 Relative energies of structures derived from *C*-lithiation and *N*-lithiation of ***2*-7** by $LiNH_2$.

entry	*C*-Lithiation[a]		*N*-Lithiation[a]	
	structures	B3LYP/6-31G*	structures	B3LYP/6-31G*
1	***2*-44**-MeOPh (vdW)	-22.8	***2*-35**-MeOPh (vdW)	-23.0
2	***2*-40**-*MeOPh* (*C*-Li.TS)	-16.6	***2*-36**-*MeOPh* (*N*-Li.TS)	-13.2
3	***2*-39**-MeOPh (C-Li.)	-32.1	***2*-37**-MeOPh (N-Li.)	-24.0
4	***2*-45**-MeOPh (inv.TS)	-23.0	***2*-43**-MeOPh (inv.TS)	-9.6
5	Deprotonation barrier	6.2	Deprotonation barrier	9.8
6	Inversion barrier	9.1	Inversion barrier	14.4

[a] All energies are relative to separated ***2*-7** and $LiNH_2$, Energies are reported in kcal/mol after ZPVE correction.

A large energetic difference (22.5 kcal/mol) between ***2*-39**-*MeOPh* and ***2*-43**-*MeOPh* questions the ***2*-43**-*MeOPh* as the racemization transition structure for ***2*-39**-*MeOPh*.

Meanwhile, the dihedral angle of C2-C3-C1-Li in ***2*-39**-*MeOPh* is -21.69 °, and results Li atom slightly above the plane of the cyclopropyl ring. Therefore, we propose an alternative racemization mechanism as shown in Scheme 2.18. The *C*-lithiated nitrile ***2*-39**-*MeOPh* might racemize by formation of a roughly flat transition structure ***2*-45**-*MeOPh*, followed by recombination of lithium and carbanion. Both methoxy groups chelate with lithium atom along the racemization pathway, and deliver lithium to the opposite face of the cyclopropyl ring. Computational study demonstrates that the ring inversion transition structure ***2*-45**-*MeOPh* is located at -23.0 kcal/mol at B3LYP/6-31G* (Scheme 2.18). The geometry of ***2*-45**-*MeOPh* shows the chelation of Li-N (2.275 Å), Li-O′(1.995 Å) and Li-O′′(1.999 Å). Apparently, racemization of the *C*-lithiated nitrile ***2*-39**-*MeOPh* requires only 9.1 kcal/mol to reach the ring inversion transition state ***2*-45**-*MeOPh*. This calculation suggests that for unsolvated structures, two identical chelating groups facilitate *C*-lithiation and racemization when both chelating groups coordinate to lithium and form two 6-member rings.

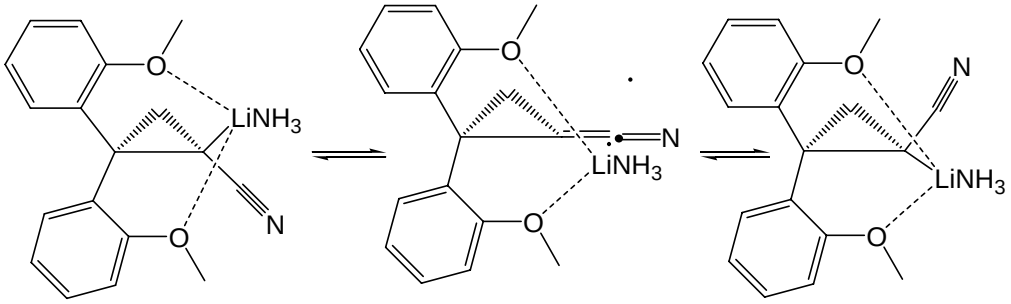

2*-39**-*MeOPh* ***2*-45**-*MeOPh* *ent*-2*-39**-*MeOPh*

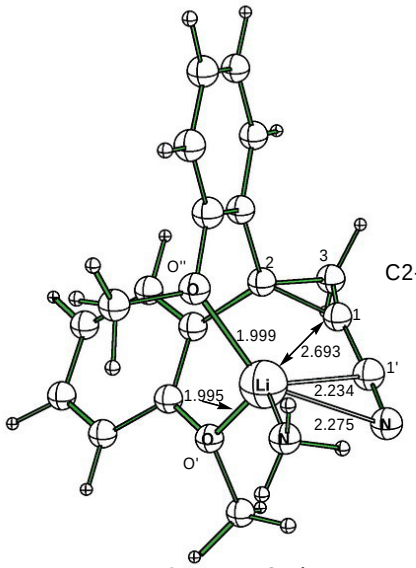

C2-C3-C1-Li: 18.23°

***2*-45**-*MeOPh*
-23.0 (1)

Scheme 2.18 Racemization of ***2*-45**-*MeOPh via* chelating group delivery. Energies are given in kcal/mol at B3LYP/6-31G*, relative to separated ***2*-7** and $LiNH_2$; the number of imaginary frequencies for each structure is given in parenthesis. Selected bond lengths are given in Å.

2.6 Conclusion

The goal of this project was to evaluate the chelating effect on configurational stability on the reaction timescale. We have designed three cyclopropylnitriles ***2*-6** ~ ***2*-8** with chelating groups, and established a synthetic route to enantiomerically enriched (*R*)-(-)-***2*-6** ~ ***2*-8**.

Configurational stability was initially evaluated by the H-D exchange. A retentive H-D exchange (in MeONa/MeOD) of (*R*)-(-)-***2*-1**, (*R*)-(-)-***2*-6** and (*R*)-(-)-***2*-7** indicated that the chelating groups did not significantly influence configurational stability of lithiated cyclopropylnitriles under this H-D exchange conditions. Note that a racemic outcome was observed for (*R*)-(-)-***2*-1** during the H-D exchange in *t*-BuOK/*t*-BuOD. We proposed that the faster deprotonation and the slower protonation led to the high possibility of racemization (Scheme 2.7) of *lithio*-(*R*)-(-)-***2*-1**. However, the deprotonation/alkylation of 2,2-disubstituted cyclopropylnitriles (*R*)-(-)-***2*-1**, (*R*)-(-)-***2*-6** and (*R*)-(-)-***2*-7** all led to the racemic corresponding alkylated cyclopropylnitriles under various conditions. Even, a racemic product (*R*)-(-)-***2*-30** was obtained for the intramolecular alkylation of (*R*)-(-)-***2*-29**, which involved a shortest delay between deprotonation and alkylation. Based on the experimental results, we concluded that the lithiated cyclopropylnitriles have low racemization barriers, and the chelating groups did not improve configurational stability during the deprotonation/alkylation reaction.

We performed computational studies on the deprotonation/racemization of ***2*-1**, ***2*-6** and ***2*-7** by $LiNH_2$ *via* the "conducted tour" mechanism to gain insights into the racemization process and the effect of chelating groups. The calculation demonstrated that for unsolvated structures, the cyclopropylnitriles ***2*-6** and ***2*-7** with chelating groups featured *C*-lithiation, which was demonstrated by the deprotonation barrier 3.6 kcal/mol and 6.2 kcal/mol respectively, compared to their *N*-lithiation (5.2 kcal/mol and 9.8 kcal/mol respectively). Though the high racemization barriers (16.1 kcal/mol and 14.4

kcal/mol) was observed for *N*-lithiation of ***2*-6** and ***2*-7** by $LiNH_2$ due to the chelating effect, our calculation indicated that the solvation significantly decrease the racemization barrier (6.2 kcal/mol) for *N*-lithiation/racemization of ***2*-7**. Interestingly, for cyclopropylnitrile ***2*-7**, the formed *C*-lithiated nitrile ***2*-39**-*MeOPh* was able to racemize *via* the ring inversion transition state ***2*-45**-*MePh,* in which the chelating groups delivered the lithium from one face to the other and was facile the ring inversion (9.1 kcal/mol inversion barrier).

Chapter 3 Evaluation of configurational stability of metalated cyclopropylnitrile: Halogen-metal exchange routes to lithiated & magnesiated cyclopropylnitriles.

3.1 Introduction.

Metalated nitriles are most commonly generated by deprotonation. However, in the previous chapter, we showed that deprotonation of several enantioenriched cyclopropylnitriles with LDA, LiHMDS and KHMDS gave metalated nitriles that racemized rapidly at temperatures down to -135 °C.

Fleming and Knochel reported that the facile halogen-metal exchange of achiral α-halonitriles with Grignard and alkyllithium reagents generated metalated nitriles in situ with various electrophiles.[154] Alkylation of conformationally constrained α-metalated nitriles exhibited electrophile-dependent alkylation stereoselectivities.[5, 154, 155] In the hope that non-deprotonation methods might provide metalated nitriles of greater configurational stability, we sought to explore metal-halogen exchange of an enantiopure bromo cyclopropylnitrile. This chapter discusses the different results obtained from lithium-halogen exchange and magnesium-halogen exchange of 1-bromo-2,2-diphenylcyclopropylnitrile. We will show that the magnesiated cyclopropylnitrile generated in this way are configurationally stable whereas the corresponding lithium derivative is not.

3.2 Synthesis of 1-bromo-2,2-diphenylcyclopropylnitrile

Our synthesis of the desired bromocyclopropylnitrile started with the known addition of dibromocarbene to 1,1-diphenylethene ***3*-1**.[156] Magnesium-bromine exchange and CO_2 trapping using a known procedure[157] gave the product ***3*-3** in 65% yield (Scheme 3.1). In order to obtain the enantiomerically pure/enriched ***3*-3**, we used Brucine ***3*-4** to resolve the racemic ***3*-3** in acetone/methanol (25:1). After recrystallization, we were able to isolate the dextrorotatory complex of compound ***3*-3** and Brucine ***3*-4** ($[\alpha]^D$ = +32.1, in EtOH, c = 0.215), which was treated with aqueous HCl to lead to the free carboxylic acid ***3*-3** ($[\alpha]^D$ = +83.4, in EtOH, c = 0.24).

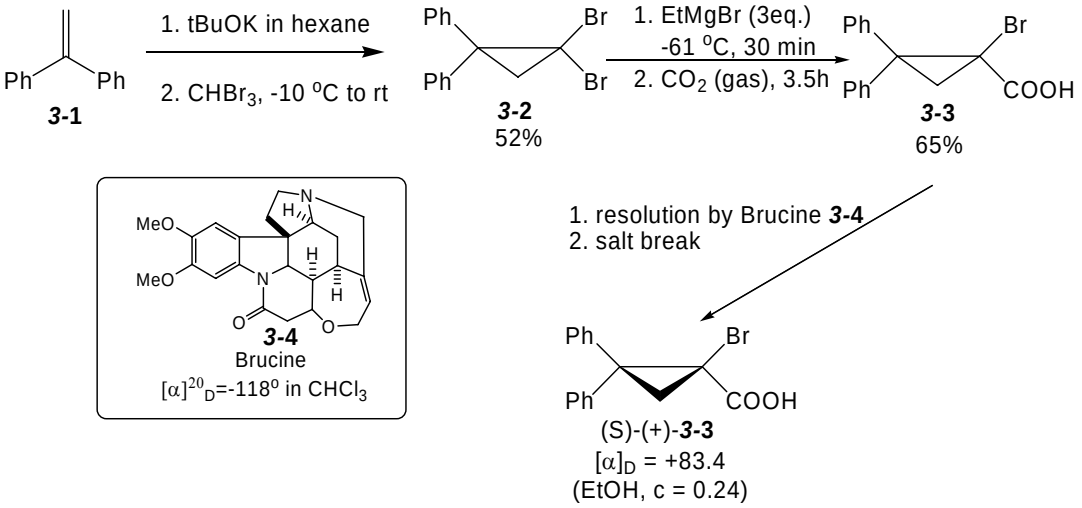

Scheme 3.1 Preparation of enantiomerically pure ***3*-3.**

The carboxylic acid ***3*-3** was directly converted to the corresponding amide ***3*-5** in 84% yield by using NHS, EDCI and NH_4OH. The conversion of amide to nitrile occurred at 80 °C upon treatment with *p*-TsCl in pyridine to give 66% yield (Scheme 3.2). Note that dehydration of bromo nitrile ***3*-5** required higher temperature than previous amide

dehydration described in Chapter 2, possibly as a result of increased steric bulk. The chiral stationary phase HPLC revealed that the product ***3*-6** was enantiomerically pure with >95% ee ($[\alpha]^D$ = +8.13, in EtOH, c = 0.16). The absolute configuration of ***3*-6** was determined as "*S*" by X-ray crystallography (Figure 3.1).

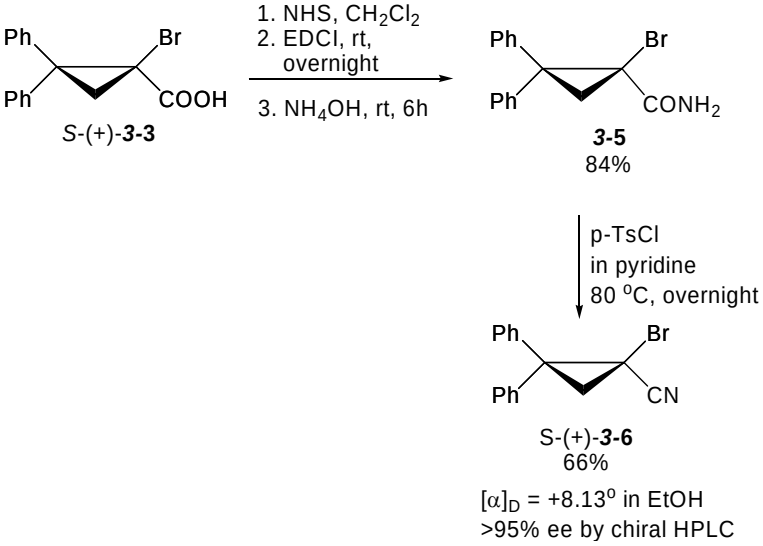

Scheme 3.2 Preparation of 1-bromo-2,2-diphenylcyclopropylnitrile ***3*-6**.

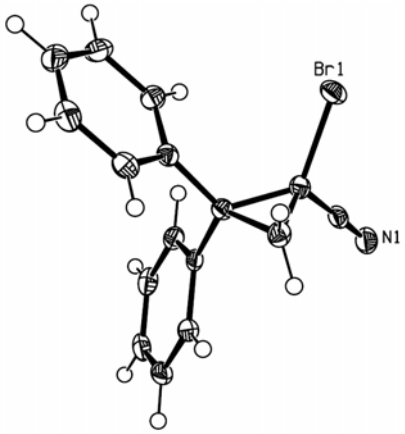

Figure 3.1 X-ray structure of 1-bromo-2,2-diphenylcyclopropylnitrile ***3*-6**.

3.3 Discovery of different behaviors of lithium-halogen exchange and magnesium-halogen exchange.

Fleming and Knochel reported the facile halogen-metal exchange of achiral α-halonitriles with Grignard and alkyllithium reagents, generating magnesiated and lithiated nitriles.[154] Magnesiated nitriles in particular appeared attractive, as they might be expected to possess improved configurational stability.[11] We explored the halogen-metal exchange to enantiomerically pure α-halocyclopropylnitriles. Initially, the lithium-halogen exchange and magnesium-halogen exchange/methylation of (*S*)-(+)-***3*-6** were carried out using in situ protocol recommended by Fleming & Knochel (1.05 equiv. *n*-BuLi or *i*-PrMgBr, Et_2O)[154], but at -100 °C instead of -78 °C. We were able to identify components in the reaction mixture by ^{1}H NMR because protons of cyclopropyl ring featured distinguishable chemical shifts and splitting. As a summary in Figure 3.2, the chemical shifts were shown for the starting material ***3*-6** (2.2 and 2.5 ppm), the methylated nitrile ***3*-7** (1.6 and 2.1 ppm), the protio-nitrile ***3*-8** (1.8, 2.0 and 2.2 ppm) and the deuterio-nitrile ***3*-9** (1.8 and 2.0 ppm). In the protio-nitrile ***3*-8**, the doublet of doublet peaks were observed due to the geminal and vicinal couplings.[158] H_a and H_b of the methylated-nitrile ***3*-7** were assigned by the correlations between H_a and Me in NOESY spectra (Figure 3.3). The chemical shifts of H_a, H_b and H_c were assigned for the protio-nitrile ***3*-8** based on typical J^2 and J^3 coupling constants in cyclopropyl ring.[158] The assignment of H_a and H_b of the bromonitrile and the deuterio-nitrile was based on the protio-nitrile and methylated-nitrile. Because of the geminal coupling, doublet peaks

were observed for the bromonitrile, methylated-nitrile, and deuterio-nitrile.

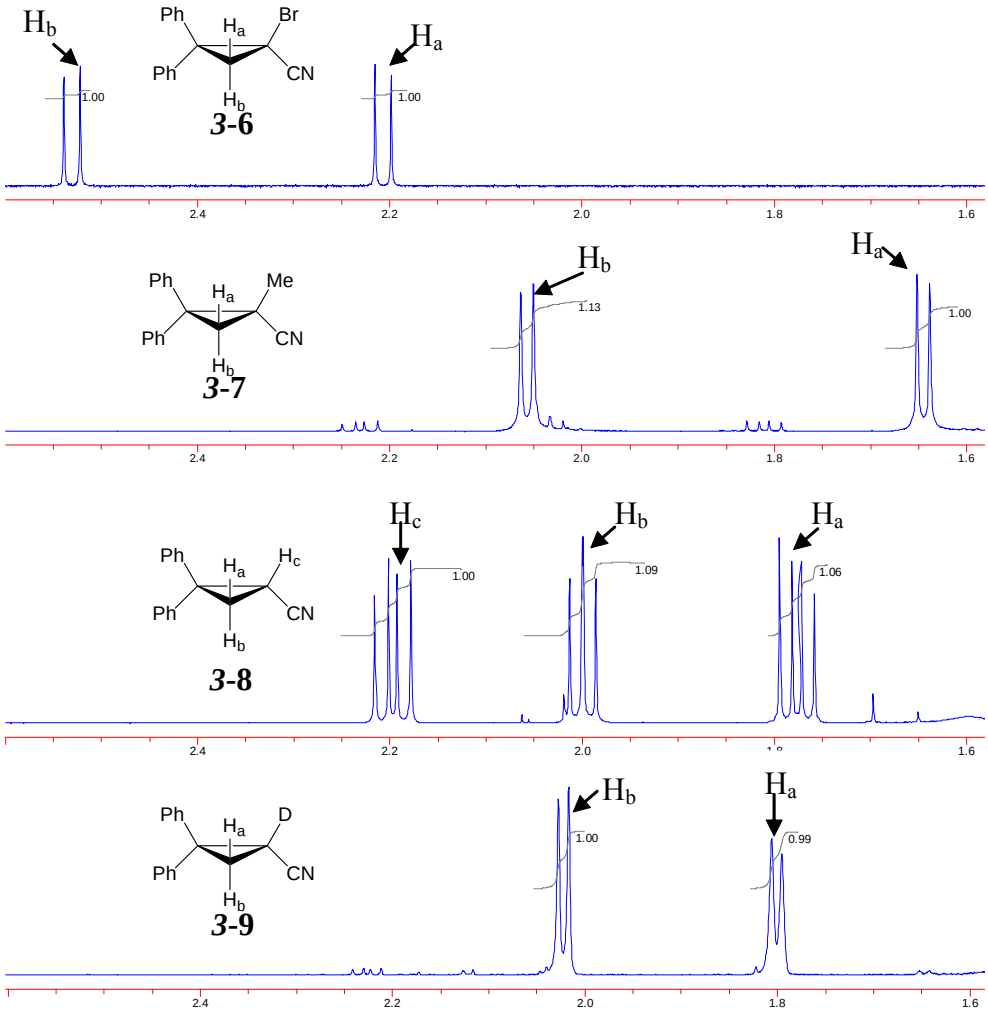

Figure 3.2 ^{1}H NMR (CDCl3) chemical shifts of cyclopropyl ring protons of ***3*-6**, ***3*-7**, ***3*-8**, and ***3*-9**. Note that the spectrum of ***3*-9** contains a small amount of ***3*-8**. Likewise, the spectrum of ***3*-7** indicates the presence of a small amount of ***3*-8** (chromatographically inseparable).

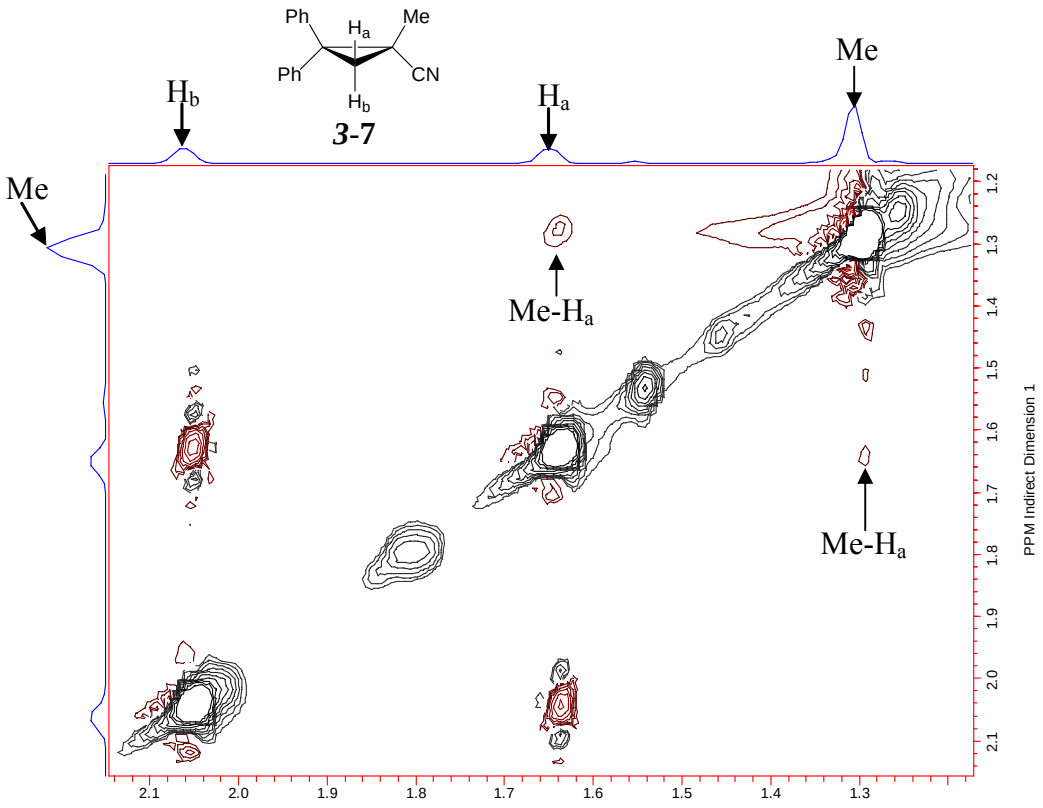

Figure 3.3 ^{1}H-^{1}H NOESY NMR of ***3*-7** in $CDCl_3$ at room temperature. Me group (δ 1.3 ppm) correlates with H_a hydrogen (δ 1.6 ppm).

When *n*-BuLi (1.05 equiv.) and CH_3I were used for exchange/methylation, followed by a NH_4Cl (aq.) quench (entry 1, Table 3.1), we were surprised to recover the starting material ***3*-6** (30 mol.%) and found that both methylated-nitrile ***3*-7** and protio-nitrile ***3*-8** were present in the crude product. To determine the origin of the protio-nitrile ***3*-8** we did a parallel reaction using CD_3I as the electrophile and D_2O for quench (entry 2, Table 3.1). Interestingly, no deuterio-nitrile ***3*-9** was detected in the crude product while the protio-nitrile ***3*-8** remained present in 25 mol.% (entry 2, Table 3.1). This result indicated that the protio-nitrile ***3*-8** did not originate from the electrophile or from the quenching step. It seemed likely that the protio-nitrile ***3*-8** was the product of E2 elimination;[159] this

possibility will be discussed later. The chiral stationary phase HPLC revealed that the methylated-nitrile ***3*-7** and the protio-nitrile ***3*-8** were both racemic, similar to results we observed in deprotonation/trapping reactions of the enantiomerically pure ***3*-8**. More interestingly, however, we found that the recovered starting material ***3*-6** was nearly racemic (~30% ee and ~9% ee in entries 1 and 2 respectively, Table 3.1).

Table 3.1 Lithium-halogen exchange/methylation and magnesium-halogen. exchange/methylation using the in-situ protocol.

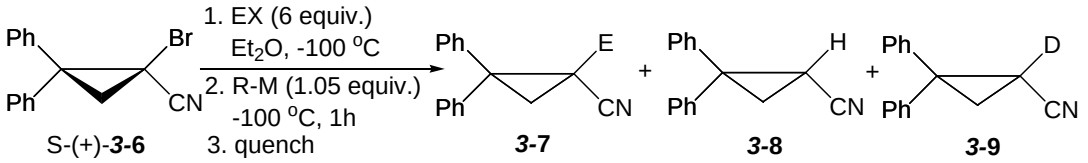

S-(+)-***3*-6** %ee >95 — ***3*-7** — ***3*-8** — ***3*-9**

entry	R-M (base)	E-X	t (min)	quench	***3*-6** mol.% (%ee)	***3*-7** mol.% (%ee)	***3*-8, *3*-9** mol. % [a] (%ee)
1	*n*-BuLi	CH_3I	60	NH_4Cl	32% (~30)	32% (0)	36%, 0%[b] (0)
2	*n*-BuLi	CD_3I	60	D_2O	23% (~9)	52% (0)	25%, 0% (0)
3	*i*-PrMgBr	CD_3I	60	NH_4Cl	48% (>95)	6% (0)	46%, 0% (69)
4	*i*-PrMgBr	CD_3I	60	D_2O	38% (>95)	7% (0)	25%, 31% (72)

[a] The mol.% was determined by ^1H NMR spectroscopy of reaction mixture (after workup) in $CDCl_3$. The protons at C1 and C3 of cyclopropyl ring feature distinguishable chemical shifts and the splitting which were used to identify components in the reaction mixture.
[b] No deuterio-reagent was used in the reaction.

Magnesium-halogen exchange/methylation of (*S*)-(+)-***3*-6** exhibited significantly different results from that of lithium-halogen exchange/methylation. When *i*-PrMgBr (1.05 equiv) and CD_3I were used for magnesium-halogen/methylation, and the reaction was quenched by NH_4Cl (aq.) (entry 3, Table 3.1), we recovered 48 mol.% of the starting material ***3*-6** with >95% ee, the protio-nitrile ***3*-8** in 46 mol.% (69% ee), while the methylated-nitrile ***3*-7** was racemic in 6 mol.% (entry 3, Table 3.1). In entry 4 Table 3.1,

an identical procedure was performed with a D_2O quench. The recovered starting material ***3*-6** and the methylated nitrile ***3*-7** were in 38 mol.% (>95% ee) and 7 mol.% (0% ee) respectively. The protio-nitrile ***3*-8** was found in 25 mol.% while the deuterio-nitrile ***3*-9** was present in 31 mol.%. The absence of the deuterio-nitrile ***3*-9** in entry 3 and the presence of it in entry 4 strongly indicated that the deuterio-nitrile ***3*-9** was formed during the quenching step. Again, we proposed that E2 elimination was the origin of the protio-nitrile ***3*-8**. The chiral stationary phase HPLC revealed 72% ee for the combined protio- (***3*-8**) and deuterio- nitriles (***3*-9**) in entry 4 Table 3.1. Though, at this point, it was not possible to determine the % ee of the protio-nitrile ***3*-8** and deuterio-nitrile ***3*-9** individually, it appeared that the formed magnesiated cyclopropylnitrile intermediate was partially configurationally stable. An additional important observation was that the unreacted bromonitrile ***3*-6** retained > 95% ee. We thus carried out additional experiments to understand the different behaviors of lithium-halogen exchange and magnesium-halogen exchange reactions of (*S*)-(+)-***3*-6**.

3.4 Lithium-halogen exchange of cyclopropylnitrile *3*-6

In order to better understand lithium-halogen exchange of 1-bromo-2,2-diphenyl cyclopropylnitrile ***3*-6**, we investigated exchange reactions by using 2.2 equiv. of *n*-BuLi or *sec*-BuLi. The use of 2.2 equiv. of organometallics for halogen-metal exchange is a standard procedure since it is believed to prevent competing E2 pathways that would consume the newly formed organometallics. The first equivalent of *n*-BuLi accomplishes

lithium-halogen exchange; the second equivalent functions as a base and causes E2 elimination of *n*-BuBr (Scheme 3.3).[159, 160] In this way, the E2 elimination between the new organolithium RLi and *n*-BuBr is avoided. In addition, given the fact that *n*-BuLi can be consumed by E2 elimination of 1-bromobutane, use of less than 2 equiv. of *n*-BuLi could result in failure to consume all the starting material.

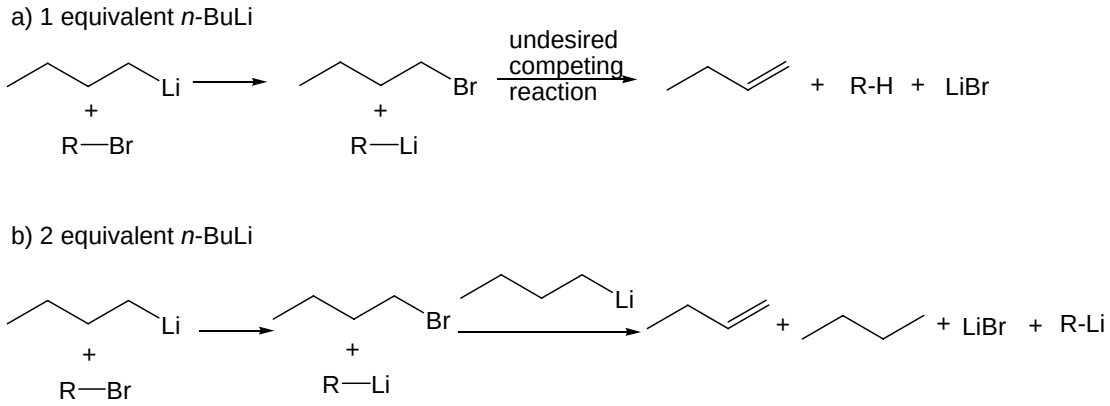

Scheme 3.3 E2 elimination during the lithium-halogen exchange.

In entry 1 Table 3.2, after 1 min of lithium-halogen exchange by *n*-BuLi, the reaction mixture was quenched by D_2O. We observed a trace of the starting material (1%), 31% of the protio-nitrile ***3*-8**, and 68% of the deuterio-nitrile ***3*-9**, both of which were racemic (entry 1, Table 3.2). When *sec*-BuLi was applied, the major product was the deuterio-nitrile ***3*-9** in 94% yield (entry 2, Table 3.2). The high conversion of the staring material within 1 min at -100 °C using 2.2 equiv. of RLi is consistent with the mechanism for halogen-metal exchange and E2 elimination shown in Scheme 3.3. Thus the recovered starting material, observed previously in reaction with 1.05 equiv *n*-BuLi (entries 1 and 2, Table 3.1), is a consequence of this dual role for *n*-BuLi.

Table 3.2 The lithium-halogen exchange/deuteration for (*S*)-(+)-***3*-6** at -100 °C.

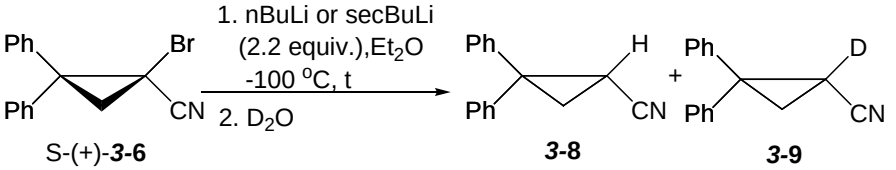

entry	R-M (base)	t (min)	***3*-6** mol.% (%ee)	***3*-8, *3*-9** mol.%[a] (%ee[b])
1	n-BuLi	1	1%	31%, 68% (1)
2	*sec*-BuLi	1	3%	3%, 94% (0)

[a] The mol.% was determined by ^{1}H NMR spectroscopy of reaction mixture (after workup) in $CDCl_3$. The protons at C1 and C3 of cyclopropyl ring feature distinguishable chemical shifts and the splitting which were used to identify components in the reaction mixture.
[b] The %ee is for ***3*-8** and ***3*-9**

The presence of the protio-nitrile ***3*-8** in entry 1 of Table 3.2, however suggests that E2 elimination of *n*-BuBr can be caused by both lithiated cyclopropylnitrile and *n*-BuLi, as shown in Scheme 3.4**.** The fact that lithium-bromine exchange of (*S*)-(+)-***3*-6** with *sec*-BuLi gives very little the protio-nitrile ***3*-8** (3%) suggests that the more basic *sec*-BuLi out-competes the lithiated cyclopropylnitrile ***3*-10** for deprotonation of 1-bromobutane.

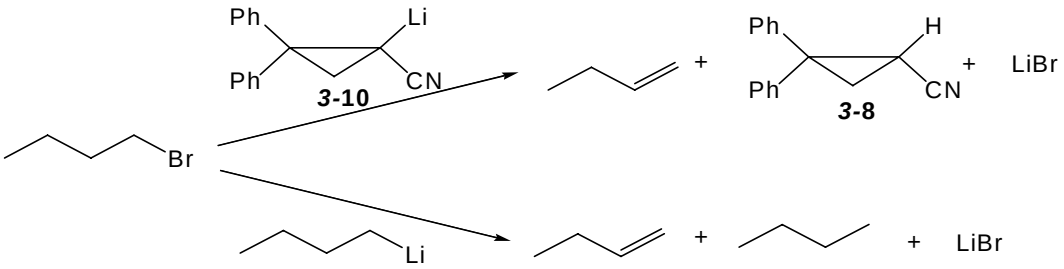

Scheme 3.4 E2 elimination of *n*-BuBr by lithiated cyclopropylnitrile ***3*-10** and *n*-BuLi.

Our proposed reaction pathway for lithium-halogen exchange/methylation using *n*-BuLi is shown in Scheme 3.5. Ate complexes, such as ***3*-11**, have been proposed as the intermediate for lithium-halogen exchange.[92] Lithiated cyclopropylnitrile ***3*-10** and

n-BuBr result from collapse of the ate complex. Because of the low barrier to inversion, the lithiated cyclopropylnitrile ***3*-10** is racemized before it can react with electrophiles. As we mentioned previously, during in situ exchange/methylation (Table 3.1), methylation competed with E2 elimination. Because only 1.05 equivalent *n*-BuLi was applied, insufficient *n*-BuLi existed to convert all the starting material (entries 1 and 2, Table 3.1). As noted earlier, in these reactions using 1.05 equiv. of *n*-BuLi, the recovered starting material was found to be racemic. To account for this observation, we propose that the lithiated intermediate ***3*-10** can react with remaining (*S*)-(+)-***3*-6** to form a new ate complex ***3*-12**.[161] Since this complex is formed from (*R/S*)-***3*-10**, and since formation of the ate complex should be reversible, a pathway now exists for racemization of the starting material.

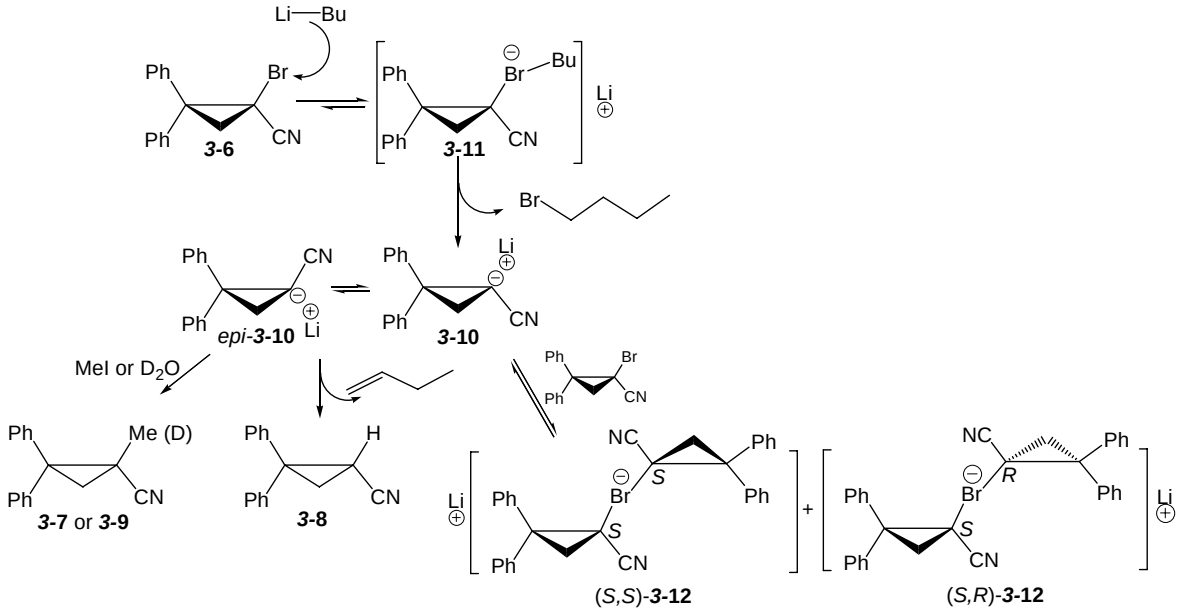

Scheme 3.5 Proposed reaction pathway for the lithium-halogen exchange/methylation using *n*-BuLi.

To support our proposed formation of the ate complex ***3*-12**, we performed the following experiments. The racemic protio-nitrile ***3*-8** was deprotonated by LDA in THF at -78 °C for 15 min, followed by adding the enantiomerically pure (*S*)-(+)-***3*-6** in THF for 30 min. This experiment was then repeated at -100 °C (entry 2, Table 3.3). Both reactions revealed that the recovered compound ***3*-6** was nearly racemic (9% ee). These results strongly suggest that a lithium-bromine exchange reaction occurred between the lithiated cyclopropylnitrile ***3*-10** and the bromonitrile ***3*-6**.

Table 3.3 Racemization of bromonitrile (*S*)-(+)-***3*-6** induced by lithiated cyclopropylnitrile ***3*-10**.

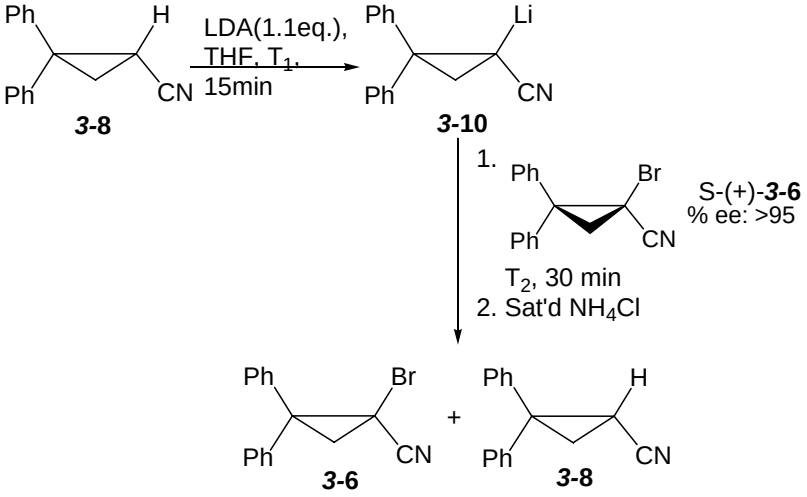

entry	T_1 (°C)	T_2 (°C)	recovered ***3*-6** mol.% (%ee)[a]	recovered ***3*-8** mol. %
1	-78	-78	73% (9)	87%
2	-78	-100	77% (4)	75%

[a] The mol.% was determined by ^{1}H NMR spectroscopy of reaction mixture (after workup) in $CDCl_3$. The protons at C1 and C3 of cyclopropyl ring feature distinguishable chemical shifts and the splitting which were used to identify components in the reaction mixture.

It is known that lithium-halogen exchange can also proceed through a single electron transfer (SET),[162] in which radical intermediates are invoked. We evaluated the possibility of a SET mechanism for the exchange reaction between ***3*-6** and ***3*-10**, as shown in

Scheme 3.6. In the SET mechanism, the single electron was transferred from ***3*-10** to (*S*)-(+)-***3*-6** in the first step (i) to afforded a radical cation ***3*-13** and a radical anion ***3*-14**. The dissociation (ii) of ***3*-13** and ***3*-14** led to a cyclopropyl radical ***3*-15**, Li^+ and Br^-. The cyclopropyl radical ***3*-15** would racemize immediately due to the low barrier expected for radicals.[163] Recombination (iii) could regenerate the radical cation ***3*-13** and the radical anion ***3*-14**. After the single electron transfer, racemic ***3*-6** and ***3*-10** would be formed. It is important to note that two cyclopropyl radicals ***3*-15** should also able to undergo radical dimerization (step v) and afford a dimer ***3*-16**.

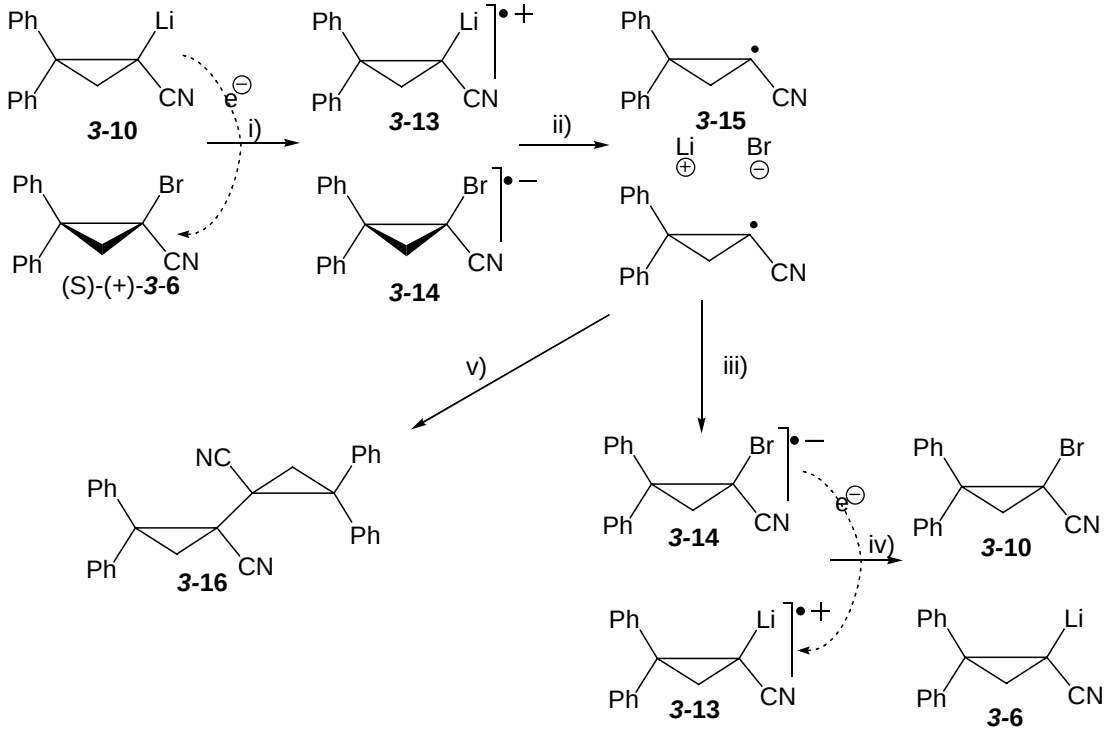

Scheme 3.6 The exchange reaction between ***3*-6** and ***3*-10** through SET mechanism.

We investigated the ^{1}H NMR of the crude product (Figure 3.4) which only showed cyclopropyl protons for the bromo nitrile ***3*-6** and that for the protio-nitrile ***3*-8**. There was no evidence for the presence of dimer ***3*-16** in the crude product which was expected

within 1.4 ppm-2.6 ppm.[164, 165] Therefore, although a SET racemization mechanism can not be ruled out, we find no evidence of the radical coupling products expected in such a mechanism.

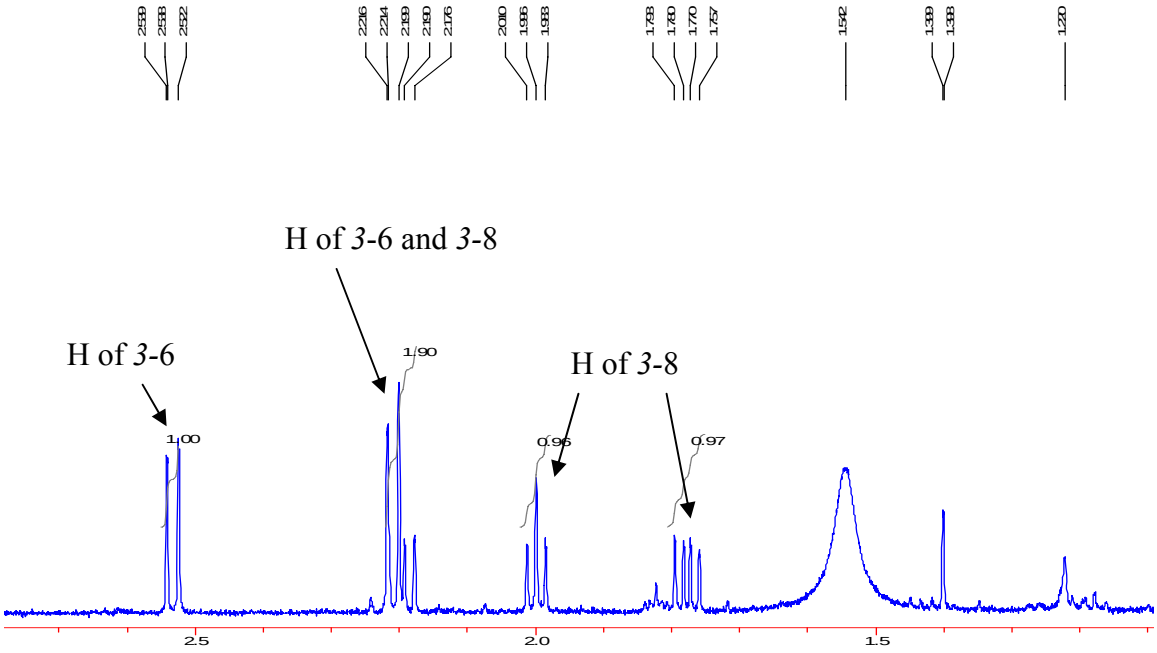

Figure 3.4 ^{1}H NMR spectrum ($CDCl_3$) of the crude product mixture from the exchange reaction between ***3*-6** and ***3*-10** (entry 2, Table 3.3).

3.5 Evaluation of configurational stability of magnesiated cyclopropylnitriles by magnesium-halogen exchange.

In order to understand the behavior of magnesiated cyclopropylnitriles, we investigated magnesium-halogen exchange/deuteration under various reaction time and temperatures. We used the 2.2 equivalents of Grignard reagents (*t*-BuMgCl, *i*-PrMgCl, EtMgBr and MeMgBr) to avoid E2 elimination between magnesiated cyclopropylnitriles and newly formed alkyl halides (such as *t*-butyl chloride, *iso*-propyl halide, or ethyl bromide). Note that although E2 elimination is impossible for CH_3Br, α-elimination to

the carbine is not impossible.

3.5.1 Evaluation of configuration stability of magnesiated cyclopropylnitriles formed from *i*-PrMgCl.

When *i*-PrMgCl was used for magnesium-halogen exchange at -135 °C, very little consumption of the starting material was observed, suggesting magnesium-bromine exchange is slow at this low temperature. The high enantiomeric excess of the recovered stating material (>95% ee) indicated that the racemization pathways observed in the presence of the lithiated nitrile might not be operative here (entry 1, Table 3.4). Meanwhile, the presence of some protio-nitrile ***3*-8** (14% yield, 87% ee) suggested that the E2 elimination was still possible at -135 °C, or that it occurred during the warm-up associated with the deuteration quench.

Table 3.4 Magnesium-halogen exchange/deuteration of enantiomerically pure ***3*-6**.

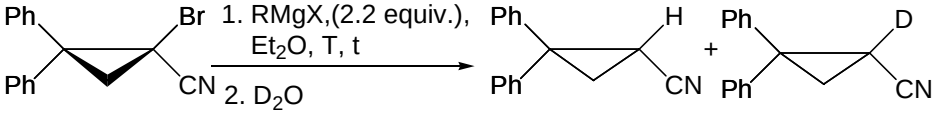

S-(+)-***3*-6**
%ee >95

***3*-8** ***3*-9**

entry	RMgX	T (°C)	t (min)	***3*-6** mol.% (%ee)[a]	***3*-8, *3*-9** mol.% (%ee)[a]
1[b]	*i*-PrMgCl	-135	1	87% (>95)	14%, 0% (87)
2	*i*-PrMgCl	-100	1	4%	6%, 90% (81)
3	*i*-PrMgCl	-100	5	5%	7%, 87% (79.2)
4	*i*-PrMgCl	-100	30	4%	8%, 89% (78.7)
5	*i*-PrMgCl	-100	180	1%	14%, 85% (67)

[a] The mol.% was determined by ^{1}H NMR spectroscopy of reaction mixture (after workup) in $CDCl_3$. The protons at C1 and C3 of cyclopropyl ring feature distinguishable chemical shifts and the splitting which were used to identify components in the reaction mixture.
[b] The solvent was Me_2O. The mixture of THF/Et_2O (3:2) and liquid N_2 reached -135 °C.

Interestingly, however when the reaction was repeated at -100 °C, 96% of the starting material was consumed, giving 90% deuterio-nitrile ***3*-9** and 6% protio-nitrile ***3*-8** (entry 2, Table 3.4). Furthermore, chiral stationary phase HPLC indicated 81% ee (retention) for the combined ***3*-8** and ***3*-9**. This result indicates that the magnesium-halogen exchange by *i*-PrMgCl is essentially complete within 1 min at -100 °C. When the magnesium-halogen exchange was allowed to proceed for 5 min, 30 min and 3 h, followed by quenching with D_2O (entry 3, 4, and 5, Table 3.4), the enantiomeric excess of the dominant deuterio-product ***3*-9** decreased slightly from 79 %ee to 67 %ee. Our proposed reaction pathway for exchange/deuteration reaction is shown in Scheme 3.7. When the Grignard reagent *i*-PrMgCl was added to the bromonitrile ***3*-6**, the magnesiated intermediate ***3*-17** was formed, followed by the deuteration. The loss of the enantiomeric purity could possibly occur during three steps. Firstly, the formation of the intermediate ***3*-17** might occur with partial loss of enantiomeric purity (step i); secondly, the intermediate ***3*-17** itself could racemize (step ii); finally, the deuteration (step iii) could occur with retention or the inversion (S_E2_{ret} or S_E2_{inv}). At the outset, it was not clear which step was responsible for the loss in % ee. However, by monitoring the % ee of ***3*-8** and ***3*-9** as a function of reaction time (before the quench), it is possible to determine the racemization rate of ***3*-17**.

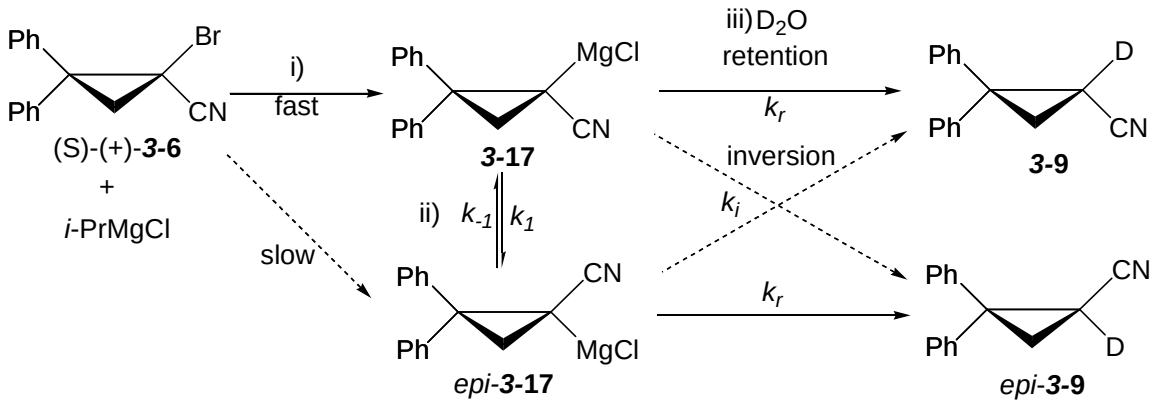

Scheme 3.7 Reaction pathway for the magnesium-halogen exchange/deuteration of (*S*)-(+)-***3*-6**.

The relationship of the enantiomeric excess of ***3*-17** and the reaction time was shown in the equation (1).[166] The relationship of the enantiomeric excess of ***3*-17** and ***3*-9** was demonstrated as the equation (2).

$$\ln [\%\ \text{ee}\ (\textbf{\textit{3}}\text{-}\mathbf{17})]_t = \ln [\%\ \text{ee}\ (\textbf{\textit{3}}\text{-}\mathbf{17})]_0 + k_{rac} \times t \qquad (1)$$

$$\%\ \text{ee}\ (\textbf{\textit{3}}\text{-}\mathbf{9}) = \frac{k_r - k_i}{k_r + k_i} \times \%\ \text{ee}\ (\textbf{\textit{3}}\text{-}\mathbf{17}) \qquad (2)$$

$$\Delta G^{\ddagger} = -RT[\ln(k_{rac}) + \ln(h/2kT)] \qquad (3)\ \text{Eyring equation}$$

The plot of In [%ee (***3*-9**)/100] *vs* time appeared linear as shown in Figure 3.5. As shown in the equation (1) and (2), we expected that the intercept of the line in Figure 3.5 was dependent on the initial stereospecificity of the magnesium-bromine exchange, as well as the rate constants of the retentive and the invertive electrophilic substitution. Although we did not know which factor contributed more to the value of the intercept, the value of the slope, which corresponded to the rate constant of the racemization of ***3*-17**, would be a constant at a certain temperature. The slope corresponding to $-k_{rac}$ of

***3*-17** indicated an estimated racemization $t_{1/2}$ of 11.3 h at -100 °C. Application of Eyring equation (3)[16] to the estimated k_{rac} for Grignard intermediate ***3*-17** indicated a barrier to inversion ($\Delta G^{\ddagger}_{rac}$) of 13.7 kcal/mol at -100 °C.

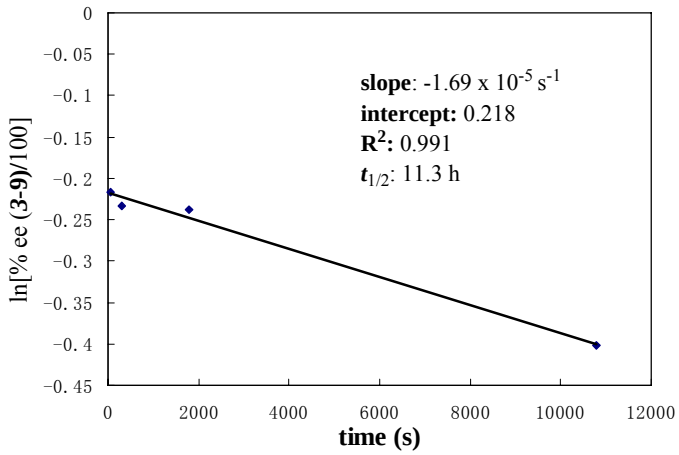

Figure 3.5 Estimation of the racemization rate of Grignard intermediate ***3*-17** at -100 °C.

We investigated the exchange/deuteration reaction at -78 °C, -42 °C and -21 °C. The yield of the protio-nitrile ***3*-8** at -42 °C and -21 °C, ranging from 14 % to 35% (entry 4-10, Table 3.5) suggested that the higher temperature facilitated the E2 elimination. Comparing the 1 min exchange/deuteration (entry 1, 4 and 9, Table 3.5), the enantiomeric excess of the deuterio-nitrile ***3*-9** decreased dramatically along with increase of temperature. The lowest value was 19 %ee for the deuterio-nitrile ***3*-9** at -21 °C (entry 9, Table 3.5).

Table 3.5 Magnesium-halogen exchange/deuteration by *i*-PrMgCl at various temperatures.

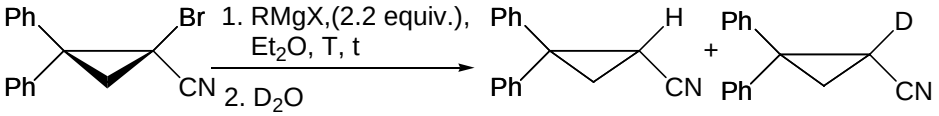

S-(+)-***3*-6**
%ee >95

***3*-8** ***3*-9**

entry	RMgX	T (°C)	t (min)	***3*-6** mol.% (%ee)[a]	***3*-8, *3*-9** mol.% (%ee)[a]
1	*i*-PrMgCl	-78	1	3%	7%, 90% (76)
2	*i*-PrMgCl	-78	5	3%	7%, 90% (75)
3	*i*-PrMgCl	-78	30	4%	9%, 88% (66)
4	*i*-PrMgCl	-42	1	2%	7%, 91% (60)
5	*i*-PrMgCl	-42	5	1%	11%, 88% (58)
6	*i*-PrMgCl	-42	30	11%	35%, 55% (49)
7	*i*-PrMgCl	-21	0.25	3%	13%, 85% (17)
8	*i*-PrMgCl	-21	0.5	1%	24%, 75% (20)
9	*i*-PrMgCl	-21	1	2%	29%, 69% (19)
10	*i*-PrMgCl	-21	5	2%	14%, 84% (6)

[a] The mol.% was determined by ^{1}H NMR spectroscopy of reaction mixture (after workup) in $CDCl_3$. The protons at C1 and C3 of cyclopropyl ring feature distinguishable chemical shifts and the splitting which were used to identify components in the reaction mixture.

The plot of ln (%ee /100) *vs* time was applied for the deuterio-nitrile ***3*-9** at -78 °C, -42 °C and -21 °C (Figure 3.6). The slope of each line, which corresponded to the racemization of ***3*-17**, demonstrated that the racemization was accelerated when the temperature increased. The Grignard intermediate ***3*-17** was still configurationally stable at -78 °C with a 2.3 h half-life; a moderate stability of ***3*-17** was observed at -42 °C with a 1.6 h half-life; however, the intermediate ***3*-17** racemized quickly at -21 °C with a 2.8 min half-life.

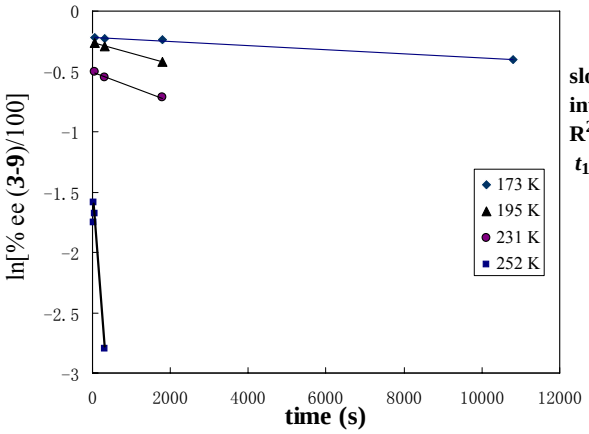

	173 K (-100 °C)	195 K (-78 °C)	231 K (-42 °C)	252 K (-21 °C)
slope	-1.69 x10^{-5}	-8.52 x 10^{-5}	-1.19 x 10^{-4}	-4.13 x 10^{-3}
intercept	-0.218	-0.265	-0.506	-1.54
R^2	0.991	1.0	0.995	0.958
$t_{1/2}$	13.7 h	2.3 h	1.6 h	2.8 min

Figure 3.6 Estimation of the racemization rate of Grignard intermediate ***3*-17** at -100 °C, -78 °C, -42 °C and -21 °C.

3.5.2 Evaluation of configurational stability of magnesiated cyclopropylnitriles by various Grignard reagents.

The widely divergent properties of the magnesiated cyclopropylnitrile relative to its corresponding lithium counterpart prompted us to explore the effectiveness of various Grignard reagents for magnesium-bromine exchange (Table 3.6). We found that the identity of Grignard reagents was very important for magnesium-halogen exchange.[115, 123] The best result was obtained when *i*-PrMgCl was used (entry 1 and 2, Table 3.6). The exchange was completed within 1 min at -100 °C and the deuterio-nitrile was obtained in high enantiomeric excess (81% ee) (entry 1, Table 3.6). Compared to *i*-PrMgCl (entry 2, Table 3.6) at -100 °C, the exchange/deuteration by *i*-PrMgBr afforded the similar mol.% of the deuterio-nitrile ***3*-9** but with less enantiomeric excess (67% ee) (entry 3, Table 3.6). Furthermore, the exchange by EtMgBr afforded 63% of the deuterio-nitrile ***3*-9** with 61% ee and recovered 37% of the starting material (entry 4 Table 3.6). More racemization was

found in the exchange reaction by MeMgBr which led to a 13 mol.% of the deuterio-nitrile ***3*-9** with 24% ee (entry 6, Table 3.6). The significantly different enantiomeric excess of the deuterio-product ***3*-9**, obtained by various Grignard reagents at -100 °C, suggested that the initially enantiomeric excess of the formed intermediate ***3*-17** depended on the type of Grignard reagents.[115] Meanwhile, the racemization did occur during the formation of the intermediate ***3*-17** (step i, Scheme 3.7).[102] Surprisingly, *t*-BuMgCl did not undergo magnesium-bromine exchange (entry 7 and 8, Table 3.6) at -100 °C and -78°C.

Table 3.6 Magnesium-halogen exchange/deuteration of (*S*)-(+)-***3*-6** by various Grignard reagents.

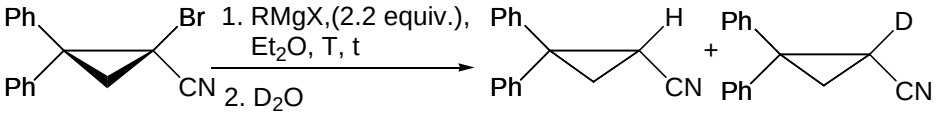

S-(+)-***3*-6**
%ee >95

***3*-8** ***3*-9**

entry	RMgX	T (°C)	t (min)	***3*-6** mol.% (%ee)[a]	***3*-8, *3*-9** mol.% (%ee)[a]
1	*i*-PrMgCl	-100	1	4%	6%, 90% (81)
2	*i*-PrMgCl	-100	30	3%	8%, 89% (79)
3	*i*-PrMgBr	-100	30	1%	14%, 86% (67)
4	EtMgBr	-100	30	37% (88)	5%, 63% (61)
5	MeMgBr	-100	5	87% (90)	0%, 13% (24)
6	MeMgBr	-78	5	65% (89)	8%, 27% (29)
7	*t*-BuMgCl	-100	30	98 (>95)	<2% combined
8	*t*-BuMgCl	-78	30	98 %(>95)	<2% combined

[a] The mol.% was determined by ^{1}H NMR spectroscopy of reaction mixture (after workup) in $CDCl_3$. The protons at C1 and C3 of cyclopropyl ring feature distinguishable chemical shifts and the splitting which were used to identify components in the reaction mixture.

3.5.3 Alkylation of the configurationally stable magnesiated cyclopropylnitrile *3*-17.

We found that the magnesiated cyclopropylnitrile intermediate ***3*-17** was configurationally stable during exchange/deuteration at -100 °C (11.3 h half life) and -78 °C (2.3 h half life). Therefore, we attempted alkylation under those conditions; results are listed in Table 3.7. Unfortunately, the intermediate ***3*-17** had very low reactivity towards electrophiles other than D_2O/H_2O. The reactions at -78 °C did not evidence formation of any alkylated products, when MeI, BnBr and MeOTf were used as electrophiles (entries 1-3, Table 3.7). A small amount of racemic methylated product ***3*-7** was obtained at -42 °C (entry 4, Table 3.7). Since the protio- ***3*-8** and the deuterio- products ***3*-9** were observed in 41% ee under these conditions (entry 4 Table 3.7), it appears that the methylation occurs *via* both retentive and invertive pathways; perhaps a SET mechanism is operative.[123]

Table 3.7 Alkylation of magnesiated intermediate ***3*-17**.

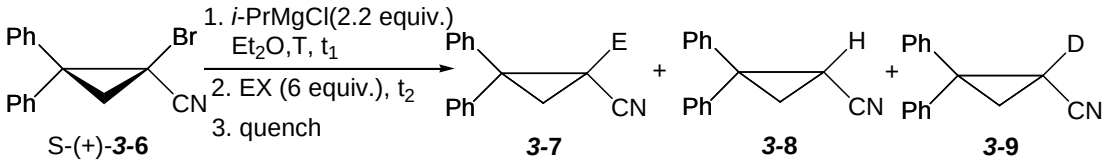

S-(+)-***3*-6**
%ee >95

***3*-7** ***3*-8** ***3*-9**

entry	E-X	Temp. (°C)	t_1, t_2 (min)	quench	***3*-6** mol.%[a] (%ee)	***3*-7** mol.%[a] (%ee)	***3*-8, *3*-9** mol.%[a] (%ee)
1	CH_3I	-78	1, 30	NH_4Cl	1%	0%	99%
2	BnBr	-78	1, 30	NH_4Cl	3%	0%	97%
3	MeOTf	-78	1, 30	NH_4Cl	19%	0%	81%
4	MeOTf	-42	2, 30	D_2O	2%	8% (6)	18%, 72% (41)

[a] The mol.% was determined by ^1H NMR spectroscopy of reaction mixture (after workup) in $CDCl_3$. The protons at C1 and C3 of cyclopropyl ring feature distinguishable chemical shifts and the splitting which were used to identify components in the reaction mixture.

3.6 Conclusion.

By investigating metal-bromine exchange on the enantiopure bromonitrile ***3*-6**, we found different behaviors of lithium-halogen and magnesium-halogen exchange. The in situ lithium-halogen exchange/methylation by *n*-BuLi (1.05 equiv.) led to a racemic mixture of the methylated product ***3*-7**, the protio-nitrile ***3*-8**, and the starting material ***3*-6**. Treatment of the racemic lithiocyclopropylnitrile with the enantiomerically pure bromocyclopropylnitrile ***3*-6** caused racemization of the bromonitrile ***3*-6**. We proposed that the racemization of the starting material ***3*-6** was due to the reversible formation of the ate complex ***3*-12**.

The Grignard intermediate ***3*-17**, formed by magnesium-halogen exchange using *i*-PrMgCl, was configurationally stable during exchange/deuteration at -100 °C. The kinetic study revealed that the racemization barrier of ***3*-17** was 13.7 kcal/mol at -100 °C leading to a racemization half life of 11.3 h. The different enantiomeric excess of the deuterio-nitrile ***3*-9**, obtained by various Grignard reagents (*i*-PrMgCl, *i*-PrMgBr, EtMgBr, MeMgBr, and *t*-BuMgCl), suggested that the configurational stability of the newly formed Grignard intermediate depended on the type of counter ion.[115] Meanwhile, the initial enantiomeric excess of the newly formed Grignard intermediate was related to the type of Grignard reagents used for exchange. We propose that the racemization can occur during the formation of the magnesiated cyclopropylnitrile. However, to date, the Grignard intermediate ***3*-17** had a very low reactivity with electrophiles other than H_2O/D_2O.

3.7 Future work.

The Grignard intermediate ***3*-17** showed an excellent configurational stability. However, our experiments suggested that the initially formed Grignard intermediate was not enantiomerically pure. Racemization occurred during the formation of the Grignard intermediate ***3*-17**. It is important to understand the relationship between configurational stability of Grignard intermediates and magnesium reagents used for Mg/Br exchange. This configurationally stable Grignard intermediate ***3*-17** will be useful for enantioselective or diastereoselective reactions. Therefore, the study of reactivity of the Grignard intermediate ***3*-17** will be explored by various electrophiles and by transmetallation. Finally, we would like to evaluate Mg/Br exchange reactions of ester and amide analogs of bromonitrile ***3*-6**. It is possible that pyramidalized enolates will be formed following halogen-metal exchange, and we would propose to study their configurational stability.

As we know, halogen-magnesium exchange reaction is reversible. The exchange will be favorable when the reaction is exothermic. The Mg/Br exchange reaction will shift to the right if the starting Grignard reagent is more basic than the newly formed organomagnesium intermediate. Based on the different basicity of organomagnesium reagents, Knochel and his co-workers successfully prepared many functionalized Grignard reagents by exchange reactions of aryl halide/heteroaryl halides and alkylmagnesium halides. Hoffmann reported 1,1-diiodoalkane underwent the Mg/I exchange, in which the iodo group might stabilize the newly formed organomagnesium

intermediate. Our studies demonstrated that the bromonitrile ***2*-6** successfully underwent the moderate stereospecific Mg/Br exchange. It will be valuable to understand a driving force of this reaction and the origin of stereospecificity (for example, ring strain and nitrile group). Therefore, we would like to evaluate the Mg/Br exchange of 2,2-disubstituted cyclopropylbromide, 2,2-disubstituted 1-alkynyl-cyclopropylbromide, and its acyclic analogs.

Chapter 4 Conformational control of acyclic compounds

4.1 Introduction.

Conformations are structures that differ due to a change of torsion angles. Stable conformations that are located at energy minima are called "conformational isomers" or "conformers". This chapter will present a brief overview of acyclic compounds with a focus on rotation about sp^3-sp^3, and sp^2-sp^3 single bonds.

4.2 Conformation of acyclic compounds: rotation of a sp^3-sp^3 bond

4.2.1 Rotation of CH_3-CH_3.

Ethane provides the simplest example of acyclic conformation. Kemp and Pitzer first established the shape of the internal energy profile for ethane in 1936, showing that it has three energy minima corresponding to the most stable staggered conformer (Figure 4.1).[167] Early measurement of heat capacities by Pitzer pointed to an effective rotation barrier in ethane of 1006 cm^{-1} (2.87 kcal/mol).[168] Since then, the barrier height of rotation about the C-C bond in ethane was investigated by IR (1024 cm^{-1}),[169] microwave (1008 cm^{-1}),[170] and Raman spectroscopy (1012 cm^{-1}).[171] An *ab initio* method (QCISD(T) or CCSDT) was attempted to predict the internal rotation barrier of ethane (about 960 cm^{-1}).[172, 173]

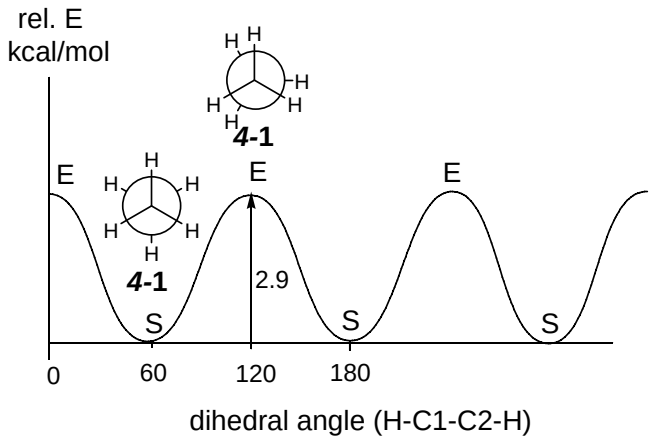

Figure 4.1 Conformation of ethane ***4*-1**.

Considerable activity has also focused on understanding the physical origin of this barrier. Three principal physical factors –electrostatic (Coulomb interaction), exchange (Pauli repulsion), and hyperconjugative interactions, are considered to be the forces that hinder internal rotations of ethane. Note that the van der Waals repulsion (or so-called steric repulsion) is caused by electrostatic and exchange interactions.

Electrostatic interaction (Coulomb interaction) involves the repulsion between the charge distributions of the CH bonds at each end of the molecule. Evaluation of the CH bond dipole moments was attempted, and then the barrier could be calculated from electrostatics.[174] However, the theoretical determination of atomic charges and bond moments has been problematic because of the difficulty of precisely defining "atomic" and "bond" components of polyatomic wave functions.[175] Pophristic and Goodman estimated the effect of Coulomb repulsion by comparing its torsional angle dependence for rigid rotation, partially relaxed rotation, and fully relaxed rotation.[176] The C-C bond stretching led to a large decrease in electrostatic repulsion energies. Thus, Goodman

proposed that Coulomb repulsion was not the origin of the staggered structural preference in ethane.[176] Baerends evaluated the Coulomb repulsion by an electronic-structure analysis method, and suggested that the origin of steric repulsion was not caused by electrostatic repulsion between electron charge clouds and nuclei.[177] However, by using density functional theory, Sadlej-Sosnowska reported that Coulomb energies (sum of the attraction and repulsion) contributed 115.8 % of the total electron-electron repulsion whereas only -14.7 % of total electron-electron repulsion was from exchange.[178]

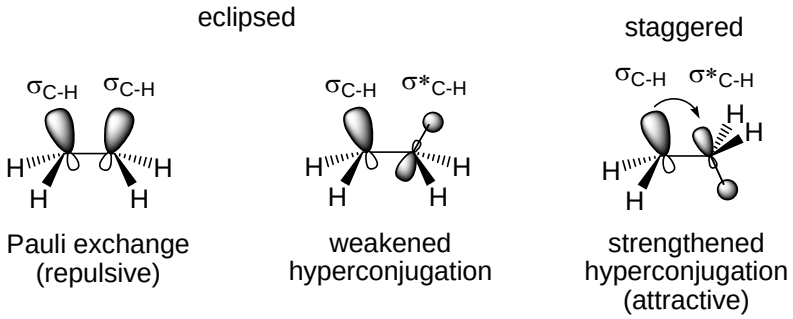

Figure 4.2 Pauli exchange, and hyperconjugation for explaining the preference for the staggered conformer of ethane.

Pitzer suggested that the overlap (exchange) repulsion between the bond orbitals due to the Pauli exclusion principle was the primary factor in the rotational barrier (Figure 4.2).[179, 180] More recently, Baerends reinvestigated the rotation round the C-C bond in ethane employing an electronic-structure analysis method, which started the formation of the C-C bond between two "prepared" methyl fragments.[177] The total bond energy was given in the sum of Pauli repulsion, electrostatic interaction, and orbital-interaction (hyperconjugation). The rotation of the C-C single bond with fixed bond length and methyl geometry led to 2.54-2.60 kcal/mol of Pauli repulsion. The sum energies of

electrostatic interaction and orbital-interaction added only 0.07 kcal/mol to the barrier energy with these geometry constrains. Baerend's analysis suggested steric repulsion (mainly Pauli repulsion) as the cause of the internal rotation barrier.[177]

Weinhold, Pophristic and Goodman recently aroused awareness of hyperconjugative interaction (Figure 4.2) accompanying internal rotations.[176, 181, 182] The hyperconjugation involved the electron transfer from a filled orbital to an unoccupied orbital, leading to delocalization of negative charges. The mixing of adjacent σ_{CH} — σ^*_{CH} orbitals was more favorable when ethane adopts the staggered rather than the eclipsed conformation (Figure 4.2).[176, 181] In addition, Pophristic and Goodman suggested that the steric repulsion in ethane were only of secondary importance and actually favored the eclipsed conformer.[176] Therefore, Weinhold, Pophristic and Goodman concluded that the hyperconjugation was primary reason for the stability of staggered conformations.

4.2.2 Rotation of XCH_2-CH_2Y.

4.2.2.1 Butane and higher alkanes (X , Y are alkyl groups)

A thermodynamic study of conformations of butane ***4*-2** was reported by Pitzer in 1940.[183] Following pioneering work of Pitzer, extensive research on the conformer enthalpy difference of *n*-butane were performed by means of Raman spectroscopy,[184, 185] NMR coupling constants and chemical shifts,[186] and ultrasonic relaxation rates,[187] and electron diffraction.[188] Due to experimental difficulties, increasing *ab initio* theoretical methods have been applied to investigate the butane torsional potential.[189-191] It is clear

that on the potential surface the *anti*-conformation is the lowest in energy with respect to the rotation of the central C-C bond. The *gauche* conformation, with a torsional angle near 60 °C (positive or negative), is about 0.8 kcal/mol higher in energy, while the highest energy (about 5.0 kcal/mol) corresponds to the *syn* or *cis* conformation with two eclipsed methyl groups. The two lower mirror-image maxima separate the *anti* conformation from the two *gauche* forms and are found at about 3.2 kcal/mol relative energy.

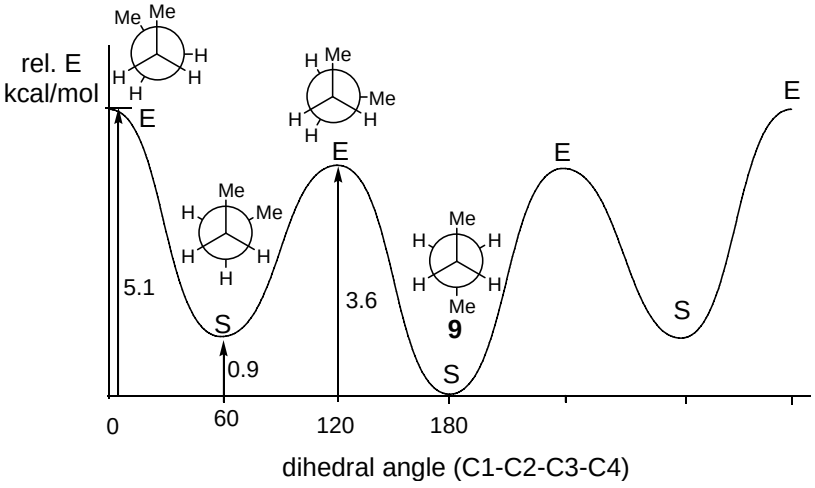

Figure 4.3 Conformations of butane ***4-2***.

Unlike ethane, the hindered rotation of *n*-butane seems to originate primarily from steric interaction (van de Waals repulsion) between the two methyl groups.[192] The steric interaction in butane and higher *n*-alkanes is minimized by adopting an *anti* conformation rather than a *gauche* conformation.[189] Some exceptions occur for branched alkanes, such as 2,3-dimethylbutane ***4-3***, which is nearly equal in enthalpy for *anti*- and *gauche*-conformations.[193] The bond angle of CH3-C1-C2 in 2,3-dimethylethane was found to be about 114 °, which was larger than the corresponding angle C1-C2-H (109 °) in butane (Figure 4.4).[194] As a result, the disordered *anti*- and *gauche*- conformation (Figure 4.4) of

2,3-dimethylbutane would enhance van der Waals repulsion in the *anti* conformer (A) but would diminish it in the *gauche* conformer (G).[194]

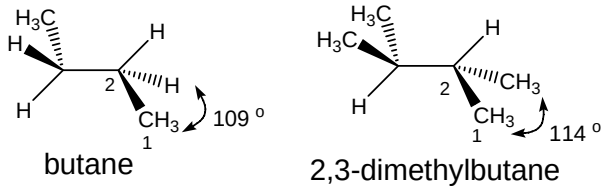

Newman projections for the conformer 2,3-dimethylbutane ***4*-3**

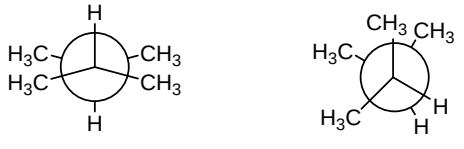

disordered *anti* disordered *gauche*

Figure 4.4 Disordered *anti* and *gauche* conformation of 2,3-dimethylbutane.

4.2.2.2 Saturated acyclic molecules with polar substituents (X or Y are polar substituents).

The electrostatic interaction, one of the physical factors hindering the internal rotation of acyclic molecules, can be evaluated by dipole moments of interested bonds. Molecules with polar substituents (XCH_2-CH_2Y) possess substantial dipole moments, and consequently respond to the electrostatic interaction. Many researchers have focused on the conformational equilibrium (*anti*/*gauche*) of 1,2-dihaloethanes. The *anti/gauche* enthalpy difference for 1,2-dibromoethane in gas phase ranged from 1.4 kcal/mol to 1.8 kcal/mol (entry 1, Table 4.1).[195, 196] The presence of a fluoro group in 1-fluoro-2-bromoethane significantly decreased the enthalpy difference to 0.57 kcal/mol (entry 3, Table 4.1).[197] 1,2-Dichloroethane showed slightly lower *anti/gauche* enthalpy

difference (0.9-1.3 kcal/mol, entry 4, Table 4.1),[198, 199] compared to 1,2-dibromoethane. The *gauche* conformer of 1-fluoro-2-chloroethane was only 0.44 kcal/mol higher in enthalpy than the *anti*-conformer (entry 5, Table 4.1).[197, 199, 200] Interestingly, the *gauche* conformation of 1,2-difluoroethane was preferred instead of the *anti* conformation. The energetic difference between *gauche* and *anti* conformations is about 0.6~0.8 kcal/mol (entry 6, Table 4.1).[201, 202]

Table 4.1 The *anti/gauche* enthalpy difference of 1,2-dihaloethane in gas phase.

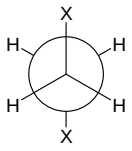

anti

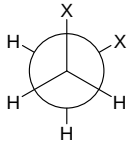

gauche

entry	compound	enthalpy difference of *anti/gauche* conformers in gas phase (kcal/mol)	
		Observ.	Calc.
1	1,2-dibromoethane (***4*-4)**	1.4-1.8 (g)[195]	1.57 [196]
2	1-bromo-2-chloroethane (***4*-5)**	1.34 (g)[197]	-
3	1-bromo-2-fluoroethane (***4*-6)**	0.57 (g)[197]	-
4	1,2-dichloroethane (***4*-7)**	0.9-1.3 (g)[198]	1.55[199]
5	1-chloro-2-fluoroethane (***4*-8)**	0.44[197]	0.38 [199]
6	1,2-difluoroethane (***4*-9)**	-0.6 ~ -0.8 (g)[201, 202]	-0.2 [203]

The large *anti/gauche* enthalpy difference of XCH_2CH_2Y (X, Y = Br or Cl) is ascribed to strong dipole-dipole repulsion (electrostatic interaction) of the C-X dipoles in the *gauche* conformation.[198] The *gauche* preference of 1,2-difluoroethane is attributed to the "gauche effect".[204] Because of the high electronegativity of fluorine, withdrawal of electrons in the C-F bond partially emptied the 2p orbital on carbon and thus facilitated hyperconjugative electron delocalization from the pseudo π system of the adjacent CH_2

group into the C-F σ* orbital.[205] This hyperconjugation was likely to be more effective in the *gauche* conformation than in the *anti* conformation (Figure 4.5).[206, 207] An alternative explanation of the "gauche effect" was given by Wiberg in bent-bond contributions to the σ part of the C-C bond which destabilized the *anti*- species relative to the *gauche* form.[208] According to Wiberg's model, the electronegative fluorine atom caused an increased *p* character in the C-F bond and thus a reduced angle between the carbon orbital pointing toward the other carbon atom and the fluorine atom. In the *anti* conformation, the C-C bond paths were bent in opposite directions, whereas in the *gauche* form they were bent in the same direction (Figure 4.5). The former (opposite bending) led to decreased overlap for σ part of the C-C bond and a poorer bond. Similar *gauche* preference is found in $NCCH_2$-CH_2CN ***4*-10**, XCH_2-CH_2CN ***4*-11** [209] and 1,2-dimethoxyethane ***4*-12**.[210]

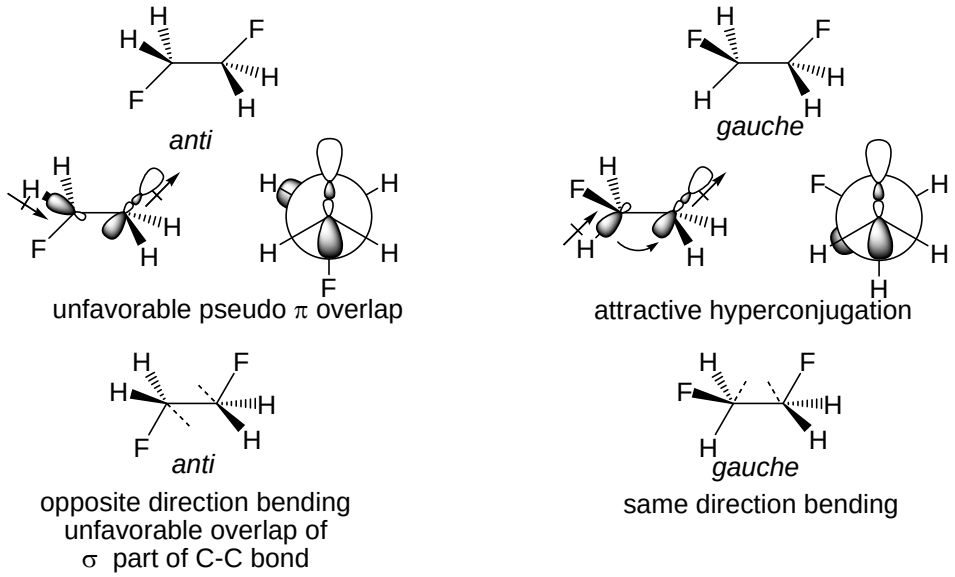

Figure 4.5 Origin of "gauche effect" in 1,2-difluoroethane: hyperconjugation or bond-bent.

Intramolecular hydrogen-bonding can also influence conformational preferences. For example, *syn* β-hydroxy ketones ***4*-13** are able to form intramolecular H-bonding in

conformation ***4*-13**A and ***4*-13**B (Table 4.2). The actual conformer population depends strongly on the nature of R1, R2 and R3. When R1 and R2 groups are small or medium in size, the conformations ***4*-13**B and ***4*-13**A should be populated leading to a vicinal coupling constant in range of 2-6 Hz (entries 1-2, Table 4.2). As the size of either the R1 or R2 group increases, the R1-R2 *gauche* interaction becomes more penalizing and the conformation ***4*-13**C will be most populated form. As shown in Table 4.2, when R_2 is *t*-butyl, the vicinal coupling constant is 10.1 Hz (entry 4, Table 4.2), which demonstrates the major conformation to be ***4*-13**C.[211, 212]

Table 4.2 Vicinal coupling constant J_{AB} of *syn* β-hydroxy ketones ***4*-13**

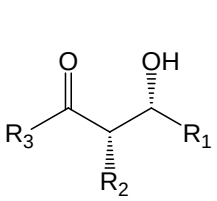

***4*-13**

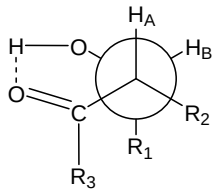

***4*-13A**

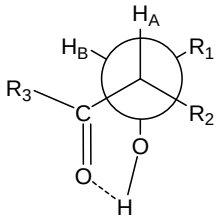

***4*-13B**

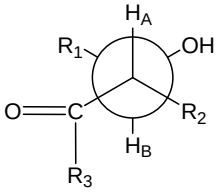

***4*-13C**

entry	R_1	R_2	R_3	J_{AB}, (Hz)
1	Ph	Me	MeO	4.7
2	Ph	Et	MeO	6.2
3	Ph	*i*-Pr	MeO	8.2
4	Ph	*t*-Bu	MeO	10.1

4.2.3 Pentane – avoidance of *syn*-pentane interaction.

The conformation of *n*-pentane ***4*-14** is more complicated than that of butane because it involves the rotation of two CH_2-CH_2 bonds. Although there are nine staggered conformations rising from the rotation of C2-C3 and C3-C4 bonds (Figure 4.6), degeneracies reduce this number to four conformations of different enthalpy, the

low-lying aa, the intermediate $(ag)^{\pm}$, the high-lying $(gg)^{\pm}$, and the unstable g^+g^-. The energetic penalty of g^+g^- conformation is caused by the severe van der Waals repulsive interaction of the methyl groups. This repulsive interaction is called "*syn*-pentane interaction" or "1,3-dimethyl eclipsing interaction", which is well known in the form of the 1,3-diaxial interaction in cyclohexane derivatives. *Ab initio* methods estimated a 3.2-3.3 kcal/mol energy increase for the *syn*-pentane interaction relative to the most stable aa conformation.[189, 213, 214] An evaluation of X-ray structural analyses of 30 arbitrarily chosen compounds containing the partial structure ***4*-15** and ***4*-16** (Figure 4.6) showed that, in 46 out of 51 of these structural elements, the specific conformation adopted is one in which the *syn*-pentane interaction is avoided.[215]

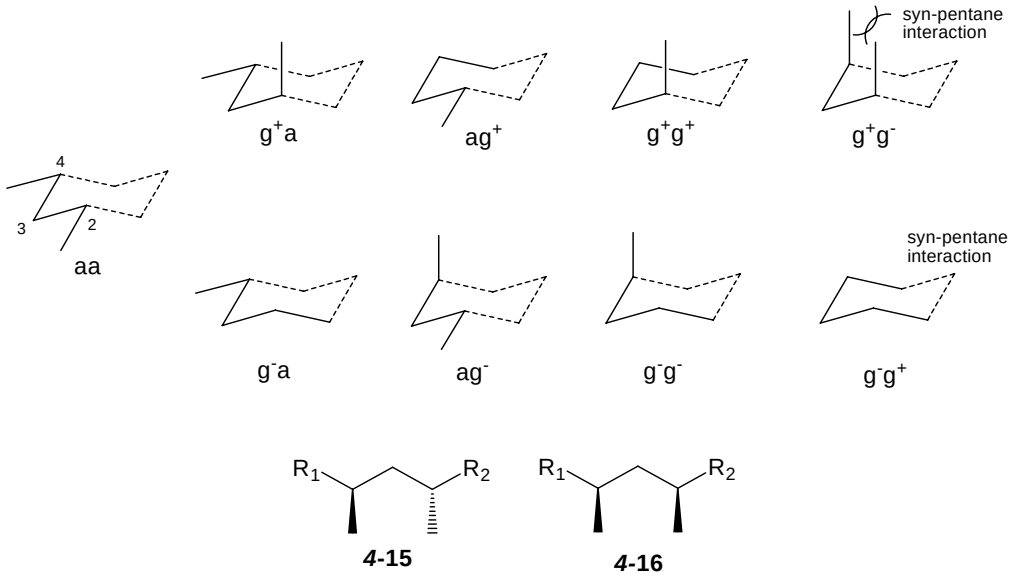

Figure 4.6 Avoidance of *syn*-pentane interaction in *n*-pentane, ***4*-15** and ***4*-16**

4.3 Conformation of unsaturated acyclic compounds: rotation of a sp^3-sp^2 bond

Three types of conformations about a sp^3-sp^2 bond can be envisioned, as shown in Figure 4.7. Conformations E are those in which the double bond C=X is eclipsed with

one of single bonds C-S, C-M or C-L respectively (with trends in size: S ≤ M ≤ L). When that double bond bisects two single bonds, the resulting conformation B is called "bisected conformation". Finally, in conformation P, the double bond is perpendicular to one of single bonds. If the X group is small and Y is large in size, conformations E will correspond to energy minima and conformations B will correspond to energy maxima. Therefore, the barrier is three fold and the highest barrier is dependent on the size of group S, M, L. In the case that conformation P with a large X group is energy minima, the rotational barrier is sixfold.

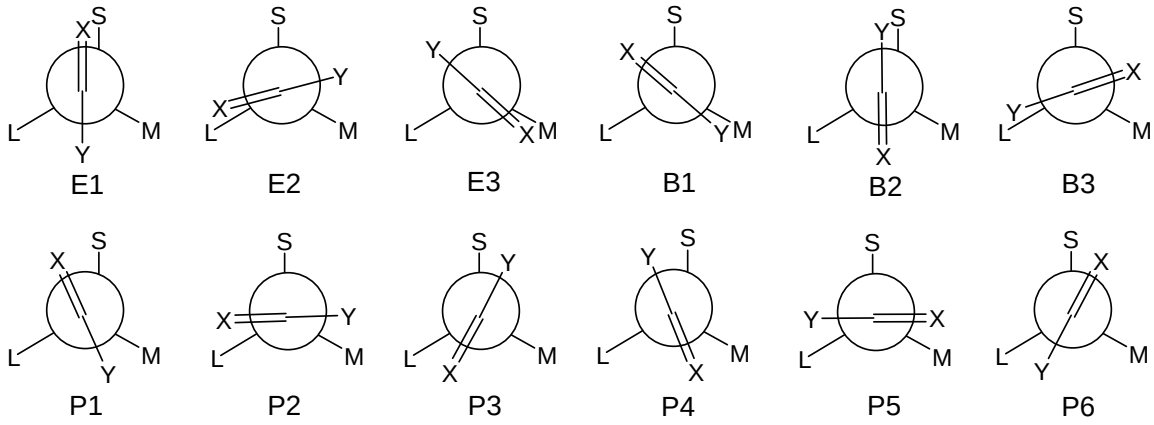

Figure 4.7 Conformation of unsaturated compounds: rotation of sp^3-sp^2 bond.[216]

4.3.1 Propene – preference of eclipsed conformation

The conformation of propene ***4*-17** is defined by rotation about the CH_3-$CH{=}CH_2$ single bond, and according to our previous classification, S = M = L = hydrogen. In addition, X = CH_2 and functions as a small group. Thus, two conformations arise from the rotation about the C2-C3 single bond: eclipsed and bisected conformation. As shown in Figure 4.8, the eclipsed conformation is lowest in energy, with the bisected

conformation 2 kcal/mol higher in energy.[217] In addition to steric arguments already presented, the eclipsed conformation allows for better overlap of the orbital for stabilizing $\sigma_{C\text{-}H} \rightarrow \pi^*_{C=C}$ hyperconjugation/σ-conjugation.[218]

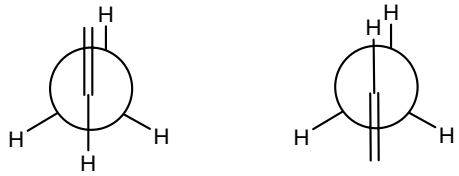

eclipsed
0 kcal/mol

bisected
2 kcal/mol

Figure 4.8 Conformation of propene ***4*-17**.

4.3.2 1-Butene.

In 1-Butene ***4*-18** (S = M = hydrogen, L = CH_3, X = CH_2), there are two possible eclipsed conformations E1 and E2 (Figure 4.9), in which H and CH_3 eclipse the CH_2 group respectively. The energies of these two eclipsed conformations are very similar, with E1 (0.53 kcal/mol) higher in energy for steric reasons.[219, 220] Similarly, two bisected transition structures B1 and B2 exist; the later one is highest in energy due to an eclipsing interaction called allylic 1,2-strain The barrier to rotation in 1-butene is 1.74 kcal/mol reflecting the energy difference between the E1 and B1 conformation.[221]

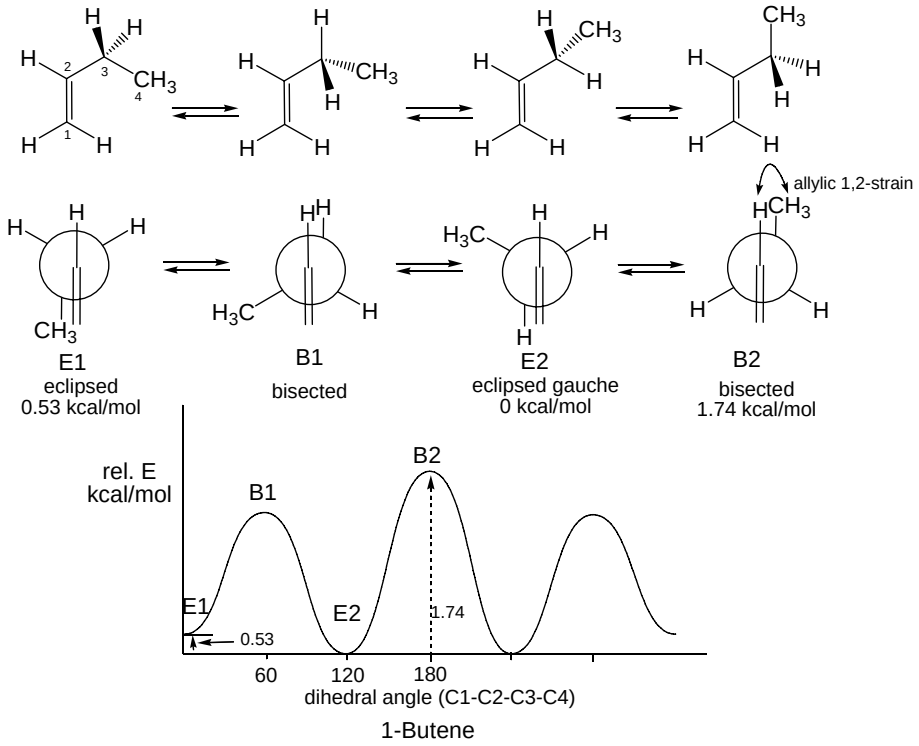

Figure 4.9 Conformation of 1-butene ***4*-18**.

4.3.3 E-2-pentene and Z-2-pentane.

2-Pentene ***4*-19** (S = M = hydrogen, L = CH_3, X = $CHCH_3$) has E and Z isomers which possess different energy profiles as shown in Figure 4.10. For E-2-pentene, two eclipsed conformations, E1 (0.6 kcal/mol) and E2 (0 kcal/mol) correspond to local minima while two bisected conformation B1 (2.12 kcal/mol) and B2 (2.45 kcal/mol) correspond to local maxima in energy profile.[222] In Z-2-pentene, the global minimum is found for the eclipsed conformations, E2. In contrast, the other eclipse conformation E1 is localized at 4.03 kcal/mol because of allylic 1,3-strain between two methyl groups.

Unlike E-2-pentene, the global maximum of Z-2-pentene is the roughly perpendicular conformation P with a 17° of dihedral angle C2-C3-C4-C5. The bisected conformation B2 is only 1.05 kcal/mol in energy relative to the E2 conformation.

However, the bisected conformation B1 does not correspond to a maximum or minimum.

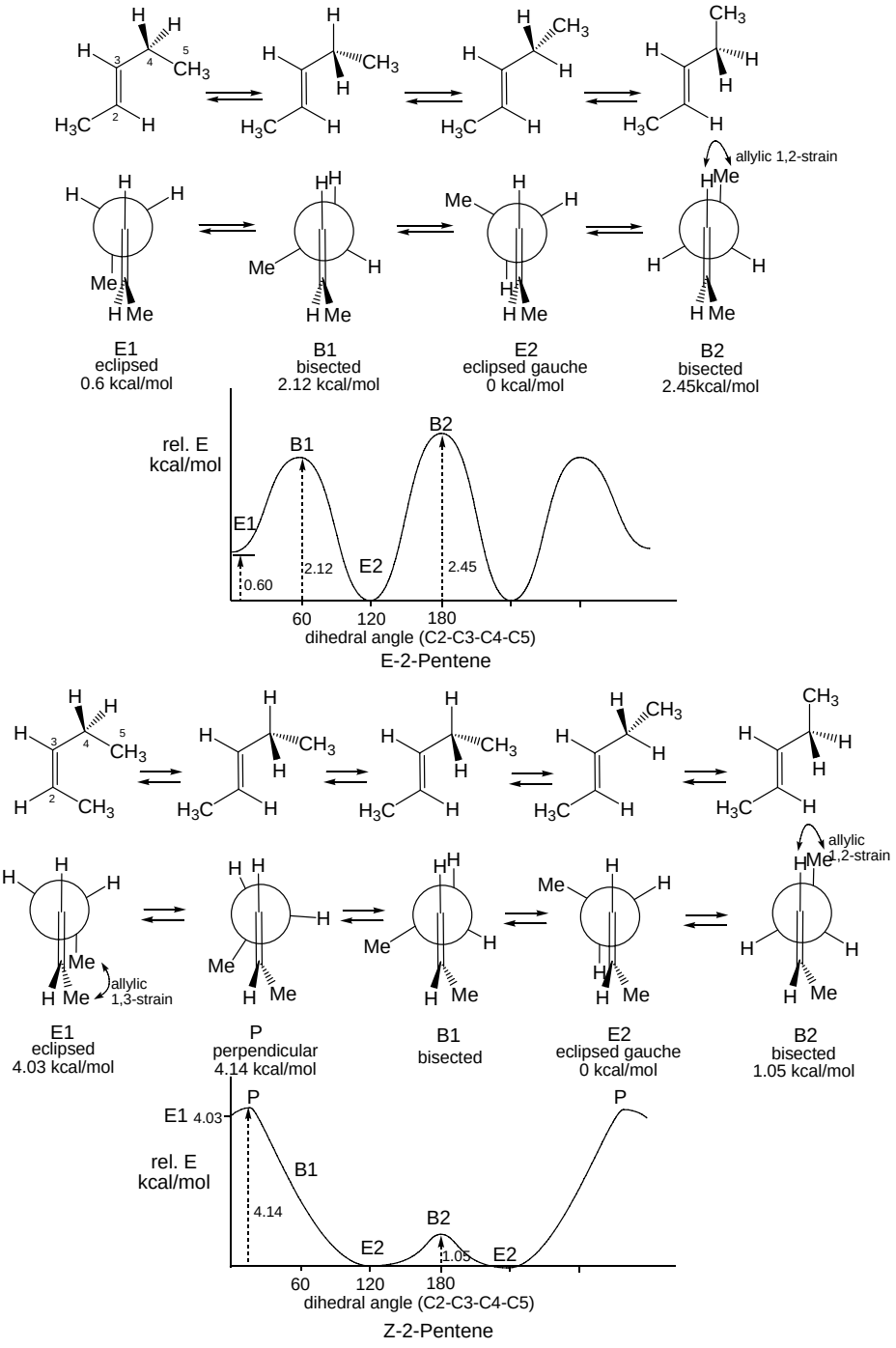

Figure 4.10 Conformation of E-2-pentene and Z-2-pentene ***4*-19**.

4.3.4 (Z)-4-Methyl-2-pentene

A quite different situation is found for (Z)-4-methyl-2-pentene ***4*-20**. A roughly perpendicular conformation (P), two eclipsed conformations (E1 and E2), and two bisected conformations (B1 and B2) can be envisioned in (Figure 4.11). The perpendicular conformation P, with 20° of the dihedral angle C2-C3-C4-C5, is found to be the maximum (4.86 kcal/mol) in energy profile. The eclipsed conformation E2 is the global minima. In contrast, the E1 conformation proved to be higher in energy compared to E2 due to allylic 1,3-strain resulting from steric interaction between the CH_3 groups. Bisected conformation B1 is another minimum at 3.4 kcal/mol.[223] Lastly, conformer B2 is neither a maximum nor a minimum in the energy profile.

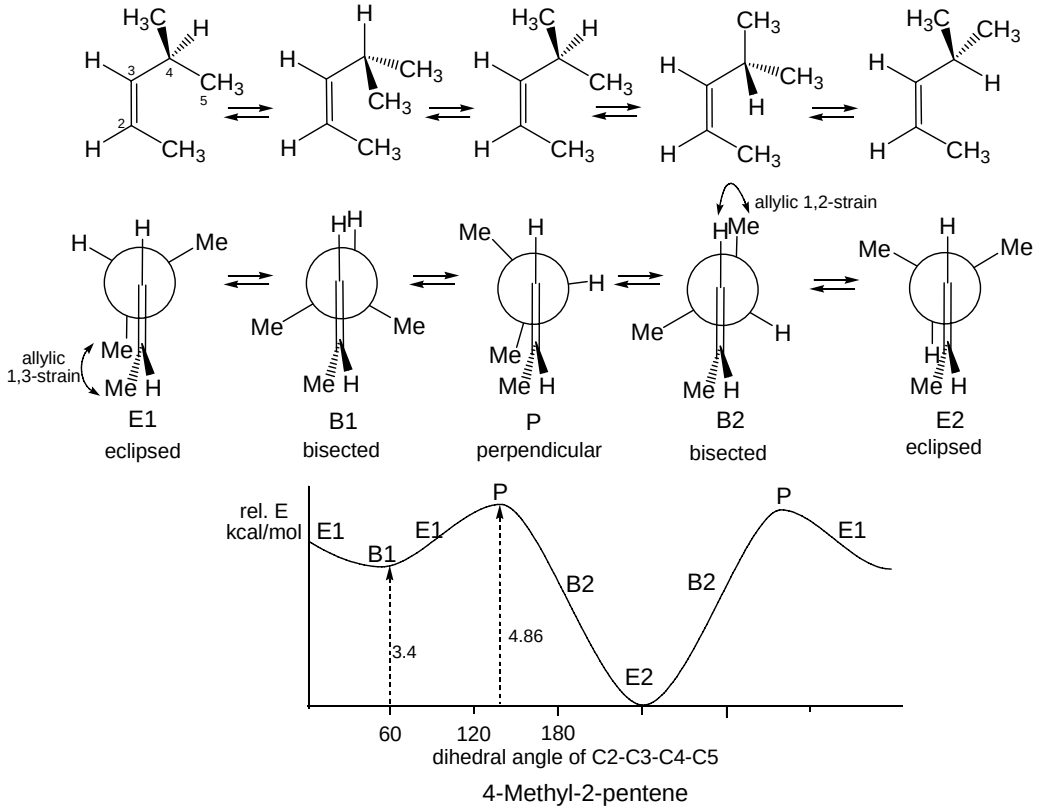

Figure 4.11 Conformation of (Z)-4-methyl-2-pentene ***4*-20**.

4.4 Conclusion

In conclusion, rotations about the sp^3-sp^3 single bond of acyclic compounds are hindered by three principle physical factors: electrostatic (Coulomb interaction), exchange (Pauli repulsion), and hyperconjugative interactions. Furthermore, intramolecular hydrogen-bonding and minimization of the *syn*-pentane interaction can also influence the conformational preference of acyclic compounds along sp^3- sp^3 bonds. For rotations about sp^3-sp^2 single bonds of unsaturated acyclic compounds, the eclipsed conformation normally is an energetic minimum in which the double bond eclipses the vicinal single bond. Meanwhile, the allylic 1,2-strain and allylic 1,3-strain should be considered during studies of rotations about sp^3-sp^2 single bonds. As a whole, conformational control of acyclic molecules is challenging, and development of new strategies to achieve this goal would be welcome.

Chapter 5 Effect of 2,6-disubstituted aryl groups on the conformation of acyclic compounds.

5.1 Introduction.

It is known that biological activities of peptides and proteins are strongly related to their conformations.[224] In general, backbone conformations of peptides are characterized by four torsional angles, ϕ, ψ, ω, and χ , as shown in Figure 5. 1.

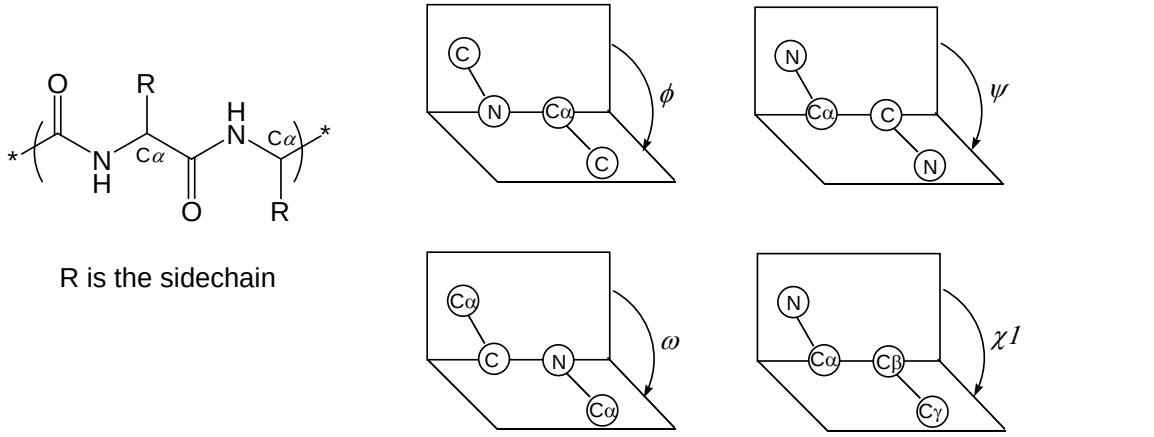

Figure 5. 1 Definition of the torsional angles of the backbone of peptides.

Hruby reported the design of polypeptides with specific conformational properties in χ space.[225] The three-dimensional arrangement of side chain moieties is characterized by torsional angles χ. The χ1 is the torsional angle about the Cα-Cβ bond for amino acid residues in peptides. Some of the subsequent torsional angles in longer side chains are defined as χ2, χ3, etc. As illustrated in Figure 5.2, each side chain χ1 torsional angle can assume three low energy staggered conformations: gauche (-) (χ1 = ~ -60 °), trans (χ1 = ~ 180 °) and gauche (+) (χ1 = ~ +60 °). The orientation of side chains is toward the

N-terminus of peptide backbone for gauche (-), toward to the *C*-terminus for trans, and over the peptide backbone for gauche (+). Conformations of the side chain moieties directly involved in the binding to receptors/acceptors are critically important for molecular recognition.[225]

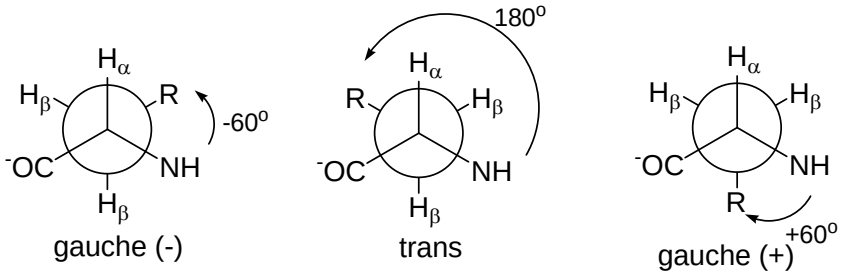

Figure 5.2 Newman projections of three staggered χ1 conformations in L-amino acids.

Hruby observed the restricted rotation about Cβ-Cγ bond of 2′,6′-dimethyl-β-methyltyrosine ***5*-1** and its analogues ***5*-2** (Figure 5.3) The rotational barriers around χ2 angle ranged from 15.1 ~ 20.1 kcal/mol, which were calculated from the coalescence temperature of the 2′,6′-methyl groups.[226]

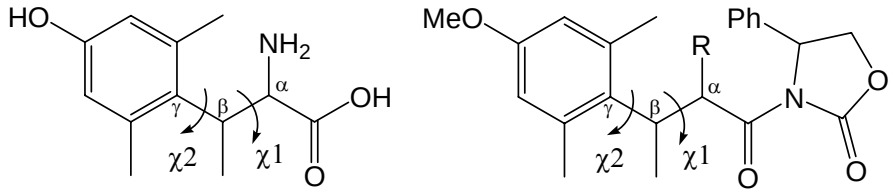

***5*-1** ***5*-2**

Figure 5.3 Structure of 2′,6′-dimethyl-β-methyltyrosine ***5*-1** and its analogues ***5*-2**.

Interestingly, each individual isomer of ***5*-1** exhibited a single preferred conformation of the χ1 angle: (2*S*, 3*S*)-***5*-1** favored gauche (-) rotamer; (2*R*, 3*R*)-***5*-1** had gauche (+) rotamer; (2*S*, 3*R*)-***5*-1** and (2*R*, 3*S*)-***5*-1** preferred trans rotamer (Figure 5.4).[227] The same conformational preference was found for 2′,6′-dimethyl-4′-methoxy-β-methyltyrosine

***5*-3**[228] and 2′,6′-dimethyl-β-methylphenylalanine ***5*-4**.[225] This focus on the divergent χ1 side-chain dihedrals is useful for peptide design, but potentially obscures a common feature of the stereoisomers: both adopt an antiperiplanar orientation of H_α and H_β in their preferred conformations.

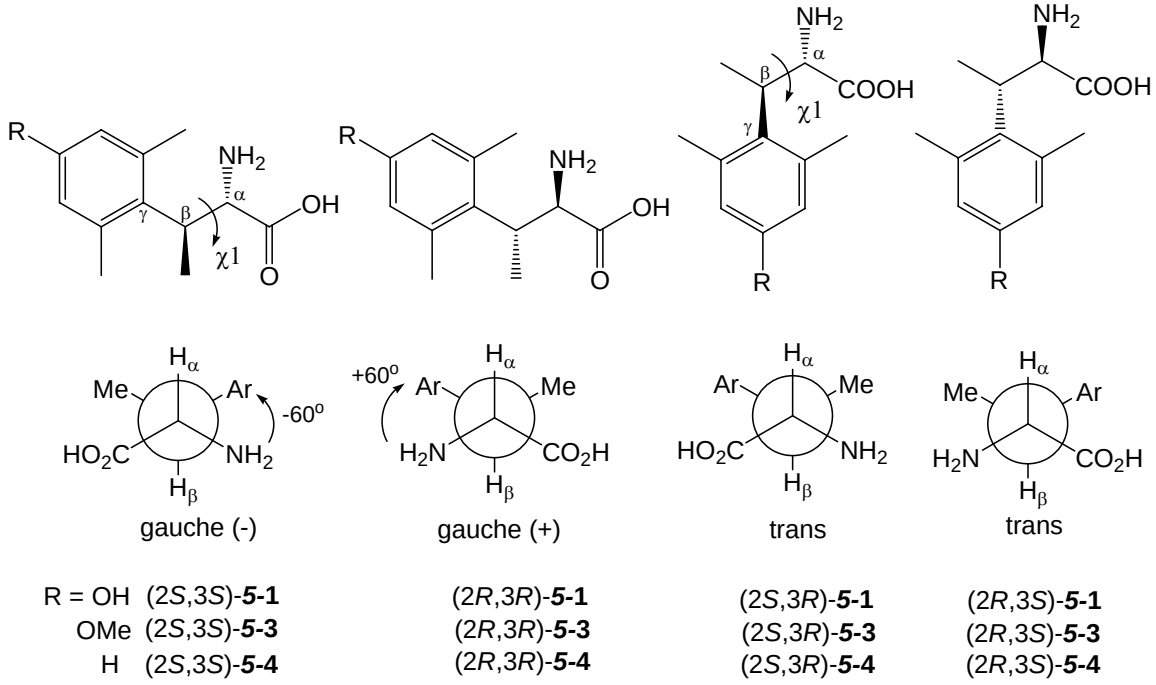

	gauche (-)	gauche (+)	trans	trans
R = OH	(2*S*,3*S*)-***5*-1**	(2*R*,3*R*)-***5*-1**	(2*S*,3*R*)-***5*-1**	(2*R*,3*S*)-***5*-1**
OMe	(2*S*,3*S*)-***5*-3**	(2*R*,3*R*)-***5*-3**	(2*S*,3*R*)-***5*-3**	(2*R*,3*S*)-***5*-3**
H	(2*S*,3*S*)-***5*-4**	(2*R*,3*R*)-***5*-4**	(2*S*,3*R*)-***5*-4**	(2*R*,3*S*)-***5*-4**

Figure 5.4 Preferred side-chain dihedrals χ1 and Newman projections of 2′,6′-dimethyl-β-methyltyrosine ***5*-1**, 2′,6′-dimethyl-4′-methoxy-β-methyltyrosine ***5*-3**, and 2′,6′-dimethyl-β-methylphenylalanine ***5*-4**.

We also noticed that the stereochemistry of nitrile aldols *anti*-***5*-5**[130] and *anti*-***5*-6** (Figure 5.5),[229] from the aldol reaction of arylacetonitriles, adopted similar antiperiplanar orientations of H2 and H3 as evidenced by X-ray crystallography and vicinal coupling constants (J^3_{23}). As a consequence, in the adopted conformation, the larger 2,6-disubstituted aryl groups were in a gauche relationship to the largest vicinal groups. Note that the terms "*anti*-" and "*syn*-" represent the standard *anti/syn* convention for aldol

stereochemistry in their extended ("zig-zag") conformation;[230] however, aldols throughout this chapter will be drawn in the conformation that they *adopt*. The terms "antiperiplanar" and "gauche" are used to depict the conformation of aldols along the C2-C3 bond. Toru et al. reported the synthesis of dithiane-derived aldols *anti*-***5*****-7** and *syn*-***5*****-7**.[231] The large vicinal coupling constant of H2 and H3 (10.0 and 10,4 Hz respectively) revealed that the H2 of *anti*-***5*****-7** and *syn*-***5*****-7** was antiperiplanar to the vicinal H3.

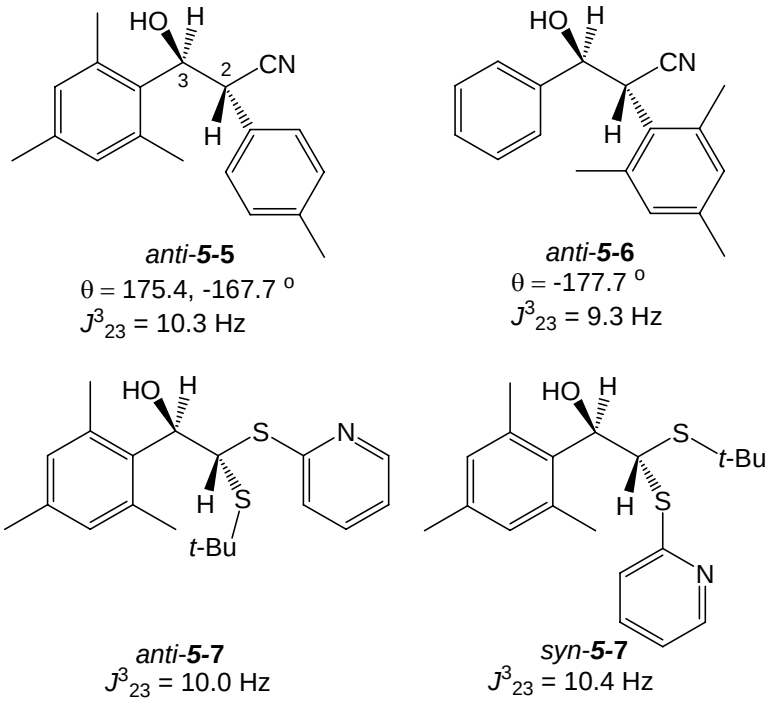

Figure 5.5 Evidence for an antiperiplanar orientation of H2 and H3. Solid-state (X-ray) dihedral angle θ (H2-C2-C3-H3) corresponds to the depicted enantiomer; where two dihedral angels are given, two molecules were presented in the asymmetric unit. The vicinal coupling constants are obtained form ^{1}H NMR ($CDCl_3$).[130, 229, 231]

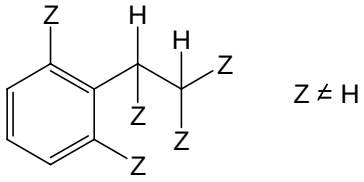

query A

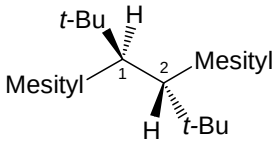

***5*-8** (BUMGOF,BUMGUL)[10]
θ = 180.0, 180.0°

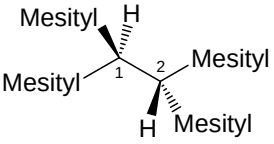

***5*-9** (TMESET)[11]
disordered-but inversion symmetry established conformation

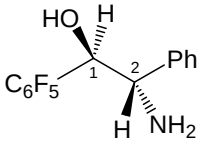

***5*-10** (OKAJIT)[12]
θ = 157.4°

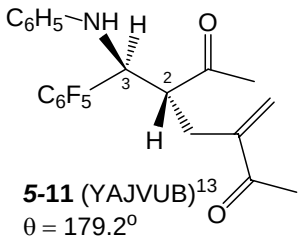

***5*-11** (YAJVUB)[13]
θ = 179.2°

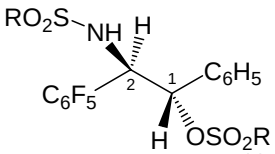

***5*-12** (ROPDEF)[14]
θ = -179.9°

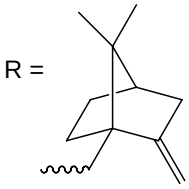

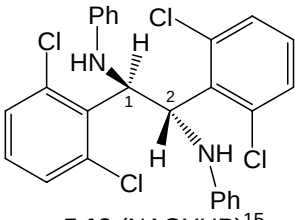

***5*-13** (NAGYUP)[15]
θ = -175.3, +179.7°

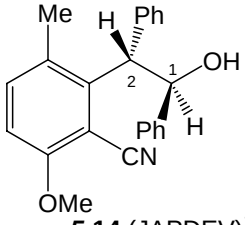

***5*-14** (JAPDEV)[16]
θ = -168.3°

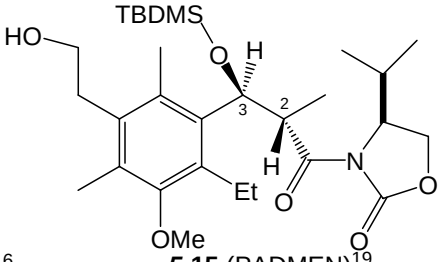

***5*-15** (PADMEN)[19]
θ = -177.8°

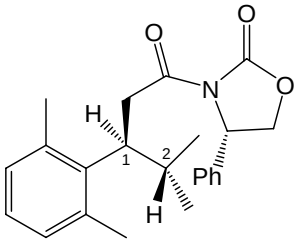

***5*-16** (RAZZAT)[17]
θ = 170.2°

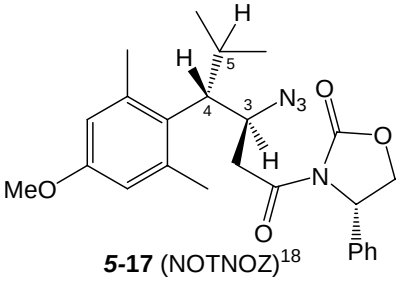

***5*-17** (NOTNOZ)[18]
θ = -166.6° (H4C4C3H3)
H5C5C4H4: -153.3°

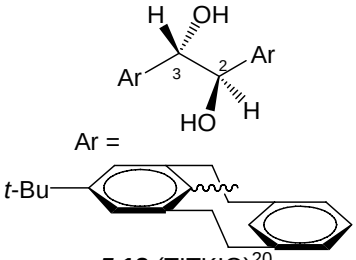

***5*-18** (TITKIQ)[20]
θ = 180°

Figure 5.6 Structures retrieved from Cambridge Structural Database search using Query A. These structures demonstrate that a 2,6-disubstituted aryl ring enforces a near antiperiplanar relationship of the geminal and vicinal hydrogens.

One of our collaborators in this effort, Professor Ian Williams (Chemistry, Hong Kong

University of Science and Technology) used the Cambridge Structural Database to search for compounds (Query A) bearing 2,6-disubstituted aryl groups. Excluding ethane units that were embedded in a ring, 13 structures provided 15 independent measurement of the dihedral angle θ. In total, 11 out of 13 structures exhibited an antiperiplanar arrangement of the geminal and vicinal hydrogens with θ ranging from -153° to +157°.[232-242] The only two structures which did not display an antiperiplanar relationship of the vicinal hydrogens were unusually crowded ethanes: (RR/SS)-1,2-di-*tert*-butyl-1,2-dimesitylethane[232] and 1,2,2-trimesitylethanol.[243]

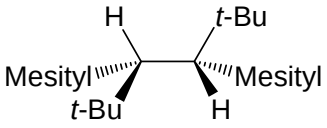

***5*-19** (BUMGUL)[10]
θ = 123.9°
note: this is the (*RR/SS*)-stereoisomer of ***2*-8**, with which it cocrystallizes in BUMGUL.

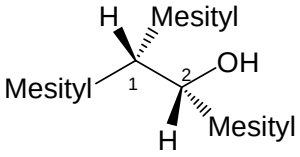

***5*-20** (CUVSUH)[21]
θ = 74.7°
note: ^{1}H NMR studies indicate that this and the θ = 180° conformations are equally populated in solution

Figure 5.7 Structures retrieved from Cambridge Structural Database search using Query A. These structures do not feature an antiperiplanar relationship of the geminal and vicinal hydrogens.

Based on these observations, it appeared that the conformational preference along the C2-C3 bond arose from the 2,6-disubstituted aryl group. In this Chapter, we will examine the generality of the conformational preference of aldols containing 2,6-disubstituted aryl group. The energetic origin of this conformational preference will be discussed in this Chapter. As reviewed in Chapter 4, *syn*-pentane interaction, allylic 1,2-strain and allylic 1,3-strain and intramolecular H-bonding provide conformational preferences of acyclic

molecules. The effect of 2,6-disubstituted aryl group on conformational preference could be another way to control acyclic conformations.

5.2 Synthesis of nitrile and ketone aldols.

To determine whether the conformational properties of nitrile aldols *anti*-***5*-5** and *anti*-***5*-6** (Figure 5.5) were general, additional nitrile aldols or ketone aldols were prepared from aldol reactions of arylacetonitrile and aldehyde or *t*-butyl ethyl ketone and aldehyde,[130] as shown in Scheme 5.1. Note that all compounds in this chapter were synthesized in racemic form.

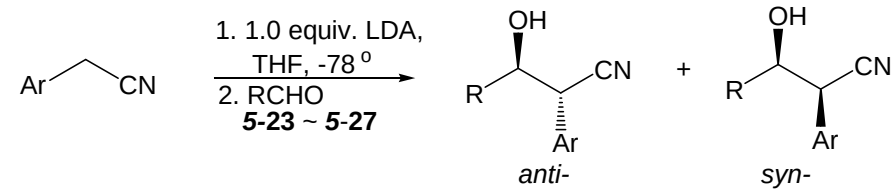

arylacetonitrile	Ar	aldehyde	R
***5*-21**	mesityl	***5*-23**	mesityl
***5*-22**	2-Naph	***5*-24**	2,6-diethylphenyl
		***5*-25**	2,6-difluorophenyl
		***5*-26**	2,6-dichlorophenyl
		***5*-27**	2,6-dibromophenyl

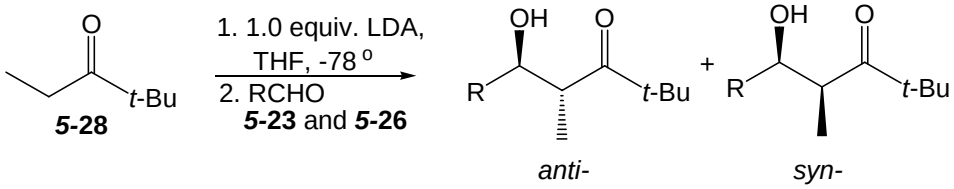

Scheme 5.1 Preparation of nitrile aldols and ketone aldols.

The aldol reaction of mesityl acetonitrile ***5*-21** and mesitaldehyde ***5*-23** was highly *anti*-selective, which was demonstrated by a ratio 20:1 for *anti/syn*- diastereomers (entry 1,

Table 5.1).[229] The aldol reactions of 2-naphthyl acetonitrile and aldehydes were moderately *anti*-selective with *anti/syn* ratios ranging from 3:1 to 1.1:1 (entries 2-6, Table 5.1). Moderate *syn*-diastereoselectivity was observed for the reaction of *t*-butyl ethyl ketone and aldehydes (entries 7 and 8, Table 5.1).

Table 5.1 Nitrile aldols and ketone aldols from the aldol reaction.

entry	Ar (nitrile) or ketone	R (aldehyde)	aldol	yield[a]	*anti:syn*[b]
1	Mesityl (***5*-21**)	Mesityl (***5*-23**)	***5*-29**	36%	20:1[c]
2	2-Naph (***5*-22**)	Mesityl (***5*-23**)	***5*-30**	53%	2.3:1
3	2-Naph (***5*-22**)	2,6-diethylphenyl (***5*-24**)	***5*-31**	29%	3:1
4	2-Naph (***5*-22**)	2,6-diflorophenyl (***5*-25**)	***5*-32**	57%	1.1:1
5	2-Naph (***5*-22**)	2,6-dichlorophenyl (***5*-26**)	***5*-33**	56%	1.8:1
6	2-Naph (***5*-22**)	2,6-dibromophenyl (***5*-27**)	***5*-34**	23%	1.3:1
7	*t*-Bu Et ketone (***5*-28**)	Mesityl (***5*-23**)	***5*-35**	22%	1:1.25
8	*t*-Bu Et ketone (***5*-28**)	2,6-dichlorophenyl (***5*-26**)	***5*-36**	66%	1:5

[a] Reported yield was isolated weight of aldols without correction for remaining starting materials.
[b] *anti:syn* ratio determined by 1H NMR.
[c] Reported *anti:syn* ratio.[229]

The preparation of aldehydes and ketones that were not commercially available is described in Scheme 5.2. The 2,6-diethylbenzaldehyde ***5*-24**[244] and 2,6-dibromobenzaldehyde ***5*-27**[245] were obtained from the reaction of corresponding lithiated benzene and N,N-dimethylformamide (DMF). The *t*-butyl ethyl ketone ***5*-28** was prepared from the chromic acid oxidation of 2,2-dimethyl-pentan-3-ol ***5*-39**.[246]

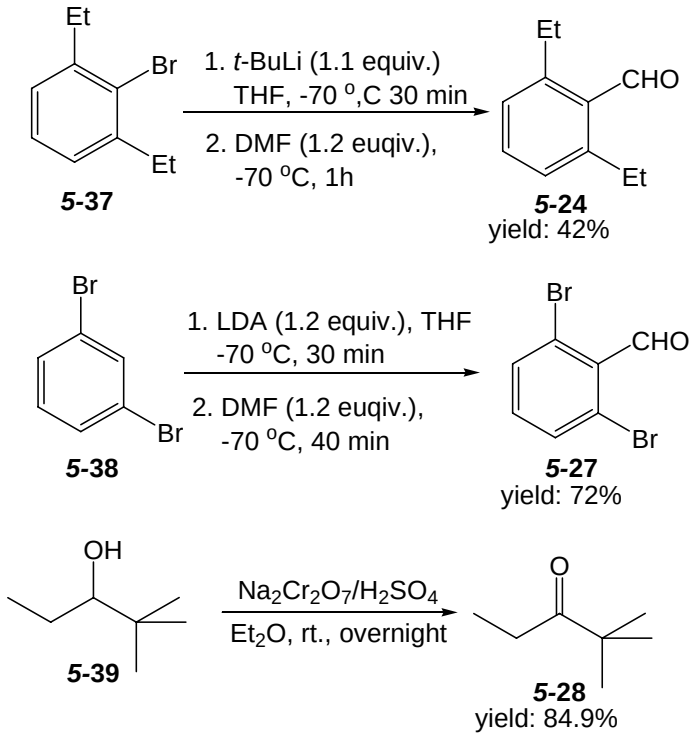

Scheme 5.2 Preparation of aldehydes ***5*-24**, ***5*-27**, and ketone ***5*-28**.

5.3 Generality of the effect of 2,6-disubstituted aryl groups on acyclic conformation in solid-state (X-ray crystallography) and in solution (^{1}H NMR).

5.3.1 Conformational preference of aldols bearing 2,6-disubstituted aryl groups, in solid state (X-ray crystallography).

Fifteen *anti*- and *syn*- nitrile and ketone aldols were prepared. After the separation of the diastereomeric aldols, we were able to get crystals from eight compounds; their structures are shown in Figure 5.8. The conformational preference in solid-state is characterized by dihedral angles θ (H2-C2-C3-H3) as given in Figure 5.8.

Nitrile aldols *anti*-***5*-5** (Figure 5.5),[130] *anti*-***5*-29**, and *anti*-***5*-30** have a mesityl group at C3. As the size of the aryl group at C2 increases from 4-Me-C_6H_5 (*anti*-***5*-5**) to naphthyl (*anti*-***5*-30**) and then to mesityl (*anti*-***5*-29**), the preference for H2 and H3 to

adopt an antiperiplanar orientation remains unchanged. Mesitaldehyde aldol *anti*-***5*-30** and 2,6-dichlorobenzaldehyde aldol *anti*-***5*-33** both feature a naphthyl group on C2 and have nearly identical dihedral angles θ, -179.5° and -174.2° respectively. Apparently, the *anti*- nitrile aldols bearing 2,6-disubstituted aryl groups feature a gauche orientation of the aryl groups on C2 and C3, which were the largest groups in size on those carbons. Only two *syn*- nitrile aldols (*syn*-***5*-32** and *syn*-***5*-33**) gave crystals. Solid-state dihedral angles θ of *syn*-***5*-32** and *syn*-***5*-33** (174.8° and -179.6° respectively) indicate an antiperiplanar relationship of H2 and H3. Note that for *syn*-diastereomeric nitrile aldols, a gauche interaction between C2- and C3-aryl groups is avoided.

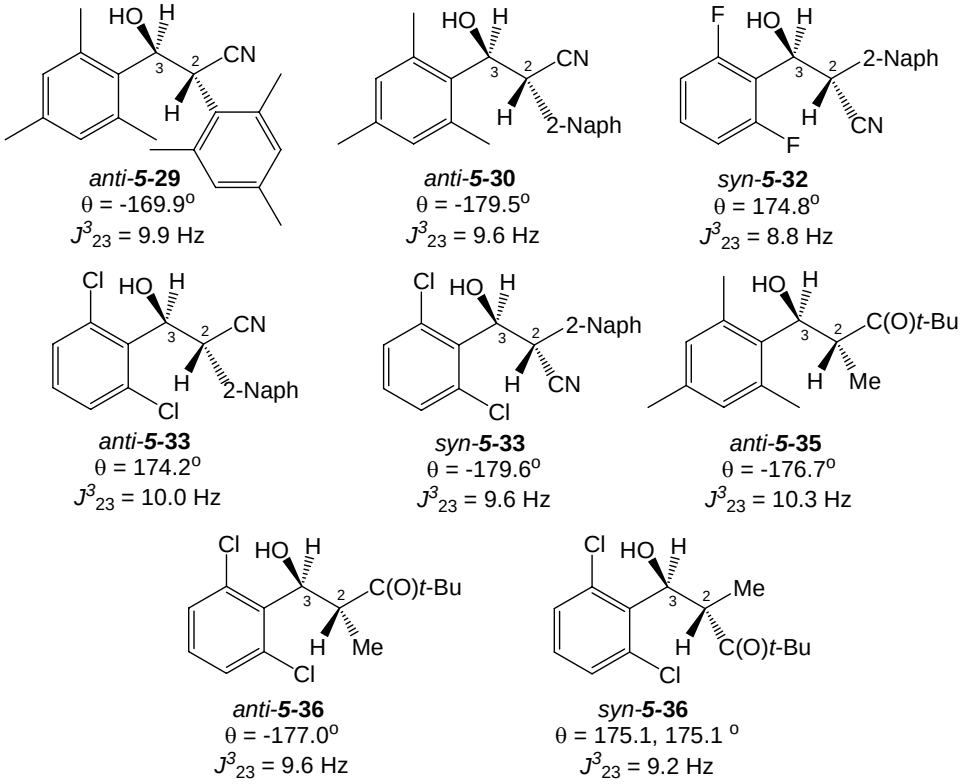

Figure 5.8 Solid-state dihedral angles θ (H2-C2-C3-H3) and vicinal coupling constants ($CDCl_3$) of nitrile and ketone aldols of 2,6-disubstituted benzaldehyde.

An antiperiplanar orientation of H2 and H3 is also seen in *anti*-***5*-35**, *anti*-***5*-36** and *syn*-***5*-36**, which are *tert*-butyl ethyl ketone aldols of mesitaldehyde and 2,6-dichlorobenzaldehyde respectively (Figure 5.8).

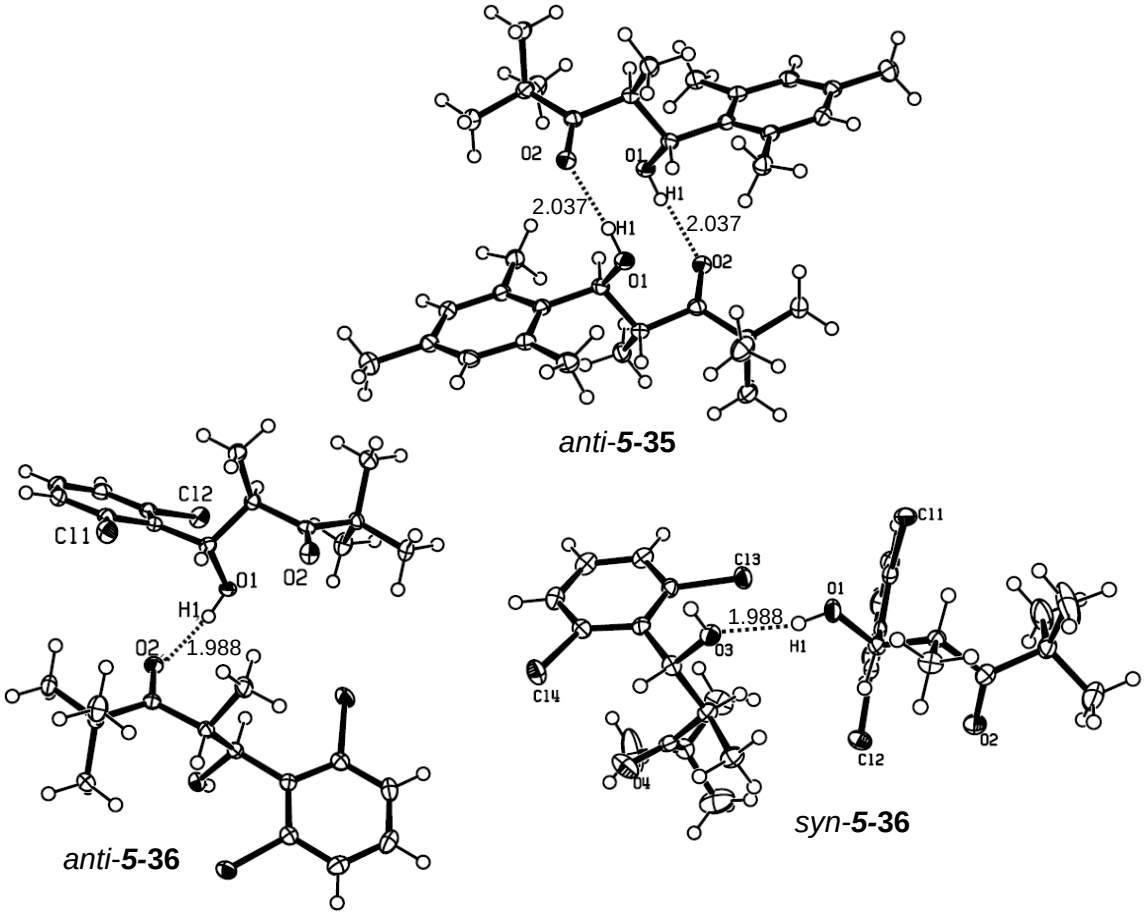

Figure 5.9 Solid-state intermolecular H-bonding in *anti*-***5*-35**, *anti*-***5*-36**, and *syn****5*-36**. The dash line shows the intermolecular H-bonding, which is given in Å.

Note the intramolecular H-bonding in β-hydroxynitriles is known to be weak,[247] and it does not play a major role in the conformational preference.[130] All X-ray structures of nitrile aldols exhibit intermolecular H-bonding between β-hydroxy and the neighboring nitrile nitrogen. Although intramolecular H-bonding in solution is very common in

β-hydroxy ketone aldols,[248] we notice that for *anti*-***5*-35**, *anti*-***5*-36** and *syn*-***5*-36**, the intermolecular H-bonding occurs between β-hydroxy and the oxygen of neighboring molecules in solid state, as shown in Figure 5.9. Thus, the conformational preference of ketone aldols is not due to the intramolecular H-bonding.

5.3.2 Conformational preference of aldols bearing 2,6-disubstituted aryl groups, in solution (^{1}H NMR)

The relationship between dihedral angles and vicinal coupling constants is given theoretically by Karplus equation.[249] A large vicinal coupling constant is obtained when the dihedral angle is close to 0° or 180°. The dihedral angle of approximately 60° gives a small vicinal coupling constant. Experimentally, an observed coupling constant in ^{1}H NMR is the weighted average of those of contributing conformers. In Scheme 5.3, conformations of *anti*-/*syn*- nitrile and ketone aldols are classified by the dihedral angle θ (H2-C2-C3-H3). When nitrile or ketone aldols do not have a single preferred conformation along the C2-C3 axis, vicinal coupling constants of H2 and H3 range from 5 to 6 Hz for *anti*-nitrile aldols,[130] 6 – 7 Hz for *syn*-nitrile aldols,[130] 7 – 10 Hz for *anti*-ketone aldols,[248] and 2 – 6 Hz for *syn*-ketone aldols.[248]

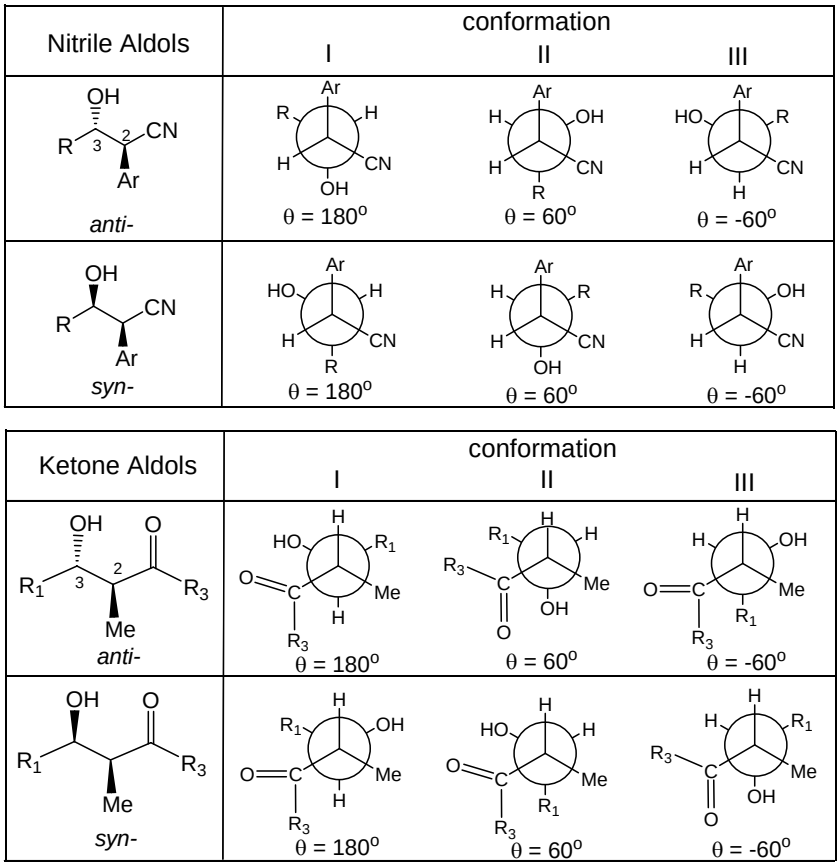

Scheme 5.3 Conformations of *anti-/syn-* nitrile and ketone aldols along C2-C3 axis, as classified by the dihedral angle θ (H2-C2-C3-H3).

As shown in the previous Figure 5.8, eight aldols demonstrate large vicinal coupling constants in solution ($CDCl_3$). Although we do not have X-ray analysis for the rest of the prepared nitrile and ketone aldols (Figure 5.10), all of the nitrile and ketone aldols examined give similar large coupling constants in solution ($CDCl_3$), ranging from 8.8 Hz to 10.3 Hz. This coupling constant gives an evidence of the significantly populated conformation I (Scheme 5.3) in solution, which features the antiperiplanar orientation of H2 and H3. The coupling constants, and the selected ^{1}H NMR/^{13}C NMR chemical shifts for all of nitrile and ketone aldols are given in Table 5.2.

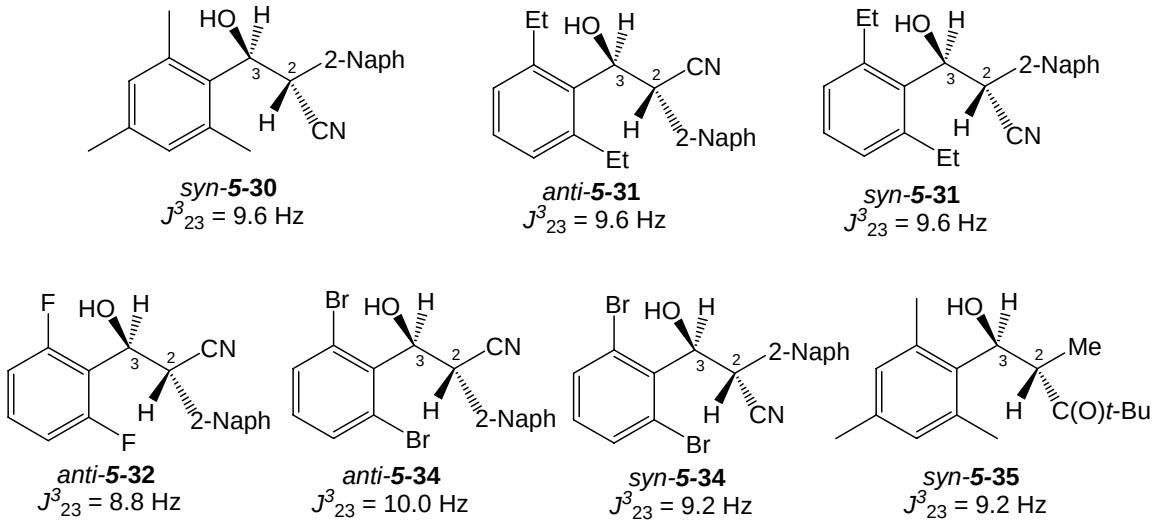

syn-***5*-30**
J^3_{23} = 9.6 Hz

anti-***5*-31**
J^3_{23} = 9.6 Hz

syn-***5*-31**
J^3_{23} = 9.6 Hz

anti-***5*-32**
J^3_{23} = 8.8 Hz

anti-***5*-34**
J^3_{23} = 10.0 Hz

syn-***5*-34**
J^3_{23} = 9.2 Hz

syn-***5*-35**
J^3_{23} = 9.2 Hz

Figure 5.10 Vicinal coupling constant ($CDCl_3$) of new prepared nitrile and ketone aldols of 2,6-disubstituted benzaldehydes, that did not form crystals.

In the conformation I of *anti*-nitrile aldols, the aryl group at C2 and –OH group at C3 are antiperiplanar, and the –CN group and the aryl group at C3 are antiperiplanar. In contrast, the conformation I of *syn*-nitrile aldols features the gauche relationship between the aryl group at C2 and the –OH group at C3 and, as well as between the -CN group at C2 and the aryl group at C3 (Scheme 5.3). With inspection of the ^{1}H NMR and ^{13}C NMR chemical shifts of nitrile aldols, an upfield shield (0.5 - 0.9 ppm, entries 2-11, Table 5.2) in the ^{1}H NMR spectrum is observed for the –OH group of *syn*-nitrile aldol ***5*-30** ~ ***5*-34** relative to their *anti*-diastereomers. This upfield shift occurs because the –OH group is gauche to the aryl group at C2, and is within the shielding cone of the aryl group at C2. The –CN group of *syn*-aldols also demonstrates similar upfield shielding (1.2 – 5.5 ppm, Table 5.2) in the ^{13}C NMR spectrum compared to the corresponding *anti*-isomers, because the –CN group is within the shielding cone of the 2,6-disubstituted aryl group at

C3. The relative stereochemistry of *anti-/syn-* **5-31** and **5-34** was assigned on the basis of the ^{1}H NMR chemical shift of the hydroxy protons and the ^{13}C NMR chemical shift of the cyano carbons.

For the ketone aldols (entry 12-15, Table 5.2), the 2-methyl group lies within the shielding cone of 2,6-disubstituted aryl group at C3. Consequently, an upfield shield (~ 0.5 ppm) is observed by ^{1}H NMR for the 2-methyl groups in *anti*-**5-35** and *anti*-**5-36** relative to their *syn*-diastereomers. However, the ^{1}H NMR chemical shifts of the –OH group of **5-35** and **5-36** are in a similar position (within 0.17 ppm of difference) for *anti*- and *syn*-diastereomers because of the absence of the aryl group at C2.

Table 5.2 Vicinal coupling constant and selected ^{1}H NMR /^{13}C NMR chemical shifts for nitrile/ketone aldols.

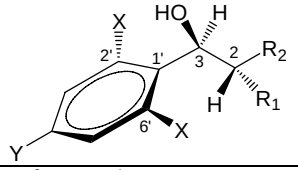

entry	aldol	R1	R2	X	Y	J^{3}_{23} (Hz)	^{1}H NMR (ppm)			^{13}C NMR (ppm)			
							-OH	Me (at C2)	*t*-Bu	-CN	-C(O)	Me (at C2)	*t*-Bu
1	*anti*-**5-29**	Mesityl	CN	Me	Me	9.9	2.04	-	-	119.2	-	-	-
2	*anti*-**5-30**	2-Naph	CN	Me	Me	9.6	2.83	-	-	120.4	-	-	-
3	*syn*-**5-30**	CN	2-Naph	Me	Me	9.6	1.92	-	-	119.0	-	-	-
4	*anti*-**5-31**	2-Naph	CN	Et	H	9.6	2.69	-	-	120.2	-	-	-
5	*syn*-**5-31**	CN	2-Naph	Et	H	9.6	2.01	-	-	118.9	-	-	-
6	*anti*-**5-32**	2-Naph	CN	F	H	8.8	3.23	-	-	119.4	-	-	-
7	*syn*-**5-32**	CN	2-Naph	F	H	8.8	2.71	-	-	118.2	-	-	-
8	*anti*-**5-33**	2-Naph	CN	Cl	H	10.0	3.44	-	-	119.8	-	-	-
9	*syn*-**5-33**	CN	2-Naph	Cl	H	9.6	2.82	-	-	114.3	-	-	-
10	*anti*-**5-34**	2-Naph	CN	Br	H	10.0	3.49	-	-	119.7	-	-	-
11	*syn*-**5-34**	CN	2-Naph	Br	H	9.2	2.85	-	-	118.0	-	-	-
12	*anti*-**5-35**	Me	C(O)*t*-Bu	Me	Me	10.3	3.78	0.78	1.22	-	220.2	15.8	26.4
13	*syn*-**5-35**	C(O)*t*-Bu	Me	Me	Me	9.2	3.68	1.27	0.83	-	218.8	16.3	25.9
14	*anti*-**5-36**	Me	C(O)*t*-Bu	Cl	H	9.6	2.67	0.82	1.16	-	218.3	15.6	26.2
15	*syn*-**5-36**	C(O)*t*-Bu	Me	Cl	H	9.2	2.84	1.30	0.86	-	217.0	16.6	25.8

All of the nitrile aldols bearing a 2,6-disubstituted aryl group at C3 demonstrate the antiperiplanar orientation of H2 and H3. In contrast, *anti*- nitrile aldols from benzaldehyde and arylacetonitrile, lacking a 2,6-disubstituted aryl group (e.g., Ar = Ph, 4-MeC_6H_4, 2-naphthyl), did not prefer the single gauche conformation along the C2-C3 axis, as indicated by vicinal coupling constants (4 – 6 Hz for *anti*-diastereomers, and 6 – 7 Hz for *syn*-diastereomers).[130] Thus, the conformational preference exhibited by the nitrile aldols ***5*-5**, ***5*-6**, and ***5*-29** ~ ***5*-34** appears to be due to the 2,6-disubstituted aryl moiety. Furthermore, we noticed the importance of the size of the 2,6-substituent. The 2,6-difluorobenzaldehyde aldols *anti*-***5*-32** and *syn*-***5*-32** exhibited a smaller vicinal coupling constant (8.8 Hz), relative to its analogues ***5*-30**, ***5*-31**, ***5*-33**, and ***5*-34** (Figure 5.8 and Figure 5.10). The smaller size of the fluoro group decreased the contribution of conformation I, resulting in the smaller coupling constant. As was also demonstrated by ketone aldol *anti*-/*syn*-***5*-35 ~ 36** (Figure 5.8 and Figure 5.10), as well as dithiane aldols *anti*-/*syn*-***5*-7** (Figure 5.5), the preference for an antiperiplanar orientation of H2 and H3 does not depend on the presence of a cyano or aryl group at C2.

5.4 Energetic origin of the effect of 2,6-disubstituted aryl groups on acyclic conformations: Experimental analysis by X-ray crystallography and ^{1}H-^{1}H NOESY NMR.

To determine how 2,6-disubstituted aryl rings at C3 and C2 might play a role in enforcing θ dihedral angle (H2-C2-C3-H3) near 180°, we examined their solid-state

orientations relative to their geminal hydrogens H3 and H2, as indicated by the dihedral angles ϕ (H3-C3-C1′-C2′) and τ (H2-C2-C1′′-C2′′) in Figure 5.11.

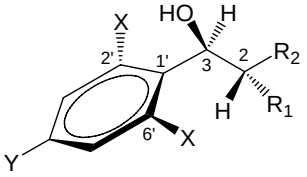

aldol	R_1	R_2	X	Y	ϕ (H3C3C1′C2′)
anti-***5*-5**	4-MeC_6H_4	CN	Me	Me	6.8, -4.2
anti-***5*-30**	2-Naph	CN	Me	Me	18.5
syn-***5*-32**	CN	2-Naph	F	H	9.1
anti-***5*-33**	2-Naph	CN	Cl	H	9.3
syn-***5*-33**	CN	2-Naph	Cl	H	12.1
anti-***5*-35**	Me	C(O)*t*-Bu	Me	Me	11.9
anti-***5*-36**	Me	C(O)*t*-Bu	Cl	H	9.3
syn-***5*-36**	C(O)*t*-Bu	Me	Cl	H	10.3

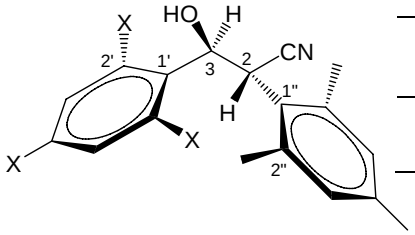

aldol	X	ϕ (H3C3C1′C2′)	τ (H2C2C1′′C2′′)
anti-***5*-6**	H	40.0	14.3
anti-***5*-29**	Me	16.2	7.5

Figure 5.11 Orientation of 2,6-disubstituted aryl rings at C3 and C2 relative to their geminal hydrogens, as indicated by the dihedral angles ϕ and τ (X-ray).

For the eight structured aldols bearing a 2,6-disubstituted aryl group at C3, dihedral angles ϕ range from 4.2 ~ 18.5° (Figure 5.11); the average dihedral angles for those eight aldols was 10.2°. For *anti*-***5*-29** bearing two mesityl groups at C2 and C3, the dihedral angles ϕ are 16.2°. Aldols *anti*-***5*-6** and *anti*-***5*-29** bearing a mesityl group at C2 feature the dihedral angle τ 14.3° and 7.5° respectively. This tendency of the 2,6-disubstituted aryl group to nearly eclipse to the corresponding geminal H derived from the

minimization of allylic 1,3-strain. This eclipsing conformation is consistent with the conformational preference about sp^2-sp^3 bond, such as that in (Z)-4-methyl-2-pentene,[223] and in amino acids ***5*-1** and ***5*-2**.[225, 227]

Inspection of Figure 5.11 leads to the insight that small ϕ dihedral angles place the C6′-X group near H2. To provide evidence of this close contact in solution, we performed additional ^{1}H NMR spectroscopic studies on *anti*-***5*-35**, because it shows nonequivalence of the mesityl *ortho*-methyl groups at room temperature. Firstly, various temperature ^{1}H NMR studies were performed for *anti*-***5*-35**. In the ^{1}H NMR spectrum of the *anti*-***5*-35**, the C2′ and C6′ methyl groups in aryl ring exhibited a broad peak with a flat top around 2.4 ~ 2.5 ppm at room temperature (21.5 °C, the coalescent temperature), and merged to a single peak at higher temperature (36.3 °C) (stacked spectra a), Figure 5.12). When the temperature was lowered to -33.4 °C, two distinct single peaks around 2.4 and 2.6 ppm were observed for the C2′ and C6′ methyl groups (stacked spectra a), Figure 5.12). The different chemical shifts for the C2′ and C6′ methyl groups are due to the restricted rotation around C3-C1′ bond. Because of the restricted rotation, the C3′ and C5′ protons also exhibited different chemical shifts at 6.8 and 6.9 ppm at -33.4 °C (stacked spectra b), Figure 5.12). The coalescence temperature for the C3′ and C5′ protons is -1.3 °C. Thus, the rotational barrier about C3-C1′ can be estimated to be in the range 14.2 to 13.7 kcal/mol, based on the coalescence temperature 21.5 and -1.3 °C respectively.[226, 250, 251]

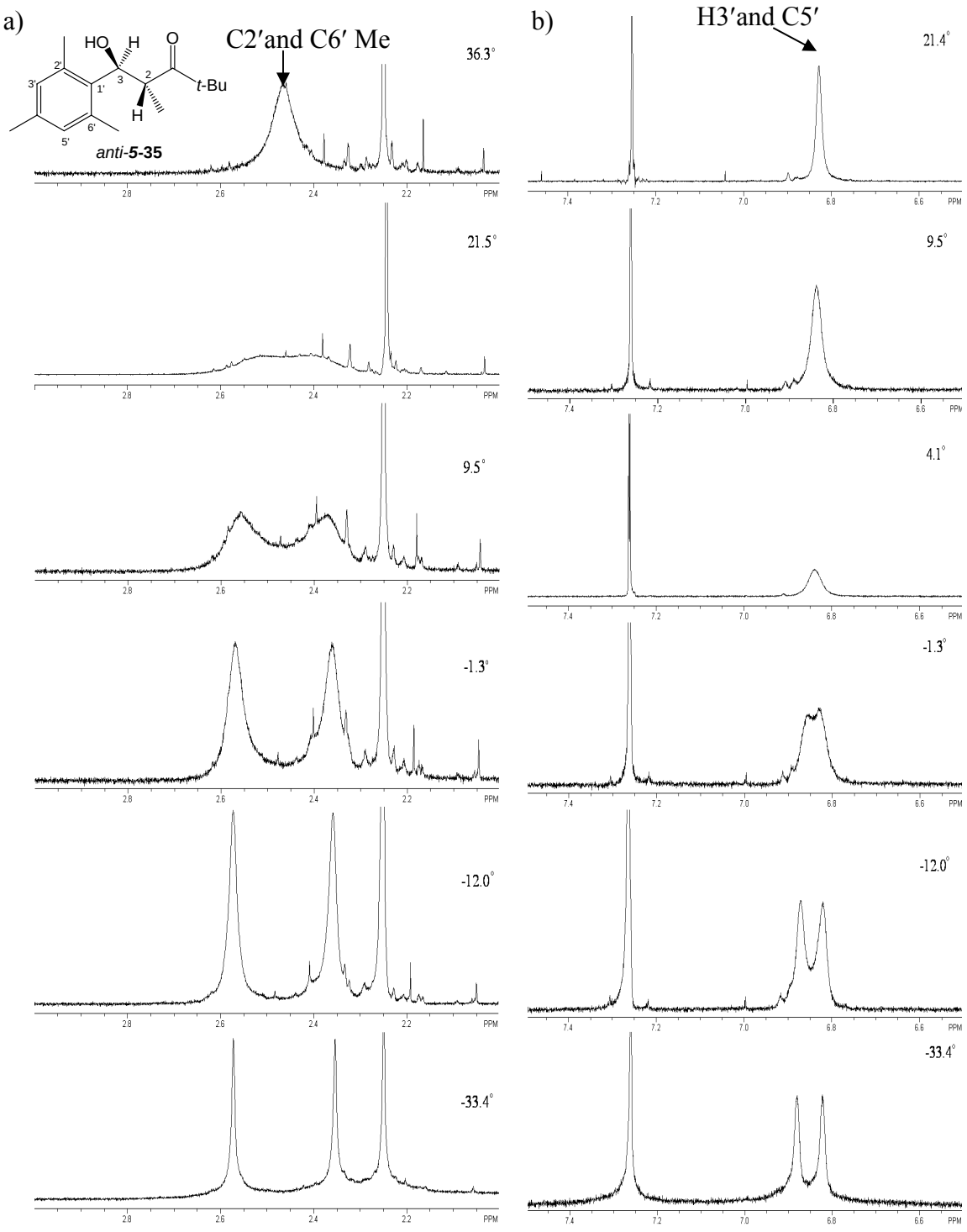

Figure 5.12 ^{1}H NMR spectra of *anti-**5**-**35*** in $CDCl_3$ at different temperatures. a) shows the coalescence (at 21.5 °C) of two mesityl methyl groups resonances at ~ 2.5 ppm; b) shows the coalescence (at -1.3 °C) of two aromatic protons resonances at ~ 6.8 ppm

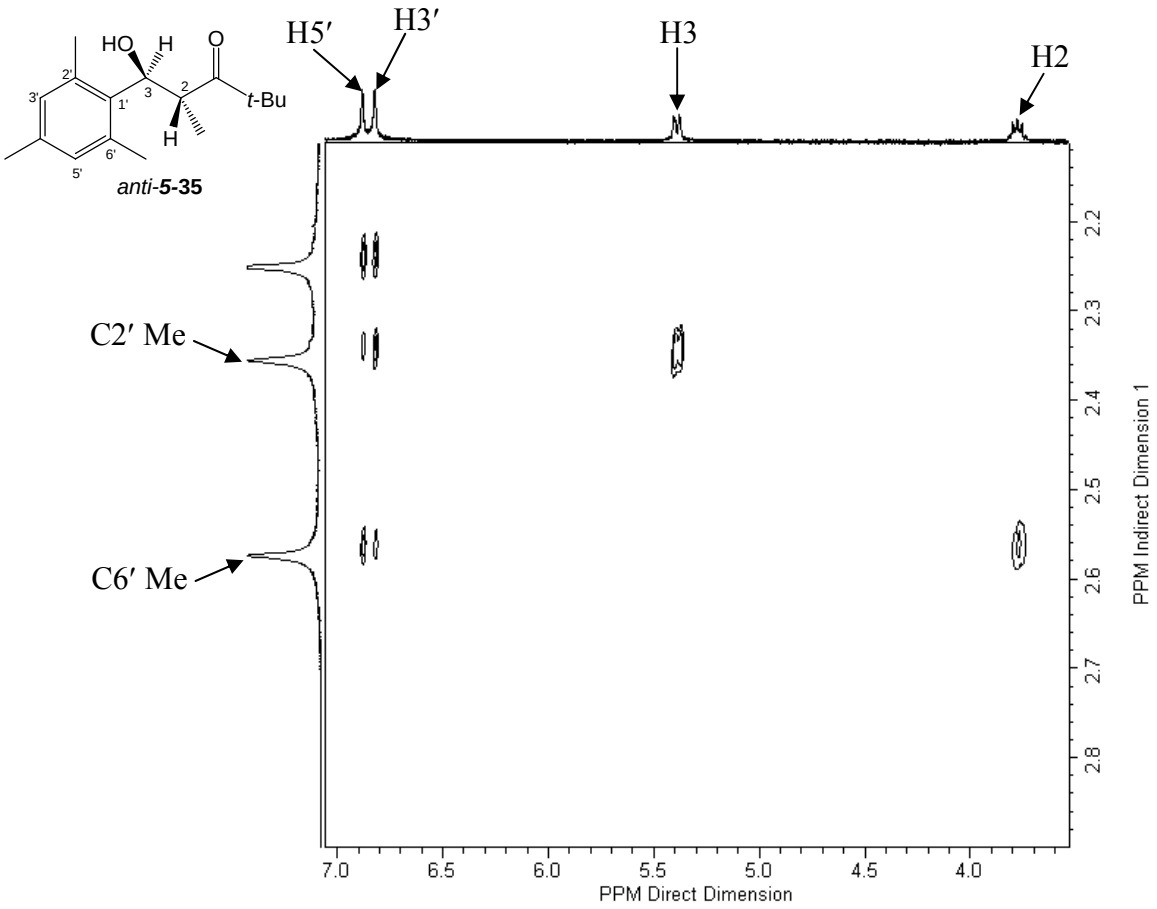

Figure 5.13 ^{1}H-^{1}H NOESY NMR of *anti*-**5-35** in $CDCl_3$ at -33.4 °C.

^{1}H-^{1}H NOESY NMR correlation at -33.4 °C reveals that the H2 is close to one of mesityl methyl group (C6′-Me) while the H3 is near the C2′-Me (Figure 5.13). The chemical shifts of the C2′-Me and the C6′-Me are at 2.355 and 2.574 ppm respectively. In Figure 5.14, the X-ray structure of *anti*-**5-35** is superimposed with selected NOESY correlations at -33.4 °C. The average distance between H2 and C6′-Me is 2.93 Å, while that between H3 and C2′-Me was 2.63 Å. Thus, the close proximity of H2 and H3 to the C6′ and C2′ substituents in the solid state structure of *anti*-**5-35** (as shown in Figure 5.14) is maintained in solution.

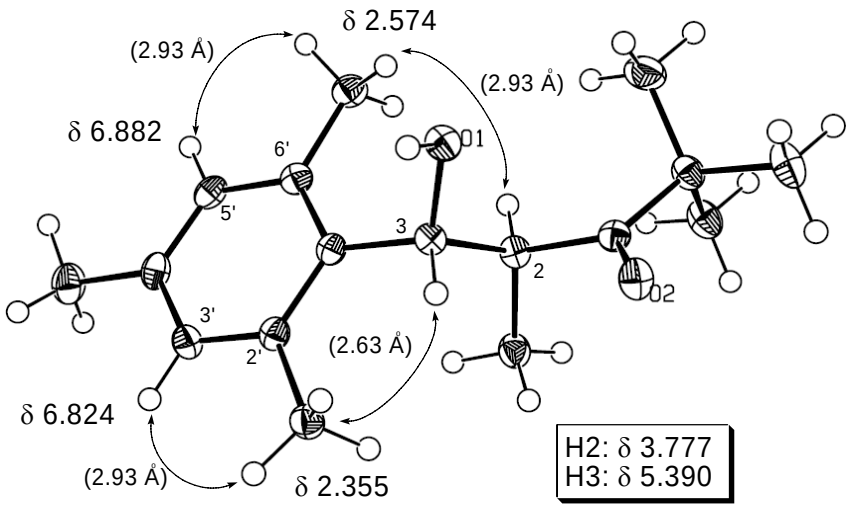

Figure 5.14 X-ray structure of *anti-**5**-**35***, superimposed with selected NOESY correlations at -33.4 °C in $CDCl_3$. Average H-H distances (X-ray) are given in parentheses.

The tendency of the 2,6-disubstituted aryl ring to nearly eclipse its geminal hydrogen should have important consequences for the energies of conformations along the C2-C3 bond (Figure 5.15). A destabilizing steric interaction of the C6′-X group with the C2 substituent occurs in conformation II and conformation III. This interaction is reminiscent of a "*syn*-pentane" interaction. In the conformation I, the C6′-X group is close to the smallest H substituent at C2, thus avoiding the "*syn*-pentane"-like interaction.

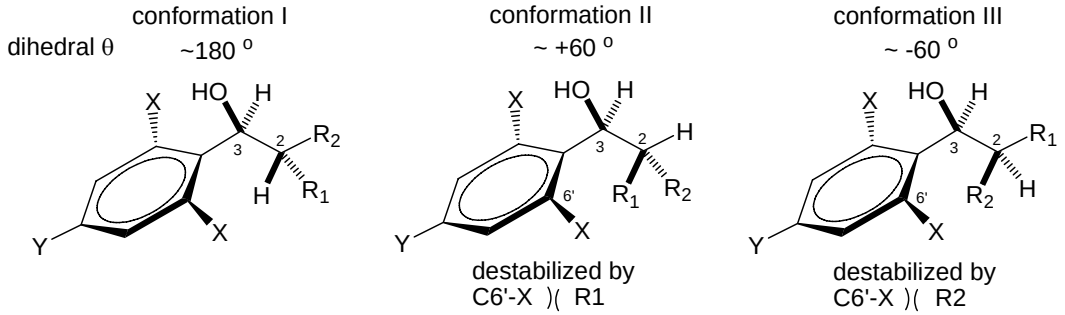

Figure 5.15 Steric interactions in conformations along the C2-C3 bond. The "*syn*-pentane" -like interaction is found in conformation II and III

5.5 Computational study: the effect of 2,6-disubstituted aryl on acyclic molecules.

To assess the magnitude of the destabilizations caused by "*syn*-pentane" –like interactions in conformations II and III, we performed conformational searches using MMFF94 mechanics method and the conformer distribution module of Spartan '04 for Windows. Although molecular mechanics-based procedures are strictly approximate, MMFF94 is particularly well parameterized to model acyclic conformations,[252] and the speed of the method allows sampling of the entire conformational space.[253] All calculated conformers were classified as conformation I, conformation II or conformation III according to the dihedral angle θ (Figure 5.15). The relative energies of the conformers from MMFF94 were used to obtain the summed Bolzmann weightings at 298K for these conformations (Table 5.3).

In 19 of 20 cases, the Bolzmann weightings of conformation I ranged from 72% to 99.8%, consistent with the ^{1}H NMR observation in solution. One exception is observed for the *syn*-***5*-36** (entry 20, Table 5.3) in which conformation III is dominant (90.3 %). Inspection of each conformation of *syn*-***5*-36** reveals that the intramolecular H-bonding is possible in conformation III of *syn*-***5*-36** because of the gauche relationship between the C(O)-*t*-Bu group and the OH group; in conformation I of *syn*-***5*-36**, the arrangement of the C(O)-*t*-Bu group and the OH group is antiperiplanar. We attribute the dominant conformation III in *syn*-***5*-36** to the overestimation of the intramolecular H-bonding stabilization of conformation III.

Table 5.3 MMFF94 summed Boltzman weightings of conformation I, II, and III at 298 K.

		298K Boltzmann Weightings of Conformer Families (number of conformers,dihedral range)		
entry	compound	Conformation I (H2C2C3H3, ~180)	Conformation II (H2C2C3H3, ~+60)	Conformation III (H2C2C3H3, ~-60)
1	*anti*-**5**-**5**	74.3% (9, 170-177 °)	2.4% (8, 67-79 °)	23.3% (15, -68 to -82 °)
2	*syn*-**5**-**5**	82.0% (8, 165-177 °)	1.5% (6, 68-73 °)	16.5% (12, -71 to -75 °)
3	*anti*-**5**-**6**	71.6% (6, 166-174 °)	12.9% (4, 69-70 °)	15.5% (4, -68 to -86 °)
4	*syn*-**5**-**6**	82.4% (8, 174-175 °, -173 to -177 °)	14.4% (4, 72-77 °)	3.2% (6, -60 to -68 °)
7	*anti*-**5**-**29**[a]	92.3% (8, 144~149 °, -167~-169 °)	4.4% (3, 60~72 °)	3.3% (4, -57~-60 °)
5	*syn*-**5**-**29**	77.1% (10, 171-180 °)	0.7% (7, 74-80 °)	2.3% (14, -71 to -87 °)
6	*anti*-**5**-**30**	73.5% (9, 170-177 °)	5.4% (8, 67-79 °)	21.0% (12, -68 to -82 °)
7	*syn*-**5**-**30**	75.4% (9, 164-177 °)	1.0% (5, 68-73 °)	23.6% (12, -72 to 76 °)
9	*anti*-**5**-**31**	77.8% (36, 164 to 180 °, -180 to -168 °)	10.5% (14, 70 to 86 °)	11.7% (16, -68 to -83°)
10	*syn*- **5**-**31**	80.6% (32, 157 to 179 °)	3.1% (10, 66 to 71 °)	16.3% (29, -69 to -75 °)
11	*anti*-**5**-**32**	76.7% (7, 163-166 °)	20.2% (6, 62-77 °)	3.1% (9, -66 to -73 °)
12	*syn*-*5*-32	72.2% (6, 168-176 °)	2.5% (8, 66-68 °)	25.3% (5, -58 to -66 °)
13	*anti*-**5**-**33**	96.9% (4, 158-162 °)	1.4% (2, 65-66 °)	1.7% (7, -66 to -77 °)
14	*syn*-**5**-**33**	88.8% (6, 162-171 °)	0.3% (6, 67-71 °)	11.0% (4, -64 to -71 °)
15	*anti*-**5**-**34**	96.9% (4, 160 to 165 °)	1.7% (4, 65 to 71 °)	1.4% (4, -66 to -77 °)
16	*syn*-**5**-**34**	87.1% (4, 161 to 172 °)	0.2% (5, 69 to 73 °)	12.8% (6, -68 to -73 °)
17	*anti*-**5**-**35**	99.8% (8, 160-179 °, -164 to -168 °)	0% (0)	0.2% (4, -59 to -72 °)
18	*syn*-**5**-**35**	96.7% (9, -161 to -172 °)	0% (2, 57 °)	3.3% (6, -73 to -86 °)
19	*anti*-**5**-**36**	97.9% (7, 159-179 °, -173°)	0.1% (2, 63-64 °)	2.1% (2, -68 to -69 °)
20	*syn*-**5**-**36**	9.4% (4, 177°，-150 to -175 °)	0.4% (2, 64-65 °)	90.3% (4, -54 to -89 °)

[a] Three members of an eclipsed conformer family were also found for *anti*-**5**-**29**; these were false minima that reverted to members of conformations I—III upon B3LYP/6-31G* optimization.

The performance of the molecular mechanics method (MMFF94) to model the conformation of the aldols ***5*-5**, ***5*-6**, and ***5*-29** ~ ***5*-36** suggests a significant energetic preference for an antiperiplanar arrangement of H2 and H3. In this conformation, *anti*-nitrile aldols, and *syn*-ketone aldols place the 2,6-disubstituted aryl group at C3 and the largest group at C2 in a gauche relationship. Because of the computational cost, we did not perform the conformational distribution using the B3LYP method. To evaluate the energetic preference of this conformation using DFT method, we took a single conformer from conformation I, II and III of each *anti*-nitrile aldol and *syn*-ketone aldol, and performed geometry optimization at B3LYP/6-31G*. The single point calculations were carried out at MP2/6-31+G*//B3LYP/6-31G*. Energies of conformers examined are reported in Table 5.4.

For *anti*- nitrile aldols and *syn*-ketone aldols (entry 1 ~ 10, Table 5.4), 9 out of 10 cases revealed that the conformer I was relatively more stable than the other two conformers at MP2/6-31+G*//B3LYP/6-31G* because of the energetic penalties of the "*syn*-pentane" –like interaction in conformer II and III. The only exception is *anti*-***5*-32** (entry 6, Table 5.4), bearing 2,6-diflurophenyl group at C3. The conformer II of *anti*-***5*-32** is only 0.35 kcal/mol more stable than conformer I. The size of 2,6-difluoro substituents is relatively small, and results in the lower energetic penalty of "*syn*-pentane" –like interaction in conformation II.

Table 5.4 Relative energies of conformer 1, 2, and 3 for *anti*- nitrile and *syn*- ketone aldols at MP2/6-31+G*//B3LYP/6-31G* and B3LYP/6-31G* (italic number). [a]

entry	aldol	Conformer I (H2C2C3H3, ~180) (kcal/mol)	Conformer II (H2C2C3H3, ~60) (kcal/mol)	Conformer III (H2C2C3H3, ~-60) (kcal/mol)
1	*anti*-**5-5**	0 *(0)*	2.15 *(2.59)*	3.74 *(1.36)*
2	*anti*-**5-6**	0 *(0)*	0.53 *(1.46)*	2.14 *(0.34)*
3	*anti*-**5-29**	0 *(0)*	1.73 *(2.23)*	3.89 *(0.79)*
4	*anti*-**5-30**	0 *(0)*	2.17 *(2.43)*	3.82 *(0.90)*
5	*anti*-**5-31**	0 *(0)*	0.93 *(2.16)*	3.86 *(0.87)*
6	*anti*-**5-32**	0 *(0)*	-0.35 *(-0.43)*	2.16 *(-0.72)*
7	*anti*-**5-33**	0 *(0)*	2.41 *(2.47)*	3.80 *(0.49)*
8	*anti*-**5-34**	0 *(0)*	1.72 *(0.89)*	7.17 *(1.45)*
9	*syn*-**5-35**	0 *(0)*	7.19 *(6.01)*	3.18 *(-0.10)*
10	*syn*-**5-36**	0 *(0)*	2.66 *(2.45)*	1.10 *(-2.73)*

[a] the italic number is the relative energy at B3LYP/6-31G*.

5.6 "*Syn*-pentane" –like effect *vs* "*t*-butyl effect".

Our ^{1}H NMR and computational studies suggest that the aldols ***5*-5**, ***5*-6** and ***5*-29** ~ ***5*-36** prefer the conformation with the antiperiplanar arrangement of H2 and H3. Interestingly, we observe these favored conformations in *anti*- nitrile aldols and *syn*- ketone aldols, in which the two large groups at C2 and C3 are gauche to each other. However, if the size of the group at C2 or C3 was to increase further, it would cause a serious penalty for the gauche interaction between the two large groups at C2 and C3. The threshold was reached in *anti*-***5*-37** that bears a *t*-butyl group at C3.[130] As depicted in Figure 5.16, the aryl group at C2 and the large *t*-butyl group at C3 were roughly antiperiplanar; consequently, the H2 and H3 dihedral was -78.5°. The aldols *anti*-***5*-38** and *anti*-***5*-39** also exhibited the gauche relationship of the H2 and H3, which had a dihedral angle θ at -89.4° and -70.6 ° from X-ray crystallography,[130] consistent with the small vicinal coupling constant in

solution (< 2.0 Hz). This antiperiplanar arrangement of a *t*-butyl group to the largest vicinal substituent[254] is known as the "*t*-butyl effect".[255] Our results show that the conformational preference induced by a 2,6-disubtituted aryl group does not overwhelm the "*t*-butyl effect".

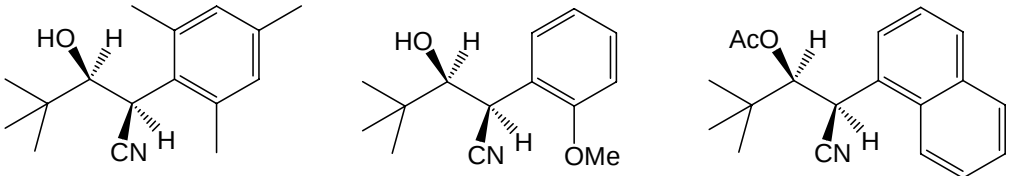

*anti-**5**-37*
θ = -78.3°
J^3_{23} = 3.9 Hz

*anti-**5**-38*
θ = -83.5°, -89.4°
J^3_{23} = <1 Hz

*anti-**5**-39*
θ = -70.6°
J^3_{23} = 2.0 Hz

Figure 5.16 The effect of *t*-butyl substitution at C3 on nitrile aldol conformation along the C2-C3 axis in the solid state (θ) and solution (J^3_{23}).

5.7 Conclusion

The 2,6-disubstituted aryl rings have steric effects on both directly attached and the adjacent sp^3 carbons. The 2,6-disubstituted ring is nearly eclipsed to the hydrogen on the directly attached carbon in order to minimize the 1,3-allylic strain. The 2,6-disubstituted ring also causes the "*syn*-pentane" –like interaction with groups on the adjacent sp^3-carbon. To minimize the "*syn*-pentane" –like interaction, the molecules adopt the conformation (along C2-C3 axis) which places the smallest hydrogen group at H2 roughly within the plane of 2,6-disubstituted aryl ring. Therefore, the antiperiplanar orientation of vicinal hydrogens (H2 and H3) is established. X-ray crystallography and the ^{1}H NMR spectroscopy reveal that the mesityl, 2,6-diethylphenyl, 2,6-diflurophenyl, 2,6-dichlorophenyl and 2,6-dibromophenyl exert this effect. The exceptions are limited to

cases in which the "*tert*-butyl effect" is dominant or unusually crowed ethanes.

Chapter 6 Experimental procedures

6.1 General information

^{1}H NMR spectra were taken on JEOL Eclipse 500, and Varian Inova 400 MHz Spectrometers; the corresponding ^{13}C NMR resonant frequencies were 125 and 100 MHz respectively. Variable temperature ^{1}H NMR and low temperature NOESY were recorded on Varian Unity 400 MHz. And chemical shifts were given in δ value with tetramethylsilane as an internal standard. High resolution mass spectra were collected on a JEOL HX110 dual focusing mass spectrometer under FAB conditions. Melting points were measured on BÜCHI B-540. Column chromatography was done with VWR silica gel 60 (60-240 mesh). TLC analyses were performed on commercial aluminum sheets coated with RDH silica gel $60F_{254}$. Tetrahydrofuran (THF) was freshly distilled from sodium/benzophenone immediately before use. All chemicals were purchased from Aldrich without further purification unless otherwise noted.

6.1 Tabulation of HPLC conditions and retention times for cyclopropylnitriles.

Reported retention times are determined from racemic and enantiomerically enriched /pure samples. The HPLC columns are not thermostatted and as a consequence retention times are subject to day to day variability.

Table 6.1 Chiral stationary phase HPLC conditions and retention times for cyclopropylnitriles.

Compound[a]	column	solvent, flowrate	fast enantiomer retention time (config.)	slow enantiomer retention time (config.)
Ph-CP-CN (***2*-1**)	AD	1% isopropylnol-hexane, 0.8 mL/min	18.1 min (R)	21.2 min (S)
Ph-CP-CN-Me (***2*-5**)	OD	6% isopropylnol-hexane, 0.5 mL/min	18.7 min	19.8 min
Ph-CP-CN-Bn (***2*-25**)	OD	1% isopropylnol-hexane, 0.8 mL/min	20.3 min	22.1 min
BnO-CH_2-CP-COOEt (***2*-21b**)	AD	1% isopropylnol-hexane, 1 mL/min	10.7 min (R)	11.7 min (S)
BnO-CP-CN (***2*-6**)	AD	2% isopropylnol-hexane, 0.8 mL/min	15.5 min (R)	15.0 min (S)
BnO-CP-CN-Me (***2*-26**)	OD	10% isopropylnol-hexane, 0.5 mL/min	21.1 min	22.7 min
MeO-Ph-CP-COOEt (***2*-21c**)	AD	1% isopropylnol-hexane, 1 mL/min	8.4 min (R)	7.2 min (S)
MeO-Ph-CP-CN (***2*-7**)	AD	1% isopropylnol-hexane, 1.0 mL/min	17.8min (R)	16.2 min (S)
BnO-$(CH_2)_3$-CP-COOEt (***2*-21d**)	OD	10% isopropylnol-hexane, 0.5 mL/min	13.1 min (R)	14.3 min (S)
TsO-$(CH_2)_3$-CP-CN (***2*-29**)	AD	15% isopropylnol-hexane, 1.0 mL/min	66.2 min (R)	70.1 min (S)
TsO$(CH_2)_3$-CP-CN-$(CH_2)_3$ (***2*-30**)	AD	6% isopropylnol-hexane, 0.5 mL/min	59.9 min	63.6min
Ph-CP-CN-Br (***3*-6**)	OD	1% isopropylnol-hexane, 0.8 mL/min	21.6 min (R)	22.6 min (S)

[a] CP stands for a cyclopropyl unit.

6.2 Synthetic procedures

Preparation of 1,1-substituted ethenes

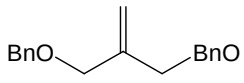

***2*-11** **1,3-Bisbenxyloxy-2-methylidenepropane**.

The NaH (1.59 g, 66 mmol, 2.2 equiv.) was added to the diol (2.42 mL, 30 mmol, 1 equiv.) in 50 mL fresh THF. The mixture was refluxed at 50 °C for 1h. After it was cooled to room temperature, benzyl bromide (9 mL, 75 mmol, 2.5 equiv.) was added into the flask. The mixture was stirred at 50 °C for another 1.5 h and then overnight at room temperature. The reaction was quenched by slowly adding sat'd NH_4Cl at room temperature. The aqueous layer was extracted by Et_2O (50 mL X 3). Combined organic layers, dried over Na_2SO_4, filtered and concentrated to give the crude product. The pure product was obtained in 97 % yield (7.10 g) after the chromatography (CH_2Cl_2). ^{1}HNMR (CD_3Cl) δ 4.08 (t, J = 1.1, 0.95 Hz, 4H), 4.53 (s, 4H), 5.27 (t, J = 1.2, 2H), 7.25-7.41 (m, 10H); ^{13}CNMR (CD_3Cl) δ 71.04, 72.32, 114.47, 127.73, 127.83, 128.52, 138.43, 142.82; HRMS (FAB) 269.154155 calcd for $C_{18}H_{21}O_2$, $[M+H]^+$ found 269.15411 (-0.2 ppm, 0.0 mmu).

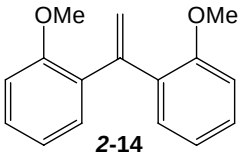

***2*-14** **1,1-Bis(*o*-methoxyphenyl)ethene.**

To a mixture of anisole (3.30 mL, 30 mmol, 1.2 equiv.) in 20 mL fresh THF/Et_2O (1:1) was added n-BuLi (10 mL, 2.5 M in hexane, 1.0 equiv.). The reaction mixture was refluxed at 50 °C for 2.5 h and the mixture was yellow. After the mixture was cooled to room temperature, EtOAc (1.3 mL, 13.3 mmol, 0.5 equiv.) was dropped in. The resulting light yellow and cloudy mixture was refluxed at 65 °C for 2h. The reaction was quenched by adding sat'd NH_4Cl after it was cooled to room temperature. Aqueous layer was

extracted by Et_2O (15 mL X 3). Combined organic layers, dried over Na_2SO_4, filtered and concentrated to give yellow solid residues. The crude alcohol was refluxed with 10 mL acetic anhydride overnight and then evaporated under reduced pressure. The crude product was recrystallized from EtOH to afford brown solids in 53% yield (1.58 g). ^{1}HNMR (CD_3Cl) δ 6.04 (s, 3H), 5.64 (s, 2H), 6.85-7.26 (m, 8H); ^{13}CNMR (CD_3Cl) δ 55.69, 111.39, 111.41, 119.02, 120.40, 128.28, 130.40, 131.95, 131.96, 144.02, 156.99; HRMS (FAB) 241.122855 calcd $C_{16}H_{17}O_2$, $[M+H]^+$ found 241.12230 (-2.3 ppm, -0.6 mmu).

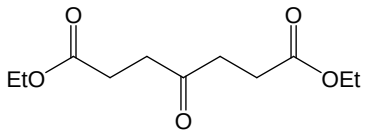

***2*-16** **Diethyl 4-oxopimelate**.[142]

To a flask containing 250 mL EtOH was added thionyl chloride (36 mL, 0.48 mol, 3.8 equiv.) dropwise at 0 °C. After completing addition, the mixture was warmed up to room temperature gently and furylacrylic acid (17.3 g, 0.125 mol, 1 equiv.) was added. The mixture was refluxed at 80 °C for 3.5 h, cooled to room temperature and concentrated. The residues were dissolved in CH_2Cl_2 (100 mL), and then washed with 5% $NaHCO_3$ (50 mL) followed by water (50 mL). The organic layer was dried over Na_2SO_4, filtered, concentrated to give the crude product. Purified by chromatography (2:1, hexane:EtOAc) to afford the product in 52% yield (14.0 g). ^{1}HNMR (CD_3Cl) δ 1.27 (t, *J* = 7.2 Hz, 6H), 2.62 (t, *J* = 6.6 Hz 4H), 2.80 (t, *J* = 6.6 Hz, 4H), 4.14 (q, *J* = 7.1, 4H); ^{13}CNMR (CD_3Cl) (ZYQ-V-80) δ 14.23, 28.05, 37.16, 60.23, 172.80, 207.15; HRMS

(FAB), 231.123249 calcd for $C_{11}H_{19}O_5$, $[M+H]^+$ found 231.1236 (+1.5 ppm, +0.3 mmu).

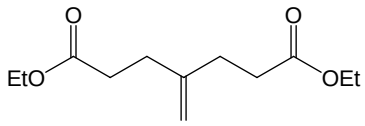

2-17 **Diethyl 4-methylidenepimelate.**[143]

The flask was charged with Zn (21.38 g, 0.33 mol), 80 mL fresh THF and CH_2Br_2 (3.56 mL, 0.051 mol, 1.2 equiv.). The mixture was stirred and cooled to -40 °C. And then $TiCl_4$ (5.75 mL, 0.052 mol, 1.2 equiv.) was added dropwise. The mixture was stirred at 5 °C for 3 days. Following 25 mL CH_2Cl_2 , diethyl 4-oxopimelate (9.58 g, 0.041 mol, 1 equiv.) in 25 mL CH_2Cl_2 was dropped in at 5 °C. The resulting mixture was stirred overnight, diluted with 120 mL Et_2O.and poured into a mixture of 50 g $NaHCO_3$ and 25 mL water. The mixture was stirred for another 3 h. And then the solid was filtered off, washed by Et_2O (150 mL X 3). The combined filtrate and ether solution was dried over Na_2SO_4, filtered, concentrated to give the crude product. Purified by chromatography (7:1, hexane: EtOAc) to afford product in 59 % yield (5.5 g). ^{1}HNMR (CD_3Cl) δ 1.29 (t, J = 7.2 Hz, 6H), 2.39 (t, J = 8.4 Hz, 4H), 2.50 (t, J = 8.0 Hz, 4H), 4.16 (q, J = 7.2, 4H), 4.81 (s, 2H); ^{13}CNMR (CD_3Cl) δ 14.28, 31.08, 32.73, 60.46, 109.88, 146.45, 173.22; HRMS (FAB), 229.143985calcd for $C_{12}H_{21}O_4$, $[M+H]^+$ found 229.14363 (-1.7 ppm, -0.4 mmu).

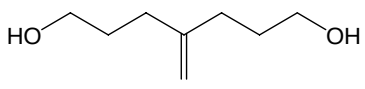

2-18 **4-Methylideneheptane-1,7-diol.**[143]

The flask was charged with $LiAlH_4$ (1.1 g, 27.5 mmol, 1.5 equiv.) in 30 mL dry Et_2O. Diethyl 4-methylidenepimelate (4.18 g, 18.3 mmol, 1 equiv.) in 15 mL Et_2O was slowly

dropped into the flask. The heat and the gas were generated during addition. After addition, the mixture was stirred at room temperature for 30 min. The 3 mL EtOAc was added to decompose the excess $LiAlH_4$. The solid was collected and added into 120 mL 20% H_2SO_4. And then the mixture was extracted by Et_2O (120 mL X 4). The combined ether layers were dried over $NaSO_4$, filtered, and concentrated to afford the oil product in 60 % yield (1.60 g). ^{1}HNMR (CD_3Cl) δ 1.74 (m, 4H), 1.92 (br, 2H), 2.15 (t, J = 7.6 Hz, 4H), 3.68 (t, J = 6.5 Hz,v4H), 4.81 (s, 2H); ^{13}CNMR (CD_3Cl) δ 30.69, 32.31, 62.56, 109.55, 148.97; HRMS (FAB) 141.091555 calcd for $C_8H_{13}O_2$, $[M+H]^+$ found 141.09082 (-5.3 ppm, -0.7 mmu).

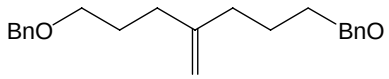

***2*-19** **1,7-Bisbenzyloxy-4-methylideneheptane**.

The NaH (0.46 g, 19.1 mmol, 2.2 equiv.) was added to the diol ***2*-18** (1.25 g, 8.7 mmol, 1 equiv.) in 30 mL fresh THF. The mixture was refluxed at 50 °C for 1h. After it was cooled to room temperature, benzyl bromide (2.6 mL, 22.0 mmol, 2.5 equiv.) was added into the flask. The mixture was stirred at 50 °C for another 1.5 h and then overnight at room temperature. The reaction was quenched by slowly adding sat'd NH_4Cl at room temperature. The aqueous layer was extracted by Et_2O (30 mL X 3). Combined organic layers, dried over Na_2SO_4, filtered and concentrated to give the crude product. The pure product was obtained in 52 % yield (7.10 g) after the chromatography (10:1, hexane: EtOAc). ^{1}HNMR (CD_3Cl) δ 1.80 (m, 4H), 2.15 (t, J = 7.6 Hz, 4H), 3.52 (t, J = 6.5 Hz, 4H), 4.54 (s, 4H), 4.78 (s, 2H), 7.29-7.39 (m, 10H); ^{13}CNMR (CD_3Cl) δ 27.99,

32.64, 70.13, 73.03, 109.35, 127.62, 127.75, 128.47, 138.74, 148.77; HRMS (FAB) 325.216755 calcd for $C_{22}H_{29}O_2$, $[M+H]^+$ found 325.21744 (+2.0 ppm, +0.7 mmu).

General procedure to synthesize 2,2-disubstituted cyclopropylnitriles

General procedure for synthesis of ethyl 2,2-disubstituted cyclopropanecarboxylate.

A two-necked round bottom flask was equipped with a equilibrium funnel containing ethyl diazoacetate (3 euqiv.) in CH_2Cl_2. Copper(I) triflate (0.01 equiv.), and ligand BOX (0.011 equiv.) in CH_2Cl_2 was added into the round bottom flask. The mixture was allowed to stirring at room temperature for 1 h under the N_2 gas. 1,1-Disubstituted ethene (1 equiv.) in 1 mL CH_2Cl_2 was added into the flask via a syringe and stirred for another 15 min. Ethyl diazoacetate in CH_2Cl_2 was very slowly dropped into the round bottom flask through the equilibrium funnel over 12-24 h. The mixture solution turned from green to yellow and then to red yellow with the formation of bubbles. The reaction mixture was stirred at room temperature for 24 h. The crude product was obtained by stripping off solvent and purified by flash column chromatography on silica gel affording the ethyl 2,2-disubstituted cyclopropylcarboxylic ester.

General procedure for synthesis of 2,2-disubstituted cyclopropanecarboxylic acid.

The round bottom flask was charged with cyclopropyl ethyl carboxylic ester (1 equiv.) in 5% NaOH in EtOH/H_2O (95:5). The mixture was yellow and stirred at room temperature for 6h. After concentrated via vacuum, the remained solid was re-dissolved in D. I. water. The aqueous solution was extracted by Et_2O once. Then, the aqueous solution was neutralized by adding 2N HCl until pH got to 2. Placed the solution in

refrigerator for a while, the oil or the precipitate was observed at the bottom of the flask. The oil or the precipitate was extracted by EtOAc. The combined extracts were dried over anhydrous Na_2SO_4, filtered and concentrated. The crude product was used for next step without further purification.

General procedure for synthesis of 2,2-disubstituted cyclopropanecarboxamide.

The round bottom flask was charged with cyclopropylcarboxylic acid (1 equiv.) and N-hydroxy succinimide (1.5 equiv.)in CH_2Cl_2. The solution was cooled in ice-water bath. After adding EDCI (1.5 equiv.) in CH_2Cl_2, the reaction mixture was stirred at room temperature for 6 h. The excess of ammonium hydroxide was added and stirred for 2 h. Separated two layers and extracted the aqueous layer by EtOAc. The combined organic layers were dried over anhydrous Na_2SO_4, filtered and concentrated. The crude product was purified by flash column chromatography on silica gel (90:10 CH_2Cl_2:MeOH).

General procedure for synthesis of 2,2-disubstituted cyclopropylnitrile.

The round bottom flask was charged with cyclopropylcarboxylic amide (1 equiv.) and *p*-toluenesulfonyl chloride (3 equiv.) in dry pyridine. The mixture was stirred at room temperature overnight. To the mixture, 2 mL water was added and then stirred for another 1 h. The reaction was quenched by adding 37% HCl slowly. The product was extracted by EtOAc. The combined organic layers were dried over Na_2SO_4, filtered and concentrated. The crude product was purified by flash column chromatography on silica gel (2:1 hexane:EtOAc).

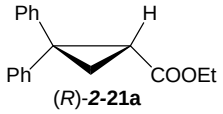

(*R*)-***2*-21a** **Ethyl 2,2-diphenylcyclopropanecarboxylate**.

To the mixture of copper triflate (100.1 mg, 0.2 mmol, 0.01 equiv.) and ligand BOX (65.5 mg, 0.22 mmol, 0.011 equiv) in 8 mL CH_2Cl_2 was added 2,2-diphenyl ethene (3.5 mL, 20mmol, 1 equiv.). After stirring for 15 min, ethyl diazoacetate (6.3 mL, 60 mmol, 3 equiv.) in 80 mL CH_2Cl_2 was slowly dropped in to flask over 24 h via an equilibrium funnel. After concentration, the crude product was purified by column chromatography on silica gel (10:1 Hexane:EtOAc) to afford ZYQ-II-50 in 80% yield (4.2 g). ^{1}HNMR (CD_3Cl) δ 1.00 (q, J = 7.1 Hz, 3H), 1.58 (dd, J = 4.9, 8.3 Hz, 1H), 2.17 (dd, J = 4.8, 6.0 Hz, 1H), 2.54 (dd, J = 6.0, 8.3 Hz, 1H), 3.90 (m, 2H), 7.16-7.36 (m, 10H); ^{13}CNMR (CD_3Cl) δ 14.10, 20.21, 29.14, 39.92, 60.54, 126.61, 127.05, 127.68, 128.37, 128.54, 129.86, 130.16, 132.51, 140.36, 144.98, 170.77; HRMS (FAB) 267.138505 calcd for $C_{18}H_{19}O_2$, $[M+H]^+$, found 267.13889 (+1.4 ppm,+0.4 mmu).

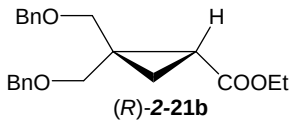

(*R*)-***2*-21b** **Ethyl 2,2-dibenzloxymethyl cyclopropanecarboxylate**.

To the mixture of copper triflate (101.7 mg, 0.2 mmol, 0.01 equiv.) and ligand BOX (66.7 mg, 0.22 mmol, 0.011 equiv) in 8 mL CH_2Cl_2 was added 2,2-disubstituted ethene (4.9 g, 20 mmol, 1 equiv.). After stirring for 15 min, ethyl diazoacetate (5.4 mL, 51 mmol, 2 equiv.) in 80 mL CH_2Cl_2 was slowly dropped in to flask over 24 h via an equilibrium funnel. After concentration, the crude product was purified by column chromatography on silica gel (5:1 Hexane:EtOAc) to afford products in 69% yield (5.0 g). ^{1}HNMR

(CD_3Cl) δ 1.15 (dd, *J* = 4.8, 8.1 Hz, 1H), 1.25-1.32 (m, 4H), 1.81 (dd, *J* = 5.7, 8.0 Hz, 1H), 3.32 (d, *J* = 9.6 Hz, 1H), 3.60 (d, *J* = 9.9 Hz, 1H), 3.77 (d, *J* = 9.9 Hz, 1H), 3.92 (d, *J* = 9.9 Hz, 1H), 4.10-4.19 (m, 2H), 4.77 (d, *J* = 4.0 Hz, 2H), 4.54 (s, 2H), 7.29-7.39 (m, 10H); ^{13}CNMR (CD_3Cl) δ 14.22, 16.72, 22.28, 30.83, 60.71, 61.42, 68.39, 72.74, 73.02, 73.09, 127.54, 127.65, 127.71, 127.73, 128.36, 128.47, 138.51, 138.69, 172.12; HRMS (FAB) 355.190934 calcd for $C_{22}H_{27}O_4$, $[M+H]^+$, found 355.19223 (+3.6 ppm, +1.3 mmu).

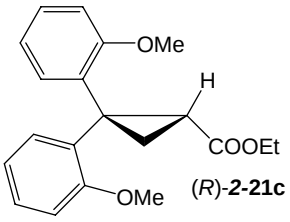

(*R*)-***2*-21c**

Ethyl 2,2-di(*o*-methoxyphenyl) cyclopropanecarboxylate.

To the mixture of copper triflate (40.8 mg, 0.08 mmol, 0.013 equiv.) and ligand BOX (25.7 mg, 0.087 mmol, 0.014 equiv) in 1 mL CH_2Cl_2 was added 2,2-substituted ethene (1.5 g, 6.25 mmol, 1 equiv.). After stirring for 15 min, ethyl diazoacetate (2 mL, 18.7 mmol, 3 equiv.) in 80 mL CH_2Cl_2 was slowly dropped in to flask over 24 h via an equilibrium funnel. After concentration, the crude product was purified by column chromatography on silica gel (7:1 Hexane:EtOAc) to afford products in 55% yield (1.12 g). ^{1}HNMR (CD_3Cl) δ 1.07 (t, *J* = 7.1 Hz, 3H), 1.46 (dd, *J* = 4.6, 8.0 Hz, 1H), 1.94 (t *J* = 5.1 Hz, 1H), 2.40 (dd, *J* = 6.2, 8.3 Hz 1H), 3.74 (s, 3H), 3.82 (s, 3H), 3.96 (q, *J* = 7.1 Hz, 2H), 6.83-7.22 (m, 8H); ^{13}CNMR (CD_3Cl) (hy-I-25, robot) δ 14.14, 20.92, 27.18, 33.05, 54.81, 55.19, 59.94, 109.74, 110.58, 119.87, 127.82, 127.90, 129.81, 131.49, 131.95, 158.21, 158.26, 172.16; HRMS (FAB) 327.159635 calcd for $C_{20}H_{23}O_4$, $[M+H]^+$, found

327.15717 (-7.5 ppm, -2.4 mmu).

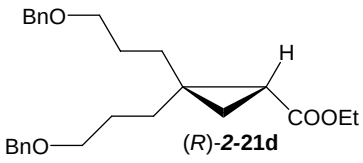

(*R*)-***2*-21d**

Ethyl 2,2-di(3-benzloxypropyl) cyclopropanecarboxylate.

To the mixture of copper triflate (23.6 mg, 0.047 mmol, 0.017 equiv.) and ligand BOX (17.6 mg, 0.06 mmol, 0.022 equiv) in 0.5 mL CH_2Cl_2 was added 2,2-disubstituted ethene (0.87 g, 2.7 mmol, 1 equiv.). After stirring for 15 min, ethyl diazoacetate (0.85 mL, 8 mmol, 3 equiv.) in 40 mL CH_2Cl_2 was slowly dropped in to flask over 12 h via an equilibrium funnel. After concentration, the crude product was purified by column chromatography on silica gel (7:1 Hexane:EtOAc) to afford products in 70% yield (0.77 g). ^{1}HNMR (CD_3Cl) δ 0.88 (dd, J = 4.4, 8.0 Hz, 1H), 1.11 (t, J = 4.8 Hz, 1H), 1.33-1.76 (m, 12H), 3.48 (m, 4H), 4.30 (q, J = 7.2 Hz, 2H), 4.52 (s, 2H), 4.53 (d, J =1.6 Hz, 2H), 7.30-7.39 (m, 10H); ^{13}CNMR (CD_3Cl) δ 14.45, 20.72, 25.22, 26.27, 26.59, 27.04, 30,29, 33.33, 60.30, 70.00, 70.54, 72.94, 73.01, 127.55, 127.63, 127.70, 127.73, 128.42, 128.47, 129.89, 138.59, 172.71; HRMS (FAB) 411.253535 calcd for $C_{26}H_{35}O_4$, $[M+H]^+$, found 411.25485 (+3.4 ppm, +1.4 mmu).

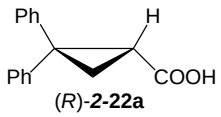

(*R*)-***2*-22a**

2,2-Diphenylcyclopropanecarboxylic acid.

The ethyl ester (*R*)-***2*-21a** (2.27 g, 8.5 mmol) in 30 mL 5% NaOH in 95%EtOH was stirred overnight. The crude carboxylic acid was obtained in 82% yield (1.71 g). ^{1}HNMR (CD_3OD) δ 1.59 (dd, J = 4.8, 8.0 Hz, 1H), 2.06 (dd, J = 4.8, 5.8 Hz, 1H), 2.49 (dd, J =

5.8, 8.1 Hz, 1H), 7.12-7.37 (m, 10H); ^{13}CNMR (CD_3Cl) δ 20.79, 27.14, 29.95, 126.78, 127.20, 127.68, 128.50, 128.60, 129.67, 131.39, 139.54, 172.47; HRMS (FAB) 239.107205 calcd for $C_{16}H_{15}O_2$, $[M+H]^+$, found 239.10739 (+0.8 ppm, 0.2 mmu).

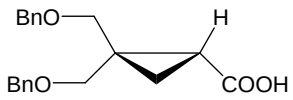

(*R*)-***2*-22b** **2,2-Dibenzloxymethyl cyclopropanecarboxylic acid**.

The ethyl ester (*R*)-***2*-21b** (2.84 g, 8.0 mmol) in 30 mL 5% NaOH in 95% EtOH was stirred overnight. The crude product was afforded in 75 % yield (1.95 g). ^{1}HNMR (CD_3OD) δ 1.09 (dd, *J* = 4.7, 1H), 1.17 (t, *J* = 6.9 Hz, 1H), 1.73 (dd, *J* = 5.8 Hz, 8.0 Hz, 1H), 3.30-3.33 (m, 2H), 3.59 (d, *J* = 10.1 Hz, 1H), 3.68 (d, *J* = 9.6 Hz, 1H), 3.85 (d, *J* = 10.1 Hz, 1H), 3.78-3.49 (m, 4H), 7.22-7.34 (m, 10H); ^{13}CNMR (CD_3Cl) δ 17.47, 22.01, 31.56, 68.20, 72.53, 73.10, 127.60, 127.71, 127.73, 128.38, 128.40, 138.20, 138.43, 177.86; HRMS (FAB) 327.159635 calcd for $C_{20}H_{23}O_4$, $[M+H]^+$, found 327.15921 (-1.3ppm, -0.4 mmu)

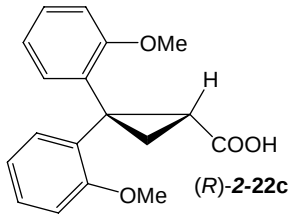

(*R*)-***2*-22c** **2,2-Di(*o*-methoxyphenyl)cyclopropanecarboxylic acid**.

The ethyl ester (*R*)-***2*-21c** (1.11 g, 3.4 mmol) in 20 mL 5% NaOH in 95% EtOH was stirred overnight. The crude product was obtained in 73% yield (0.74 g). ^{1}HNMR (CD_3Cl) δ 1.55 (dd, *J* = 4.8, 8.3 Hz, 1H), 1.92 (t, *J* = 5.1 Hz, 1H), 2.40 (dd, *J* = 6.2, 8.0 Hz, 1H), 3.71 (s, 3H), 3.83 (s, 3H), 6.68-7.70 (m, 8H); ^{13}CNMR (CD_3Cl) δ 21.33, 26.69, 33.26,

54.64, 55.04, 109.85, 110.47, 119.73, 119.80, 127.62, 127.73, 127.85, 131.29, 131.79, 158.04, 158.12, 174.90; HRMS (FAB) 299.128335 calcd for $C_{18}H_{19}O_4$, $[M+H]^+$, found 299.12677 (-5.1ppm, -1.5 mmu).

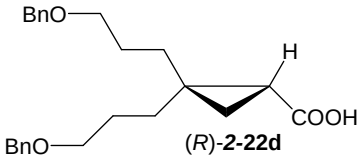

(*R*)-***2*-22d** **2,2-Di(3-benzloxypropyl) cyclopropanecarboxylic acid**.

The ethyl ester (*R*)-***2*-21d** (1.87 g, 4.6 mmol) in 20 mL 5% NaOH in 95% EtOH was stirred overnight. The crude product was obtained in 66% yield (1.14 g). ^{1}HNMR (CD_3Cl) δ 0.93 (t, *J* = 4.4 Hz, 1H), 1.11 (t, *J* = 5.1 Hz, 1H), 1.34-1.73 (m, 9H), 3.40-3.51 (m, 4H), 4.47-4.52 (m, 4H), 7.25-7.37 (m, 10H); ^{13}CNMR (CD_3Cl) δ 21.72, 25.13, 26.02, 26.53, 26.92, 31.72, 33.43, 69.05, 70.39, 72.88, 73.00, 127.57, 127.67, 127.71, 127.77, 128.44, 128.47, 138.52, 138.62, 178.81; HRMS (FAB) 383.222235 calcd for $C_{24}H_{31}O_4$, $[M+H]^+$, found 383.22100 (-3.2 ppm, -1.2 mmu).

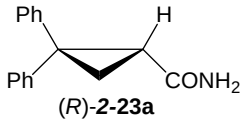

(*R*)-***2*-23a** **2,2-Diphenylcyclopropanecarboxamide**.

To the mixture of acid (*R*)-***2*-22a** (1.61 g, 6.8 mmol, 1 equiv.) and NHS (1.17g, 10.2 mmol, 1.5 equiv.) in 40 mL CH_2Cl_2 was added EDCI (1.98 g, 10.2 mmol, 1.5 equiv.) in 50 mL CH_2Cl_2. After stirring for 6 h, 50 mL ammonium hydroxide was added and stirred overnight. Purified by silica gel (9:1, CH_2Cl_2:AcOEt) to give the pure product in 83% yield (1.34 g). ^{1}HNMR (CD_3Cl) δ 1.68 (dd, *J* = 5.2, 8.4 Hz, 1H),2.16 (t, *J* =5.2 Hz, 1H), 2.37 (dd, *J* = 6.0, 8.4 Hz,1H), 5.19-5.41 (d, br, 1H), 7.20-7.42 (m, 10H); ^{13}CNMR (CD_3Cl)

δ 20.11, 30.61, 39.19, 126.45, 127.08, 127.33, 128.46, 129.81, 139.84, 145.12, 171.68; HRMS (FAB) 238.123189 calcd for $C_{16}H_{16}NO$, $[M+H]^+$, found 238.12346 (+1.3 ppm, +0.3 mmu).

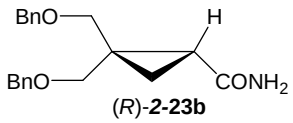

(*R*)-***2*-23b**

2,2-Dibenzloxymethyl cyclopropanecarboxamide.

To the mixture of acid (*R*)-***2*-22b** (1.19 g, 3.7 mmol, 1 equiv.) and NHS (0.63g, 5.5 mmol, 1.5 equiv.) in 20 mL CH_2Cl_2 was added EDCI (1.05 g, 5.5 mmol, 1.5 equiv.) in 10 mL CH_2Cl_2. After stirring for 6 h, 20 mL ammonium hydroxide was added and stirred overnight. Purified by silica gel (9:1, CH_2Cl_2:MeOH) to give the pure product in 76% yield (0.91 g). ^{1}HNMR (CD_3Cl) δ 1.08 (dd, *J* = 4.8, 8.0 Hz, 1H), 1.34 (t, *J* = 4.8 Hz, 1H), 1.64 (1H), 3.45 (d, *J* 10.0 Hz, 1H), 3.65 (dd, *J* = 9.6, 10.0 Hz, 2H), 3.85 (d, *J* = 10.0 Hz, 1H), 4.45-4.57 (m, 4H), 5.35 (br, 1H), 5.79 (br, 1H), 7.29-7.39 (m, 10H); ^{13}CNMR (CD_3Cl) δ 15.24, 23.55, 29.82, 68.48, 72.85, 73.04, 127.53, 127.65, 127.74, 128.30, 128.39, 138.16, 138.46, 172.94; HRMS (FAB) 326.175619 calcd for $C_{20}H_{24}NO_3$, $[M+H]^+$ found 326.17661 (+3.0 ppm, +1.0 mmu).

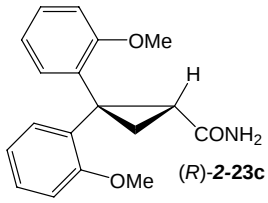

(*R*)-***2*-23c**

2,2-Di(*o*-methoxyphenyl) cyclopropanecarboxamide.

To the mixture of acid (*R*)-***2*-22c** (0.74 g, 2.5 mmol, 1 equiv.) and NHS (0.45g, 3.9 mmol, 1.5 equiv.) in 10 mL CH_2Cl_2 was added EDCI (0.73 g, 3.9 mmol, 1.5 equiv.) in 5 mL CH_2Cl_2. After stirring for 6 h, 20 mL ammonium hydroxide was added and stirred

overnight. Purified by silica gel (9:1, CH_2Cl_2:MeOH) to give the pure product in 97% yield (0.71 g). ^{1}HNMR (CD_3Cl) δ 1.49 (dd, *J* = 5.3, 8.5 Hz, 1H), 1.88 (dd, *J* = 5.1, 6.0 Hz, 1H), 2.27 (dd, *J* = 6.2, 8.3 Hz, 1H), 3.77 (s, 3H) 3.83 (s 3H), 5.15 (br, 1H), 5.34 (br, 1H), 6.72-7.66 (m, 8H); ^{13}CNMR (CD_3Cl) δ 20.18, 28.80, 32.05, 55.03, 55.17, 110.41, 110.59, 119.87, 120.02, 127.87, 128.11, 131.24, 131.49, 158.13, 158.50, 173.58; HRMS (FAB) 298.144319 calcd for $C_{18}H_{20}NO_3$, $[M+H]^+$ found 298.14386 (-1.4 ppm, -0.4 mmu).

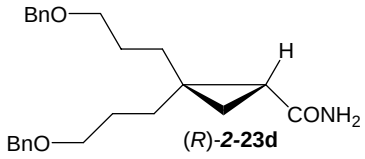

(*R*)-***2*-23d** **2,2-Di(3-benzloxypropyl) cyclopropanecarboxamide**.

To the mixture of acid (*R*)-***2*-22d** (1.10 g, 2.9 mmol, 1 equiv.) and NHS (0.52 g, 4.5 mmol, 1.5 equiv.) in 20 mL CH_2Cl_2 was added EDCI (0.81 g, 4.2 mmol, 1.5 equiv.) in 10 mL CH_2Cl_2. After stirring for 6 h, 25 mL ammonium hydroxide was added and stirred overnight. Purified by silica gel (9:1, CH_2Cl_2:MeOH) to give the pure product in 80% yield (0.87 g). ^{1}HNMR (CD_3Cl) δ 0.75 (dd, J = 4.4, 7.6 Hz, 1H), 1.08 (t, J = 4.8 Hz, 1H), 1.28-1.69 (m, 9H), 3.46 (m, 4H), 4.49 (d, J = 6.0 Hz, 4H), 5.67 (br, 1H), 5.79 (br, 1H), 7.21-7.38 (m, 10H); ^{13}CNMR (CD_3Cl) δ 19.65, 25.16, 26.80, 27.11, 27.78, 29.59, 33.72, 70.29, 70.88, 73.13, 73.20, 127.73, 127.89, 127.93, 127.95, 128.59, 128.68, 138.67, 138.84, 174.07; HRMS (FAB) 382.238219 calcd for $C_{24}H_{32}NO_3$, $[M+H]^+$ found 382.2387 (+1.3 ppm, +0.5 mmu).

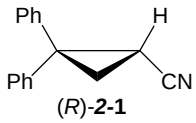

(*R*)-***2*-1** **2,2-Diphenyl cyclopropylnitrile**.

The mixture of amide (*R*)-***2*-23a** (1.31, 5.5 mmol, 1 equiv.) and p-TsCl (3.22 g, 16.9 mmol, 3 equiv.) in 20 mL pyridine was stirred overnight. The crude product was purified by column (3:1, hexane:EtOAc) to give the nitrile in 88% yield (1.07 g). ^{1}HNMR (CD_3Cl) δ 1.81 (dd, *J* =5.2, 9.2 Hz, 1H), 2.02 (t, *J* = 6.0 Hz, 1H), 2.22 (dd, *J* = 5.6, 9.2 Hz, 1H), 7.19-7.44 (m, 10H); ^{13}CNMR (CD_3Cl) δ 12.32, 21.11, 38.37, 119.57, 127.49, 127.87, 128.03, 128.89, 128.95, 129.46, 139.00, 142.41; HRMS (FAB) 220.112623 calcd for $C_{16}H_{14}N$, $[M+H]^+$ found 220.1133 (+3.1 ppm, +0.7 mmu).

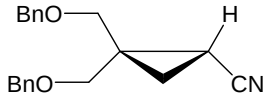

(*R*)-***2*-6** **2,2-Dibenzloxymethyl cyclopropylnitrile**.

The mixture of amide (*R*)-***2*-23b** (1.50 g, 4.6 mmol, 1 equiv.) and p-TsCl (2.63 g,13.8 mmol, 3 equiv.) in 20 mL pyridine was stirred overnight. The crude product was purified by column (3:1, hexane:EtOAc) to give the nitrile in 83% yield (1.16 g). ^{1}HNMR (CD_3Cl) δ 1.11 (t, *J* = 5.6 Hz, 1H), 1.27 (dd, *J* = 5.2, 8.8 Hz, 1H), 1.59 (dd, *J* = 5.6, 8.8 Hz, 1H), 3.52 (d, *J* = 1.6 Hz, 2H), 3.65 (d, *J* = 10.4 Hz, 1H), 3.70 (d, *J* = 10.0 Hz, 1H), 4.47 (s, 2H), 4.55 (d, *J* = 2.0 Hz, 2H), 7.25-7.37 (m, 10H); ^{13}CNMR (CD_3Cl) δ 6.03, 15.94, 28.47, 70.01,70.83,73.27, 73.58, 119.97, 127.73, 127.91, 127.93, 127.95, 128.55, 128.58, 137.84, 137.94; HRMS (FAB) 308.165054 calcd for $C_{20}H_{22}NO_2$, $[M+H]^+$ found 308.1649 (-0.5 ppm, -0.2 mmu).

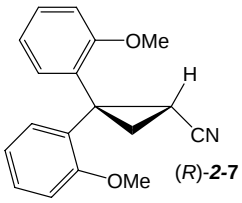

(*R*)-***2*-7** **2,2-Di(*o*-methoxyphenyl) cyclopropylnitrile**.

The mixture of amide (*R*)-***2*-23c** (0.67 g, 2.3 mmol, 1 equiv.) and p-TsCl (1.30 g, 6.7 mmol, 3 equiv.) in 10 mL pyridine was stirred overnight. The crude product was purified by column (3:1, hexane:EtOAc) to give the nitrile in 54% yield (0.34 g). ^{1}HNMR (CD_3Cl) δ 1.61 (dd, *J* = 5.3, 9.0 Hz, 1H), 1.82 (t, *J* = 5.7 Hz, 1H), 2.11 (dd, *J* = 6.0, 9.0 Hz, 1H), 3.82 (s, 3H), 3.87 (s, 3H), 6.74-7.65 (m, 8H); ^{13}CNMR (CD_3Cl) δ 10.90, 21.42, 30.88, 55.17, 55.31, 110.53, 110.83, 119.94, 120.10, 120.72, 127.00, 128.53, 129.00, 129.60, 130.92, 131.56, 158.13, 158.50; HRMS (FAB) 280.133754 calcd for $C_{18}H_{18}NO_2$, $[M+H]^+$ found 280.1344 (+2.3 ppm, +0.6 mmu).

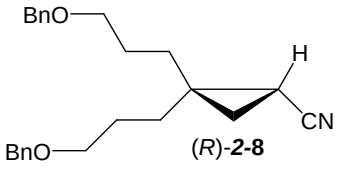

(*R*)-***2*-8** **2,2-Di(3-benzloxypropyl) cyclopropylnitrile**.

The mixture of amide (*R*)-***2*-23d** (0.67 g, 1.8 mmol, 1 equiv.) and p-TsCl (1.12 g, 5.3 mmol, 3 equiv.) in 10 mL pyridine was stirred overnight. The crude product was purified by column (3:1, hexane:EtOAc) to give the nitrile in 70% yield (0.45 g). ^{1}HNMR (CD_3Cl) δ 0.96-1.02 (m, 2H), 1.24 (dd, *J* = 5.4, 8.6 Hz, 1H), 1.34-1.52 (m, 2H), 1.62-1.93 (m, 6H), 3.46-3.57 (m, 4H), 4.51 (s, 2H), 4.54 (s, 2H), 7.29-7.40 (m, 10H); ^{13}CNMR (CD_3Cl) δ 9.45, 20.98, 26.40, 26.47, 27.69, 29.34, 31.56, 69.54, 70.09, 73.01, 73.09, 120.80, 127.65, 127.75, 128.48, 128.52, 138.39, 138.52; HRMS (FAB) 364.227654 calcd for $C_{24}H_{30}NO_2$,

$[M+H]^+$ found 364.22644 (-3.4 ppm, -1.2 mmu).

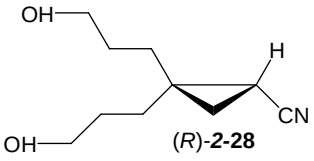

(*R*)-***2*-28** **2,2-Di(3-hydroxypropyl) cyclopropylnitrile**.

The 10 mL round bottom flask was charged with 33.7 mg (0.03 mmol) of 10% Palladium on active carbon. The flask was reflushed by H_2 gas for three times. The corresponding nitrile (*R*)-***2*-8** (59.6 mg, 0.16 mmol) in 5 mL MeOH was transferred to the flask which was filled with H_2 gas. The reaction was stirred at room temperature under the H_2 gas overnight. After filtering off the carbon, the crude product was 20.4 mg in 68 % yield which was used for the next step without further purification. ^{1}HNMR (CD_3Cl) δ 0.97 (t, *J* = 5.2 Hz, 1H), 1.02 (dd, *J* = 5.1, 8.7 Hz, 1H), 1.24 (dd, *J* = 5.5, 8.7, 1H), 1.33-1.82 (m, 8H), 3.64 (t, *J* = 6.3 Hz, 2H), 3.69 (t, *J* = 6.2 Hz, 2H); ^{13}CNMR (CD_3Cl) δ 9.41, 21.02, 27.69, 28.89, 28.97, 29.03, 31.15, 62.04, 62.35, 120.87; HRMS (FAB) 184.133754 calcd for $C_{10}H_{18}NO_2$, $[M+H]^+$ found 184.13332 (-2.5 ppm, -0.5 mmu).

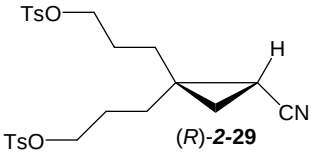

(*R*)-***2*-29** **2,2-Di(3-(*p*-toluenesulfonyloxy)-propyl) cyclopropylnitrile**.

A 10 mL round bottom flask was charged with the nitrile (*R*)-***2*-28** (20.4 mg, 0.11 mmol) and p-TsCl (63.8 mg, 0.33 mmol), followed by adding pyridine 3mL at 0 °C. The reaction mixture was placed in the fridge overnight. Next day, the 3mL 1N HCl was added to the reaction mixture. The product was extracted by Et_2O (5mL x 3). The ether layers were combined, dried by Na_2SO_4, concentrated to yield the crude product (47.5

mg). Purified on PTLC (EtOAc:hexane 1:1) and led to a product (29 mg) in 53% yield. ^{1}HNMR (CD_3Cl) δ 0.93 (t, J = 5.2 Hz, 1H), 1.00 (dd, J = 5.2, 8.8 Hz, 1H), 1.21 (dd, J = 5.4, 8.6, 1H), 1.34-1.89 (m, 8H), 2.50 (d, 6H), 4.01-4.11 (m, 2H), 7.38-7.82 (m, 8H); ^{13}CNMR (CD_3Cl) δ 9.61, 21.01, 21.89, 25.82, 27.11, 28.86, 29.14, 29.96, 31.04, 69.77, 70.14, 120.31, 128.09, 128.14, 130.18, 133.08, 145.18, 145.29; HRMS (FAB) 492.151458 calcd for $C_{24}H_{30}NO_6S_2$, $[M+H]^+$ found 492.1516 (+3.0 ppm, +0.2 mmu).

General procedure for H-D exchange of 2,2-disubstituted cyclopropylnitriles

The prepared base solution (1 M, 0.5 mL, 0.5 mmol) was added to 2,2-disubstituted cyclopropylnitrile (0.017 mmol). After warmed at 50 °C (or at room temperature) for a certain time period, the reaction was quenched by adding saturated NH_4Cl. Products were extracted by Et_2O (2 mL x 3). After organic layers were combined, dried over Na_2SO_4, concentrated in vacuo, the obtained crude product was used for ^{1}H NMR analysis. The purified product (by PTLC, Hexane: CH_2Cl_2(1:1)) was used for measurement of the enantiomeric excess.

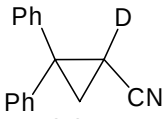

***2*-2** **1-Deuterio-2,2-diphenyl-cyclopropylnitrile**.

Compound (*R*)-***2*-1** (3.8 mg, 0.017 mmol) was added to a base solution NaOMe/CD_3OD (1 M). After stirred at 50 °C for 3 days, the titled compound were obtained in 97% yield (3.7 mg, >99% deuteration). HPLC analysis indicated >99% ee (*R*).^{1}H NMR (CD_3Cl) δ1.80 (d, J = 5.2 Hz, 1H), 2.02 (d, J =5.6 Hz, 1H), 7.17-7.53 (m,

10H); ^{13}C NMR (CD_3Cl) δ 12.32, 21.00, 38.28, 119.55, 127.49, 127.87, 128.03, 128.58, 128.89, 128.95, 129.47, 129.90, 138.99, 142.39; HRMS (FAB) 221.1189 calcd for $C_{16}H_{13}DN$, $[M+H]^+$ found 221.11850 (-1.8 ppm, -0.4 mmu).

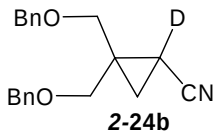

***2*-24b** **1-Deuterio-2,2-dibenzyloxymethyl-cyclopropylnitrile**.

Enantioenriched compound (*R*)-***2*-6** (6.4 mg, 0.020 mmol, 86% ee) was added to a base solution NaOMe/CD_3OD (1 M). After stirred at 50 °C for 1 days, the titled compound was isolated in 70% yield (4.5 mg, >99% deuteration). HPLC analysis indicated 81% ee (*R*). ^{1}HNMR ($CDCl_3$) δ 1.10 (d, *J* = 5.0 Hz, 1H), 1.23 (d, *J* = 5.2 Hz, 1H), 3.52 (d, *J* = 2.0 Hz, 2H), 3.59 (d, *J* = 10.5 Hz, 1H), 3.79 (d, *J* = 10.5 Hz, 1H), 4.46 (s, 2H), 4.54 (d, *J* = 3.5 Hz, 2H), 7.25-7.37 (m, 10H); ^{13}CNMR (CD_3Cl) δ 7.80, 15.94, 29.78, 69.95, 70.81, 73.26, 73.56, 119.79, 127.70, 127.87, 127.90, 127.93, 128.51, 128.55, 138.83, 139.03.

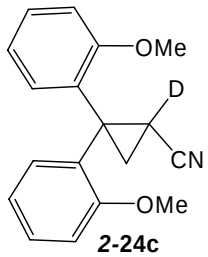

***2*-24c** **1-Deuterio-2,2-di(*o*-methoxylphenyl)-cyclopropylnitrile**

Enantioenriched compound (*R*)-***2*-7** (4.7 mg, 0.017 mmol, 96% ee) was added to a base solution NaOMe/CD_3OD (1 M). After stirred at 50 °C for 8 days, the titled compound starting material was recovered in 87% yield (4.1 mg, >56% deuteration). HPLC analysis indicated 94% ee (*R*). ^{1}H NMR data were deduced by inspection of a

mixture of ***2*-7** and ***2*-24c**. ^{1}HNMR ($CDCl_3$) δ 1.60 (d, *J* = 5.2 Hz, 1H), 1.83 (d, *J* =5.5 Hz, 1H), 3.83 (s, 3H), 3.88 (s, 3H), 6.77-7.67 (m, 8H); ^{13}C NMR ($CDCl_3$) δ 11.02, 21.43, 30.90, 55.30, 55.45, 110.64, 110.94, 120.06, 120.23, 120.87, 127.09, 128.67, 129.13, 129.66, 131.06, 131.70, 158.25, 158.62.

General in situ protocol for deprotonation/alkylation of 2,2-disubstituted cyclopropyl nitriles

At a certain temperature under N_2 gas, to a stirred solution of 2,2-disubstituted cyclopropylnitrile (0.10 mmol, 1.0 equiv.) in anhydrous solvent (1 mL), the electrophile was added. The reaction was quenched at -100 °C by the addition of saturated aqueous NH_4Cl (2 mL) and extracted with Et_2O (3 x 5mL). The combined extracts were dried over Na_2SO_4, filtered, and concentrated. The crude product was purified by PTLC.

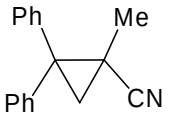

***2*-5** **2,2-Diphenyl-1-methyl-cyclopropylnitrile**.

^{1}HNMR (CD_3Cl) δ 1.29 (s, 3H), 1.63 (d, *J* = 5.3 Hz, 1H), 2.04 (d, *J* =5.3 Hz, 1H), 7.17-7.53 (m, 10H); ^{13}CNMR (CD_3Cl) δ 16.71, 19.91, 26.41, 42.90, 122.73, 127.54, 127.67, 128.56, 128.85, 128.91, 129.21, 129.39, 139.45, 141.56 ; HRMS (FAB) 234.128274 calcd for $C_{17}H_{16}N$, $[M+H]^+$ found 234.12860 (+1.4 ppm, +0.3 mmu).

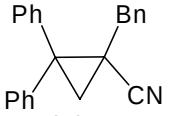

***2*-25** **1-Benzyl-2,2-diphenylcyclopropylnitrile**.

^{1}HNMR (CD_3Cl) δ 1.91 (d, *J* = 5.5 Hz, 1H), 2.04 (d, *J* = 5.7 Hz, 1H), 2.18 (d, *J*

=14.9 Hz, 1H), 3.14 (d, *J* = 14.9 Hz, 1H), 7.15-7.55 (m, 15H); ^{13}CNMR (CD_3Cl) (ZYQ-II) δ 23.66, 25.41, 38.97, 43.93, 121.90, 127.39, 127.89, 127.94, 128.86, 129.05, 129.13, 129.18, 129.47, 129.54, 137.36, 139.40, 141.48; HRMS (FAB) 310.159574 calcd for $C_{23}H_{20}N$, $[M+H]^+$ found 310.15850 (+3.5 ppm, +1.1 mmu).

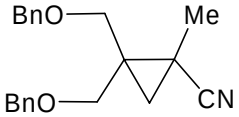

***2*-26** **2,2-Di(benzloxylmethyl)-1-methyl-cyclopropylnitrile**.

^{1}HNMR (CD_3Cl) δ 0.96 (d, *J* = 5.6 Hz, 1H), 1.33 (d, *J* = 5.4 Hz, 1H); 1.48 (s, 3H), 3.43, (d, *J* = 10.0 Hz, 1H), 3.62 (d, *J* = 10.0 Hz, 1H), 3.76 (d, *J* = 10.4 Hz, 1H), 3.83 (d, *J* = 10.0 Hz, 1H), 4.51 (d, *J* = 5.6 Hz, 2H), 4.56 (s, 2H), 7.30-7.40 (m, 10H); ^{13}CNMR (CD_3Cl) δ 13.61, 16.87, 23.50, 31.50, 68.38, 72.35, 73.41, 73.59, 122.74, 127.95, 127.97, 128.05, 128.63, 128.65, 138.07, 138.21; HRMS (FAB) 322.180704 calcd for $C_{21}H_{24}NO2$, $[M+H]^+$ found 322.17750 (+9.9ppm, +3.2mmu).

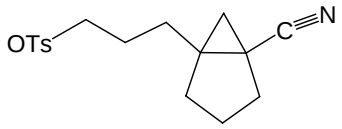

***2*-30** **5-(3-(*p*-toluenesulfonyloxy)-propyl)-bicyclo[3,1,0] hexane-1-carbonitrile**.

^{1}HNMR (CD_3Cl) δ 0.88 (d, *J* = 5.2 Hz, 1H), 1.06 (d, *J* = 5.6 Hz, 1H), 1.16 2.08 (m, 12H), 2.29 (s, 3H), 4.10 (t, *J* = 6.0 Hz, 2H), 7.39 (d, *J* = 8.0, 2H), 7.83 (dd, *J* = 6.6, 1.8 Hz, 2H); ^{13}CNMR (CD_3Cl) δ14.19, 19.93, 20.61, 21.74, 26.97, 29.79, 30.08, 30.13, 30.46, 70.01, 122.20, 128.00, 130.00, 144.56; HRMS (FAB) 320.132041 calcd for $C_{17}H_{22}NO_3S$, $[M+H]^+$ found 320.13000 (-6.4 ppm, -2.0 mmu).

Synthesis of 1-bromo-2,2-diphenyl-cyclopropylnitrile

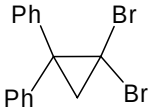

3-2 **1,1-Dibromo-2,2-diphenyl cyclopropane**.

A mixture of potassium *tert*-butoxide (1.40 g, 12.5 mmol, 1.5 equiv.) and 1,1-diphenylethene (1.76 mL, 10 mmol, 1.0 equiv.) in 20 mL hexane was cooled in an ice-salt bath (-10 °C). Bromoform (2.4 mL, 27.4 mmol, 2.2 equiv.) in 5 mL hexane was added dropwise with stirring over 15 min. The temperature rose to room temperature gently and the mixture was stirred overnight. Water was added and the product was extracted by CH_2Cl_2 (20 mL X 3). The organic layers were combined, dried over Na_2SO_4, filtered and concentrated to give the yellow brown residues. Filtered and collected the solid on the filter paper. The solid was washed by cooled hexane until it was white. The white solid product was in 52% yield (1.78 g). ^{1}HNMR (CD_3Cl) δ 2.45 (s, 2H), 7.17-7.45 (m, 10H); ^{13}CNMR (CD_3Cl) δ 33.84, 34.47, 45.05, 127.27, 128.39, 129.16, 141.85; HRMS (FAB) 350.938397 calcd for $C_{15}H_{13}Br^{79}{}_2$, $[M+H]^+$ found 351.9266 (+5.6 ppm, +2.0 mmu).

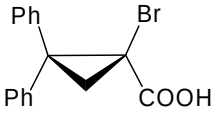

(*S*)-(+)-***3-3*** **(*S*)-(+)-1-Bromo-2,2-diphenyl cyclopropylcarboxylic acid**.

The round bottom flask containing dibromo-2,2-diphenylcyclopropane (1.50 g, 4.3 mmol, 1.0 equiv.) in 20 mL fresh THF was placed in -61 °C chloroform-dry ice bath. The EtMgBr (12 mL, 1.0 M in THF, 3.0 equiv.) was added into the flask dropwise and the

mixture was stirred at -61 °C for 30 min. CO_2 gas was cannulated to the mixture for 3.5 h. The reaction was quenched by adding 5 mL water. After it got to room temperature, two layers were separated and organic layer was washed by 10% $NaHCO_3$ (15 mL X 3). Combined aqueous layers were neutralized by 37% HCl until pH was equal to 1. Then the product was extracted from aqueous solution by using Et_2O (25 mL X 4). The organic layers were combined and dried over Na_2SO_4, filtered and concentrated to give the product in 65% yield (0.89 g).

The resolution of 1-bromo-2,2-diphenyl cyclopropylcarboxylic acid was carried out by using (-) Brucine. The mixture of acid (2.62 g, 8.25 mmol, 1 equiv.) and brucine (3.25 g, 8.25 mmol, 1 equiv.) was dissolved in 70 mL acetone and 5 mL methanol. The solution was warmed at 60 °C for 30 min. When it was cooled to room temperature, it was placed in the refrigerator. The solid crystal was collected in 80% yield (2.35 g, $[\alpha]^D$ = +31.6, c = 0.22 in EtOH). The acid/brucine salt was dissolved in water and CH_2Cl_2, followed by adding 37% HCl until pH got to 1. The carboxylic acid was extracted by CH_2Cl_2. Combined organic layers, dried over Na_2SO_4, filtered and concentrated to afford the enantiomerically pure 1-bromo-2,2-diphenylcyclopropylcarboxylic acid ($[\alpha]^D$ = +83.4, c = 0.24 in EtOH). ^{1}HNMR (CD_3Cl) δ 2.07 (d, *J* = 6.4 Hz, 1H), 2.73 (d, *J* = 6.4 Hz, 1H), 7.16-7.47 (m, 10H); ^{13}CNMR (CD_3Cl) δ 28.55, 38.11, 46.54, 127.64, 127.75, 128.53, 128.68, 128.56, 129.60, 140.28, 141.48, 173.88; HRMS (FAB) 317.017716 calcd for $C_{16}H_{14}Br^{79}O_2$, $[M+H]^+$ found 317.02084 (+9.8 ppm, +3.1 mmu).

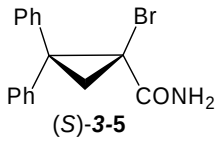

(*S*)-***3*-5** **(*S*)-1-Bromo-2,2-diphenyl cyclopropanecarboxamide**.

To the mixture of (+)-acid *(S)*-***3*-3** (0.89 g, 2.8 mmol, 1 equiv.) and NHS (0.48 g, 4.2 mmol, 1.5 equiv.) in 15 mL CH_2Cl_2 was added EDCI (0.80 g, 4.2 mmol, 1.5 equiv.) in 15 mL CH_2Cl_2 dropwise. After stirred for 6 h, the excess ammonium hydroxide (20 mL) was added and stirred overnight. Regular work-up was performed. After purified by column chromatograph (1:1, hexane:EtOAc), the pure product was in 84% yield (0.73 g). ^{1}HNMR (CD_3Cl) δ 2.02 (d, J = 6.0 Hz, 1H), 2.82 (d, J = 6.0 Hz, 1H), 5.64 (br, 1H), 6.81 (br, 1H), 7.13-7.45 (m, 10H); ^{13}CNMR (CD_3Cl) δ 27.36, 45.83, 127.14, 127.30, 128.24, 128.40, 128.54, 129.37, 140.30, 142.05, 168.66; HRMS (FAB), 316.033700 calcd for $C_{16}H_{15}Br^{79}ON$, $[M+H]^+$ found 316.0315 (-7.0 ppm, -2.2 mmu).

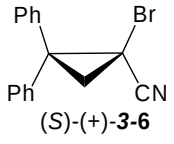

(*S*)-(+)-***3*-6** **(*S*)-(+)-1-Bromo-2,2-diphenyl cyclopropylnitrile**.

The mixture of (*S*)-***3*-5** (0.22 g, 0.7 mmol, 1 equiv.) and ρ-TsCl (0.42 g, 2.2 mmol, 3 equiv.) in 7 mL pyridine was stirred at 80 °C for 1 day. After the regular work-up for cyclopropyl nitrile, the crude product was purified by chromatography (2:1, hexane:EtOAc) to afford nitrile in 66% yield (0.14 g, $[\alpha]^D$ = +8.1, c = 0.16 in EtOH, >99.5 %ee by chiral HPLC). ^{1}HNMR (CD_3Cl) δ 2.21 (d, J = 6.8 Hz, 1H), 2.53 (d, J = 6.8 Hz, 1H), 7.23-7.51 (m, 10H); ^{13}CNMR (CD_3Cl) δ 18.65, 30.03, 44.57, 118.32, 128.09, 128.27, 128.65, 128.72, 129.07, 129.26, 138.83, 139.14; HRMS (FAB) 298.023135 calcd

$C_{16}H_{12}BrN$, $[M+H]^+$ found 298.02057 (-8.5 ppm, -2.5 mmu).

General protocol for the in situ metal-bromine exchange/methylation of (*S*)-(+)-*3*-6

At -100 °C under nitrogen, to a stirred solution of (*S*)-(+)-**5** (0.025 mmol) and the electrophile (0.15 mmol, CH_3I or CD_3I) in anhydrous Et_2O (1.0 mL) the base was added (0.026 mmol) and the mixture was stirred for 1h. The reaction was quenched by addition of saturated aqueous NH_4Cl or D_2O at -100 °C, and extracted with Et_2O (5 mL x 3). The combined extracts were dried over anhydrous Na_2SO_4, filtered, and concentrated. The crude product was analyzed by ^1H NMR spectra. These ^1H NMR spectra were very clean; no unidentified materials were present in any significant amount. Preparative TLC(50/50 CH_2Cl_2/hexane) was performed to isolate ***3*-6** from ***3*-7a,b/*3*-8/*3*-9**; note that ***3*-8/*3*-9** and ***3*-7a,b** were coincident by TLC. Total mass balance following chromatography ranged from 60-70%.

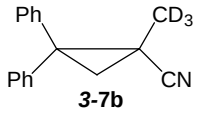

***3*-7b** **2,2-diphenyl-1-trideuteriomethyl-cyclopropylnitrile**.

^1H NMR (CD_3Cl) δ 1.63 (d, J = 5.2 Hz, 1H), 2.04 (d, J = 5.6 Hz, 1H), 7.17-7.51 (m, 10H); $^{13}CNMR$ (CD_3Cl) δ 16.6, 26.5, 43.0, 122.9, 127.69, 127.83, 129.00, 129.06, 129.37, 129.53, 139.6, 141.7; HRMS (FAB) 237.1471 calcd for $C_{17}H_{13}D_3N$, $[M+H]^+$ found 237.1451 (+8.4 ppm, +2.0 mmu).

General protocol for sequential magnesium-bromine exchange/deuteration of (*S*)-(+)-*3*-6.

At the indicated temperature under nitrogen, to a stirred solution of (*S*)-(+)-***3*-6** (0.025 mmol) in anhydrous Et_2O (1.0 mL) the Grignard reagent (0.055 mmol) was added and the mixture was stirred for 1 min, 5 min, or 30 min. The reaction was quenched by D_2O, and extracted with Et_2O (3 x 5 mL). The combined extracts were dried over anhydrous Na_2SO_4, filtered, and concentrated, and analyzed as described as above for the in situ reaction of (*S*)-(+)-***3*-6**.

General procedure for synthesis of nitrile aldols.

An oven-dried 50 mL round bottom flask equipped with stirring bar and septum was charged with nitrile (1 mmol) and fresh THF (10 mL), and cooled to -78 °C. The LDA (1.5 M, 0.7 mL, 1.05 mmol) was added via syringe, and the mixture was stirred at -78 °C for 30 min. Aldehyde (1 mmol) was added into the mixture. If mesitaldehyde was used, borontrifluoride etherate (1 mmol) was added to activate the aldehyde. After 30 min at -78 °C, the reaction was quenched by addition of saturated aqueous NH_4Cl and allowed to warm up to room temperature. The 5 mL 1N HCl was poured into the reaction mixture and extracted with Et_2O (3 x 15 mL). The combined organic extracts were dried (Na_2SO_4), and concentrated *in vacuo* to give the crude product.

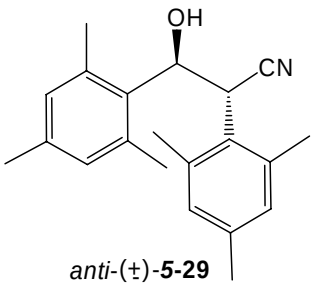

anti-(±)-***5*-29**

(2*RS*,3*RS*)-3-hydroxy-2,3-di(2,4,6-trimethylphenyl) propanenitrile.

Reaction of mesitylacetonitrile (0.1607 g, 1mmol), mesitaldehyde (0.145 mL, 1mmol) and borontrifluoride etherate (0.124 mL, 1mmol) was performed as above. The ratio of *anti:syn*- diastereomers was over 20:1. The *anti*-diastereomer (0.1101 g, 35.5 %) was isolated from a mixture of *anti*- and *syn*- aldols by column chromatography with ethyl acetate/hexane (1:4). ^{1}H NMR ($CDCl_3$): 1.31-2.85 (br, 6H), 1.58 (br, 3H), 2.20 (d, 6H), 2.69 (br, 3H), 4.82 (d, J = 9.9 Hz, 1H), 5.45 (d, J = 9.9 Hz, 1H), 6.61-6.87 (m, 4H); ^{13}C NMR ($CDCl_3$): 14.28, 19.73, 20.30, 20.85, 38.02, 69.42, 119.21, 125.72, 129,51, 129.72, 130.18 (br), 130.74, 132.70, 136.96, 137.18, 137.46, 137.09, 138.08; HRMS (FAB): 290.19087 calcd for $C_{21}H_{24}N$, $[M\text{-}OH]^+$, found 290.19293 (+7.0 ppm, +2.0); Element analysis: C, 82.04; H, 8.20; N, 4.56 calcd for $C_{21}H_{25}NO$, found C, 81.89; H, 8.26; N, 4.47. mp: 167.3 – 168.7 °C.

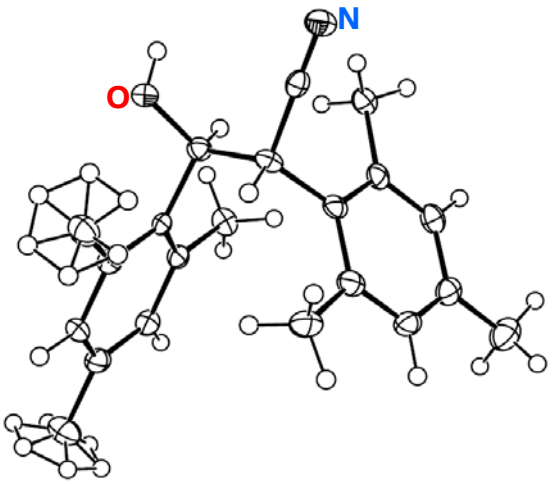

Figure 6.1 Thermal ellipsoid (50% probability) of anti-5-29. (X-ray is obtained from Michael's thesis).

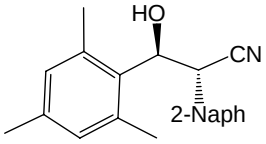

anti-(±)-**5-30**

(***RS*.3*RS*)-3-hydroxy-3-(2,4,6-trimethylphenyl)-2-(2-naphthyl)-propanenitrile**.

Reaction of 2-naphthylacetonitrile (0.1661 g, 1mmol), mesitaldehyde (0.145 mL, 1 mmol) and borontrifluoride etherate (0.124 mL, 1 mmol) was performed as above. The ratio of *anti*- and *syn* diastereomers was 2.3:1. The *anti*-diastereomer (0.1148 g, 36.6%) was isolated from a mixture of *anti*- and *syn*- aldols by column chromatography with ethyl acetate/hexane (1:5). The crystals of *anti*-(±)-**5-30** were obtained from CH_2Cl_2/Hexane. ^{1}H NMR ($CDCl_3$): 2.13 (br, 6H), 2.20 (s, 3H), 2.83 (d, J = 3.5 Hz, 1H), 4.58 (d, J = 9.6 Hz, 1H), 5.25 (dd, J = 3.5, 9.6 Hz, 1H), 6.695-7.79 (m, 9H); ^{13}C NMR ($CDCl_3$): 20.71, 20.88, 44.43, 73.50, 120.38, 125.75, 126.64, 126.68, 127.71, 127.74, 128.03, 128.41, 129.63, 130.40, 131.45, 132.86, 133.00, 136.82, 138.00; HRMS (FAB): 298.15957 calcd for $C_{22}H_{20}N$, $[M\text{-}OH]^+$, found 298.15802 (-5.3 ppm, -1.6 mmu).

mp: 148.3 – 150.8 °C.

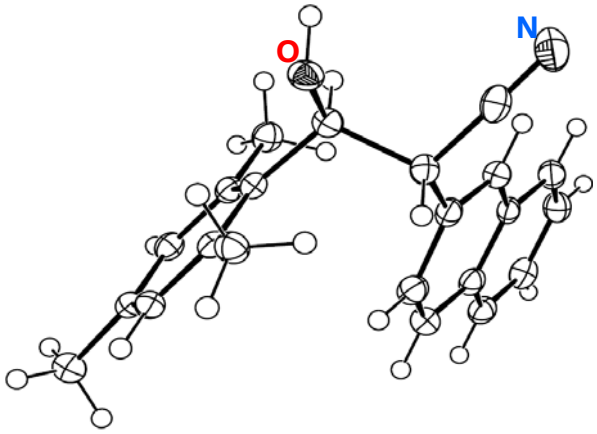

Figure 6.2 Thermal ellipsoid (50% probability) of *anti*-***5*-30**.

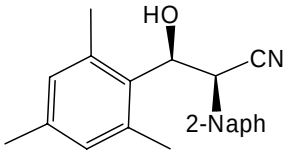

syn-(±)-***5*-30**

(2*RS*,3*SR*)-3-hydroxy-3-(2,4,6-trimethylphenyl)-2-(2-naphthyl) propanenitrile.

Data on *syn*-(±)-***5*-30** were deduced by inspection of a *anti*:*syn* mixture (6:1) of ***5*-30**, obtained during isolation of *anti*-(±)-***5*-30**. ^{1}H NMR ($CDCl_3$): 1.92 (d, J = 3.2, 1H), 2.26 (s, 3H), 2.52 (br, 6H), 4.49 (d, J = 9.6 Hz, 1H), 5.46 (dd, J = 3.0, 9.4 Hz, 1H), 6.88-7.92 (m, 9H); ^{13}C NMR ($CDCl_3$): 21.12, 43.60, 73.59, 119.00, 125.85, 127.06, 127.13, 128.05, 128.20, 128.25, 129.47, 131.22, 132.22, 133.38, 133.52, 136.85, 138.48; HRMS (FAB): 298.15957 calcd for $C_{22}H_{20}N$, $[M\text{-}OH]^+$, found 298.16141(+6.1 ppm, +1.8 mmu); Element analysis: C, 83.78; H, 6.71;N, 4.44 calcd for $C_{22}H_{21}NO$, found C, 83.52; H, 6.74;N, 4.51.

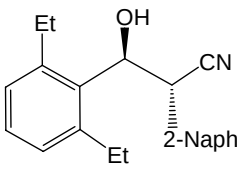

anti-(±)-***5*-31**

(2*RS*,3*RS*)-3-(2,6-diethylphenyl)-3-hydroxy-2-(2-naphthyl)-

propanenitrile.

Reaction of 2-naphthylacetonitrile (0.1019 g, 0.6 mmol), 2,6-diethylbenzaldehyde (0.0976 g, 0.6 mmol) and borontrifluoride etherate (0.076 mL, 0.6 mmol) was performed as above. The ratio of *anti*:*syn* diastereomers was 3:1. The *anti*-diastereomer (0. 0451g, 22.8 %) was isolated from a mixture of *anti*- and *syn*- aldols by column chromatography with ethyl dichloromethane/hexane (1:1). ^{1}H NMR ($CDCl_3$): 1.05 (br, 6H), 2.44 (br, 4H), 2.89 (d, J = 4.0 Hz, 1H), 4.55 (d, J = 9.6 Hz, 1H), 5.43 (dd, J = 3.8, 9.8 Hz, 1H), 6.91-7.73 (m, 10 H); ^{13}C NMR ($CDCl_3$): 16.24 (br), 26.31, 45.72, 73.16, 120.18, 125.64, 126.63, 126.68, 127.68, 127.77, 127.89, 127.99, 128.38, 128.85, 129.48, 132.84, 132.97, 133.20, 143.39; HRMS (FAB): 312.175224 calcd for $C_{23}H_{22}N$, $[M\text{-}OH]^+$ found 312.17487 (-1.1 ppm, -0.4 mmu).

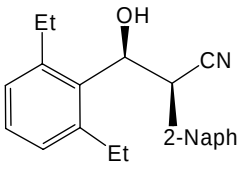

syn-(±)-***5*-31**

(2*RS*,3*RS*)-3-(2,6-diethylphenyl)-3-hydroxy-2-(2-naphthyl)-propanenitrile.

The *syn*-diastereomer (0. 0115g, 5.8%) was isolated from a mixture of *anti*- and *syn*-aldols by column chromatography with ethyl dichloromethane/hexane (1:1). ^{1}H NMR ($CDCl_3$): 1.29 (br, 6H), 2.01 (d, J = 3.2 Hz, 1H), 2.79-3.05 (br, 4H), 4.49 (d, J = 9.6 Hz, 1H), 5.50 (dd, J = 3.2, 10.0 Hz, 1H), 7.10-7.94 (m, 10 H); ^{13}C NMR ($CDCl_3$): 16.10, 16.96, 26.21, 27.47, 44.73, 73.19, 118.87, 125.64, 126.84, 126.95, 127.02, 127.92, 128.08, 129.13, 129.32, 129.42, 131.23, 133.28, 133.41, 133.84, 142.69, 143.86; HRMS (FAB):

312.175224 calcd for $C_{23}H_{22}N$, $[M\text{-}OH]^+$ found 312.17490 (-1.1 ppm, -0.3 mmu).

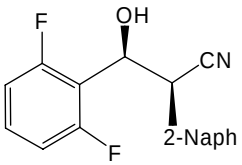

syn-(±)-**5-32**

(2RS,3SR)-3-(2,6-difluorophenyl)-3-hydroxy-2-(2-naphthyl) propanenitrile.

Reaction of 2-naphthylacetonitrile (0.334 g, 2 mmol) and 2′,6′-diflurobenzaldehyde (0.256 mL, 2 mmol) was performed as above. The ratio of *anti*:*syn* diastereomers was 1.1:1. The *syn*-diastereomer (0.1668 g, 29.9 %) was isolated from a mixture of *anti*- and *syn*-aldols by column chromatography with ethyl acetate/hexane (1:3). The crystals were obtained from CH_2Cl_2/hexane. ^{1}H NMR ($CDCl_3$): 2.71 (d, J = 7.1 Hz, 1H), 4.53 (d, J = 8.8 Hz, 1H), 5.44 (t, J = 8.0 Hz, 1H), 6.91-7.90 (m, 10H); ^{13}C NMR ($CDCl_3$): 44.43, 68.84, 112.15, 112.09, 112.32, 112.35, 118.21, 125.56, 127.00, 127.02, 127.89, 128.08, 128.36, 129.35, 129.65, 131.12, 133.32, 160.18, 162.11; HRMS (FAB): 310.10434 calcd for $C_{19}H_{14}F_2NO$, $[M+H]^+$, found 310.10535 (+3.0 ppm, +0.9).

mp: 156.7 – 157.9 °C.

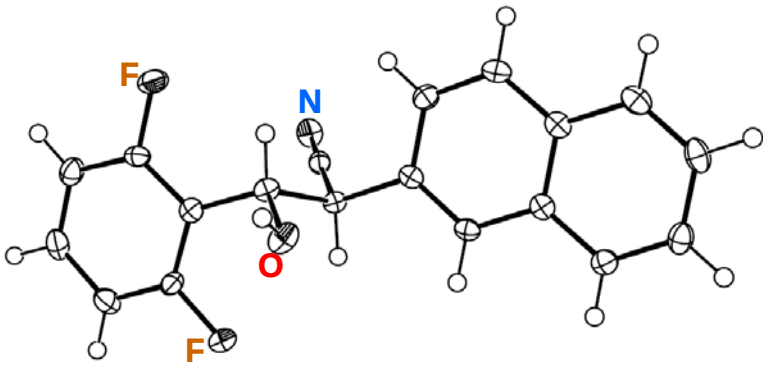

Figure 6.3 Thermal ellipsoid (50% probability) of *syn*-**5-32.**

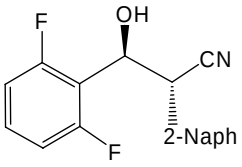

anti-(±)-***5*-32**

(2*RS*,3*RS*)-3-(2,6-difluorophenyl)-3-hydroxy-2-(2-naphthyl) propanenitrile.

Data on *anti-(*±)-***5*-32** were deduced by inspection of a *anti*:*syn* mixture (1:1.8) of ***5*-32**, obtained during isolation of *syn-(*±)-***5*-32**. ^{1}H NMR ($CDCl_3$): 3.23 (d, J = 7.8, 1H), 4.50 (d, J = 8.8 Hz, 1H), 5.49 (t, J = 8.2 Hz, 1H), 6.73-7.90 (m, 10H); ^{13}C NMR ($CDCl_3$): 45.04, 69.00, 11.87, 111.90, 112.03, 112.06, 119.41, 125.12, 126.78, 126.84, 127.78, 128.02, 129.03, 129.12, 130.83, 133.14, 160.11, 162.06; HRMS (FAB): 310.10434 calcd for $C_{19}H_{14}F_2NO$, $[M+H]^+$, found 310.10434 (-0.1 ppm, +0.0 mmu); Element analysis: C, 73.78; H, 4.24; N, 4.53 calcd for $C_{19}H_{13}F_2NO$, found C, 72.99; H, 4.30; N, 4.51.

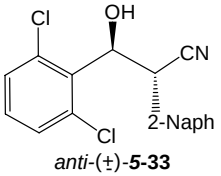

anti-(±)-***5*-33**

(2*RS*,3*RS*)-3-(2,6-dichlorophenyl)-3-hydroxy-2-(2-naphthyl) propanenitrile.

Reaction of 2-naphthylacetonitrile (0.334 g, 2 mmol) and 2,6-dichlorobenzaldehyde (0.4169 g, 2 mmol) was performed as above. The ratio of *anti*:*syn* diastereomers was 1.8:1. The *anti*-diastereomer (0.2225g, 32.5 %) was isolated from a mixture of *anti*- and *syn*-aldols by column chromatography with ethyl acetate/hexane (1:3). The crystals were obtained from CH_2Cl_2/hexane. ^{1}H NMR ($CDCl_3$): 3.44 (d, J = 9.2 Hz, 1H), 4.95 (d, J = 10.0 Hz, 1H), 5.90 (dd, J = 9.2, 10.0 Hz 1H), 7.02-7.74 (m, 10H); ^{13}C NMR ($CDCl_3$): 43.53, 73.73, 119.76, 125.39, 126.68, 126.77, 127.75, 127.91, 128.00, 128.70, 129.57, 130.32,

132.88, 133.03; HRMS (FAB): 342.04525 calcd for $C_{19}H_{14}{}^{35}Cl_2NO$, $[M+H]^+$ found 342.04266 (-7.5 ppm, -2.6 mmu).

mp: 154.0 -155.2 °C.

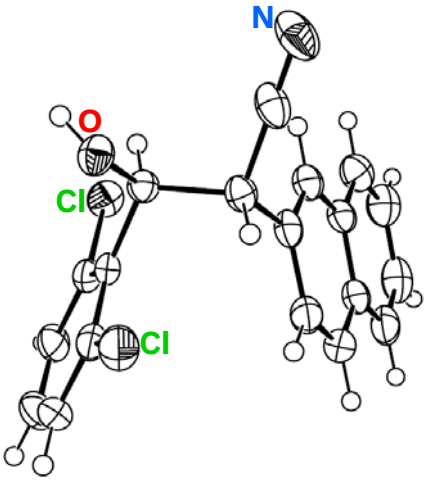

Figure 6.4 Thermal ellipsoid (50% probability) of *anti*-***5*-33.**

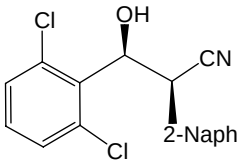

syn-(±)-***5*-33**

(2*RS*,3*SR*)-3-(2,6-dichlorophenyl)-3-hydroxy-2-(2-naphthyl) propanenitrile.

The *syn*-diastereomer (0.1572 g, 23.0 %) was isolated from a mixture of *anti*- and *syn*-aldols by column chromatography with ethyl acetate/hexane (1:3). The crystals were obtained from CH_2Cl_2/hexane. ^{1}H NMR ($CDCl_3$): 2.82 (d, J = 8 Hz, 1H), 4.85 (d, J = 9.6 Hz, 1H), 5.87 (dd, J = 8.0, 9.6 Hz, 1H), 7.02-7.94 (m, 10H); ^{13}C NMR ($CDCl_3$): 42.35, 73.73, 114.29, 125.67, 126.99, 127.93, 128.09, 128.41, 129.43, 130.19, 130.63, 133.39, 133.67, 135.41, 137.31; HRMS (FAB): 342.04525 calcd for $C_{19}H_{14}{}^{35}Cl_2NO$, $[M+H]^+$, found 342.04349 (-5.1 ppm, -1.8 mmu); Element analysis: C, 66.68; H, 3.83; N, 4.09 calcd for $C_{19}H_{13}Cl_2NO$, found C, 66.58; H, 3.84; N, 4.06.

mp: 173.2 – 175.6 °C.

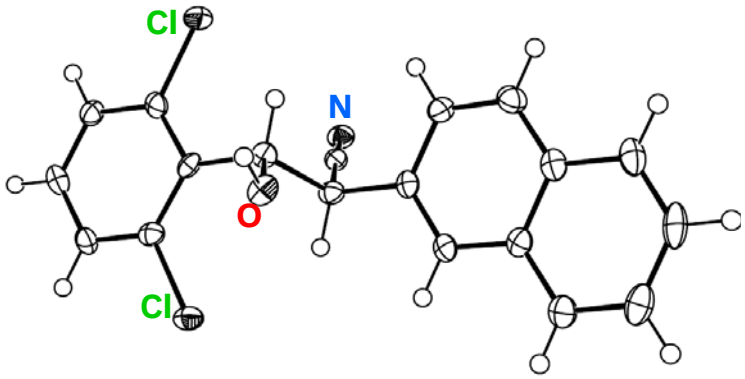

Figure 6.5 Thermal ellipsoid (50% probability) of *syn*-***5*-33.**

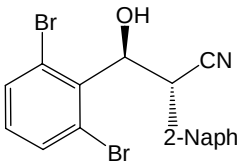

anti-(±)-***5*-34**

(2*RS*,3*RS*)-3-(2,6-dibromophenyl)-3-hydroxy-2-(2-naphthyl) propanenitrile.

Reaction of 2-naphthylacetonitrile (0.0671 g, 0.4 mmol) and 2,6-dibromobenzaldehyde (0.1061 g, 0.4 mmol) was performed as above. The ratio of *anti*:*syn* diastereomers was 4:3. The *anti*-diastereomer (0. 034g, 13.6 %) was isolated from a mixture of *anti*- and *syn*- aldols by column chromatography with ethyl acetate/hexane (1:9). ^{1}H NMR ($CDCl_3$): 3.55 (d, J = 8.8 Hz, 1H), 5.10 (d, J = 10.4 Hz, 1H), 5.90 (dd, J = 8.8, 10.0 Hz, 1H), 6.86-7.34 (m, 10 H); ^{13}C NMR ($CDCl_3$): 43.28, 76.93, 119.73, 125.62, 126.65, 126.75, 127.75, 128.01, 128.12, 128.60, 130.10, 130.93, 133.01, 133.04, 133.73(br), 135.08; HRMS (FAB): 429.944211 calcd for $C_{19}H_{14}{}^{79}Br_2NO$, $[M+H]^+$ found 429.94525 (+2.3 ppm, +1.0 mmu).

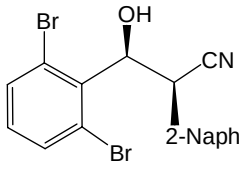

syn-(±)-***5-34***

(2*RS*,3*RS*)-3-(2,6-dibromophenyl)-3-hydroxy-2-(2-naphthyl) propanenitrile.

The *syn*-diastereomer (0. 0235g, 9.4%) was isolated from a mixture of *anti*- and *syn*-aldols by column chromatography with ethyl acetate/hexane (1:9). ^{1}H NMR ($CDCl_3$): 2.86 (d, J = 8.0 Hz, 1H), 4.98 (d, J = 9.6 Hz, 1H), 5.88 (dd, J = 8.0, 9.6 Hz, 1H), 7.07-7.95 (m, 10 H); ^{13}C NMR ($CDCl_3$): 42.11, 77.10, 117.98, 125.71, 126.97, 127.92, 128.10, 128.42, 129.42, 130.26, 131.27, 133.35, 133.39, 133.73,134.83(br), 135.93; HRMS (FAB): 429.944211 calcd for $C_{19}H_{14}{}^{79}Br_2NO$, $[M+H]^+$ found 429.94119 (-7.0 ppm, -3.0 mmu)

General procedure for synthesis of ketone aldols

The 2,2-dimethyl-3-pentanone was obtained by the chromic acid oxidation of 2,2-dimethyl-pentan-3-ol (2.4 mL, 17 mmol).[256]

An oven-dried 50 mL round bottom flask equipped with stirring bar and septum was charged with fresh THF (10 mL), and cooled to -78 °C. The LDA (1.5 M, 0.7 mL, 1.05 mmol) was added via syringe, followed by 2,2-dimethyl-3-pentanone (1 mmol). The mixture was stirred at -78 °C for 30 min. Aldehyde (1 mmol) was added into the mixture. If mesitaldehyde was used, borontrifluoride etherate (1 mmol) was added. After 4 hours at -78 °C, the reaction was quenched by addition of saturated aqueous NH_4Cl and allowed to warm up to room temperature. The 5 mL 1N HCl was poured into the reaction mixture and extracted with Et_2O (3 x 15 mL). The combined organic extracts were dried (Na_2SO_4), and

concentrated *in vacuo* to give the crude product.

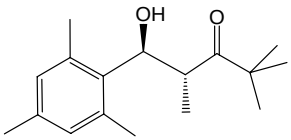

anti-(±)-***5*-35**

(2*RS*,3*SR*)-5-hydroxy-2,2,4-trimethyl-5-(2,4,6-trimethyl-phenyl)pentanone

Reaction of 2,2-dimethyl-3-pentanone (0.117 g, 1 mmol), mesitaldehyde (0.145 mL, 1 mmol) and borontrifluoride etherate (0.125 mL, 1 mmol) was performed as above. The ratio of *anti*:*syn* diastereomers was 1:1.25. The *anti*-diastereomer (26.5 mg, 10.0 %) was isolated from a mixture of *anti*- and *syn*- aldols by column chromatography with ethyl acetate/hexane (1:10).The crystals were obtained from CH_2Cl_2/hexane. ^{1}H NMR ($CDCl_3$): 0.78 (d, J = 6.9 Hz, 3H), 1.22 (s, 9H), 2.24 (s, 3H), 2.29-2.62 (br, 6H), 3.78 (dq, J = 10.2, 7.0, 1H), 5.40 (d, J = 10.3 Hz, 1H), 6.83 (s, 2H); ^{13}C NMR ($CDCl_3$): 15.79, 20.85, 26.43, 44.54, 45.00, 73.29, 129.35, 132.81, 134.42, 137.09, 220.21; HRMS (FAB): 245.19054 calcd for $C_{17}H_{25}$, $[M\text{-}OH]^+$ found 245.18999 (-2.2 ppm, -0.5 mmu).

mp: 106.0 – 106.8 °C.

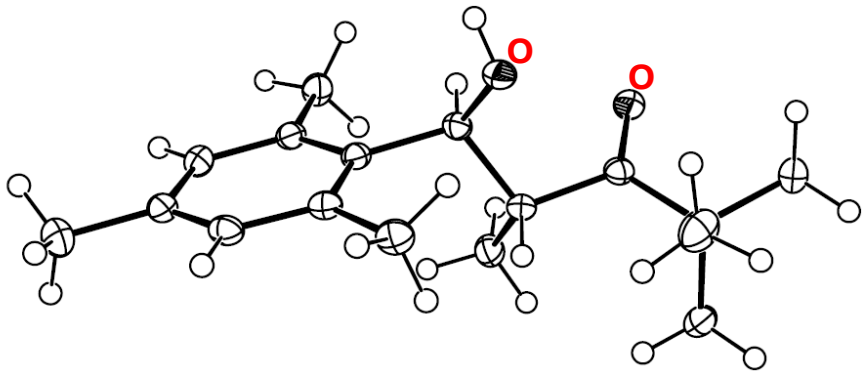

Figure 6.6 Thermal ellipsoid (50% probability) of *anti*-***5*-35.**

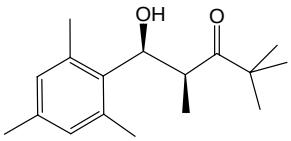

syn-(±)-**5-35**

(2*RS*,3*RS*)-5-hydroxy-2,2,4-trimethyl-5-(2,4,6-trimethylphenyl) pentanone.

The *syn*-diastereomer (31.3 mg, 11.6 %) was isolated from a mixture of *anti*- and *syn*-aldols by column chromatography with ethyl acetate/hexane (1:10). ^{1}H NMR ($CDCl_3$): 0.83 (s, 9H), 1.27 (d, J = 6.9 Hz, 3H), 2.20, (s, 3H), 2.40 (s, 6H), 3.68 (dq, J = 8.9, 6.8 Hz, 1H), 5.22 (d, J = 9.2 Hz, 1H), 6.75 (s, 1H); ^{13}C NMR ($CDCl_3$): 16.31, 20.81, 20.94, 25.87, 44.78, 44.83, 72.43, 130.32, 135.26, 136.67, 137.02, 218.76; HRMS (FAB): 245.19054 calcd for $C_{17}H_{25}$, $[M\text{-}OH]^+$ found 245.18940 (-4.6 ppm, -0.1 mmu);

Elemental analysis: C, 77.82; H, 9.99; N, 0.00 calcd for $C_{17}H_{26}O_2$, found C, 77.56; H, 9,98; N, 0.00.

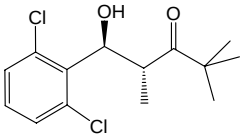

anti-(±)-**5-36**

(2*RS*,3*SR*)-5-(2,6-dichlorophenyl)-5-hydroxy-2,2,4-trimethyl pentanone.

Reaction of 2,2-dimethyl-3-pentanone (0.340 g, 2.9 mmol) and 2,6-dichlorobenzaldehyde (0.825 g, 3.6 mmol) was performed as above. The ratio of *anti*:*syn* diastereomers was 1:5. The *anti*-diastereomer (0.0932g, 10.8 %) was isolated from a mixture of *anti*- and *syn*- aldols by column chromatography with ethyl acetate/hexane (1:8).The crystals were obtained from CH_2Cl_2/hexane. ^{1}H NMR ($CDCl_3$): 0.82 (d, J = 7.2, 3H), 1.16 (s, 9H), 2.67 (d, J = 8.4 Hz, 1H), 4.05 (dq, J = 10.3, 7.1 Hz, 1H), 5.74 (dd, J = 8.0 Hz, 9.6 Hz, 1H), 7.11-7.36 (m, 3H); ^{13}C NMR ($CDCl_3$): 15.59, 26.23, 43.62, 45.00, 76.85,

129.40, 135.97, 218.28; HRMS (FAB): 289.07621 calcd for $C_{14}H_{19}{}^{35}Cl_2O_2$, $[M+H]^+$ found 289.07760 (+4.8 ppm, +1.4 mmu).

mp: 119.3 – 123.2 °C.

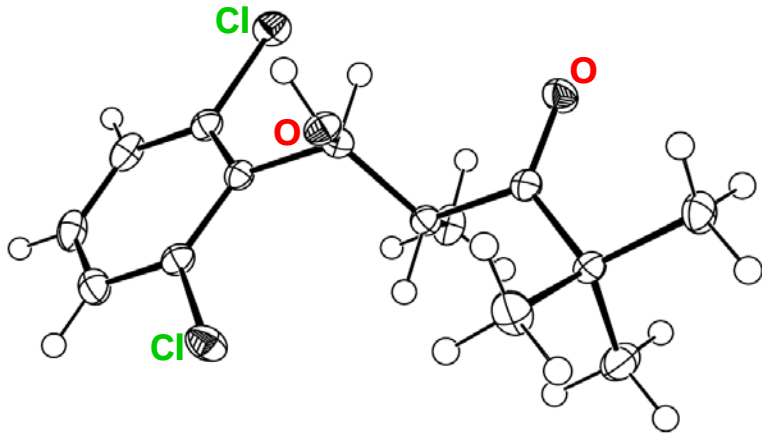

Figure 6.7 Thermal ellipsoid (50% probability) of *anti*-***5*-36.**

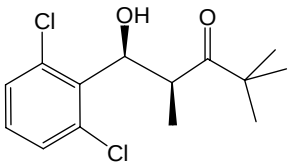

syn-(±)-***5*-36**

(2*RS*,3*SR*)-5-(2,6-dichlorophenyl)-5-hydroxy-2,2,4-trimethyl pentanone.

The *syn*-diastereomer (0.4748 g, 55.1 %) was isolated from a mixture of *anti*- and *syn*-aldols by column chromatography with ethyl acetate/hexane (1:8). The crystals were obtained from CH_2Cl_2/hexane. ^{1}H NMR ($CDCl_3$): 0.86 (s, 9H), 1.30 (d, J = 6.8, 3H), 2.84 (d, J = 9.2 Hz, 1H), 4.00 (dq, J = 9.6, 6.8 Hz, 1H), 5.51 (t, J = 9.2 Hz, 1H), 7.06-7.25 (m, 3H); ^{13}C NMR ($CDCl_3$): 16.55, 25.84, 44.56, 44.78, 73.12, 129.40, 129.52, 135.05, 136.67, 217.02; HRMS (FAB): 289.07621 calcd for $C_{14}H_{19}{}^{35}Cl_2O_2$, $[M+H]^+$ found 289.0767 (+1.7 ppm, +0.5 mmu); Elemental analysis: C, 58.14; H, 6.27; N, 0.00; calcd for $C_{14}H_{18}Cl_2O_2$, found C, 58.21; H, 6.42; N, 0.00.

mp: 64.0 – 67.0 °C.

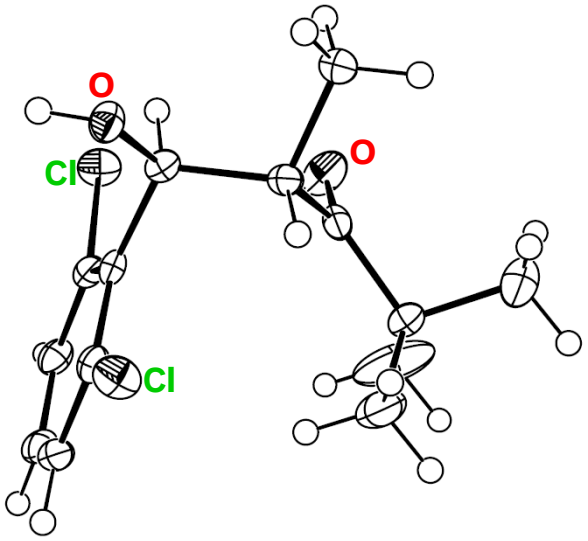

Figure 6.8 Thermal ellipsoid (50% probability) of *anti*-***5*-36.**

6.2 X-ray structure determination summary.

The chosen crystal was cut (0.11 x 0.15 x 0.23 mm^3) and mounted on a nylon CryoLoop™ (Hampton Research) with Krytox® Oil (DuPont) and centered on the goniometer of an Oxford Diffraction PX Ultra™ diffractometer equipped with an Onyx™ CCD detector an Cu radiation. The data collection routine, unit cell refinement, and data processing were carried out with the program CrysAlis.[257] The structure was solved by direct methods and refined using SHELXTL NT.[258] The asymmetric unit of the structure comprises one crystallographically independent molecule. The final refinement model involved anisotropic displacement parameters for non-hydrogen atoms and a riding model for all hydrogen atoms. The absolute configuration was established from anomalous dispersion effects (Flack parameter = 0.03(18)). Eight CIF files for crystal structures of nitrile aldols and ketone aldols in Chapter 5 are available in the supporting information of *J. Org. Chem.* **2006**, *71*, 8835

(http://pubs3.acs.org/acs/journals/supporting_information.page?in_coden=joceah&in_volume=71&in_start_page=8835). The thermal ellipsoid plots of these nitrile and ketone aldols have been presented in previous section of Chapter 6.

X-ray analysis for (*R*)-(-)-*2*-7.

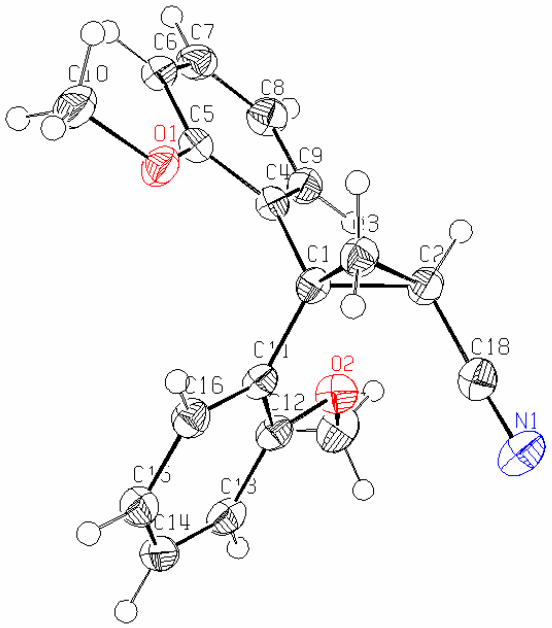

Figure 6.9 Thermal ellipsoid (50% probability) of (*R*)-(-)-***2*-7.**

Table 6.2 Crystal data and structure refinement.

Identification code	**(*R*)-(-)-*2*-7**
Empirical formula	$C_{18}H_{17}NO_2$
Formula weight	279.33
Temperature	100(2) K
Wavelength	1.54178 Å
Crystal system	Orthorhombic
Space group	$P2_12_12_1$
Unit cell dimensions	a = 8.3593(2) Å; b = 11.0321(2) Å; c = 15.8165(2) Å
Volume	1458.61(5) $Å^3$
Z	4
Density (calculated)	1.272 Mg/m^3
Absorption coefficient	0.661 mm^{-1}
F(000)	592

Crystal size	0.23 x 0.15 x 0.11 mm^3
Theta range for data collection	4.89 to 67.08°.
Index ranges	-8<=h<=9, -13<=k<=11, -18<=l<=18
Reflections collected	7872
Independent reflections	2579 [R(int) = 0.0305]
Completeness to theta = 67.08°	99.5 %
Absorption correction	None
Refinement method	Full-matrix least-squares on F^2
Data / restraints / parameters	2579 / 0 / 192
Goodness-of-fit on F^2	1.094
Final R indices [I>2sigma(I)]	R1 = 0.0278, wR2 = 0.0695
R indices (all data)	R1 = 0.0295, wR2 = 0.0702
Absolute structure parameter	0.03(18)
Largest diff. peak and hole	0.105 and -0.150 e.$Å^{-3}$

Table 6. 3 Atomic coordinates (x 10^4) and equivalent isotropic displacement parameters ($Å^2$x 10^3) for (*R*)-(-)-***2-7***. U(eq) is defined as one third of the trace of the orthogonalized U^{ij} tensor.

	x	y	z	U(eq)
O(1)	4519(1)	8253(1)	4127(1)	31(1)
O(2)	9734(1)	10590(1)	4101(1)	32(1)
N(1)	7578(2)	13112(1)	3093(1)	39(1)
C(1)	6645(2)	10033(1)	3685(1)	24(1)
C(2)	6831(2)	10850(1)	2911(1)	27(1)
C(3)	5192(2)	10487(1)	3233(1)	28(1)
C(4)	7040(2)	8712(1)	3552(1)	24(1)
C(5)	5917(2)	7828(1)	3790(1)	26(1)
C(6)	6256(2)	6605(1)	3679(1)	30(1)
C(7)	7722(2)	6252(1)	3348(1)	34(1)
C(8)	8838(2)	7110(1)	3115(1)	33(1)
C(9)	8493(2)	8331(1)	3218(1)	28(1)
C(10)	3373(2)	7381(1)	4399(1)	41(1)
C(11)	7065(1)	10528(1)	4543(1)	24(1)
C(12)	8665(2)	10786(1)	4739(1)	26(1)
C(13)	9087(2)	11214(1)	5535(1)	30(1)
C(14)	7914(2)	11365(1)	6143(1)	31(1)
C(15)	6328(2)	11104(1)	5966(1)	32(1)
C(16)	5915(2)	10687(1)	5165(1)	27(1)

C(17)	11399(2)	10605(1)	4307(1)	38(1)
C(18)	7274(2)	12101(1)	3022(1)	29(1)

Table 6.4 Bond lengths [Å] and angles [°] for (*R*)-(-)-***2*-7**.

O(1)-C(5)	1.3668(16)	O(1)-C(10)	1.4237(15)
O(2)-C(12)	1.3661(15)	O(2)-C(17)	1.4288(17)
N(1)-C(18)	1.1498(17)	C(1)-C(3)	1.4953(17)
C(1)-C(11)	1.5046(17)	C(1)-C(4)	1.5082(17)
C(1)-C(2)	1.5274(16)	C(2)-C(18)	1.4395(17)
C(2)-C(3)	1.5146(17)	C(4)-C(9)	1.3894(18)
C(4)-C(5)	1.4049(18)	C(5)-C(6)	1.3903(18)
C(6)-C(7)	1.388(2)	C(7)-C(8)	1.379(2)
C(8)-C(9)	1.3879(19)	C(11)-C(16)	1.3868(17)
C(11)-C(12)	1.4022(18)	C(12)-C(13)	1.3894(18)
C(13)-C(14)	1.384(2)	C(14)-C(15)	1.385(2)
C(15)-C(16)	1.3913(19)		

C(5)-O(1)-C(10)	117.52(10)	C(12)-O(2)-C(17)	117.83(11)
C(3)-C(1)-C(11)	119.96(11)	C(3)-C(1)-C(4)	115.74(10)
C(11)-C(1)-C(4)	115.16(10)	C(3)-C(1)-C(2)	60.13(8)
C(11)-C(1)-C(2)	118.98(10)	C(4)-C(1)-C(2)	115.86(10)
C(18)-C(2)-C(3)	116.48(11)	C(18)-C(2)-C(1)	119.66(11)
C(3)-C(2)-C(1)	58.89(8)	C(1)-C(3)-C(2)	60.98(8)
C(9)-C(4)-C(5)	118.41(11)	C(9)-C(4)-C(1)	122.44(11)
C(5)-C(4)-C(1)	119.13(11)	O(1)-C(5)-C(6)	123.79(11)
O(1)-C(5)-C(4)	115.97(11)	C(6)-C(5)-C(4)	120.24(12)
C(7)-C(6)-C(5)	119.99(12)	C(8)-C(7)-C(6)	120.39(12)
C(7)-C(8)-C(9)	119.60(13)	C(8)-C(9)-C(4)	121.36(12)
C(16)-C(11)-C(12)	118.57(11)	C(16)-C(11)-C(1)	121.61(11)
C(12)-C(11)-C(1)	119.75(11)	O(2)-C(12)-C(13)	123.85(12)
O(2)-C(12)-C(11)	115.36(11)	C(13)-C(12)-C(11)	120.79(12)
C(14)-C(13)-C(12)	119.38(13)	C(13)-C(14)-C(15)	120.82(12)
C(14)-C(15)-C(16)	119.38(12)	C(11)-C(16)-C(15)	121.05(12)
N(1)-C(18)-C(2)	177.43(15)		

Table 6.5 Anisotropic displacement parameters ($Å^2 x\ 10^3$) for (*R*)-(-)-***2*-7**. The anisotropic displacement factor exponent takes the form: $-2\pi^2[\ h^2\ a^{*2}U^{11} + ... + 2\ h\ k\ a^*\ b^*\ U^{12}\ ]$

	U^{11}	U^{22}	U^{33}	U^{23}	U^{13}	U^{12}
O(1)	32(1)	26(1)	35(1)	0(1)	9(1)	-6(1)
O(2)	20(1)	37(1)	39(1)	-4(1)	4(1)	-1(1)
N(1)	39(1)	26(1)	53(1)	1(1)	5(1)	-1(1)
C(1)	23(1)	24(1)	26(1)	2(1)	1(1)	-2(1)
C(2)	29(1)	24(1)	28(1)	2(1)	3(1)	-1(1)
C(3)	27(1)	26(1)	30(1)	2(1)	-2(1)	-1(1)
C(4)	27(1)	24(1)	22(1)	1(1)	-1(1)	-1(1)
C(5)	31(1)	27(1)	21(1)	0(1)	-1(1)	-2(1)
C(6)	38(1)	25(1)	27(1)	1(1)	-2(1)	-5(1)
C(7)	44(1)	24(1)	33(1)	-3(1)	-5(1)	4(1)
C(8)	33(1)	31(1)	35(1)	-3(1)	1(1)	5(1)
C(9)	29(1)	27(1)	29(1)	1(1)	1(1)	-1(1)
C(10)	45(1)	33(1)	44(1)	-4(1)	14(1)	-14(1)
C(11)	23(1)	19(1)	28(1)	1(1)	1(1)	0(1)
C(12)	25(1)	21(1)	33(1)	0(1)	1(1)	1(1)
C(13)	30(1)	23(1)	37(1)	2(1)	-7(1)	-1(1)
C(14)	41(1)	25(1)	28(1)	-2(1)	-4(1)	-1(1)
C(15)	36(1)	30(1)	29(1)	0(1)	4(1)	0(1)
C(16)	25(1)	27(1)	30(1)	1(1)	2(1)	-1(1)
C(17)	20(1)	39(1)	56(1)	6(1)	3(1)	-2(1)
C(18)	26(1)	30(1)	32(1)	2(1)	4(1)	2(1)

Table 6.6 Hydrogen coordinates (x 10^4) and isotropic displacement parameters ($Å^2$x 10^3) for (*R*)-(-)-***2-7***.

	x	y	z	U(eq)
H(2)	7201	10450	2379	32
H(3A)	4541	11115	3517	33
H(3B)	4573	9897	2892	33
H(6)	5485	6010	3829	36
H(7)	7958	5415	3282	40
H(8)	9837	6866	2885	40
H(9)	9266	8919	3058	34
H(10A)	3834	6885	4851	61
H(10B)	3077	6860	3922	61
H(10C)	2419	7799	4611	61
H(13)	10171	11400	5660	36

H(14)	8200	11652	6689	37
H(15)	5530	11208	6387	38
H(16)	4827	10509	5042	33
H(17A)	11593	10075	4793	58
H(17B)	11725	11434	4447	58
H(17C)	12020	10316	382	58

Table 6.7 Torsion angles [°] for (*R*)-(-)-***2*-7**.

C(3)-C(1)-C(2)-C(18)	104.81(13)	C(11)-C(1)-C(2)-C(18)	-5.09(17)
C(4)-C(1)-C(2)-C(18)	-149.03(11)	C(11)-C(1)-C(2)-C(3)	-109.90(13)
C(4)-C(1)-C(2)-C(3)	106.16(12)	C(11)-C(1)-C(3)-C(2)	108.29(12)
C(4)-C(1)-C(3)-C(2)	-106.34(11)	C(18)-C(2)-C(3)-C(1)	-110.19(12)
C(3)-C(1)-C(4)-C(9)	121.45(13)	C(11)-C(1)-C(4)-C(9)	-91.50(14)
C(2)-C(1)-C(4)-C(9)	53.83(16)	C(3)-C(1)-C(4)-C(5)	-60.00(15)
C(11)-C(1)-C(4)-C(5)	87.04(14)	C(2)-C(1)-C(4)-C(5)	-127.63(12)
C(10)-O(1)-C(5)-C(6)	1.79(18)	C(10)-O(1)-C(5)-C(4)	-178.13(11)
C(9)-C(4)-C(5)-O(1)	178.94(10)	C(1)-C(4)-C(5)-O(1)	0.34(16)
C(9)-C(4)-C(5)-C(6)	-0.98(18)	C(1)-C(4)-C(5)-C(6)	-179.59(11)
O(1)-C(5)-C(6)-C(7)	-178.58(11)	C(4)-C(5)-C(6)-C(7)	1.34(19)
C(5)-C(6)-C(7)-C(8)	-1.1(2)	C(6)-C(7)-C(8)-C(9)	0.5(2)
C(7)-C(8)-C(9)-C(4)	-0.1(2)	C(5)-C(4)-C(9)-C(8)	0.37(19)
C(1)-C(4)-C(9)-C(8)	178.92(12)	C(3)-C(1)-C(11)-C(16)	44.31(17)
C(4)-C(1)-C(11)-C(16)	-101.25(14)	C(2)-C(1)-C(11)-C(16)	114.57(13)
C(3)-C(1)-C(11)-C(12)	-138.60(11)	C(4)-C(1)-C(11)-C(12)	75.84(14)
C(2)-C(1)-C(11)-C(12)	-68.35(15)	C(17)-O(2)-C(12)-C(13)	12.19(18)
C(17)-O(2)-C(12)-C(11)	-167.92(11)	C(16)-C(11)-C(12)-O(2)	178.99(11)
C(1)-C(11)-C(12)-O(2)	1.81(16)	C(16)-C(11)-C(12)-C(13)	-1.12(18)
C(1)-C(11)-C(12)-C(13)	-178.29(11)	O(2)-C(12)-C(13)-C(14)	-179.03(11)
C(11)-C(12)-C(13)-C(14)	1.08(18)	C(12)-C(13)-C(14)-C(15)	-0.43(19)
C(13)-C(14)-C(15)-C(16)	-0.16(19)	C(12)-C(11)-C(16)-C(15)	0.52(18)
C(1)-C(11)-C(16)-C(15)	177.64(11)	C(14)-C(15)-C(16)-C(11)	0.12(19)

6.3 Computational Details.

Computational details: Racemization of 2,2-disubtituted cyclopropylnitriles *via* the "conducted tour" mechanism.

Geometry optimizations and frequency calculations were performed using

Gaussian03[259] at B3LYP/6-31G*. All stationary points were characterized as minima (zero imaginary frequencies) or transition states (one imaginary frequency) by vibrational frequency analysis. The displacement of the imaginary frequencies corresponded to the molecular motion for deprotonation and ring inversion transition structures. Zero-point vibration energies at B3LYP/6-31G* were calculated from corrected frequencies (correction factor = 0.9804).

Table 6.8 Calculated energies for racemization of 2,2-disubstituted cyclopropylnitriles *via* the "conducted tour" mechanism.

Structure	ε_0 (hartrees) (nimag)	ZPVE (kJ/mol)	Corr ZPVE (kJ/mol)	Z corr ε_0 (hartrees)	Relative E (kcal/mol)
$LiNH_2$	-63.47145740 (0)	14.65	13.3901	-63.450119	
***2*-1**	-672.23897151 (0)	637.2378	624.7479391	-672.0010178	
2*-35-*Ph	-735.74914832 (0)	705.0816	691.2620006	-735.4858608	-21.8
2*-36-*Ph	-735.73536554 (1)	694.737	681.1201548	-735.4759408	-15.6
2*-37-*Ph	-735.75143769 (0)	709.7575	695.846253	-735.4864041	-22.1
2*-38-*Ph	-735.75622377 (0)	710.0471	696.1301768	-735.4910821	-25.1
2*-39-*Ph	-735.74435255 (1)	706.3145	692.4707358	-735.4806046	-18.5
***2*-6**	-979.90131476 (0)	963.0207	944.1454943	-979.5417091	
2*-35-*BnO	-1043.41805366 (0)	1029.7001	1009.517978	-1043.033549	-26.2
2*-36-*BnO	-1043.40684152 (1)	1021.7159	1001.690268	-1043.025318	-21.0
2*-37-*BnO	-1043.43188686	1036.7239	1016.404112	-1043.044759	-33.2

	(0)				
2*-39-*BnO	-1043.44198106 (0)	1036.825	1016.50323	-1043.054816	-39.5
2*-40-*BnO	-1043.41806813 (1)	1022.5793	1002.536746	-1043.036222	-27.9
2*-43-*BnO	-1043.40402675 (1)	1030.9488	1010.742204	-1043.019056	-17.1
2*-44-*BnO	-1043.42695682 (0)	1030.9985	1010.790929	-1043.041967	-31.5
$LiNH_2$•$2Me_2O$	-373.57905327 (0)	495.1093	485.4051577	-373.3941724	
***2*-7**	-901.28461595 (0)	810.1848	794.3051779	-900.9820814	
2*-35-*MeOPh	-964.79682387 (0)	878.1065	860.8956126	-964.4689264	-23.0
2*-36-*MeOPh	-964.77744650 (1)	868.184	851.1675936	-964.4532542	-13.2
2*-37-*MeOPh	-964.79976000 (0)	882.0174	864.729859	-964.4704021	-24.0
2*-39-*MeOPh	-964.81281589 (0)	882.366	865.0716264	-964.4833278	-32.1
2*-40-*MeOPh	-964.78290285 (1)	868.3788	851.3585755	-964.4586378	-16.6
2*-43-*MeOPh	-964.77573986 (1)	878.9251	861.698168	-964.4475367	-9.6
2*-44-*MeOPh	-964.79733489 (0)	880.5844	863.3249458	-964.4685121	-22.8
2*-45-*MeOPh	-964.79681370 (1)	878.4055	861.1887522	-964.4688046	-23.0
2*-35-S_2-*MeOPh	-1274.88156444 (0)	1308.1057	1282.466828	-1274.393099	-10.6
2*-36-S_2-*MeOPh	-1274.87563903 (1)	1296.9995	1271.57831	-1274.391321	-9.5
2*-37-S_2-*MeOPh	-1274.89215710 (0)	1312.1711	1286.452546	-1274.402174	-16.3
2*-43-S_2-*MeOPh	-1274.88111072 (1)	1308.8639	1283.210168	-1274.392362	-10.1

Computational details: Conformational distribution of nitrile aldols and ketone

aldols.

Conformational search of nitrile aldols and ketone aldols in Chapter 5 was performed using the MMFF94 molecular mechanics method[260] and the conformer distribution module of Spartan 04 for Windows.[261] All conformers were classified as conformation I, conformation II, conformation III, according to the dihedral angle H2-C2-C3-H3. MMFF94 relative energies of the conformers were then used to calculate the summed Boltzmann weightings at 298 K for these conformations.

The geometry optimization at B3LYP/6-31G* was performed for the conformers of *anti*-nitriles and *syn*-nitriles which had lowest MMFF94 relative energy in each conformation groups. Zero-point vibration energies at B3LYP/6-31G* were calculated from corrected frequencies (correction factor = 0.9804). Single point electronic energies were calculated at MP2/6-31+G*//B3LYP/6-31G*.

Table 6.9 MMFF94 conformation distribution for *anti*-**5**-**5** .

Conformer #	Relative E (kCal/mol)	Boltzmann Weightings at 298K	Dihedral angles for H2-C2-C3-H3
Molecule001	0.0000000000	1.0000E+00	170.38
Molecule012	0.0122571015	9.7968E-01	170.42
Molecule023	0.0122950117	9.7962E-01	170.57
Molecule027	0.9847026390	1.9216E-01	-78.13
Molecule028	1.0174881700	1.8190E-01	-78.25
Molecule029	1.0408219500	1.7492E-01	-78.09
Molecule030	1.4530524300	8.7693E-02	-81.34
Molecule031	1.4762041800	8.4358E-02	-81.21
Molecule032	1.4878933900	8.2722E-02	-80.72
Molecule002	1.5105262400	7.9645E-02	-80.51
Molecule003	1.7688184600	5.1673E-02	77.80
Molecule004	1.8002179300	4.9025E-02	78.45
Molecule005	2.0454654800	3.2510E-02	177.24
Molecule006	2.1427553000	2.7621E-02	177.02
Molecule007	2.1525114100	2.7173E-02	177.07

Molecule008	2.1537720400	2.7116E-02	173.42
Molecule009	2.1804163200	2.5932E-02	-68.31
Molecule010	2.1850373200	2.5732E-02	173.53
Molecule011	2.1971804200	2.5214E-02	173.49
Molecule013	2.1996431400	2.5110E-02	-68.22
Molecule014	2.2438516400	2.3318E-02	-68.29
Molecule015	2.2627973800	2.2590E-02	-68.20
Molecule016	5.25115823	1.5136E-04	-82.29
Molecule017	5.27531324	1.4536E-04	-82.32
Molecule018	5.31520752	1.3596E-04	-82.47
Molecule019	5.33929205	1.3058E-04	-82.50
Molecule020	5.39462294	1.1903E-04	78.88
Molecule021	5.40433347	1.1711E-04	78.95
Molecule022	5.43373001	1.1148E-04	79.23
Molecule024	6.34659839	2.4161E-05	67.28
Molecule025	6.3686709	2.3284E-05	67.28
Molecule026	6.44116711	2.0622E-05	67.57

Table 6. 10 MMFF94 conformation distribution for *syni*-***5*-5**

Conformer #	Relative E (kCal/mol)	Boltzmann Weightings at 298K	Dihedral angles for H2-C2-C3-H3
Molecule001	0.0000000000	1.0000E+00	165.74
Molecule012	0.017912263	9.7044E-01	165.76
Molecule020	0.112814341	8.2781E-01	165.02
Molecule021	0.128537124	8.0630E-01	165.05
Molecule022	0.238813616	6.7031E-01	176.98
Molecule023	0.25546718	6.5187E-01	177.03
Molecule024	0.605889966	3.6244E-01	175.33
Molecule025	0.621194007	3.5327E-01	175.39
Molecule026	0.760086247	2.7994E-01	-73.66
Molecule002	0.775286848	2.7291E-01	-73.71
Molecule003	0.802286179	2.6084E-01	-73.77
Molecule004	0.817193481	2.5441E-01	-73.82
Molecule005	2.12807599	2.8308E-02	68.48
Molecule006	2.13688261	2.7894E-02	68.55
Molecule007	2.21190756	2.4600E-02	67.85
Molecule008	2.22097962	2.4229E-02	67.93
Molecule009	2.44648127	1.6607E-02	-71.07
Molecule010	2.47358968	1.5870E-02	-71.11
Molecule011	2.52281864	1.4614E-02	-71.12
Molecule013	2.54971046	1.3970E-02	-71.17
Molecule014	4.02840605	1.1736E-03	-74.72
Molecule015	4.04103182	1.1490E-03	-74.69
Molecule016	4.11361276	1.0175E-03	-74.76
Molecule017	4.12640827	9.9590E-04	-74.73
Molecule018	6.16733247	3.2623E-05	73.33
Molecule019	6.17642527	3.2130E-05	73.34

Table 6.11 MMFF94 conformation distribution for *anti-**5**-**6***

Conformer #	Relative E (kCal/mol)	Boltzmann Weightings at 298K	Dihedral angles for H2-C2-C3-H3
Molecule001	0	1.0000E+00	169.83
Molecule007	0.027849128	9.5442E-01	170.04
Molecule008	0.23938081	6.6967E-01	166.71
Molecule009	0.747556686	2.8588E-01	69.61
Molecule010	0.804283314	2.5997E-01	69.94
Molecule011	0.851533783	2.4018E-01	-78.84
Molecule012	1.08799855	1.6163E-01	-85.84
Molecule013	1.09930206	1.5860E-01	-86.11
Molecule014	1.15836836	1.4366E-01	174.85
Molecule002	1.1595071	1.4339E-01	174.90
Molecule003	1.20501814	1.3286E-01	174.24
Molecule004	1.37860428	9.9340E-02	-68.03
Molecule005	4.498643	5.3386E-04	70.13
Molecule006	4.54500269	4.9397E-04	70.59

Table 6.12 MMFF94 conformation distribution for *syn-**5**-**6***

Conformer #	Relative E (kCal/mol)	Boltzmann Weightings at 298K	Dihedral angles for H2-C2-C3-H3
Molecule001	0	1.0000E+00	-175.83
Molecule011	0.034994533	9.4307E-01	-175.45
Molecule012	0.395518877	5.1556E-01	-173.02
Molecule013	0.400690648	5.1111E-01	-172.96
Molecule014	0.672504033	3.2418E-01	72.21
Molecule015	0.719513919	2.9963E-01	72.30
Molecule016	0.930569757	2.1040E-01	174.26
Molecule017	0.945563808	2.0518E-01	174.57
Molecule018	1.36666507	1.0135E-01	-177.06
Molecule002	1.38709223	9.7938E-02	-176.84
Molecule003	1.75792378	5.2624E-02	-64.99
Molecule004	1.77431569	5.1199E-02	-64.77
Molecule005	2.09583335	2.9879E-02	-68.32
Molecule006	3.78532874	1.7633E-03	-59.74
Molecule007	3.79023089	1.7489E-03	-59.84
Molecule008	4.13002941	9.8987E-04	77.32
Molecule009	4.17889683	9.1208E-04	77.36
Molecule010	4.33984645	6.9654E-04	-64.50

Table 6.13 MMFF94 conformation distribution for *anti-**5**-**29***

Conformer #	Relative E (kCal/mol)	Boltzmann Weightings at	Dihedral angles for

		298K	H2-C2-C3-H3
Molecule001	0	1.0000E+00	-167.62
Molecule012	0.0060004	9.9000E-01	-167.64
Molecule023	0.059962745	9.0444E-01	-167.39
Molecule025	0.826620622	2.5042E-01	-108.86
Molecule026	0.858041635	2.3758E-01	-108.92
Molecule027	0.875290244	2.3081E-01	-109.30
Molecule028	1.52663508	7.7524E-02	-169.10
Molecule029	1.5790895	7.1004E-02	-168.98
Molecule030	1.60729698	6.7727E-02	-168.92
Molecule002	1.65924562	6.2083E-02	-168.81
Molecule003	1.74469653	5.3803E-02	72.45
Molecule004	1.79006407	4.9866E-02	72.43
Molecule005	1.82976452	4.6658E-02	72.64
Molecule006	2.03904528	3.2861E-02	-57.91
Molecule007	2.071744	3.1110E-02	-57.86
Molecule008	2.10037344	2.9653E-02	-57.83
Molecule009	2.29470807	2.1414E-02	-60.41
Molecule010	3.24532052	4.3568E-03	144.66
Molecule011	3.37891108	3.4833E-03	144.45
Molecule013	3.38721683	3.4351E-03	144.50
Molecule014	3.52100553	2.7455E-03	144.30
Molecule015	5.30978801	1.3720E-04	-103.92
Molecule016	5.3579235	1.2657E-04	-104.46
Molecule017	6.03532096	4.0697E-05	149.13
Molecule018	6.09064542	3.7095E-05	73.22
Molecule019	6.15009473	3.3579E-05	73.30
Molecule020	6.1689115	3.2537E-05	149.00
Molecule021	6.33468515	2.4648E-05	148.80
Molecule022	6.8497134	1.0402E-05	60.47
Molecule024	6.95436607	8.7296E-06	60.46

Table 6.14 MMFF94 conformation distribution for *anti-**5**-**30***

Conformer #	Relative E (kCal/mol)	Boltzmann Weightings at 298K	Dihedral angles for H2-C2-C3-H3
Molecule001	0	1.0000E+00	170.27
Molecule012	0.055976073	9.1050E-01	171.28
Molecule023	0.287283301	6.1804E-01	171.56
Molecule024	1.12927902	1.5083E-01	-77.86
Molecule025	1.14526366	1.4685E-01	-77.90
Molecule026	1.16305707	1.4254E-01	-77.97
Molecule027	1.17912177	1.3875E-01	-78.01
Molecule028	1.50698277	8.0119E-02	76.83
Molecule029	1.60001315	6.8558E-02	-81.06
Molecule002	1.61673597	6.6664E-02	-81.18
Molecule003	1.66480113	6.1508E-02	78.05
Molecule004	1.70362763	5.7635E-02	78.61

Molecule005	2.01010241	3.4493E-02	177.55
Molecule006	2.08045511	3.0659E-02	176.40
Molecule007	2.10239094	2.9553E-02	177.28
Molecule008	2.20772078	2.4773E-02	173.14
Molecule009	2.23050483	2.3845E-02	174.20
Molecule010	2.25438843	2.2910E-02	174.28
Molecule011	2.4934425	1.5351E-02	-68.36
Molecule013	2.5245478	1.4571E-02	-68.34
Molecule014	2.55736909	1.3792E-02	-68.35
Molecule015	2.58836514	1.3094E-02	-68.33
Molecule016	5.21176953	1.6168E-04	78.20
Molecule017	5.3578836	1.2658E-04	79.53
Molecule018	5.53997476	9.3305E-05	-82.49
Molecule019	5.57737798	8.7639E-05	-82.57
Molecule020	6.29836003	2.6195E-05	67.63
Molecule021	6.37205046	2.3153E-05	67.92
Molecule022	6.49370635	1.8885E-05	67.86

Table 6.15 MMFF94 conformation distribution for *syn*-***5*-30**

Conformer #	Relative E (kCal/mol)	Boltzmann Weightings at 298K	Dihedral angles for H2-C2-C3-H3
Molecule001	0	1.0000E+00	165.73
Molecule012	0.018918129	9.6881E-01	165.95
Molecule020	0.039296497	9.3630E-01	166.01
Molecule021	0.086873689	8.6458E-01	165.03
Molecule022	0.118919396	8.1939E-01	163.86
Molecule023	0.40711856	5.0564E-01	-73.33
Molecule024	0.450993758	4.6981E-01	-73.41
Molecule025	0.454314068	4.6720E-01	176.63
Molecule026	0.45774406	4.6453E-01	177.03
Molecule002	0.509166192	4.2619E-01	-73.39
Molecule003	0.553541952	3.9566E-01	-73.50
Molecule004	0.820563741	2.5297E-01	174.99
Molecule005	0.827585286	2.5002E-01	175.31
Molecule006	1.86371748	4.4078E-02	67.73
Molecule007	2.04300119	3.2644E-02	67.91
Molecule008	2.17645151	2.6105E-02	-70.79
Molecule009	2.25393553	2.2928E-02	-70.83
Molecule010	2.33338159	2.0071E-02	-70.53
Molecule011	2.41163658	1.7605E-02	-70.59
Molecule013	3.89016857	1.4793E-03	-74.10
Molecule014	3.97825524	1.2764E-03	-74.12
Molecule015	4.07926508	1.0777E-03	-74.16
Molecule016	4.16611891	9.3181E-04	-74.20
Molecule017	5.97696639	4.4876E-05	72.05
Molecule018	6.13236724	3.4591E-05	72.03
Molecule019	6.16055735	3.2996E-05	72.51

Table 6.16 MMFF94 conformation distribution for *anti*-**5-31**

Conformer #	Relative E (kCal/mol)	Boltzmann Weightings at 298K	Dihedral angles for H2-C2-C3-H3
Molecule001	0	1.0000E+00	171.82
Molecule012	0.015264842	9.7476E-01	173.66
Molecule023	0.015269216	9.7475E-01	173.68
Molecule034	0.451490062	4.6942E-01	179.42
Molecule045	0.481780199	4.4620E-01	178.87
Molecule056	1.02638931	1.7920E-01	-76.83
Molecule067	1.0486511	1.7264E-01	-76.87
Molecule078	1.0486604	1.7264E-01	-76.89
Molecule089	1.09741332	1.5910E-01	69.61
Molecule002	1.25693399	1.2180E-01	70.23
Molecule003	1.256934	1.2180E-01	70.23
Molecule004	1.25693401	1.2180E-01	70.22
Molecule005	1.67433318	6.0533E-02	173.22
Molecule006	1.67900343	6.0062E-02	175.45
Molecule007	1.67900504	6.0061E-02	175.43
Molecule008	1.67900805	6.0061E-02	175.47
Molecule009	1.76404024	5.2088E-02	177.80
Molecule010	1.78905567	4.9950E-02	176.37
Molecule011	1.78905568	4.9950E-02	176.37
Molecule013	2.04666325	3.2444E-02	-179.88
Molecule014	2.08807118	3.0270E-02	179.58
Molecule015	2.20136668	2.5038E-02	-82.19
Molecule016	2.2256023	2.4042E-02	-82.31
Molecule017	2.37653	1.8671E-02	-67.89
Molecule018	2.40023269	1.7945E-02	-67.88
Molecule019	2.41487625	1.7510E-02	-179.85
Molecule020	2.45895625	1.6264E-02	179.62
Molecule021	2.49178968	1.5393E-02	176.88
Molecule022	2.54770476	1.4017E-02	79.08
Molecule024	2.5635894	1.3649E-02	-77.97
Molecule025	2.60050551	1.2830E-02	75.19
Molecule026	2.61074418	1.2612E-02	-77.75
Molecule027	2.66551391	1.1507E-02	79.57
Molecule028	2.70790454	1.0718E-02	78.71
Molecule029	2.71862877	1.0527E-02	-77.72

Molecule030	2.74487437	1.0074E-02	-77.70
Molecule031	2.86137073	8.2885E-03	-176.69
Molecule032	2.897179	7.8060E-03	-179.59
Molecule033	2.89718386	7.8059E-03	-179.57
Molecule035	2.99457795	6.6309E-03	-176.75
Molecule036	3.06788528	5.8647E-03	76.09
Molecule037	3.20912211	4.6291E-03	78.07
Molecule038	3.20912213	4.6291E-03	78.07
Molecule039	3.41830583	3.2608E-03	179.19
Molecule040	3.41830912	3.2608E-03	179.17
Molecule041	3.45702443	3.0561E-03	177.59
Molecule042	3.55382217	2.5986E-03	80.40
Molecule043	3.6344626	2.2703E-03	80.90
Molecule044	3.70783946	2.0077E-03	-82.83
Molecule046	3.71937136	1.9693E-03	-68.24
Molecule047	3.73119534	1.9307E-03	-68.43
Molecule048	3.76482678	1.8249E-03	-82.57
Molecule049	3.93721816	1.3672E-03	120.40
Molecule051	4.00484554	1.2208E-03	-179.23
Molecule050	4.00484554	1.2208E-03	-179.23
Molecule052	4.00484638	1.2208E-03	-179.23
Molecule053	4.06002475	1.1130E-03	-179.76
Molecule054	4.19240864	8.9166E-04	-68.42
Molecule055	4.36904445	6.6329E-04	86.21
Molecule057	4.6383499	4.2247E-04	-177.11
Molecule058	4.72255385	3.6690E-04	-176.34
Molecule059	4.75425794	3.4792E-04	-178.07
Molecule060	4.75426079	3.4792E-04	-178.06
Molecule061	4.8445006	2.9911E-04	164.08
Molecule062	4.87138679	2.8594E-04	-176.42
Molecule063	4.8713877	2.8594E-04	-176.43
Molecule064	4.98203242	2.3757E-04	-168.02

Table 6.17 MMFF94 conformation distribution for *syn*-**5-31**

Conformer #	Relative E (kCal/mol)	Boltzmann Weightings at 298K	Dihedral angles for H2-C2-C3-H3
Molecule001	0	1.0000E+00	170.51
Molecule023	0.024306275	9.6010E-01	170.77
Molecule034	0.095466048	8.5222E-01	166.73

Molecule045	0.121438287	8.1594E-01	166.88
Molecule056	0.267093314	6.3929E-01	178.59
Molecule067	0.267093315	6.3929E-01	178.59
Molecule078	0.267093394	6.3929E-01	178.59
Molecule089	0.269304958	6.3693E-01	178.34
Molecule002	0.346071866	5.6008E-01	-73.03
Molecule003	0.45336093	4.6795E-01	-72.82
Molecule004	0.851315821	2.4027E-01	175.16
Molecule005	0.855468281	2.3861E-01	175.37
Molecule007	0.855468382	2.3861E-01	175.37
Molecule006	0.855469951	2.3861E-01	175.37
Molecule008	1.00167322	1.8678E-01	161.74
Molecule009	1.03914713	1.7541E-01	161.71
Molecule010	1.34147144	1.0572E-01	71.36
Molecule011	1.34147177	1.0571E-01	71.36
Molecule013	1.47583797	8.4409E-02	-73.52
Molecule014	1.47583867	8.4409E-02	-73.52
Molecule015	1.54411602	7.5287E-02	71.45
Molecule016	1.5765107	7.1311E-02	157.40
Molecule017	1.60098256	6.8447E-02	-72.99
Molecule018	1.60098341	6.8447E-02	-73.00
Molecule019	1.60390614	6.8112E-02	157.04
Molecule020	1.70369474	5.7628E-02	165.60
Molecule021	1.72213805	5.5875E-02	168.43
Molecule022	1.72512603	5.5596E-02	165.75
Molecule024	1.74223793	5.4025E-02	168.67
Molecule025	1.92218057	3.9966E-02	-72.09
Molecule026	1.92218067	3.9966E-02	-72.09
Molecule027	2.03227705	3.3236E-02	-71.78
Molecule028	2.04875404	3.2331E-02	177.88
Molecule029	2.05410585	3.2042E-02	178.17
Molecule030	2.05410585	3.2042E-02	178.17
Molecule031	2.05883125	3.1790E-02	-73.71
Molecule032	2.07261728	3.1064E-02	168.08
Molecule035	2.07638907	3.0869E-02	168.14
Molecule033	2.07638907	3.0869E-02	168.14
Molecule036	2.13631362	2.7920E-02	-70.69
Molecule037	2.13631443	2.7920E-02	-70.70
Molecule038	2.16963487	2.6405E-02	-73.55
Molecule039	2.16963489	2.6405E-02	-73.55

Molecule040	2.29662362	2.1345E-02	-70.21
Molecule041	2.46283864	1.6158E-02	170.42
Molecule042	2.46680113	1.6051E-02	170.58
Molecule043	2.46680113	1.6051E-02	170.58
Molecule044	2.50844206	1.4970E-02	174.22
Molecule046	2.52076341	1.4664E-02	174.44
Molecule047	2.52076341	1.4664E-02	174.44
Molecule048	2.85791782	8.3366E-03	-71.82
Molecule049	2.99458718	6.6308E-03	-71.15
Molecule050	3.06392037	5.9038E-03	68.20
Molecule051	3.2126962	4.6015E-03	-74.54
Molecule052	3.22329557	4.5205E-03	70.43
Molecule053	3.22329597	4.5205E-03	70.43
Molecule055	3.26166576	4.2391E-03	68.14
Molecule054	3.26166576	4.2391E-03	68.14
Molecule057	3.33753456	3.7332E-03	-74.04
Molecule058	3.33753476	3.7332E-03	-74.05
Molecule059	3.47558207	2.9625E-03	-70.77
Molecule060	3.50817668	2.8051E-03	-69.49
Molecule061	3.66032282	2.1741E-03	-68.85
Molecule062	3.69537867	2.0501E-03	-70.08
Molecule063	3.92644354	1.3921E-03	-71.28
Molecule065	4.093952	1.0515E-03	-70.85
Molecule064	4.09395213	1.0515E-03	-70.85
Molecule066	4.71999203	3.6847E-04	-69.48
Molecule068	4.92312195	2.6220E-04	-68.68
Molecule069	4.97620248	2.3990E-04	66.39
Molecule070	4.97620316	2.3990E-04	66.41

Table 6.18 MMFF94 conformation distribution for *anti*-**5-32**

Conformer #	Relative E (kCal/mol)	Boltzmann Weightings at 298K	Dihedral angles for H2-C2-C3-H3
Molecule001	0	1.0000E+00	166.20
Molecule012	0.040291998	9.3474E-01	165.70
Molecule016	0.317512371	5.8752E-01	68.17
Molecule017	0.326973447	5.7828E-01	163.69
Molecule018	0.358523977	5.4852E-01	163.19
Molecule019	0.35852567	5.4851E-01	163.20
Molecule020	0.467678849	4.5686E-01	67.86
Molecule021	1.03353881	1.7707E-01	164.22
Molecule022	1.05640724	1.7042E-01	163.58

Molecule002	1.56366848	7.2861E-02	-73.05
Molecule003	1.58875041	6.9864E-02	-73.31
Molecule004	3.16230202	5.0068E-03	-65.57
Molecule005	3.16230404	5.0068E-03	-65.57
Molecule006	3.19434038	4.7452E-03	-65.58
Molecule007	4.00344402	1.2237E-03	-70.91
Molecule008	4.01216265	1.2059E-03	-70.71
Molecule009	4.51604283	5.1853E-04	75.85
Molecule010	4.70951953	3.7500E-04	76.79
Molecule011	5.08230782	2.0083E-04	-70.88
Molecule013	5.13747693	1.8311E-04	-70.83
Molecule014	8.39453359	7.8223E-07	62.58
Molecule015	8.50446638	6.5067E-07	61.54

Table 6.19 MMFF94 conformation distribution for *syn*-***5*-32**

Conformer #	Relative E (kCal/mol)	Boltzmann Weightings at 298K	Dihedral angles for H2-C2-C3-H3
Molecule001	0	1.0000E+00	173.84
Molecule012	0.01944349	9.6796E-01	174.14
Molecule013	0.554536924	3.9500E-01	-66.00
Molecule014	0.671069062	3.2496E-01	-66.09
Molecule015	1.87350013	4.3362E-02	168.17
Molecule016	1.87868632	4.2987E-02	168.00
Molecule017	2.32896079	2.0220E-02	65.56
Molecule018	2.32896138	2.0220E-02	65.66
Molecule019	2.48962302	1.5449E-02	66.58
Molecule002	2.48962303	1.5449E-02	66.58
Molecule003	2.57203023	1.3457E-02	175.52
Molecule004	2.59305254	1.2992E-02	174.52
Molecule005	3.10764724	5.4868E-03	-58.71
Molecule006	3.21327008	4.5971E-03	-57.67
Molecule007	5.95991151	4.6176E-05	67.03
Molecule008	5.95991151	4.6176E-05	67.03
Molecule009	6.11527135	3.5596E-05	68.44
Molecule010	6.2750565	2.7237E-05	-58.33
Molecule011	8.37163807	8.1281E-07	67.51

Table 6.20 MMFF94 conformation distribution for *anti*-***5*-33**

Conformer #	Relative E (kCal/mol)	Boltzmann Weightings at 298K	Dihedral angles for H2-C2-C3-H3
Molecule001	0	1.0000E+00	162.42
Molecule006	0.02240019	9.6317E-01	161.41
Molecule007	0.303020348	6.0196E-01	158.99
Molecule008	0.304875358	6.0009E-01	158.03
Molecule009	2.16216287	2.6737E-02	66.61

Molecule010	2.33623098	1.9975E-02	65.51
Molecule011	2.71686211	1.0558E-02	-77.05
Molecule012	2.75992286	9.8237E-03	-77.38
Molecule013	2.75992949	9.8236E-03	-77.37
Molecule002	2.7664775	9.7164E-03	-75.61
Molecule003	2.80299956	9.1398E-03	-75.77
Molecule004	3.38549482	3.4451E-03	-66.40
Molecule005	3.39428842	3.3947E-03	-66.46

Table 6.21 MMFF94 conformation distribution for *syn*-**5-33**

Conformer #	Relative E (kCal/mol)	Boltzmann Weightings at 298K	Dihedral angles for H2-C2-C3-H3
Molecule001	0	1.0000E+00	171.12
Molecule009	0.01547386	9.7441E-01	171.24
Molecule010	1.18347224	1.3774E-01	-70.20
Molecule011	1.29993115	1.1333E-01	-70.52
Molecule012	1.84943337	4.5146E-02	161.78
Molecule013	1.87013405	4.3607E-02	161.83
Molecule014	2.52906632	1.4461E-02	166.83
Molecule015	2.5404549	1.4188E-02	168.63
Molecule016	3.24618626	4.3505E-03	-64.54
Molecule002	3.43433735	3.1744E-03	-64.37
Molecule003	3.78925815	1.7518E-03	66.97
Molecule004	3.78925893	1.7518E-03	66.98
Molecule005	3.96674198	1.3013E-03	68.55
Molecule006	3.96674198	1.3013E-03	68.55
Molecule007	6.78431692	1.1606E-05	68.87
Molecule008	6.94905839	8.8076E-06	71.25

Table 6.22 MMFF94 conformation distribution for *anti*-**5-34**

Conformer #	Relative E (kCal/mol)	Boltzmann Weightings at 298K	Dihedral angles for H2-C2-C3-H3
Molecule001	0	1.0000E+00	159.67
Molecule005	0.016605855	9.7257E-01	160.65
Molecule006	0.169898961	7.5233E-01	164.86
Molecule007	0.178508815	7.4155E-01	163.81
Molecule008	2.30035121	2.1213E-02	71.27
Molecule009	2.3775322	1.8640E-02	-76.54
Molecule010	2.41592524	1.7479E-02	-76.67
Molecule011	2.48644401	1.5532E-02	70.66
Molecule012	2.55880922	1.3759E-02	65.71
Molecule002	2.70732512	1.0728E-02	64.83
Molecule003	3.04096809	6.1352E-03	-66.40

Molecule004	3.04648442	6.0787E-03	-66.43

Table 6.23 MMFF94 conformation distribution for *syn*-**5-34**

Conformer #	Relative E (kCal/mol)	Boltzmann Weightings at 298K	Dihedral angles for H2-C2-C3-H3
Molecule001	0	1.0000E+00	171.85
Molecule008	0.010396148	9.8274E-01	171.89
Molecule009	1.35600434	1.0317E-01	161.21
Molecule010	1.38757523	9.7858E-02	161.42
Molecule011	1.47862296	8.4017E-02	-72.38
Molecule012	1.49267688	8.2062E-02	-69.90
Molecule013	1.5664445	7.2523E-02	-72.49
Molecule014	1.58378075	7.0448E-02	-69.90
Molecule015	3.0382033	6.1636E-03	-67.15
Molecule002	3.19415882	4.7466E-03	-66.97
Molecule003	3.60379906	2.3900E-03	69.39
Molecule004	3.76725028	1.8175E-03	70.56
Molecule005	6.62743532	1.5095E-05	71.14
Molecule006	6.79141598	1.1469E-05	72.71
Molecule007	6.791416	1.1469E-05	72.72

Table 6.24 MMFF94 conformation distribution for *anti*-**5-35**

Conformer #	Relative E (kCal/mol)	Boltzmann Weightings at 298K	Dihedral angles for H2-C2-C3-H3
Molecule001	0	1.0000E+00	160.33
Molecule008	0.01839945	9.6965E-01	160.52
Molecule009	1.90315059	4.1261E-02	161.36
Molecule010	1.92296873	3.9914E-02	161.58
Molecule011	2.38500657	1.8408E-02	173.92
Molecule012	3.69497236	2.0515E-03	179.46
Molecule013	3.81593733	1.6752E-03	-72.01
Molecule014	3.90202769	1.4502E-03	-72.14
Molecule015	3.90290321	1.4481E-03	175.75
Molecule002	7.59369838	2.9916E-06	-59.31
Molecule003	7.64115749	2.7630E-06	-59.48
Molecule004	8.68720688	4.7910E-07	172.70
Molecule005	9.46521788	1.3015E-07	-167.83
Molecule006	9.46955927	1.2921E-07	-163.78
Molecule007	9.47345966	1.2837E-07	-167.85

Table 6.25 MMFF94 conformation distribution for *syn-**5**-**35***

Conformer #	Relative E (kCal/mol)	Boltzmann Weightings at 298K	Dihedral angles for H2-C2-C3-H3
Molecule001	0	1.0000E+00	-167.24
Molecule012	0.065858562	8.9555E-01	-167.01
Molecule015	0.133357085	7.9981E-01	-170.37
Molecule016	0.149645972	7.7829E-01	-170.16
Molecule017	1.74192235	5.4054E-02	-73.21
Molecule018	1.82819271	4.6781E-02	-73.09
Molecule019	1.85645446	4.4618E-02	-161.13
Molecule020	1.94041169	3.8764E-02	-160.99
Molecule021	2.43680802	1.6878E-02	-166.26
Molecule002	2.46797391	1.6020E-02	-166.05
Molecule003	2.67849858	1.1259E-02	-75.46
Molecule004	2.76167534	9.7949E-03	-75.50
Molecule005	5.98983104	4.3919E-05	-171.82
Molecule006	6.98262823	8.3260E-06	56.86
Molecule007	7.02990832	7.6920E-06	56.87
Molecule008	7.33819083	4.5896E-06	-86.04
Molecule009	7.34881122	4.5087E-06	-86.33

Table 6. 26 MMFF94 conformation distribution for *anti-**5**-**36***

Conformer #	Relative E (kCal/mol)	Boltzmann Weightings at 298K	Dihedral angles for H2-C2-C3-H3
Molecule001	0	1.0000E+00	178.04
Molecule004	0.536776323	4.0693E-01	164.47
Molecule005	1.27019433	1.1912E-01	179.02
Molecule006	2.04898978	3.2318E-02	-67.55
Molecule007	2.46236099	1.6171E-02	165.15
Molecule008	3.97130094	1.2914E-03	63.95
Molecule009	6.59018217	1.6067E-05	63.21
Molecule010	7.43523319	3.9011E-06	175.06
Molecule011	7.44644364	3.8285E-06	159.96
Molecule002	7.57480791	3.0878E-06	-172.73
Molecule003	9.47181348	1.2872E-07	-69.08

Table 6. 27 MMFF94 conformation distribution for *syn-**5**-**36***

Conformer #	Relative E (kCal/mol)	Boltzmann Weightings at 298K	Dihedral angles for H2-C2-C3-H3
Molecule001	0	1.0000E+00	-74.59
Molecule005	1.42627683	9.1716E-02	-75.60
Molecule006	1.74637814	5.3652E-02	-167.68
Molecule007	1.94145907	3.8696E-02	177.48

Molecule008	2.30814121	2.0938E-02	-175.15
Molecule009	3.22735325	4.4899E-03	63.56
Molecule010	6.04835394	3.9818E-05	65.40
Molecule011	6.14050647	3.4123E-05	-54.34
Molecule012	6.67391413	1.3964E-05	-89.37
Molecule002	7.41354295	4.0454E-06	-150.06

Table 6. 28 Calculated energies for *anti*-nitrile aldols and *syn*-ketone aldols: Most stable conformer in the group of Conformation I, II and III.

Structure	Confor-mation	Energy basis	ε_0 (hartrees) (nimag)	Corr ZPVE (hartrees)	Z corr ε_0 (hartrees)	Relative E (kcal/mol)
anti-**5**-**5**	I	B3LYP/6-31G*	-866.636066	0.352873	-866.283193	0.00
		MP2/6-31+G*//B3				
		LYP/6-31G*	-863.871146	0.352873	-863.518273	0.00
	II	B3LYP/6-31G*	-866.632259	0.353215	-866.279044	2.60
		MP2/6-31+G*//B3				
		LYP/6-31G*	-863.868056	0.353215	-863.514841	2.15
	III	B3LYP/6-31G*	-866.634082	0.352897	-866.281185	1.26
		MP2/6-31+G*//B3				
		LYP/6-31G*	-863.865208	0.352897	-863.512311	3.74
anti-**5**-**6**	I	B3LYP/6-31G*	-827.318698	0.325362	-826.993336	0.00
		MP2/6-31+G*//B3				
		LYP/6-31G*	-824.699656	0.325362	-824.374294	0.00
	II	B3LYP/6-31G*	-827.316925	0.325913	-826.991012	1.46
		MP2/6-31+G*//B3				
		LYP/6-31G*	-824.699356	0.325913	-824.373443	0.53
	III	B3LYP/6-31G*	-827.318476	0.325689	-826.992787	0.34
		MP2/6-31+G*//B3				
		LYP/6-31G*	-824.696568	0.325689	-824.370879	2.14
anti-**5**-**29**	I	B3LYP/6-31G*	-945.262354	0.409085	-944.853269	0.00
		MP2/6-31+G*//B3				
		LYP/6-31G*	-942.212260	0.409085	-941.803175	0.00
	II	B3LYP/6-31G*	-945.259520	0.40983	-944.849690	2.25
		MP2/6-31+G*//B3				
		LYP/6-31G*	-942.210251	0.40983	-941.800421	1.73
	III	B3LYP/6-31G*	-945.261750	0.409773	-944.851977	0.81
		MP2/6-31+G*//B3				
		LYP/6-31G*	-942.2066122	0.409773	-941.796839	3.98
anti-**5**-**30**	I	B3LYP/6-31G*	-980.961791	0.372536	-980.589255	0.00
		MP2/6-31+G*//B3				
		LYP/6-31G*	-977.864771	0.372536	-977.492235	0.00

	II	B3LYP/6-31G*	-980.958277	0.372892	-980.585385	2.43
		MP2/6-31+G*//B3				
		LYP/6-31G*	-977.861669	0.372892	-977.488777	2.17
	III	B3LYP/6-31G*	-980.960102	0.372287	-980.587815	0.90
		MP2/6-31+G*//B3				
		LYP/6-31G*	-977.858428	0.372287	-977.486141	3.82
anti-**5**-**31**	I	B3LYP/6-31G*	-1020.267563	0.402495	-1019.865068	0.00
		MP2/6-31+G*//B3				
		LYP/6-31G*	-1017.028632	0.402495	-1016.626137	0.00
	II	B3LYP/6-31G*	-1020.264395	0.402765	-1019.861630	2.16
		MP2/6-31+G*//B3				
		LYP/6-31G*	-1017.027424	0.402765	-1016.624659	0.93
	III	B3LYP/6-31G*	-1020.266283	0.402599	-1019.863684	0.87
		MP2/6-31+G*//B3				
		LYP/6-31G*	-1017.022580	0.402599	-1016.619981	3.86
anti-**5**-**32**	I	B3LYP/6-31G*	-1061.482514	0.27251	-1061.210004	0.00
		MP2/6-31+G*//B3				
		LYP/6-31G*	-1058.405961	0.272594	-1058.133367	0.00
	II	B3LYP/6-31G*	-1061.483620	0.272939	-1061.210681	-0.43
		MP2/6-31+G*//B3				
		LYP/6-31G*	-1058.406859	0.272939	-1058.133920	-0.35
	III	B3LYP/6-31G*	-1061.48376396	0.272619	-1061.211145	-0.72
		MP2/6-31+G*//B3				
		LYP/6-31G*	-1058.40254387	0.272619	-1058.129925	2.16
anti-**5**-**33**	I	B3LYP/6-31G*	-1782.197024	0.269371	-1781.927653	0.00
		MP2/6-31+G*//B3				
		LYP/6-31G*	-1778.415433	0.269371	-1778.146062	0.00
	II	B3LYP/6-31G*	-1782.193603	0.269879	-1781.923724	2.47
		MP2/6-31+G*//B3				
		LYP/6-31G*	-1778.412095	0.269879	-1778.142216	2.41
	III	B3LYP/6-31G*	-1782.196529	0.269664	-1781.926865	0.49
		MP2/6-31+G*//B3				
		LYP/6-31G*	-1778.409669	0.269664	-1778.140005	3.80
anti-**5**-**34**	I	B3LYP/6-31G*	-6005.21937718	0.268532	-6004.950845	0.00
		MP2/6-31+G*//B3				
		LYP/6-31G*	-5999.251961	0.268532	-5998.983429	0.00
	II	B3LYP/6-31G*	-6005.218256	0.268827	-6004.949429	0.89
		MP2/6-31+G*//B3				
		LYP/6-31G*	-5999.249515	0.268827	-5998.980688	1.72
	III	B3LYP/6-31G*	-6005.216756	0.268214	-6004.948542	1.45
		MP2/6-31+G*//B3	-5999.240222	0.268214	-5998.972008	7.17

		LYP/6-31G*				
syn-***5*-35**	I	B3LYP/6-31G*	-813.925740	0.397085	-813.528655	0.00
		MP2/6-31+G*//B3				
		LYP/6-31G*	-811.252845	0.397085	-810.855760	0.00
	II	B3LYP/6-31G*	-813.916455	0.39738	-813.519075	6.01
		MP2/6-31+G*//B3				
		LYP/6-31G*	-811.241681	0.39738	-810.844301	7.19
	III	B3LYP/6-31G*	-813.926506	0.397697	-813.528806	-0.10
		MP2/6-31+G*//B3				
		LYP/6-31G*	-811.248389	0.397697	-810.850692	3.18
syn-***5*-36**	I	B3LYP/6-31G*	-1615.156227	0.293743	-1614.862484	0.00
		MP2/6-31+G*//B3				
		LYP/6-31G*	-1611.799883	0.293743	-1611.506140	0.00
	II	B3LYP/6-31G*	-1615.152519	0.293937	-1614.858582	2.45
		MP2/6-31+G*//B3				
		LYP/6-31G*	-1611.795830	0.293937	-1611.501893	2.66
	III	B3LYP/6-31G*	-1615.161502	0.29466	-1614.866842	-2.73
		MP2/6-31+G*//B3				
		LYP/6-31G*	-1611.799053	0.29466	-1611.504393	1.10

References

1. Yamamoto, H.; Oshima, K., *Main Group Metals in Organic Synthesis*. Wiley-VCH: Weinheim, 2004; Vol. 1.
2. Hodgson, D. M., *Topics in Organometallic Chemistry*. Springer: Verlag Berlin Heidelberg New York, 2003; Vol. 5.
3. Yoshifuji, S.; Tanaka, K.; Nitta, Y., A novel synthesis of L-ω-carbamoyl-α-amino acids from L-α,ω-diamino acids by ruthenium tetroxide oxidation method. . *Chem. Pharm. Bull.* **1985,** *33*, 1749-1751.
4. Miles, W. H.; Rivera, S. L.; Rosario, J. D. d., Diastereselective reactions of a simple secondary Grignard reagent. *Tetrahedron Lett.* **1992,** *33*, 305-308.
5. Fleming, F. F.; Gudipati, S.; Zhang, Z.; Liu, W.; Steward, O. W., Cyclic nitriles: Diastereoselective alkylations. *J. Org. Chem.* **2005,** *70*, 3845-3849.
6. Jones, D. M.; Nilsson, B.; Szelke, M., A short stereocontrolled synthesis of hydroxyethylene dipeptide isosteres. *J. Org. Chem.* **1993,** *58*, 2286-2290.
7. Stratmann, O.; Kaiser, B.; Frohlich, R.; Meyer, O.; Hoppe, D., The configurational stability of an enantioenriched alpha-thiobenzyllithium derivative and the stereochemical course of its electrophilic substitution reactions; Synthesis of enantiomerically pure, tertiary benzylic thiols. *Chem. -Eur. J.* **2001,** *7*, 423-435.
8. Clayden, J., *Organolithiums: Selectivity for Synthesis*. Elsevier Science: Oxford, 2002; Vol. 23.
9. Hirsch, R.; Hoffmann, R. W., Chiral organometallic reagents .5. A test on the configurational stability of chiral organolithium compounds based on kinetic resolution - scope and limitations. *Chem. Ber.* **1992,** *125*, 975-982.
10. Bryant, R. G., The NMR time scale. *J. Chem. Educ.* **1983,** *60*, 933-935.
11. Witanowski, M.; Roberts, J. D., Proton magnetic resonance spectroscopy. Configurational stability of neohexyl(3,3-dimethylbutyl) organometallic compounds. *J. Am. Chem. Soc.* **1966,** *88*, 737-741.
12. Fraenkel, G.; Duncan, J. H.; Martin, K.; Wang, J., Stereochemistry of solvation of benzylic lihthium compounds: Structure and dynamic behavior. *J. Am. Chem. Soc.* **1999,** *121*, 10538-10544.
13. Hofmann, R. W.; Julius, M.; Chemla, F.; Ruhland, T.; Frenzen, G., Configurational stability of chiral organolithium compounds on the time scale of their addition to aldehydes. *Tedrahedron* **1994,** *50*, 6049-6060.
14. Hoffmann, R. W.; Julius, M.; Chemla, F.; Ruhland, T.; Frenzen, G., Configurational stability of chiral organolithium compounds on the time-scale of their addition to aldehydes. *Tetrahedron* **1994,** *50*, 6049-6060.
15. Öki, M., In *Top. Stereochem.*, John Wiley & Sons. Inc.: New York, 1983; Vol. 14, p 14.
16. Eyring, H., The activated complex and the absolute rate of chemical reactions. *Chem. Rev.* **1935,** *17*, 65-77.

17. Reich, H. J.; Dykstra, R. R., Effects of ion-pair separation on inversion and rotation of sulfur-stabilized, selenium-stabilized, and silicon-stabilized organolithium reagents. *Angew. Chem., Int. Ed. Engl.* **1993,** *32*, 1469-1470.
18. Hoffmann, R. W.; Dress, R. K.; Ruhland, T.; Wenzel, A., Chiral organometallic reagents .16. Enantiomerization of alpha-thio-substituted, alpha-seleno-substituted, and alpha-telluro-substituted alkyllithium compounds - kinetic and mechanistic studies. *Chem. Ber.* **1995,** *128*, 861-870.
19. Ahlbrecht, H.; Harbach, J.; Hoffmann, R. W.; Ruhaland, T., Chiral organometallic reagents XII. On the racemization of alpha-hetero-substituted benzyllithium compounds. *Liebigs Ann. Chem.* **1995,** *1995*, 211-216.
20. Kawabata, T.; Suzuki, H.; Nagae, Y.; Fuji, K., A chiral nonracemic enolate with dynamic axial chirality: Direct asymmetric alpha-methylation of alpha-amino acid derivatives. *Angew. Chem., Int. Ed. Engl.* **2000,** *39*, 2155-2157.
21. Panek, E. J.; Neff, B. L.; Chu, H.; Panek, M. G., Cis-trans isomerizations of 1-lithio-1-phenyl-1-butene. Solvent effects on the rate of isomerization and on nuclear magnetic resonance spectra. *J. Am. Chem. Soc.* **1975,** *97*, 3996-4000.
22. Letsinger, R. L., Formation of optically active 1-methylheptyllithium. *J. Am. Chem. Soc.* **1950,** *72*, 4842-4842.
23. Applequist, D. E.; Peterson, A. H., The Configurational Stability of cis- and trans-2-Methylcyclopropyllithium and Some Observations on the Stereochemistry of their Reactions with Bromine and Carbon Dioxide *Journal of the American Chemical Society* **1961,** *83*, 862-865.
24. Curtin, D. Y.; Koehl Jr., W. J., Effect of solvent on the steric stability of lithium reagents. *J. Am. Chem. Soc.* **1962,** *84*, 1967-1973.
25. Kerrick, S. T.; Beak, P., Asymmetric deprotonations: enantioselective syntheses of 2-substituted tert-(butoxycarbonyl)pyrrolidines *J. Am. Chem. Soc.* **1991,** *113*, 9708-9710.
26. Gawley, R. E.; Hart, G.; Goicoechea-Pappas, M.; Smith, A. L., Oxazoline-mediated asymmetric alkylation of amines *J. Org. Chem.* **1986,** *51*, 3076-3078.
27. Gawley, R. E.; Hart, G. C.; Bartolotti, L. J., Chiral dipole-stabilized anions: Experiment and theory in nonbenzylic systems. 100% Stereoselective deprotonation and two-electron vs single-electron transfer in the chemistry of lithium and copper piperidinooxazolines. *J. Org. Chem.* **1989,** *54*, 175-181.
28. Pearson, W. H.; Lindbeck, A. C., Stereochemical studies on chiral, nonconjugated, nitrogen-substituted carbanions generated by tin-lithium exchange *J. Am. Chem. Soc.* **113,** *113*, 8546-8548.
29. Reich, H. J.; Medina, M. A.; Bowe, M. D., Stereochemistry of a cyclohexyllithium reagent. A case of higher configurational stability in strongly coordinating media *J. Am. Chem. Soc.* **1992,** *114*, 11003-11004.
30. Clark, T.; Schleyer, P. V. R., Proposal for the mechanism of inversion of

alkyl-lithium. *J. Chem. Soc., Chem. Commun.* **1978**, 137-138.
31. Reich, H. J.; Kulicke, K. J., Chelation effects in chiral organolithium reagents. *J. Am. Chem. Soc.* **1995,** *117*, 6621-6622.
32. Hoell, D.; Schnieders, C.; Müllen, K., 1-Lithio-1-phenylcyclopropanes - Structure and dynamics. *Angew. Chem., Int. Ed. Engl.* **1983,** *22*, 243-244.
33. Chong, J. M.; Park, S. B., Enantiomerically enriched tert-BOC-protected alpha-aminoorganolithiums: preparation and configurational stability. *J. Org. Chem.* **1992,** *57*, 2220-2222.
34. Wittig, G.; Pockels, U.; Dröge, H., Replaceability of aromatically bound hydrogen by lithium with the aid of phenyllithium. *Ber. Dtsch. Chem. Ges. B* **1938,** *71*, 1903-1912.
35. Negishi, E.; Swanson, D. R.; Rousset, C. J., Clean and convenient procedure for converting primary alkyl iodides and alpha, omega-diiodoalkanes into the corresponding alkyllithium derivatives by treatment with *tert*-butyllithium *J. Org. Chem.* **1990,** *55*, 5406-5409.
36. Basu, A.; Thayumanavan, S., Configurational stability and transfer of stereochemical information in the reactions of enantioenriched organolithium reagents. *Angew. Chem., Int. Ed. Engl.* **2002,** *41*, 716-738.
37. Beak, P.; Basu, A.; Gallagher, D. J.; Park, Y. S.; Thayumanavan, S., Regioselective, diastereoselective, and enantioselective lithiation-substitution sequences: Reaction pathways and synthetic applications. *Acc. Chem. Res.* **1996,** *29*, 552-560.
38. Linderman, R. J.; Ghannam, A., Synthetic utility and mechanistic studies of the aliphatic reverse Brook rearrangement *J. Am. Chem. Soc.* **1990,** *112*, 2392-2398.
39. Carstens, A.; Hoppe, D., Generation of a configurationally stable, enantioenriched α-oxy-α-methylbenzyllithium: Stereodivergence of its electrophilic substitution. *Tedrahedron* **1994,** *50*, 6097-6108.
40. Burchat, A. F.; Chong, J. M.; Park, S. B., Observations on Sn-Li exchange in α-aminoorganostannanes and the configurational stability of non-stabilized α-aminoorganolithiums. *Tetrahedron Lett.* **1993,** *34*, 51-54.
41. Park, Y. S.; Boys, M. L.; Beak, P., (-)-Sparteine-mediated -lithiation of *N*-Boc-*N*-(p-methoxyphenyl)benzylamine: Enantioselective syntheses of (*S*) and (*R*) mono- and disubstituted N-Boc-benzylamines. *J. Am. Chem. Soc.* **1996,** *118*, 3757-3758.
42. Kaiser, B.; Hoppe, D., Preparation and detection of enantiomerically enriched and configurationally stable alpha-thioalkyllithium compounds. *Angew. Chem., Int. Ed. Engl.* **1995,** *34*, 323-325.
43. Brickmann, K.; Brueckner, R., [2,3]-Thia-Wittig rearrangements proceeding with complete inversion or with partial loss of configuration at the carbanionic center. *Chem. Ber.* **1993,** *126*, 1227-1239.
44. Obrien, P.; Powell, H. R.; Raithby, P. R.; Warren, S., Investigation of the configurational stability of lithiated phosphine oxides using the Hoffmann test: X-ray structures of
(2S(*),3S(*),4R(*))2-(N,N-dibenzylamino)-4-diphenylphosphinoyl-1-phenylp entan-3-ol

and (2S(*),4S(*))-2-(N,N-dibenzylamino)-4-diphenylphinoyl-1-phenylpentan-3-o ne. *J. Chem. Soc., Perkin Trans. 1* **1997**, 1031-1039.
45. Still, W. C.; Sreekumar, C., alpha.-Alkoxyorganolithium reagents. A new class of configurationally stable carbanions for organic synthesis. *J. Am. Chem. Soc.* **1980,** *102*, 1201-1202.
46. Jephcote, V. J.; Pratt, A. J.; Thomas, E. J., Synthesis and absolute configuration of optically active E-1-alkoxymethoxy-but-2-eny(tri-n-butyl)stannanes: Stereoselective reactions with aldehydes. *J. Chem. Soc., Chem. Commun.* **1984**, 800-802.
47. Chan, P. C. M.; Chong, J. M., Asymmetric reduction of acylstannanes. Preparation of enantiomerically enriched alpha-alkoxystannanes. *J. Org. Chem.* **1988,** *53*, 5584-5586.
48. Chong, J. M.; Mar, E. K., An expeditious enantioselective synthesis of γ-lactones. *Tetrahedron Lett.* **1990,** *31*, 1981-1984.
49. Matteson, D. S.; Tripathy, P. B.; Sarkar, A.; Sadhu, K. M., A stereospecific convergent coupling of nucleophilic and electrophilic chiral carbons. *J. Am. Chem. Soc.* **1989,** *111*, 4399-4402.
50. Gawley, R. E.; Zhang, Q., 2-Lithio-N-methylpiperidine and 2-lithio-N-methylpyrrolidine: Configurationally and chemically stable unchelated .alpha.-aminoorganolithiums. *J. Am. Chem. Soc.* **1993,** *115*, 7515-7516.
51. Low, E.; Gawley, R. E., Solution structure of unstabilized cyclic -aminoorganolithiums by ^{13}C, ^{15}N, and ^{6}Li NMR spectroscopy. *J. Am. Chem. Soc.* **2000,** *122*, 9562-9563.
52. Hoffmann, R. W.; Koberstein, R., The stereochemistry of a retro-carbolithiation reaction. *J. Chem. Soc., Chem. Commun.* **1999**, 33-34.
53. Hoffmann, R. W.; Koberstein, R., Chiral organometallic reagents. Part XXV. The stereochemistry of the ring opening of cyclopropylallyllithium compounds. *J. Chem. Soc., Perkin Trans. 2* **2000**, 595-602.
54. Beak, P.; Reitz, D. B., Dipole-stabilized carbanions: Novel and useful intermediates. *Chem. Rev.* **1978,** *78*, 275-316.
55. Haeffner, F.; Brandt, P.; Gawley, R. E., A theoretical investigation into the inversion barrier of dipole-stabilized -aminoorganolithiums. *Org. Lett.* **2002,** *4*, 2101-2104.
56. Marr, F.; Fröhlich, R.; Hoppe, D., A Highly enantioenriched, configurationally stable α-thioallyllithium compound and the stereochemical course of its electrophilic alkylation. *Org. Lett.* **1999,** *1*, 2081-2083.
57. Gross, K. M. B.; Beak, P., Complex-induced proximity effects: The effect of varying directing-group orientation on carbamate-directed lithiation reactions. *J. Am. Chem. Soc.* **2001,** *123*, 315-321.
58. Gross, K. M. B.; Jun, Y. M.; Beak, P., Asymmetric deprotonations: Lithiation of N-(tert-butoxycarbonyl)indoline with sec-butyllithium/(-)-sparteine. *J. Org. Chem.* **1997,** *62*, 7679-7689.

59. Elworthy, T. R.; Meyers, A. I., The configurational stability of chiral lithio α-amino carbanions. The effect of Li-O vs. Li-N complexation. *Tetrahedron* **1994,** *50*, 6089-6096.
60. Hoffmann, R. W.; Ruehl, T.; Harbach, J., Chiral organometallic reagents. VIII. On the configurational stability of α-hetero-substituted benzyllithium compounds. *Liebigs Ann. Chem.* **1992**, 725-730.
61. Hoppe, D.; Carstens, A.; Krámer, T., Generation of a configurationally stable chiral benzyllithium derivative, and the capricious stereochemistry of its electrophilic substitution. *Angew. Chem., Int. Ed. Engl.* **1990,** *29*, 1424-1425.
62. Hammerschmidt, F.; Hanninger, A., Chiral carbanions. Part 1. Configurational stability and reactions of α-acyloxy-substituted a-methylbenzyllithium compounds. *Chem. Ber.* **1995,** *128*, 1069-1077.
63. Derwing, C.; Hoppe, D., Synthesis of enantioenriched tertiary benzylic alcohols via stereospecific lithiation of secondary benzyl carbamates - design of dialkylcarbamates, cleavable under basic, mild conditions. *Synthesis* **1996**.
64. Hammerschmidt, F.; Hanninger, A.; Völlenke, H., Proof of inversion of configuration on stannylation of a configurationally stable, tertiary benzyllithium compound from a single-crystal X-Ray structure analysis. *Chem. -Eur. J.* **1997,** *3*, 1728-1732.
65. Hammerschmidt, F.; Hanninger, A.; Simov, B. P.; Vollenkle, H.; Werner, A., Chiral carbanions, III - Configurational stability and stannylation of dipole-stabilised cyclic tertiary benzylic alpha-oxycarbanions, which occurs with retention or inversion configuration depending on R and X of R_3SnX used. *Eur. J. Org. Chem.* **1999**, 3511-3518.
66. Faibish, N. C.; Park, Y. S.; Lee, S.; Beak, P., A mechanistic and structural investigation of the (-)-sparteine mediated asymmetric benzylic lithiation substitution reactions of N-boc-N-(p-methoxyphenyl)benzylamine. *J. Am. Chem. Soc.* **1997,** *119*, 11561-11570.
67. Nakamura, S.; Nakagawa, R.; Watanabe, Y.; Toru, T., Enantioselective reactions of configurationally unstable α-thiobenzyllithium compounds. *Angew. Chem., Int. Ed. Engl.* **2000,** *39*, 353-355.
68. Nakamura, S.; Nakagawa, R.; Watanabe, Y.; Toru, T., Highly enantioselective reactions of configurationally labile -thioorganolithiums using chiral bis(oxazoline)s *via* two different enantiodetermining steps. *J. Am. Chem. Soc.* **2000,** *122*, 11340-11347.
69. Gawley, R. E.; Zhang, Q., Search for configurationally stable, aracemic α-amino organolithiums. *Tetrahedron* **1994,** *50*, 6077-6088.
70. Walborsky, H. M.; Hornyak, F. M., Cyclopropanes : The cyclopropyl carbanion. *J. Am. Chem. Soc.* **1955,** *77*, 6026-6029.
71. Walborsky, H. M.; Hornyak, F. M., Cyclopropanes. III. Rate of racemization of 2,2-diphenylcyclopropyl cyanide. *J. Am. Chem. Soc.* **1956,** *78*, 872-873.
72. Impastato, F. J.; Walborsky, H. M., Cyclopropanes. XIV. The Haller-bauer

cleavage reaction. *J. Am. Chem. Soc.* **1962,** *84*, 4838-4843.
73. Walborsky, H. M.; Impastato, F. J.; Young, A. E., Cyclopropanes. XV. The optical stability of 1-methyl-2,2-diphenylcyclopropyllithium. *J. Am. Chem. Soc.* **1964,** *86*, 3283-3288.
74. Periasamy, M. P.; Walborsky, H. M., Cyclopropanes. 39. The configurational stability of the 1-isocyano-2,2-diphenylcyclopropyl anion. *J. Am. Chem. Soc.* **1977,** *99*, 2631-2638.
75. Hopkinson, A. C.; McKinney, M. A.; Lien, M. H., A theoretical study of alpha-substituted isopropyl and cyclopropyl anions. *J. Comput. Chem.* **1983,** *4*, 513-523.
76. Newton, M. D.; Schulman, J. M., Theoretical studies of bicyclobutane. *J. Am. Chem. Soc.* **1972,** *94*, 767-773.
77. Walborsky, H. M., Cyclopropyl carbanion. *Record Chem. Progr. (Kresge-Hooker Sci. Lib.)* **1962,** *23*, 75-91.
78. Walborsky, H. M.; Motes, J. M., Cyclopropanes. XXV. The cyclopropyl anion. *J. Am. Chem. Soc.* **1970,** *92*, 2445-2450.
79. Grignard, V., Some new organometallic combinations of magnesium and their application to the synthesis of alcohols and hydrocarbons. *C. R. Hebd. Seances Acad. Sci. Ser.* **1900,** *130*, 1322.
80. Prevost, C., The action of alpha-ethylenic bromides on organomagnesium bromides-collected results. *Bull. Soc. Chim. Fr.* **1931,** *49*, 1372.
81. Urion, E., A functional exchange between [organic] magnesium compounds and halogen derivatives. *C. R. Hebd. Seances Acad. Sci. Ser.* **1934,** *198*, 1244-1246.
82. Ila, H.; Baron, O.; Wagner, A. J.; Knochel, P., Functionalized magnesium organometallics as versatile intermediates for the synthesis of polyfunctional heterocycles. *J. Chem. Soc., Chem. Commun.* **2006**, 583-593.
83. Abarbri, M.; Thibonnet, J.; Berillon, L.; Dehmel, F.; Rottlander, M.; Knochel, P., Preparation of new polyfunctional magnesiated heterocycles using a chlorine-, bromine-, or iodine-magnesium exchange. *J. Org. Chem.* **2000,** *65*, 4618-4634.
84. Rottländer, M.; Boymond, L.; Bérillon, L.; Leprêtre, A.; Varchi, G.; Avolio, S.; Laaziri, H.; Quéguiner, G.; Ricci, A.; Cahiez, G.; Knochel, P., New polyfunctional magnesium reagents for organic synthesis. *Chem. -Eur. J.* **2000,** *6*, 767-770.
85. Thibonnet, J.; Knochel, P., Preparation of functionalized alkenylmagnesium bromides via a bromine-magnesium exchange. *Tetrahedron Lett.* **2000,** *41*, 3319-3322.
86. Tamborski, C.; Moore, G. J., Synthesis of polyfluoroaromatic magnesium compounds through the exchange reaction. *J. Organomet. Chem.* **1971,** *26*, 153-156.
87. Smith, C. F.; Moore, G. J.; Tamborski, C., Synthesis and reactions of some pentabromophenyl organometallics. *J. Organomet. Chem.* **1972,** *42*, 257-265.
88. Burton, D. J.; Yang, Z.-Y., Fluorinated organometallics: Perfluoroalkyl and functionalized perfluoroalkyl organometallic reagents in organic synthesis. *Tetrahedron* **1992,** *48*, 189-275.
89. Chambers, R. D.; Musgrave, W. K. R.; Savory, J., Organometallic and metalloid

compounds made from heptafluoro-2-iodopropane, and their properties. *J. Chem. Soc.* **1962**, 1993-1999.
90. Mukaiyama, T.; Soai, K.; Sato, T.; Shimizu, H.; Suzuki, K., Enantioface-differentiating (asymmetric) addition of alkyllithium and dialkylmagnesium to aldehydes by using (2S,2'S)-2-hydroxymethyl-1-[(1-alkylpyrrolidin-2-yl)methyl]pyrrolidines as chiral ligands. *J. Am. Chem. Soc.* **1979,** *101*, 1455-1460.
91. Marko, I. E.; Chesney, A.; Hollinshead, D. M., Asymmetric grignard addition to aldéhydes. An example of inverse temperature dependence of enantiomeric excess. *Tetrahedron: Asymmetry* **1994,** *5*, 569-572.
92. Bailey, W. F.; Patricia, J. J., The mechanism of the lithium - halogen Interchange reaction : A review of the literature. *J. Organomet. Chem.* **1988,** *352*, 1-46.
93. Ward, H. R.; Lawler, R. G.; Cooper, R. A., Chemically induced dynamic nuclear polarization evidence for one-electron transfers during some halogen-metal exchange reactions. *J. Am. Chem. Soc.* **1969,** *91*, 746-748.
94. Lepley, A. R.; Landau, R. L., Free radical iodide-lithium interchange *J. Am. Chem. Soc.* **1969,** *91*, 748-749.
95. Ashby, E. C.; Pham, T. N., Single electron transfer in metal halogen exchange. The reaction of organolithium compounds with alkyl halides. *J. Org. Chem.* **1987,** *52*, 1291-1300.
96. Villiéras, J., Preparation and properties of gem-halogenated Gringnard reagents. *Bull. Soc. Chim. Fr.* **1967**, 1520-1532.
97. Wittig, G.; Schöllkopf, U., Zum chemismus der halogen-lithium-austauschreaktion. *Tetrahedron* **1958,** *3*, 91-93.
98. Sunthankar, S. V.; Gilman, H., Halogen-metal interconversion and metalation in the naphthalene series. *J. Org. Chem.* **1951,** *16*.
99. Farnham, W. B.; Calabrese, J. C., Novel hypervalent (10-I-2) iodine structures *J. Am. Chem. Soc.* **1986,** *108*, 2449-2451.
100. Müller, M.; Stiasny, H.-C.; Brönstrup, M.; Burton, A.; Hoffmann, R. W., Chiral organometallic reagents. Part XXIV.1 Iodine ate-complexes as intermediates in the iodine–lithium exchange reaction on 1,1-diiodoalkanes. *J. Chem. Soc., Perkin Trans. 2* **1999**, 731-736.
101. Reich, H. J.; Bevan, M. J.; Gudmundsson, B. Ö.; Puckett, C. L., Are ate complexes true intermediates in lithium-metalloid exchange? Subtle effects of ion-pair structure in lithium-tellurium and lithium-selenium exchange reactions. *Angew. Chem., Int. Ed. Engl.* **2002,** *41*, 3436-3439.
102. Hoffmann, R. W.; Bronstrup, M.; Muller, M., The second step of the halogen/metal exchange reaction. *Org. Lett.* **2003,** *5*, 313-316.
103. Müller, M.; Brönstrup, M.; Knopff, O.; Schulze, V.; Hoffmann, R. W., Energetics of iodine ate complexes, Intermediates in the iodine/magnesium exchange on 1,1-diiodoalkanes. *Organometallics* **2003,** *22*, 2931-2937.

104. Schulze, V.; Bronstrup, M.; Bohm, V. P. W.; Schwerdtfeger, P.; Schimeczek, M.; Hoffmann, R. W., alpha-Iodoalkyl-iodine ate complexes as observable intermediates in the iodine magnesium exchange reaction. *Angew. Chem., Int. Ed. Engl.* **1998,** *37*, 824-826.
105. Böhm, V. P. W.; Schulze, V.; Brönstrup, M.; Müller, M.; Hoffmann, R. W., Evidence for an iodine ate complex as an observable intermediate in the iodine/magnesium exchange on 1,1-diiodoalkane. *Organometallics* **2003,** *22*, 2925-2930.
106. Knochel, P.; Dohle, W.; Gommermann, N.; Kneisel, F. F.; Kopp, F.; Korn, T.; Sapountzis, I.; Vu, V. A., Highly functionalized organomagnesium reagents prepared through halogen-metal exchange. *Angew. Chem., Int. Ed. Engl.* **2003,** *42*, 4302-4320.
107. Yoshino, T.; Manabe, Y., Solvent effect on cis-trans isomerization in Grignard reagent formation from β-bromostyrenes. *J. Am. Chem. Soc.* **1963,** *85*, 2860-2861.
108. Whitesides, G. M.; Witanowski, M.; Roberts, J. D., Magnetic resonance spectroscopy. The configurational stability of primary Grignard reagents. 3,3-Dimethylbutylmagnesium chloride. *J. Am. Chem. Soc.* **1965,** *87*, 2854-2862.
109. Whitesides, G. M.; Roberts, J. D., Nuclear magnetic resonance spectroscopy. The configurational stability of primary Grignard reagents. Structure and medium effects. *J. Am. Chem. Soc.* **1965,** *87*, 4878-4888.
110. Walborsky, H. M.; Young, A. E., Cyclopropanes. XVI. An optically active Grignard reagent and the mechanism of Grignard formation. *J. Am. Chem. Soc.* **1964,** *86*, 3288-3296.
111. Jensen, F. R.; Nakamaye, K. L., Preparation of geometrically isomeric Grignard reagents and the stereochemical courses of their reactions. *J. Am. Chem. Soc.* **1966,** *88*, 3437-3438.
112. Schulze, V.; Hoffmann, R. W., Discrimination of enantiotopic iodine atoms by an iodine/magnesium exchange reaction. *Chem. -Eur. J.* **1999,** *5*, 337-344.
113. Hoffmann, R. W.; Nell, P. G., alpha-Chloroalkylmagnesium reagents of >90 % ee by sulfoxide/magnesium exchange. *Angew. Chem., Int. Ed. Engl.* **1999,** *38*, 338-340.
114. Hoffmann, R. W.; Hölzer, B.; Knopff, O.; Harms, K., Asymmetric synthesis of a chiral secondary Grignard reagent. *Angew. Chem., Int. Ed. Engl.* **2000,** *39*, 3072-3074.
115. Hoffmann, R. W.; Nell, P. G.; Leo, R.; Harms, K., Chiral organometallic reagents, Part 26: Highly enantimerically enriched α-haloalkyl Grignard reagents. *Chem. -Eur. J.* **2000,** *6*, 3359-3365.
116. Charreau, P.; Julia, M.; Verpeaux, J.-N., A convenient preparation of mono- or gem-di-halogenoalkenes from α-sulfonyl carbanions and halogenolithiocarbenoïds. *J. Organomet. Chem.* **1989,** *379*, 201-210.
117. Satoh, T.; Takano, K.; Ota, H.; Someya, H.; Matsuda, K.; Koyama, M., Magnesium alkylidene carbenoids: Generation from 1-halovinyl sulfoxides with Grignard reagents and studies on their property, mechanism, and some synthetic uses. *Tetrahedron* **1998,** *54*, 5557-5574.
118. Ashby, E. C.; Laemmle, J.; Neumann, H. M., Mechanisms of Grignard reagent

addition to ketones *Acc. Chem. Res.* **1974,** *7*, 272-280.
119. Griller, D.; Ingold, K. U.; Krusic, P. J.; Fischer, H., Configuration of the tert-butyl radical *J. Am. Chem. Soc.* **1978,** *100*, 6750-6752.
120. Hoffmann, R. W.; Holzer, B., Concerted and stepwise Grignard additions, probed with a chiral Grignard reagent. *J. Chem. Soc., Chem. Commun.* **2001**, 491-492.
121. Holzer, B.; Hoffmann, R. W., Kumada-Corriu coupling of Grignard reagents, probed with a chiral Grignard reagent. *J. Chem. Soc., Chem. Commun.* **2003**, 732-733.
122. Hoffmann, R. W.; Holzer, B.; Knopff, O., Amination of Grignard reagents with retention of configuration. *Org. Lett.* **2001,** *3*, 1945-1948.
123. Hoffmann, R. W., The quest for chiral Grignard reagents. *Chem. Soc. Rev.* **2003,** *32*, 225-230.
124. Gawley, R. E., A proposal for (slight) modification of the hughes-ingold mechanistic descriptors for substitution reactions. *Tetrahedron Lett.* **1999,** *40*, 4297-4300.
125. Nagle, D. G.; Gerwick, W. H., Structure and stereochemistry of constanolactones A-G, lactonized cyclopropyl oxylipins from the red marine alga Constantinea simplex. *J. Org. Chem.* **1994,** *59*, 7227-7237.
126. Seo, Y.; Cho, K. W.; Rho, J.-R.; Shin, J.; Kwon, B.-M.; Bok, S.-H.; Song, J.-I., Solandelactones A-I, lactonized cyclopropyl oxylipins isolated from the hydroid Solanderia secunda. *Tetrahedron* **1996,** *52*, 10583-10596.
127. Niwa, H.; Wakamatsu, K.; Yamada, K., Halicholactone and neohalicholactone, two novel fatty acid metabolites from the marine sponge Halichondria okadai Kadota. *Tetrahedron Lett.* **1989,** *30*, 4543-4546.
128. Pelish, H. E.; Peterson, J. R.; Salvarezza, S. B.; Rodriguez-Boulan, E.; Chen, J.-L.; Stamnes, M.; Macia, E.; Feng, Y.; Shair, M. D.; Kirchhausen, T., Secramine inhibits Cdc42-dependent functions in cells and Cdc42 activation *in vitro*. *Nat. Chem. Biol.* **2006,** *2*, 39-46.
129. Arseniyadis, S.; Kyler, K.; Watt, D. S., Addition and substitution reactions of nitrile-stabilized carbanions. *Org. React.* **1984,** *31*, 1-364.
130. Carlier, P. R.; Lo, K. M.; Lo, M. M.-C.; Williams, I. D., Anti-selective aldol reaction of benzylic nitriles and synthesis of gamma-amino alcohols. *J. Org. Chem.* **1995,** *60*, 7511-7517.
131. Davies, H. M. L.; Antoulinakis, E. G., Intermolecular metal-catalyzed carbenoid. *Org. React.* **2001,** *57*, 1-326.
132. Doyle, M. P.; McKervey, M. A.; Ye, T., *Modern Catalytic Methods for Organic Synthesis with Diazo Compounds : From Cyclopropanes to Ylides*. Wiley & Sons: New York, 1998.
133. Dowd, P.; Kaufman, C.; Paik, Y. H., Protected ester, nitrile, carbinol and carbinyl amine cyclopropanone hydrates. *Tetrahedron Lett.* **1985,** *26*, 2283-2286.
134. Felpin, F.-X.; Doris, E.; Wagner, A.; Valleix, A.; Rousseau, B.; Mioskowsk, C., Rearrangement of α-amino cyclopropanone hydrate: A novel route to labeled amino acids. *J. Org. Chem.* **2001,** *66*, 305-308.

135. Jacobsen, E. N.; Pfaltz, A.; Yamamoto, H., *Comprehensive Asymmetric Catalysis*. Springer-Verlag: Berlin: New York, 1999; Vol. II.
136. Moser, W. R., The mechanism of copper-catalyzed addition of diazoalkanes to olefins. I. Steric effects. *J. Am. Chem. Soc.* **1969,** *91*, 1135-1140.
137. Salomon, R. G.; Kochi, J. K., Copper(I) catalysis in cyclopropanations with diazo compounds. The role of olefin coordination. *J. Am. Chem. Soc.* **1973,** *95*, 3300-3310.
138. Evans, D. A.; Woerpel, K. A.; Hinman, M. M.; Faul, M. M., Bis(oxazo1ines) as chiral ligands in metal-catalyzed asymmetric reactions. Catalytic, asymmetric cyclopropanation of olefins. *J. Am. Chem. Soc.* **1991,** *113*, 726-728.
139. Evans, D. A.; Woerpel, K. A.; Scott, M. J., Bis(oxazolines) as Ligands for Self-Assembling Chiral Coordination Polymers - Structure of a Copper(I) Catalyst for the Enantioselective Cyclopropanation of Olefins. *Angew. Chem., Int. Ed. Engl.* **1992,** *31*, 430-432.
140. Westwell, A. D.; Williams, J. M. J., Auxiliary accelerated reactions: Towards the use of catalytic chiral auxiliaries. *Tetrahedron* **1997,** *53*, 13063-13078.
141. Granoth, I.; Segall, Y.; Leader, H.; Alkabets, R., Chemical consequences of hydride addition to aromatic olefins. *J. Org. Chem.* **1976,** *41*, 3682-3687.
142. Gutman, A. L.; Zuobi, K.; Bravdo, T., Lipase-catalyzed preparation of optically active γ-butyrolactones in organic solvents. *J. Org. Chem.* **1990,** *55*, 3546-3552.
143. Qiu, W.; Burton, D. J., Preparation of fluorinated 1,2- and α,ω-diols. *J. Org. Chem.* **1993,** *58*, 419-423.
144. Fraile, J. M.; Garcia, J. I.; Martinez-Merino, V.; Mayoral, J. A.; Salvatella, L., Theoretical (DFT) insights into the mechanism of copper-catalyzed cyclopropanation reactions. Implications for enantioselective catalysis. *J. Am. Chem. Soc.* **2001,** *123*, 7616-7625.
145. Motes, J. M.; Walborsky, H. M., Cyclopropane XXVII. The cyclopropyl anion. *J. Am. Chem. Soc.* **1969,** *91*, 3697-3699.
146. Reich, H. J.; Dykstra, R. R., Structure effects of ion pair separation: planar and pyramidal sulfur and silicon substituted carbanions. *J. Am. Chem. Soc.* **1993,** *115*, 7041-7042.
147. Carlier, P. R.; Lucht, B. L.; Collum, D. B., $^{6}Li/^{15}N$ NMR-based solution structural determination of Et_2O- and TMEDA-solvated lithio-phenylacetonitrile and a LiHMDS mixed aggregate. *J. Am. Chem. Soc.* **1994,** *116*, 11602-11603.
148. Carlier, P. R.; Lo, C. W. S., $^{7}Li/^{31}P$ NMR studies of lithiated arylacetonitriles in THF-HMPA solution: characterization of HMPA-solvated monomers, dimers and separated ion pairs. *J. Am. Chem. Soc.* **2000,** *122*, 12819-12823.
149. Carlier, P. R., Configurational stability of chiral lithiated cyclopropylnitriles: A density functional study. *Chirality* **2003,** *15*, 340-347.
150. Boche, G.; Langlotz, I.; Marsch, M.; Harms, K.; Frenking, G., [*tert*-Butylcyanide-lithium bis(trimethylsilyl)-amide]$_2$, a model of the intermediate RCN-MR' complex formed in reactions of cynaides RCN with organometallic

compounds R'M. *Angew. Chem., Int. Ed. Engl.* **1993,** *32*, 1171-1173.
151. Koch, R.; Wiedel, B.; Anders, E., Theoretical study of the deprotonation of nitriles, RCH_2CN: Ab initio and PM3 calculations of intermediate aggregates and transition states. *J. Org. Chem.* **1996,** *61*, 2523-2529.
152. Pearson, W. H.; Lindbeck, A. C.; Kampf, J. W., Configurational stability of chiral, nonconjugated nitrogen-substituted organolithium compounds generated by tin-lithium exchange of N-[(1-tri-N-butylstannyl)alkyl]imidazolidin-2-ones and N-[(1-tri-N-butylstannyl)alkyl]oxazolidin-2-ones. *J. Am. Chem. Soc.* **1993,** *115*, 2622-2636.
153. Tomasi, J.; Cammi, R.; Mennucci, B.; Cappelli, C.; Corni, S., Molecular properties in solution described with a continuum solvation model. *Phys. Chem. Chem. Phys.* **2002,** *4*, 5697-5712.
154. Fleming, F. F.; Zhang, Z.; Knochel, P., Metalated nitriles: Halogen-metal exchange with α-halonitriles. *Org. Lett.* **2004,** *6*, 501-503.
155. Fleming, F. F.; Zhang, Z.; Wei, G.; Steward, O. W., Metalated nitriles: Electrophile-dependant alkylations. *Org. Lett.* **2005,** *7*, 447-449.
156. Maruyama, K.; Imahori, H., [2 + 4] Photocyclization between quinones and allenes via photoinduced electron transfer. *J. Org. Chem.* **1989,** *54*, 2692-2702.
157. Baird, M. S.; Nizovtsev, A. V.; Bolesov, I. G., Bromine-magnesium exchange in *gem*-dibromocyclopropanes using Grignard reagents. *Tetrahedron* **2002,** *58*, 1581-1593.
158. Friebolin, H., *Basic One-and Two-Dimensional NMR Spectroscopy.* 4 ed.; Wiley-VCH: Weinheim, 2005.
159. Corey, E. J.; Beames, D. J., Mixed cuprate reagents of type R_1R_2CuLi which allow selective group transfer. *J. Am. Chem. Soc.* **1972,** *94*, 7210-7211.
160. Seebach, D.; Neumann, H., Bromine-lithium exchange in vinyl and aryl bromides with tert-butylithium. Ring enlargement via dibromocarbene adducts. *Chem. Ber.* **1974,** *107*, 847-853.
161. Zefirov, N. S.; Makhon'kov, D. I., X-philic reactions. *Chem. Rev.* **1982,** *82*, 615-624.
162. Bryce-Smith, D., Organometallic compounds of the alkali metals. VI. Evidence for the formation of free alkyl radicals during certain Wurtz reactions. Homolytic reactions between alkyllithium compounds and alkyl halides. *J. Chem. Soc.* **1956**, 1603-1610.
163. Lien, M. H.; Hopkinson, A. C., A theoretical study of α-substituted cyclopropyl and isopropyl radicals. *J. Comput. Chem.* **1985,** *6*, 274.
164. Baron, W. J.; Henrick, M. E.; Maitland Jones, J., Reactions of diphenylcarbene with alkenes, alkynes, and alkenynes. *J. Am. Chem. Soc.* **1973,** *95*, 6286-6294.
165. Jończyk, A.; Włostowska, J.; Mąkosza, M., Reactions of tosylhydrazones of benzaldehyde and benzophenone with cyanoalkenes in a basic two-phase system. *Tetrahedron* **2001,** *57*, 2827-2832.
166. Carlier, P. R.; Lam, P. C.-H.; DeGuzman, J. C.; Zhao, H., Memory of chirality

trapping of low inversion barrier 1,4-benzodiazepin-2-one enolates. *Tetrahedron: Asymmetry* **2005,** *16*, 2998-3002.
167. Kemp, J. D.; Pitzer, K. S., Hindered rotation of the methyl groups in ethane. *J. Chem. Phys.* **1936,** *4*, 749-750.
168. Pitzer, K. S., Potential energies for rotation about single bonds. *Discuss. Farady Soc.* **1951**, 66-73.
169. Weiss, S.; Leroi, G. E., Direct observation of the infrared torsional spectrum of C_2H_6, CH_3CD_3, and C_2D_6. *J. Chem. Phys.* **1968,** *48*, 962-967.
170. Hirota, E.; Saito, S.; Endo, Y., Barrier to internal rotation in ethane from the microwave spectrum of CH_3CHD_2. *J. Chem. Phys.* **1979,** *71*, 1183-1187.
171. Moazzen-Ahmadi, N.; Gush, H. P.; Halpern, M.; Jagannath, H.; Leung, A.; Ozier, I., The torsional spectrum of CH_3CH_3. *J. Chem. Phys.* **1988,** *88*, 563-577.
172. Lee, J. S., Accurate theoretical prediction of relative energy: Barriers to linearity, inversion, and internal rotation in polyatomic molecules. *J. Phys. Chem. A* **1997,** *101*, 8762-8767.
173. Császár, A. G.; Allen, W. D.; Schaefer III, H. F., In pursuit of the ab initio limit for conformational energy prototypes. *J. Chem. Phys.* **1998,** *108*, 9751-9764.
174. Lassettre, E. N.; Laurence B. Dean, J., An electrostatic theory of the potential barriers hindering rotation around single bonds. *J. Chem. Phys.* **1949,** *17*, 317-332.
175. Reed, A. E.; Weinhold, F., Some remarks on the C-H bond dipole moment. *J. Chem. Phys.* **1986,** *84*, 2428-2430.
176. Pophristic, V.; Goodman, L., Hyperconjugation not steric repulsion leads to the staggered structure of ethane. *Nature* **2001,** *411*, 565-568.
177. Bickelhaupt, F. M.; Baerends, E. J., The case for steric repulsion causing the staggered conformation of ethane. *Angew. Chem., Int. Ed. Engl.* **2003,** *42*, 4183-4188.
178. Sadlej-Sosnowska, N., Energy barriers to internal rotation: Hyperconjugation and electrostatic description. *J. Phys. Chem. A* **2003,** *107*, 8671-8676.
179. Sovers, O. J.; Kern, C. W.; Pitzer, R. M.; Karplus, M., Bond-function analysis of rotational barriers: ethane. *J. Chem. Phys.* **1968,** *49*, 2592-2599.
180. Pitser, R. M., The barrier to internal rotation in ethane. *Acc. Chem. Res.* **1983,** *16*, 207-210.
181. Weinhold, F., A new twist on molecular shape. *Nature* **2001,** *411*, 539-541.
182. Weinhold, F., Rebuttal to the Bickelbaupt-Baerends case for steric repulsion causing the staggered conformation of ethane. *Angew. Chem., Int. Ed. Engl.* **2003,** *42*, 4188-4194.
183. Pitzer, K. S., The vibration frequencies and thermodynamic functions of long chain hydrocarbons. *J. Chem. Phys.* **1940,** *8*, 711-720.
184. Rosenthal, L., An inverstigation of the conformational equilibrium of *n*-butane in a solvent using Raman spectroscopy. *J. Chem. Phys.* **1982,** *76*, 817-820.
185. Compton, D. A. C.; Montero, S.; Murphy, W. F., Low-frequency raman spectrum and asymmetric potential function for internal rotation of gaseous n-butane. *J. Phys.*

Chem. **1980,** *84*, 3587-3591.
186. Woller, P. B.; Edgar W. Garbisch, J., The conformational analysis of *n*-butane. *J. Am. Chem. Soc.* **1972,** *94*, 5310-5314.
187. Piercy, J. E.; Rao, M. G. S., Ultrasonic relaxation due to trans—gauche rotational isomerism in the liquid normal paraffins. *J. Chem. Phys.* **1967,** *46*, 3951-3959.
188. Bonham, R. A.; Bartell, L. S., The molecular structure and rotational isomerization of n-butane. *J. Am. Chem. Soc.* **1959,** *81*, 3491-3496.
189. Wiberg, K. B.; Murcko, M. A., Rotational barriers. 2. Energies of alkane rotamers. An examination of gauche interactions. *J. Am. Chem. Soc.* **1988,** *110*, 8029-8038.
190. Allinger, N. L.; Grev, R. S.; Yates, B. F.; Henry F. Schaefer, I., The *syn* rotational barrier in butane. *J. Am. Chem. Soc.* **1990,** *112*, 114-118.
191. Allinger, N. L.; Fermann, J. T.; Allen, W. D.; Schaefer, H. F., The torsional conformations of butane: Definitive energetics from ab initio methods. *J. Chem. Phys.* **1997,** *106*, 5143-5150.
192. Schreiner, P. R., Teaching the right reasons: Lessons from the mistaken origin of the rotational barrier in ethane. *Angew. Chem., Int. Ed. Engl.* **2002,** *41*, 3579-3581.
193. Boyd, R. H., Molecular structures and thermodynamic functions of 2-methylbutane and 2,3-dimethylbutane. *J. Am. Chem. Soc.* **1975,** *97*, 5353-5357.
194. Rüchardt, C.; Beckhaus, H.-D., Towards an understanding of the carbon-carbon bond. *Angew. Chem., Int. Ed. Engl.* **1980,** *19*, 429-440.
195. Abraham, R. J.; Bretschneider, E., Medium effects on rotational and conformational equilibria. In *Internal Rotation in Molecules*, Orville-Thomas, W. J., Ed. Wiely: New York, 1974.
196. Abraham, R. J.; Parry, K., A calculation of the rotamer energies of halogenoethanes. *J. Chem. Soc., Chem. Commun.* **1969**, 963-964.
197. Huang, J.; Hedberg, K., Conformational analysis. 14. The dihaloethanes $ClCH_2CH_2F$, $BrCH_2CH_2F$, and $BrCH_2CH_2Cl$. Investigations of the molecular structures, rotameric compositions, anti and gauche energy and entropy differences, and barriers hindering internal rotation by gas-phase electron diffraction augmented by rotational constants and ab initio calculation. *J. Am. Chem. Soc.* **1990,** *112*, 2070-2075.
198. Došen-Mićović, L.; Jeremić, D.; Allinger, N. L., Treatment of electrostatic effects within the molecular-mechanics method. 2. *J. Am. Chem. Soc.* **1983,** *105*, 1723-1733.
199. Chuang, Y.-Y.; Truhlar, D. G., Statistical thermodynamics of bond torsional modes. *J. Chem. Phys.* **2000,** *112*, 1221-1228.
200. Durig, J. R.; Liu, J.; Little, T. S., Conformational analysis, barriers to internal rotation, *ab initio* calculations, and vibratinal assignment of 1-chloro-2-fluoroethane. *J. Phys. Chem.* **1991,** *95*, 4664-4672.
201. Abraham, R. J.; Kemp, R. H., Rotational isomerism. Part XI. The nuclear magnetic resonance spectra and rotational isomerism of 1,2-difluoro- and 1,1,2-trifluoroethane. *J. Chem. Soc. B* **1971**, 1240-1245.
202. Hirano, T.; Nonoyama, S.; Miyajima, T.; Kurita, Y.; Kawamura, T.; Sato, H.,

Gas-phase ^{19}F and ^{1}H high-resolution n.m.r. spectroscopy: application to the study of unperturbed conformational energies of 1,2-difluoroethane. *J. Chem. Soc., Chem. Commun.* **1986**, 606-607.
203. Durig, J. R.; Liu, J.; Little, T. S., Conformational anaylsis, barriers to internal rotation, vibrational assignment, and *ab initio* calculations of 1,2-difuoroethane. *J. Phys. Chem.* **1992,** *96*, 8224-8233.
204. Wolfe, S., Gauche effect. Stereochemical consequences of adjacent electron pairs and polar bonds *Acc. Chem. Res.* **1972,** *5*, 102-111.
205. Rablen, P. R.; Hoffmann, R. W.; Hrovat, D. A.; Borden, W. T., Is hyperconjugation responsible for the "*gauche* effect" in 1-fluoropropane and other 2-substituted-1-fluoroethanes? *J. Chem. Soc., Perkin Trans. 2* **1999**.
206. Radom, L.; Lathan, W. A.; Hehre, W. J.; Pople, J. A., Molecular orbital theory of the electronic structure of organic compounds. XVII Internal rotation in 1,2-disubstituted ethanes. *J. Am. Chem. Soc.* **1973,** *95*, 693-698.
207. Allinger, N. L.; Chang, S. H. M., Conformational analysis—CXXIII : Carboxylic acids and esters in force field calculations. *Tetrahedron* **1977,** *33*, 1561-1567.
208. Wiberg, K. B.; Murcko, M. A.; Laidig, K. E.; MacDougall, P. J., Origin of the "gauche effect" in substituted ethanes and ethenes. *J. Phys. Chem.* **1990,** *94*, 6956-6959.
209. Park, P. J. D.; Pethrick, R. A.; Thomas, B. N., Infrared and raman band intensities and conformational change. In *Internal Rotation in Molecules*, Orville-Thomas, W. J., Ed. Wiley-Interscience: New York, 1974.
210. Matsuura, H.; Miyauchi, N.; Murata, H.; Sakakibara, M., Vibrational spectra and rotational isomerism of 2-chloro- and 2-bromoethyl methyl sulfides. *Bull. Chem. Soc. Jpn.* **1979,** *52*, 344-350.
211. Canceill, J.; Basselier, J. J.; Jacques, J., Stereochemistry of the Reformatskii reaction. II. Ir and N.M.R. spectra of β-hydroxy esters formed. Determination of their mixtures. Results. *Bull. Soc. Chim. Fr.* **1967**, 1024-1030.
212. Canceill, J.; Jacques, J., Stereochemistry of the reduction of β-keto esters, β-keto amides, and β-keto nitriles by hydrides. *Bull. Soc. Chim. Fr.* **1970**, 2180-2187.
213. Tsuzuki, S.; Schafer, L.; Gotb, H. i.; luvathingal, E.; Jemmis, D.; Hosoya, H.; Siam, K.; Tanabe, K.; Ösawa, E., Investigation of intramolecular interactions in *n*-alkanes. Cooperative energy increments associated with GG and GTG' sequences. *J. Am. Chem. Soc.* **1991,** *113*, 4665-4671.
214. Mirkin, N. G.; Krimm, S., Ab initio studies of the conformation dependence of the spectra of stable conformers of n-pentane and n-hexane. *J. Phys. Chem.* **1993,** *97*, 13887-13895.
215. Hoffmann, R. W., Flexible molecules with defined shape-conformational design. *Angew. Chem., Int. Ed. Engl.* **1992,** *31*, 1124-1134.
216. Eliel, E. L.; Wilen, S. H.; Mander, L. N., *Stereochemistry of Organic Compounds.* 1 ed.; Wiley: New York, 1994.
217. Lowe, J. P., Barriers to internal rotation about single bonds. *Prog. Phys. Org.*

Chem. **1968,** *6*, 1-80.
218. Wiberg, K. B.; Martin, E., Barriers to rotation adjacent to double bonds. *J. Am. Chem. Soc.* **1985,** *107*, 5035-5041.
219. Hemelrijk, D. V.; Enden, L. V. d.; Geise, H. J.; Sellers, H. L.; Schaefer, L., Structure determination of 1-butene by gas electron diffraction, microwave spectroscopy, molecular mechanics, and molecular orbital constrained electron diffraction. *J. Am. Chem. Soc.* **1980,** *102*, 2189-2195.
220. Durig, J. R.; Compton, D. A. C., Spectroscopic and thermodynamic study of the conformational properties and torsional potential functions of 1-butene. *J. Phys. Chem.* **1980,** *84*, 773-781.
221. Karabatsos, G. J.; Fenoglio, D. J., Rotational isomerism about sp^2-sp^3 carbon-carbon single bonds. In *Top. Stereochem.*, Eliel, E. L.; Allinger, N. L., Eds. Wiley-Interscience: New York, 1970; Vol. 5, p 167.
222. Smith, G. D.; Paul, W., United atom force field for molecular dynamics simulations of 1,4-polybutadiene based on quantum chemistry calculations on model molecules. *J. Phys. Chem. A* **1998,** *102*, 1200-1208.
223. Broeker, J. L.; Hoffmann, R. W.; Houk, K. N., Conformational analysis of chiral alkenes and oxonium ions:Ab initio molecular orbital calculations and an improved MM2 force field. *J. Am. Chem. Soc.* **1991,** *113*, 5006-5017.
224. Hruby, V. J., Design in topographical space of peptide and peptidomimetic ligands that affect behavior. A chemist's glimpse at the mind-body problem. *Acc. Chem. Res.* **2001,** *34*, 389-397.
225. Hruby, V. J.; Li, G.; Haskell-Luevano, C.; Shenderovich, M., Design of peptides, proteins, and peptidomimetics in Chi space. *Biopolymers* **1997,** *43*, 219-266.
226. Jiao, D.; Russell, K. C.; Hruby, V. J., Locally constrained tyrosine analogues with restricted side chain dynamics. *Tetrahedron* **1993,** *49*, 3511-3520.
227. Qian, X.; Shenderovich, M. D.; Kövér, K. E.; Davis, P.; Horváth, R.; Zalewska, T.; Yamamura, H. I.; Porreca, F.; Hruby, V. J., Probing the stereochemical requirements for receptor recognition of δ opioid agonists through topographic modifications in position 1. *J. Am. Chem. Soc.* **1996,** *118*, 7280-7290.
228. Liao, S.; Shenderovich, M. D.; Zhang, Z.; Maletinska, L.; Slaninova, J.; Hruby, V. J., Substitution fo the side-chain-constrained amino acids β–methyl-2',6'-dimethyl-4'-methoxytyrosine in position 2 of a bicyclic oxytocin analogues provides unique insights into the bioactive topography of oxytocin antagonists. *J. Am. Chem. Soc.* **1998,** *120*, 7393-7394.
229. Carlier, P. R.; Lo, C. W.-S.; Lo, M. M.-C.; Wan, N. C.; Williams, I. D., HMPA promotes retro-aldol reaction, resulting in *syn*-selective addition of lithiated 1-naphthylacetonitrile to aromatic aldehydes *Org. Lett.* **2000,** *2*, 2443-2445.
230. Masamune, S.; Ali, S. A.; Snitman, D. L.; Garvey, D. S., Highly stereoselective aldol condensation using an enantioselective chiral enolate. *Angew. Chem., Int. Ed. Engl.* **1980,** *19*, 557-558.

231. Nakamura, S.; Ito, Y.; Wang, L.; Toru, T., Enantioselective reaction of α-lithiated dithioacetals using chiral bis(oxazoline)s: New chiral formyl anion equivalents. *J. Org. Chem.* **2004,** *69*, 1581-1589.
232. Eichin, K. H.; Beckhaus, H. D.; Hellmann, S.; Fritz, H.; Peters, E. M.; Peters, K.; Von Schnering, H. G.; Rüechardt, C., Thermolabile hydrocarbons. XVIII. 1-Substituted neopentyl radicals and their dimers. *Chem. Ber.* **1983,** *116*, 1787-1821.
233. Postma, H. J.; Van Bolhuis, F., Crystal structure of s-tetramesitylethane (TME). . *Acta Crystallogr., Sect. B: Struct. Sci.* **1975,** *B31*, 1792.
234. Korenaga, T.; Tanaka, H.; Ema, T.; Sakai, T., Intermolecular oxygen atom ....π interaction in the crystal packing of chiral amino alcohol bearing a pentafluorophenyl group. *J. Fluorine Chem.* **2003,** *122*, 201-205.
235. Liu, X.; Zhao, J.; Jin, G.; Zhao, G.; Zhu, S.; Wang, S., An unexpected highly diastereoselective double Baylis–Hillman reaction of per- (or poly)fluorophenyl aromatic aldimines with methyl vinyl ketone *Tetrahedron* **2005,** *61*, 3841-3851.
236. Sakai, T.; Kubo, K.; Kashino, S.; Uneyama, K., Synthesis of enantiomerically pure (1R,2S)- and (1S,2R)-2-Amino-1,2-bis(pentafluorophenyl)ethanols *Tetrahedron: Asymmetry* **1996,** *7*, 1883-1886.
237. Schindler, W.; Knoch, F.; Kisch, H., Heterogeneous photocatalysis. Part XIV. Semiconductor-catalyzed photoaddition. γ,δ-Unsaturated amines from cyclopentene and Schiff bases. *Chem. Ber.* **1996,** *129*, 925-932.
238. Siriwardane, U.; Crenshaw, L.; Khanapure, S. P.; Biehl, E. R., Structure of anti-2-(2-cyano-3-methoxy-6-methylphenyl)-1,2-diphenyl-1-ethanol. *Acta Crystallogr., Sect. C: Cryst. Struct. Commun.* **1989,** *C45*, 1463-1465.
239. Liao, S.; Han, Y.; Qui, W.; Bruck, M.; Hruby, V. J., Syntheses of highly constrained β-aryl isohexanoic acid derivatives via asymmetric Michael addition. *Tetrahedron Lett.* **1996,** *37*, 7917-7920.
240. Han, Y.; Liao, S.; Qiu, W.; Cai, C.; Hruby, V. J., Total asymmetric synthesis of highly constrained amino acids β-isopropyl-2′,6′-dimethyl-tyrosines. *Tetrahedron Lett.* **1997,** *38*, 5135-5138.
241. Clive, D. L. J.; Yu, M.; Sannigrahi, M., Synthesis of optically pure (+)-puraquinonic acid and assignment of absolute configuration to natural (-)-puraquinonic acid. Use of radical cyclization for asymmetric generation of a quaternary center. *J. Org. Chem.* **2004,** *69*, 4116-4125.
242. Ishi-i, T.; Sawada, T.; Mataka, S.; Tashiro, M., Intramolecular O–H ....π hydrogen bond found in [2.2]metacyclophane systems: spectral properties and X-ray crystallographic analysis of 8-hydroxymethyl[2.2]metacyclophanes. *J. Chem. Soc., Perkin Trans. 1* **1996**, 1887-1891.
243. Biali, S. E.; Rappoport, Z., Stable simple enols. 8. Synthesis and keto, enol equilibria of the elusive 2,2-dimesitylethanal and 1,2,2-trimesitylethanone. Conformations of 1,2,2-trimesitylethanone and 1,2,2-trimesitylethanol. *J. Am. Chem. Soc.* **1985,** *107*, 1007-1015.

244. Carlier, P. R.; Lam, P. C.-H.; Wong, D. M., Catalytic asymmetric synthesis of protected tryptophan regioisomers. *J. Org. Chem.* **2002,** *67*, 6256-6259.
245. Luliński, S.; Serwatowski, J., Regiospecific metalation of oligobromobenzenes. *J. Org. Chem.* **2003,** *68*, 5384-5387.
246. Brown, H. C.; Garg, C. P.; Liu, K.-T., The oxidation of secondary alcohols in diethyl ether with aqueous chromic acid. A convenient procedure for the preparationof ketones in high epimeric purity. *J. Org. Chem.* **1971,** *36*, 387-390.
247. Allerhand, A.; Schleyer, P. v. R., Nitriles and isonitriles as proton acceptors in hydrogen bonding: Correlation of ΔvOH with acceptor structure. *J. Am. Chem. Soc.* **1963,** *85*, 866-870.
248. Heathcock, C. H., The aldol addition reaction. In *Asymmetric Synthesis*, Morrison, J. D., Ed. Academic Press: Orlando, 1984; Vol. 3, pp 111-212.
249. Karplus, M., Vicinal proton coupling in nuclear magnetic resonance. *J. Am. Chem. Soc.* **1963,** *85*, 2870-2871.
250. Chandross, E. A.; Sheley Jr, C. F., Some 9-aryl fluorenes. Ring-current effects on nuclear magnetic resonance spectra, carbonium ions, and the 9-mesitylfluorenyl radical *J. Am. Chem. Soc.* **1968,** *90*, 4345-4354.
251. Medina, E.; Moyano, A.; Pericàs, M. A.; Riera, A., nantioselective syntheses of conformationally rigid, highly lipophilic mesityl-substituted amino acids. *Helv. Chim. Acta* **2000,** *83*, 972-988.
252. Halgren, T. A.; Nachbar, R. B., Merck molecular force field. IV. conformational energies and geometries for MMFF94. *J. Comput. Chem.* **1996,** *17*, 587-615.
253. Young, D., *Computational Chemistry*. Wiley-Interscience: New York, 2001; p 179-192.
254. Cauwberghs, S.; Tinant, P. J. D. C.; Declercq, J. P., Factors affecting ease of ring formation. The effect of anchoring substitution on the rate of an intramolecular diels-alder reaction with furan-diene. *Tetrahedron Lett.* **1988,** *29*, 2493-2496.
255. Hoffmann, R. W.; Stahl, M.; Schopfer, U.; Frenking, G., Conformation design of hydrocarbon backbones: A modular approach. *Chem. -Eur. J.* **1998,** *4*, 559-566.
256. Brown, H. C.; Garg, C. P.; Liu, K.-T., Oxidation of secondary alcohols in diethyl ether with aqueous chromic acid. Convenient procedure for the preparation of ketones in high epimeric purity. . *J. Org. Chem.* **1977,** *36*, 387-390.
257. *CrysAlis*, V1.171; Oxford Diffraction: Wroclaw, Poland, 2004.
258. Sheldrick, G. M. *SHELXTL NT v6.12*, Bruker Analytical X-ray Systems, Inc.: Madison, WI, 2001.
259. Frisch, M. J.; Trucks, G. W.; Schlegel, H. B.; Scuseria, G. E.; Robb, M. A.; Cheeseman, J. R.; Zakrewski, V. G.; Montgomery, J. A.; Stratmann, R. E.; Burant, J. C.; Dapprich, S.; Millam, J. M.; Daniels, A. D.; Kudin, K. N.; Strain, M. C.; Farkas, O.; Tomasi, J.; Barone, V.; Cossi, M.; Cammi, R.; Mennucci, B.; Pomelli, C.; Adamo, C.; Clifford, S.; Ochterski, J.; Petersson, G. A.; Ayala, P. Y.; Cui, Q.; Morokuma, K.; Salvador, P.; Dannenberg, J. J.; Malick, D. K.; Rabuck, A. D.; Raghavachari, K.; Foresman, J. B.;

Cioslowski, J.; Ortiz, J. V.; Baboul, A. G.; Stefanov, B. B.; Liu, G.; Liashenko, A.; Piskorz, P.; Komaromi, I.; Gomperts, R.; Martin, R. L.; Fox, D. J.; Keith, T.; Al-Laham, M. A.; Peng, C. Y.; Nanayakkara, A.; Challacombe, M.; Gill, P. M. W.; Johnson, B.; Wong, M. W.; Andres, J. L.; Gonzalez, C.; Head-Gordon, M.; Replogle, E. S.; Pople, J. A. *Gaussian 03*, Pittsburgh, PA, 2003.
260. Halgren, T. A., Merck molecular force field. I. Basis, form, scope, parameterization, and performance of MMFF94. *J. Comput. Chem.* **1996,** *17*, 490-519.
261. Kong, J.; White, C. A.; Krylov, A. I.; Sherrill, D.; Adamson, R. D.; Furlani, T. R.; Lee, M. S.; Lee, A. M.; Gwaltney, S. R.; Adams, T. R.; Ochsenfeld, C.; Gilbert, A. T. B.; Kedziora, G. S.; Rassolov, V. A.; Maurice, D. R.; Nair, N.; Shao, Y.; Besley, N. A.; Maslen, P. E.; Dombroski, J. P.; Daschel, H.; Zhang, W.; Korambath, P. P.; Baker, J.; Byrd, E. F. C.; Voorhis, T. V.; Oumi, M.; Hirata, S.; Hsu, C.-P.; Ishikawa, N.; Florian, J.; Warshel, A.; Johnson, B. G.; Gill, P. M. W.; Head-Gordon, M.; Pople, J. A., Q-Chem 2.0: a high-performance ab initio electronic structure program package. *J. Comput. Chem.* **2000,** *21*, 1532-1548.